Oxygen Challenge MRI

Development of a Novel Technique and Application to Acute Stroke Patients

Krishna A. Dani
BSc (Hons), MBChB, MRCP (Glasg)

A thesis submitted which fulfills the requirements of the University of Glasgow for the degree of Doctor of Philosophy

Institute of Neurosciences and Psychology
University of Glasgow

April, 2011

Abstract

The treatment of hyperacute ischaemic stroke has been revolutionised by the concept of potentially salvageable tissue – the 'ischaemic penumbra'. However, current therapeutic practice is to administer thrombolytic therapy with recombinant tissue plasminogen activator after exclusion of intra-cerebral haemorrhage, with 'time since onset' used as a surrogate marker for the presence or absence of the ischaemic penumbra. The ability to identify the penumbra on an individual basis would enable bespoke treatment plans on the basis of underlying pathophysiology. The most commonly employed penumbral image technique is multi-modal magnetic resonance imaging (MRI) to identify a region of perfusion-diffusion mismatch. However, this approach remains to be validated. Moreover, a systematic review presented as an appendix to this thesis highlights the marked heterogeneity for its application.

This thesis focusses on the development of a novel MRI technique (Oxygen Challenge) and is the first to report findings from human acute ischaemic stroke. The rationale for this technique is that it is sensitive to deoxyhaemoglobin, which is produced as a consequence of oxidative metabolism. It therefore has the potential to discriminate tissue compartments based on metabolic activity. For this study, 35 subjects with acute ischaemic stroke were imaged with transient hyperoxia (Oxygen Challenge) applied during continuous T2*-weighted MRI. Exploratory analyses suggested the following;

- Oxygen Challenge precipitates a T2*-weighted signal increase in healthy tissue

- This signal increase is partly dependent on the underlying cerebral blood volume, as suggested by univariate and multivariate analyses

- In general, higher concentrations of oxygen precipitate greater T2*-weighted signal increases, but oxygen may influence T2*-weighted signal intensity in a bi-modal manner

- The signal changes in operationally defined infarct core are attenuated, suggesting a metabolic influence on Oxygen Challenge results

- Signal increases in the hyperacute perfusion-diffusion mismatch region were sometimes exaggerated, consistent with increased oxygen extraction fraction. However, small volumes of tissue acquired from only a few subjects limited definitive conclusions in this study

- Oxygen Challenge may detect regions of crossed cerebellar diaschsis, although further confirmation is required

- Maps of ‘percentage signal change’ allowed rapid evaluation of whole brain Oxygen Challenge data

- Improvements in signal-to-noise ratio are required before this technique can be applied in clinical practice.

On the basis of these data it is concluded that the technique is encouraging and further validation is warranted.

Table of Contents

List of Tables

List of Figures

List of Publications

Papers

- **Hyperintense Vessel Sign on Fluid Attenuated Inversion Recovery Magnetic Resonance Imaging is Reduced by Gadolinium.** Dani KA, Latour L, Warach S. American Journal of Neuroradiology *(in press)*.
- **T2*-weighted Magnetic Resonance Imaging with Hyperoxia in Acute Ischemic Stroke;** Dani KA, Santosh C, Brennan D, McCabe C, Holmes WM, Condon B, Hadley DM, Macrae IM, Shaw M, Muir KW. Annals of Neurology 2010; 68 (1); 37-47.
- **Do Iodinated Contrast Agents Impair Fibrinolysis in Acute Stroke; A Systematic Review**; Dani KA and Muir KW. American Journal of Neuroradiology. 2010; Jan; 31(1)170-4
- **Brain Lesion Volume and Capacity for Consent in Stroke Trials: Potential Regulatory Barriers to the Use of Surrogate Markers.** KA Dani, MT McCormick. KW Muir. Stroke. 2008 Aug;39(8):2336-40
- **CT and MR perfusion imaging in ischemic stroke: definitions and thresholds.** KA Dani, RGR Thomas, FM Chappell, K Shuler, KW Muir, JM Wardlaw. *Annals of Neurology. 2011. In press.*
- **Perfusion imaging with CT and MR in acute ischaemic stroke – 2. Heterogeneity of acquisition and post processing parameters. A Systematic Review.** KA Dani, RGR Thomas, FM Chappell, K Shuler, KW Muir, JM Wardlaw. *Stroke. In press*

Abstracts

- **Oxygen Challenge MRI: Signal Dependence on Tissue Type and Oxygen Concentration.** Dani KA, Santosh C, Brennan D, Condon B, Hadley D, McCabe C, Holmes W, Macrae IM, Muir KM. Presented as a poster at the annual Scottish Imaging Network (2010) meeting, Edinburgh 2010.
- **Magnetic Resonance Spectroscopy May Be Helpful in Acute Stroke.** Dani KA, An l, Henning E, Shen J, Warach S. This was presented as a poster as the European Stroke Conference, Barcelona, 2010.
- **Under-Reporting and Heterogeneity of Acquisition Parameters for Acute Stroke Brain Perfusion Studies.** Dani KA, Thomas RGR, Chappel FM, Shuler K, Wardlaw J, Muir KW. This was presented as a poster as the European Stroke Conference, Barcelona, 2010.
- **Thresholds for tissue viability on CT and MR perfusion imaging in acute ischemic stroke.** Dani KA, Thomas RGR, Chappel FM, Shuler K, Wardlaw JM. This was presented as a poster as the European Stroke Conference, Barcelona, 2010.
- **Hyperintense Vessel Sign on Fluid Attenuated Inversion Recovery Magnetic Resonance Imaging is Reduced by Gadolinium.** Dani KA, Latour L, Warach S. This was presented as a poster as the International Stroke Conference, San Antonio, 2010. Stroke. 2010. 41 (4); E369.
- **Pilot Results of in vivo Brain Glutathione Measurements in Stroke Patients Using Magnetic Resonance Spectroscopy. An L, Dani KA, Shen J, Warach S.** This was presented as a poster as the International Stroke Conference, San Antonio, 2010. Stroke. 2010. 41 (4); E386.
- **Oxygen Challenge with T2*MRI as a Metabolic Biomarker In Acute Ischemic Stroke Patients** Dani KA, Santosh C, Brennan D, Macrae IM, Condon B, Hadley D, Muir KW. Oral Presentation at the International Stroke Conference 2009**, Date:** FEB 17-20, 2009 San Diego CA Stroke. 2009**;** 40**:** 4 E116-E116

- **Oxygen Challenge T2* Weighted MRI as a Measurement Tool for Brain Metabolism.** Dani KA, Santosh C, Brennan D, Macrae IM, Condon B, McCabe C, Holmes W, Hadley D, Muir KW. Presented by Professor Muir at the Annual SINAPSE meeting, Edinburgh 2009.
- **Comparison of perfusion weighted MRI and single photon emission computed tomography for assessment of cerebrovascular reserve in symptomatic carotid territory stenosis**. McSorley ST, Dani KA; Patterson J; Muir KM; Poster Presentation by T. McSorely at the Annual Meeting of the Association-of-British-Neurologists**,** Date**:** NOV 14-16, 2007 London. JNNP. 2008;79;3;345
- **Transient Hyperoxia During T2* weighted MRI to Image Brain Metabolic Activity: An Alternative definition of penumbra in Acute Ischaemic Stroke?** Dani KA, Santosh C, Brennan D, Macrae IM, Condon B, Hadley D, Muir KW. Poster presentation at the UK Stroke Forum, Harrogate, December 2007
- **The Use of Oxygen Challenge with T2* Sensitive MR in the Delineation of Metabolic Tissue Compartments in Acute Stroke.** Santosh C, Dani KA, Brennan D, Condon B, Macrae IM, Hadley DM, , Muir KW. Presented by Dr Santosh at the British Society of Neuroradiology Annual Meeting, 2007.
- **Mapping of Brain Metabolism using Oxygen Challenge with Magnetic Resonance Imaging in Acute Stroke Patients.** Dani KA, Santosh C, Brennan D, Condon B Macrae IM, Hadley DM, Muir KW**.** Presented as an oral presentation at the European Stroke Conference, Glasgow, May 2007
- **Do Iodinated Contrast Agents Impair Fibrinolysis in Acute Stroke? A Systematic Review.** KA Dani, KW Muir. Presented as a poster at the European Stroke Conference, Glasgow, May 2007
- **The Use of Oxygen as a Contrast Agent and Metabolic Biotracer in Acute Stroke Patients**.Dani KA, Muir KW, Brennan D, Condon B, Macrae IM, Hadley DM, Santosh C. Presented as a poster at Brain 07, Osaka, Japan, May 2007

Acknowledgments

I am very grateful to my supervisor, Professor Keith W Muir, who welcomed me into his research group and seeded an enthusiasm for the use of imaging, especially MRI, to elicit brain pathophysiology. It is thanks to his research and clinical guidance that I had the opportunity to pursue research in acute stroke. The skills I learned from him extend far beyond those attained from working on the studies presented in this thesis.

I am also grateful for the support of my advisor Professor I Mhairi Macrae, who provided useful advice throughout the duration of my research period and, in particular, encouraged scientific rigor. I am also very am grateful to Dr Celestine Santosh who is a strong proponent of the Oxygen Challenge technique. He provided useful discussions and ensured that the patients recruited into the study completed the imaging protocol. I am grateful to Ms Isobel McDonald and her fellow radiographers, without whom, this study would never have happened.

I am very grateful to the University of Glasgow Clinical Research Fellow committee who provided me with the opportunity to take the Clinical Research Fellow post and who provided me with the first year's funding. I am also very thankful to the Patrick Berthoud Committee who had faith in me to complete the studies presented in this thesis, and provided a further 3 years of funding. I am indebted to the Stroke Consultants at the Southern General Hospital who allowed me to recruit patients under their care. These people were Dr Phil Birschel, Dr Tracey Baird, Dr George Duncan, Dr Fozia Nair, Dr Ian Reeves and Dr Margaret Roberts. I am grateful to Dr David Brennan, Dr Rosario Holmes and Dr Fergal McVerry for useful discussions concerning the post-processing of images. I am grateful to Dr Steven Warach of the National Institutes of Health for allowing me to attend his laboratory for a year. Although I did not pursue work directly related to this thesis, I received excellent training in stroke research skills related to MRI.

Finally I must acknowledge the support of my loving wife, Claribel, who provided the support for me to complete these projects, including tolerating a year apart during my 'USA year'. She encouraged constant motivation and energy. I am also grateful for the support of my mother, father, and sister Melanie.

Author's Declaration

All analyses are the work of the author unless otherwise stated.

Krishna A. Dani BSc (Hons), MBChB, MRCP (Glasg)

University of Glasgow, April 2011

Abbreviations

ACA – anterior cerebral artery
ADC - apparent diffusion coefficient
AIF – arterial input function
AUC – area under the curve
ANOVA – analysis of variance, statistical testing
ASL – arterial spin labelling
ASPECTS - Alberta Stroke Programme Early CT Score
ASSET – An implementation of sensitivity encoding produced by GE
BBB – blood brain barrier
BOLD – blood oxygenation level dependant imaging
CBF – cerebral blodd flow
CBOS - on haemoglobin saturation for oxygen
CBV – cerebral blood volume
CCD – crossed cerebellar diaschisis
CDM – clinical-diffusion mismatch
CI – confidence interval
cm – centimetres
CMB – cortical microbleed
$CMRO_2$ – cerebral metabolic rate for oxygen
CO_2 – carbon dioxide
COPD – chronic obstructive pulmonary disease
CT – computed tomography
CTA – computed tomography angiography
CTp – computed tomography perfusion
d – days
DSA – digital subtraction angiography
DSC – dynamic susceptibility contrast
DWI - diffusion weighted imaging in magnetic resonance imaging
ECTD – European Clinical Trials Directive
EPI – echo planar imaging in magnetic resonance imaging
FAT - first arrival time of hyperoxic blood
FiO_2 – fraction of inspired oxygen concentration
FLAIR - fluid attenuated inversion recovery in magnetic resonance imaging
fMRI – functional magnetic resonance imaging
FMISO - ^{18}F-fluormisonidazole
FMZ - flumazenil
FOV - field of view
GE – General Electric
GIC – gradient of incline of the T2* signal intensity curves
GRE – gradient echo sequences in magnetic resonance imaging
h – hours
H_2O – water
Hct - haematocrit
HICAS – hyperintense internal carotid artery sign
HMCAS – hyperintense middle cerebral artery sign
HU – Hounsfield Units
ia – intra-arterial
ICA – internal carotid artery
ICH – intra-cerebral haemorrhage
IQR – inter-quartile range

iv -intravenous
KD – thesis author
l – litre
Lac – lactate
MAP – mean arterial blood pressure
MIP – maximum intensity projection
mm – millimetres
mM – millimoles
MMP – matrix metalloproteinase
MRA – magnetic resonance angiography
mRS – modified Rankin Scale
ms - milliseconds
MCA – middle cerebral artery
MCAO – middle cerebral artery occlusion
MR – Magnetic Resonance
MR-COMI – magnetic resonance derived cerebral metabolic rate for oxygen index
MRI – Magnetic Resonance Imaging
MREC – Multi-centre Research Ethics Committee
MRI – Magnetic Resonance Imaging
MRS – Magnetic Resonance Spectroscopy
MTT – mean transit time
N_2O – nitrous oxide
NAA – N-acetyl aspartate
NCCT – non-contrast computed tomography
NEX – number of exitations performed during MR sequences
NIHSS –National Institutes of Health Stroke Scale
NMR – nuclear magnetic resonance
NNT- - number neeed to treat
OEF – oxygen extraction fraction
OR – odds ratio
pCO_2 –tension of carbon dioxide
pO_2 – tension of oxygen
PACS – partial anterior circulation syndrome
PET – positron emission tomography
pTMS - pseudo time to maximum signal of the T2* signal intensity curve (80% of TMS)
PSC – percentage signal changes of T2* signal intensity curves
PWI - perfusion weighted imaging
rtPA – recombinant tissue plasmonogen activator
s – seconds
SE – spin echo sequences in magnetic resonance imaging
SENSE – sensitivity encoding in MRI
SNR – signal to noise ratio
SPECT – single photon emission tomography
SVD – singular value deomposition
tPA – tissue plasminogen activator
T1 – longitudinal relaxation of spins in magnetic resonance imaging
TACS – total anterior circulations syndrome
TCD – transcranial doppler
TE - Echo time
TI – inversion time
TIA – transient ischaemic attack
TIBI – thrombolysis in brain ischaemi

TIMI – thrombolysis in myocardial infarction
TMAX – time to the peak of the deconvolved curve in perfusion analysis
TMS – time to maximum signal of the T2* signal intensity curve
TTP – time to peak
TR- Repetition time
UK – United Kingdom
USA – United States of America
yrs - years

1 Introduction

Stroke is a potentially catastrophic disease. Not only is it the second leading cause of death worldwide(1) but it also imposes substantial morbidity – 6% of the total budget of the United Kingdom's National Health Service is consumed by stroke care. Approximately 80% of stroke is ischaemic in nature (2), the subtype which will be considered in this thesis. The remainder of strokes are accounted for by primary intracerebral haemorrhage (ICH) and subarachnoid haemorrhage. Data from stroke registries (3) indicate that most ischaemic strokes are within the anterior circulation (carotid territory) and most of these are within the territory supplied by large (proximal) arteries. Such strokes manifest as significant, often devastating, neurological deficit. This, coupled with the large volume of tissue amenable to study, has lead to a focus on such anterior circulation strokes due to proximal arterial occlusion by many acute imaging based studies. Moreover, advances in our understanding of the pathophysiology of ischemic stroke have fuelled developments in stroke imaging. This chapter will commence with a brief review of the pathophysiology of stroke before describing the current status of stroke imaging, with particular focus on Magnetic Resonance Imaging (MRI) of large vessel ischaemic stroke.

1.1 Events Leading to Cell Death

Large vessel strokes are usually due to vessel occlusion by thrombus. Potential sources of thrombus include embolism from plaques on atheromatous large vessels such as the carotid artery or aorta, or from a cardiac source. The site of arterial occlusion depends, in part, on the size of the thrombus, since it will lodge in an artery of comparable size. This occlusion impedes the passage of blood, thus reducing cerebral blood flow (CBF) to the brain territories distal to the clot. There might either be complete occlusion of the vessel, or alternatively some residual flow may be detected around the clot - a good prognostic sign with respect to therapy (4). The magnitude of reduction in CBF not only depends on this residual flow but also on the anatomical compensatory mechanisms which may be able to divert blood flow to hypoperfused regions– the

collateral vessels(5). Reversal of flow in the ophthalmic or anterior communicating arteries(6, 7), from the posterior communicating artery, or from retrograde flow through leptomeningeal anastomoses(5) may provide this collateral support. However, if CBF drops below a critical threshold, a cascade of events is set in train which may ultimately result in cell death, which may occur by five major mechanisms, each of which with its own temporal course. These events, which have been extensively reviewed and conceptualized(8, 9) are 1) excitotoxity, 2) peri-infarct depolarisation, 3) oxidative stress, 4) inflammation and 5) apoptosis, and are illustrated below(Figure 1-1).

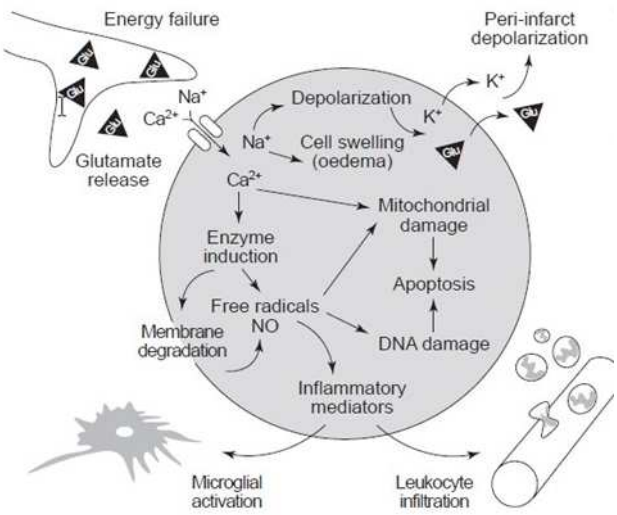

Figure 1-1 Mechanisms of Cell Death after Stroke.
Illustrated by Dirnagl and colleagues. Reproduced from 'Dirnagl U, Iadecola C, Moskowitz MA. Pathobiology of ischaemic stroke: an integrated view. Trends in Neurosciences. 1999;22:391-397' with permission from Elsevier.

Excitotoxity may occur after a few minutes of glucose and oxygen deprivation due to severely reduced CBF. Failure of the energy dependent Na^+-K^+-ATPase pumps precipitates a shift of K^+ ions from the intra- to extra-cellular space, with a movement of Na^+, Ca^{++} and Cl^- ions in the opposite direction. The extra-cellular K^+ precipitates neuronal depolarization, stimulating glutamate release into the synaptic cleft thereby activating N-methyl-D-aspartate (NMDA) and 2-amino-3-(3-hydroxy-5-methylisoxazol-4-yl) proprionate (AMPA) receptors, precipitating an influx of Ca^{++} to cells, and stimulation of potentially lethal intracellular phospholipases and proteases. The increase in Na^+ ions leads to cellular swelling, lysis, and necrotic cell death. Peri-infarct depolarisations,

which also occur within minutes after stroke, have been described in animal models where the propagation of depolarisations is observed beyond the infarct. The duration of these depolarisations is correlated to infarct size(10). Tissue acidosis occurring after anaerobic glycolysis may also lead to cell death by a number of mechanisms. The next process, ‘oxidative stress’, describes the imbalance between potentially toxic oxygen free radicals and the physiological defence mechanisms against them –antioxidants. Ischemia and reperfusion contribute to the generation of reactive oxygen species through a number of mechanisms including the generation of a mitochondrial transition pore (MTP) which can subsequently release free radicals. Whilst the processes described so far start after a matter of minutes, inflammatory and apoptotic cascades evolve over hours to days and also contribute to infarct expansion. Inflammatory changes include the infiltration of leukocytes, activation of microglia, and expression of potentially detrimental inflammatory cytokines. Apoptotic pathways occur in the peri-infarct region and involve the generation of caspases which can cleave DNA repair enzymes such as poly-(ADP-ribose_-polymerase (PARP), ultimately leading to programmed cell death.

In summary, cellular death may occur through a number of different mechanisms operating over different time scales. This has lead to the concept that patients with stroke may still have salvageable tissue at the time they present to hospital, and therefore some of these patients may be treated. This concept will be expanded in the following sections.

1.2 The Ischaemic Penumbra

1.2.1 The Concept of the Ischaemic Penumbra

The observation of different cascades each with their own time course is reflected by other observations that following arterial occlusion, all of the ‘tissue at risk’ may not become infarcted immediately, and also not at the same time. Many of these pivotal observations were made in the 1970’s by Symon and his group, who used the hydrogen clearance technique to measure cerebral

blood flow (CBF) in a baboon model of middle cerebral artery (MCA) occlusion(11). It became apparent that a number of CBF thresholds could be defined. Firstly, blood flow could be lowered to a 'benign' level without electrical function becoming affected (oligaemia). Secondly, the threshold for complete electrical failure (as measured by the obliteration of somatosensory evoked responses) was higher than that for the disturbance of ion homeostasis (defined as a massive increase in extracellular potassium [K^+] and used a surrogate marker for cell death). Furthermore, a pharmacologically induced increase in mean arterial blood pressure restored electrical function, suggesting the potentially salvageable nature of the ischaemic tissue. Not only did these observations lead to the concept of flow thresholds, but the concept of the 'ischaemic penumbra' was born(12). In an analogy to the 'almost shadow' state seen during a solar eclipse, this term describes a state of functionally inactive but structurally intact neurons, which can be salvaged by restoring cerebral blood flow. This is distinct from the region of tissue which will inevitably proceed to infarction (core) and the hypoperfused region which will never proceed to infarction, benign oligaemia. Although the original definition was based upon the mismatch between the state of electrical dysfunction and perturbed ion homeostasis, the concept has since been variously defined depending of the nature of the scientific study. A more clinically relevant definition is that stated by Baron in 1999 which emphasizes its potentially salvageable nature(13).

"a severely ischaemic, functionally impaired tissue at risk of infarction, that will be saved if reperfused before it is irreversibly damaged, but that otherwise will be progressively recruited into the core until maximum infarct extension is reached".

Given that this tissue compartment represents a genuine potential therapeutic target, the last 30 years has seen vigorous research into further defining and identifying this tissue state, and into targeting therapies towards salvaging it.

1.2.2 Key Principles of the Ischaemic Penumbra

A large number of observations have generated some important principles underlying the definition of the penumbra, which will be discussed here.

1.2.2.1 The Penumbra is Biologically Compromised

Although the penumbra is potentially viable, it exists in a compromised state and the cascade of ischaemic events which creates the core is also applicable to the penumbra. It has been hypothesised(14) however, that in the penumbra peri-infarct depolarisations may be central to these events and contribute to energy depletion, lactic acidosis, differential gene expression and selective neuronal loss. Proof of compromised penumbral tissue comes from animal histology studies which have shown a clear zone of neuronal damage within a few millimetres of the infarct(15). Others have shown neuronal damage in a scattered or microfocal pattern(16) within the presumed penumbral region. Gene expression in the penumbra is also different from that in normal tissue and infarct core (17). In particular, denatured proteins appear to stimulate the synthesis of a heat shock protein known as HSP70, and such expression is noted to coincide with regions of penumbra(18). Therefore, there is good evidence that the penumbra is biologically compromised.

1.2.2.2 Flow Thresholds are Specific for Different Pathophysiological Processes

Much attention has been focussed on identifying the thresholds which distinguish oligaemia from penumbra, and penumbra from core. However, the large body of studies of the ‘penumbra’ has used various surrogate markers for the penumbral and infarction threshold. Despite a range of methodologies to study a range of different biological processes, Hossman(14) concluded a rank order of CBF thresholds for the disruption of different processed could still be established (Figure 1-2).

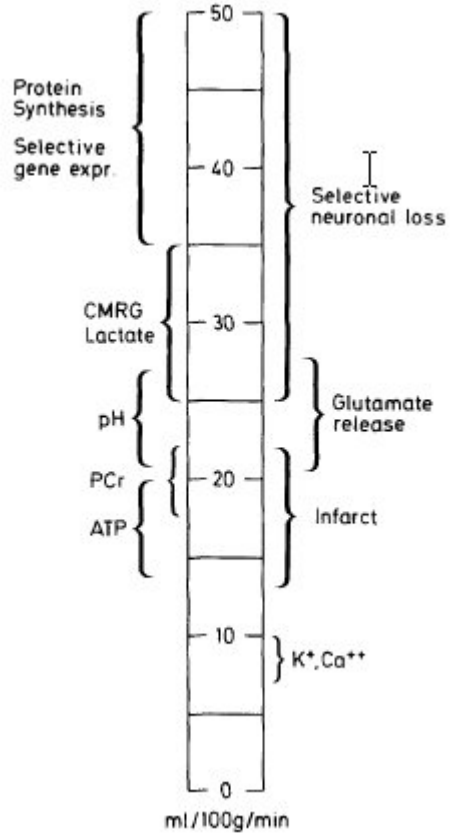

Figure 1-2 Flow Thresholds as Described by Hossman
Numerical values indicate CBF in ml/100g/min. CMRG=cerebral metabolic rate of glucose. PCr=phosphocreatine depletion. ATP = adenosine triphosphate depletion. K^{+}=potassium ions. Ca^{++} = calcium ions. Reproduced from ' Hossmann KA. Viability thresholds and the penumbra of focal ischemia.[see comment]. Ann.Neurol. 1994;36:557-565' with permission from John Wiley and Sons.

In particular, protein synthesis is disturbed well above the threshold for the penumbra / oligaemic border and that for electrical failure. As might be expected, when CBF falls further there is electrical failure (15-25ml/100g/min), and disturbance of glucose metabolism and anaerobic glycolysis. With more severe hypoperfusion there is energy failure, disturbance of ion homeostasis and infarction.

1.2.2.3 The Cerebral Blood Flow Threshold for Tissue Infarction is Dynamic and Increases with Time

The CBF threshold which distinguishes infarct core from penumbra is dynamic. Jones and colleagues(19) performed MCA occlusion in unanaesthetised monkeys for variable periods of time (15-30 minutes, 2-3 hours, or permanently) with

concomitant measures of CBF. The study demonstrated that infarction thresholds depended not only on the degree of hypoperfusion, but also the duration. For example the CBF infarction threshold was 10-12ml/100g/min after 2-3 hours of occlusion, but rose to 18ml/100g/min after permanent occlusion (Figure 1-3). In man, the volume of penumbra has been shown to progressively decline with time(20) but in a minority of human strokes may be present as long as 48 hours post ictus(21).

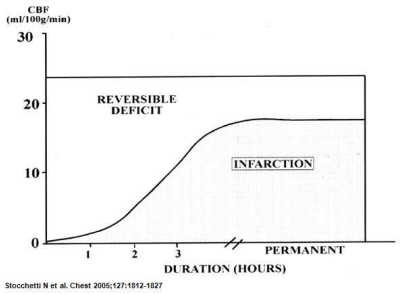

Figure 1-3. CBF thresholds for Infarction Increase with Time.
The x-axis denotes time in hours, and the y-axis denotes locally measured CBF in ml/100g/min. Reproduced from an adaptation of 'Jones TH, Morawetz RB, Crowell RM et al. Thresholds of focal cerebral ischemia in awake monkeys. J.Neurosurg. 1981;54:773', courtesy of the American College of Chest Physicians.

1.2.2.4 Assessment of Haemodynamic Status Solely Using Measures of CBF is Inaccurate

CBF measurements alone do not provide a full description of the haemodynamic status of the tissue. Under normal circumstances CBF is dependent on the interaction between the cerebral perfusion pressure (CPP) and the cerebrovascular resistance (CVR) which is dependent, in part, on the diameter of local vasculature diameter. Lassen(22) described a range of mean arterial pressures between which the local vasculature could, by changes in vessel diameter, respond to changes in systemic arterial pressure in order to maintain a constant cerebral blood flow - a phenomenon termed ‘autoregulation’. However, beyond the extremes of this range (typically less than 60mmHg or greater than 160mmHg) autoregulation can no longer be maintained. The sequence of haemodynamic events following hypoperfusion has been reviewed by Markus and is summarised as follows (Figure 1-4).

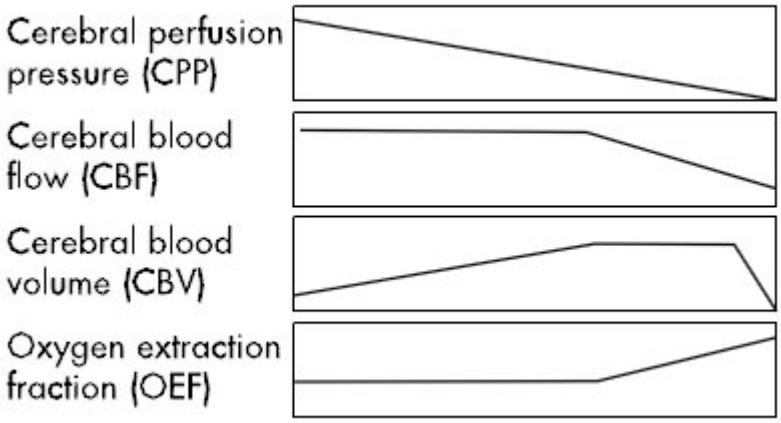

Figure 1-4. Sequence of Haemodynamic Perturbations after Ischaemia.
After arterial occlusion there is a reduction in cerebral perfusion pressure. CBF is maintained by a increase in cerebral blood volume (CBV) and when maximal dilatation has been achieved there is an increase in oxygen extraction fraction. The line diagrams illustrate the relative changes for each parameter. Reproduced from 'Markus. Cerebral Perfusion and Stroke. Journal of Neurology, Neurosurgery and Psychiatry. 75(3);' with permission from BMJ Publishing Group Ltd.'

The first response to severe hypoperfusion is the dilatation of pre-capillary arterioles with its associated increase in cerebral blood volume (CBV). Thereafter, oxygen action fraction from the blood to the tissue (normally 30-40%) increases – a phenomenon coined ‘misery perfusion’(23). If this is insufficient for metabolic demands then neurological symptoms ensue. If perfusion is not restored and the cerebral metabolic rate for oxygen ($CMRO_2$) falls, so too does the CBV(24). This implies that penumbral tissue should have preserved or increased CBV. These data indicate that knowledge of the CBF alone cannot distinguish penumbra from core, and that additional assessment of CBV, OEF, and $CMRO_2$ provides a more comprehensive description of the haemodynamic and viability state of the tissue. Modern imaging techniques have sought to image some or all of these modalities.

1.2.2.5 Timely Restoration of Cerebral Blood Flow Salvages the Penumbra

In concert with the results suggesting that the threshold for infarction is time dependent, Jones and colleagues(19) also reported results for functional recovery. After release of an MCA occlusion after 15 minutes, all monkeys made a rapid and full recovery. Release of occlusion at later time points, when the volume of penumbra was likely to have diminished, led to the clinical

improvement in only a proportion of the animals, and an overall lesser degree of clinical improvement. Consistent with this, the volume of penumbra in man which escapes infarction due to reperfusion is highly correlated with neurological recovery(25, 26). These observations, and others like them, mean that the penumbra is not just an academic curiosity, but a genuine therapeutic target.

1.2.2.6 Clinical Operational Criteria Have Been Devised to Define the Penumbra

In order to be clear that studies are really investigating what is genuinely penumbral tissue, a number of generally accepted criteria have been developed(27). These include 1) Hypoperfusion <20ml/100g/min, 2) the presence of a neurological deficit, 3) perturbation of normal physiology / biochemistry, 4) uncertain fate, and finally 5) evidence that salvage of the compartment defined by the criteria for penumbra is associated with improved outcome. Novel penumbral imaging techniques should ideally be assessed against this standard.

1.3 Recombinant Tissue Plasminogen Activator for Acute Ischemic Stroke

The concept of the penumbra has led to the development of a number of different reperfusion strategies. Intra-venous recombinant tissue plasminogen activator (rtPA) is the only proven reperfusion therapy for use in acute ischemic stroke. The rationale is to aid clot lysis, leading to reperfusion, penumbral salvage and improved clinical outcome.

Tissue plasminogen activator (tPA) is a naturally occurring serine protease which activates plasminogen to form plasmin, which subsequently breaks down fibrin. This achieves lysis of the clots, which are composed of fibrin meshes and activated platelets. The therapeutic attractiveness of ‘tPA’ is that it targets fibrin bound plasminogen specifically, therefore targeting plasminogen in the

clot rather than in plasma(28), potentially reducing bleeding side effects. Recombinant DNA technology has allowed the production of rtPA(29) which has facilitated modifications of 'tPA' such as reduction of half life, and an increase in fibrin specificity. Although it is effective for clot lysis, it has side effects which include intra-cranial haemorrhage due to a direct effect of proteases on haemostatic plugs, and is potentially neurotoxic(30-33).

The first blinded randomised controlled clinical trial showing efficacy was the report from the National Institute of Neurological Disorders and Stroke rtPA Stroke Study Group (NINDS trial) in 1995(34). This trial was actually two trials; Part 1 (phase IIb trial, 291 patients) and Part 2 (Phase III trial). Both trials used the same protocol; after exclusion of haemorrhage by non contrast CT of the brain (NCCT) rtPA was administered within 3h using the now approved dosing regimen. Although part 1 was negative($p=0.06$), part 2 was positive for its end point; there was a 12% absolute increase in the number of subjects with minimal or no disability at 3 months in the rtPA arm. This corresponded to an odds ratio (OR) for a favourable outcome of 1.7 (95% confidence interval (CI) 1.2-2.4). Rates of symptomatic intracranial haemorrhage were acceptable, (~7%). A recent re-analysis of the data showed that the number needed to treat (NNT) to have 1 patient experiencing a better outcome (at least 1 grade improvement on the mRS) was '3.1' and the NNT to have a normal or near normal outcome was '8'(35). A separate study also showed that all subgroups of stroke benefited from this therapy(36). Reassuringly, results from the Safe Implementation of Thrombolysis in Stroke-Monitoring Study (SITS-MOST) registry(37) showed that in clinical practice, outcomes pertaining to symptomatic haemorrhage, mortality, and functional outcome in clinical practice were comparable (and sometimes better) to those achieved in the trials.

These results were followed up by the European Stroke Study (ECASS) III(38) which was a prospective double blind randomised controlled trial which administered rtPA or placebo to subjects in the 3 - 4.5h time window. A NCCT was obtained to exclude patients with primary intracerebral haemorrhage (ICH) or major established infarction. This study showed that the proportion of subjects with a mRS score of 0-1 at 90d was greater with rtPA compared to placebo (52.4% vs 45.2%). Again, the rates of symptomatic intra-cerebral haemorrhage (any bleeding associated with an increase of 4 or more NIHSS

points) were acceptable in this study (2.4% with rtPA vs 0.2% in placebo). Again, 'real world' results reported in the Safe Implementation of Treatments in Stroke – International Stroke Thrombolysis Registry (SITS-ISTR)(39) suggest that this approach is safe; results from 664 patients who had rtPA between 3 - 4.5h (median 195 minutes) did not differ from those obtained from 11864 patients who had rtPA below 3h (median 140 minutes) with respect to symptomatic intra-cerebral haemorrhage at 24h, and mortality and independence at 3 months. Recently, updated NNT estimates based on the 6 rtPA trials were published(40). The NNTB (number need to treat to gain any benefit) and NNTH (number needed to treat to harm) for 90 minute intervals up to 6 h were reported. At all points up to 4.5h the NNTB outweighed the NNTH. At 4.5-6h, the NNTH outweighed the NNTB. The NNTB at 0-90mins, 91-180mins, 181-270mins, and 271-360mins were 3.6, 4.3, 5.9, and 19.3 respectively. Therefore, all studies seem to point towards an upper limit of 4.5h for rtPA administration, in the context of studies which used only NCCT to select subjects for rtPA. Other potential reperfusion strategies such as intra-arterial thrombolysis(41, 42) and mechanical retrieval(43) offer promise but direct randomised evidence showing superiority to intravenous rtPA is lacking, and in certain situations may be harmful(44).

In summary, rtPA is a selective fibrinolytic which is proven to be of benefit in patients with acute ischaemic stroke. However, although the penumbra may exist up to 48h(21), strategies using NCCT are only effective up to 4.5h. The next sections discuss the currently employed imaging strategies to better identify subjects who may benefit from rtPA.

1.4 Principles of Magnetic Resonance Imaging

1.4.1 Signal Generation

A comprehensive description of the principles of Magnetic Resonance Imaging (MRI) is beyond the scope of this introduction. However, basic principles will be briefly considered. MRI is based on the concept of Nuclear Magnetic Resonance (NMR) which describes the properties of nuclear spins. Atoms which contain an uneven nuclear mass such as hydrogen (^{1}H), spin about their own axes – they

precess. This gyroscopic motion is analogous to the movement of a spinning top. Clinical MRI measures the spins from protons (^1H) since water (H_2O) is abundant in the brain. During scanning a subject is placed in the MR scanner and is subjected to an external magnetic field (B_0) which causes spins to align with the magnetic field (z direction). Spins will align either in a direction parallel to the magnetic field (the lower energy state) or anti-parallel (the higher energy state). There are always slightly more spins in the lower energy parallel state and the difference can be estimated at 0.003% per Tesla. This difference creates a magnetisation parallel to the magnetic field – longitudinal magnetisation. However, precession is still asynchronous; the protons do not rotate in phase and therefore there is no magnetisation in the transverse (x-y) plane (Figure 1-5).

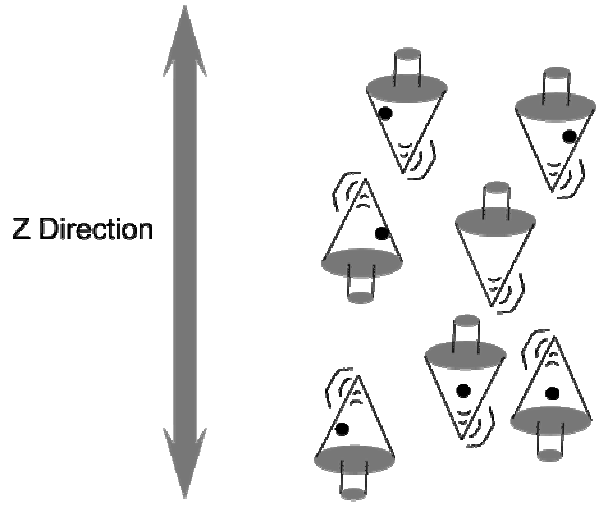

Figure 1-5. Demonstration of the Parallel and Anti-parallel States.
When protons are subjected to an external magnetic field (B0) they align in the plane of the magnetic field (Z-direction). They align either parallel (spinning tops pointing down) or anti-parallel (spinning tops pointing up) to this field. Slightly more protons align in the parallel state thus creating magnetisation. However the protons are precessing out of phase (note different position of the black spots on the spinning tops) and hence there is no transverse magnetisation, hence the MR signal cannot be measured without further changes.

The magnetisation in this phase is static and therefore cannot be measured. Therefore magnetisation is tipped into the transverse plane by excitation. This is achieved by applying electromagnetic radiation (B_1) at the same frequency as that of the precessing spins - the Larmor frequency. In response, some spins move from a low energy (parallel) state to a high energy (anti-parallel) state, and thus longitudinal magnetisation decreases. Secondly, the protons start to

precess in a synchronous manner; they become ‘in phase’ with each other. This means that there is now net magnetisation in the transverse (x-y) direction since the different directions of precession by individual protons no longer cancel each other out. After the radiofrequency pulse is over and spins re-establish equilibrium and move from a high energy anti-parallel state to the more stable parallel state, longitudinal magnetisation recovers by a time constant T1 (Figure 1-6). Given that total magnetisation remains constant, the increase in longitudinal magnetisation is offset by a decrease in transverse magnetisation. This results from spins interacting with one another and gradually becoming out of phase, and is therefore also known as spin-spin relaxation. This occurs at a time constant T2. Spins can also become out of phase because of external magnetic field inhomogeneities according to the time constant T2’. The time constant which describes signal decay due to the combined effects of spin-spin interactions and magnetic field inhomogeneities is known as T2* and will be exploited in some of the studies described later. This can be defined as 1/T2*=1/T2 + 1/T2’. The signal changes described above are measured by receiver coils which ultimately allow image formation. Image acquisition parameters can be adjusted to weight tissue contrast to highlight differences in longitudinal or transverse relaxation between tissues. The T1 and T2 curves are shown below (Figure 1-6).

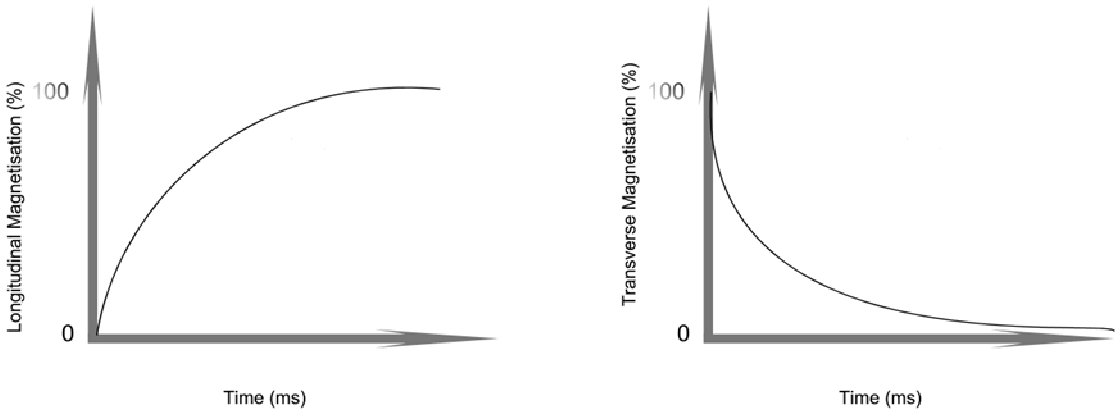

Figure 1-6. T1 and T2 Relaxation Curves.

After B1 is applied at time = 0, longitudinal magnetisation starts to recover (see T1 curve - left) and transverse magnetisation starts to decay (see T2 curve right).

1.4.2 MR Sequences

In order to achieve contrast between different types of tissue, a variety of pulse sequences may be applied. The figure below (Figure 1-7) illustrates a classification of different types of contrast.

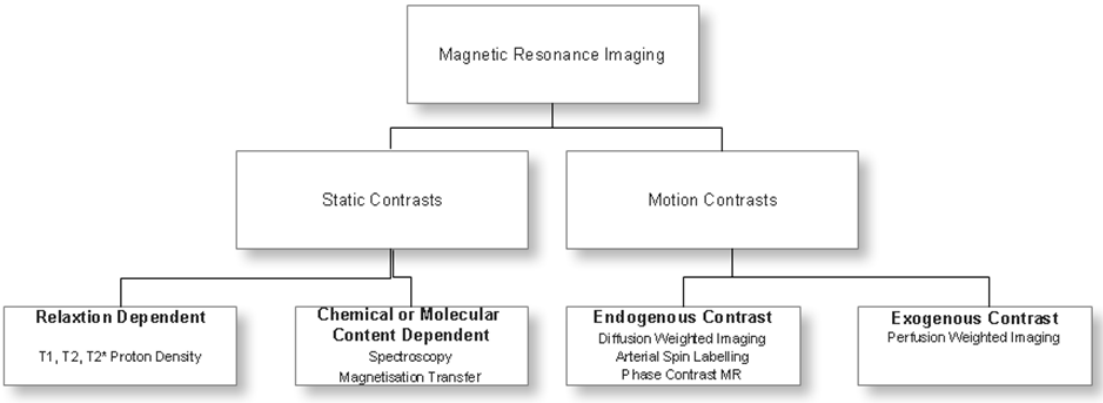

Figure 1-7. Classification of MR Sequences.

These contrasts may be produced by a number of different pulse sequences; over one hundred different types exist. In this section some basic sequences will be discussed. These are denoted by a number of different acronyms which vary between scanner manufacturers. Work forming this thesis was conducted with a General Electric (GE) scanner and therefore notation by this manufacturer will be adopted unless otherwise specified.

1.4.2.1 Spin Echo Sequences (SE)

The 'spin echo' (SE) sequence consists of a 90º radiofrequency pulse, followed by a pulse at 180º, and is the 'classic' MR pulse sequences. The first pulse tips the longitudinal magnetisation into the x-y plane. When protons start to dephase the 180 º pulse refocuses the spins and thus reduces the dephasing from external field inhomogeneities. Therefore any signal decay will be due to spin-spin effects rather than magnetic field homogeneities i.e. T2 rather than T2*.

1.4.2.2 Gradient Echo Sequences (GRE)

Gradient echo (GRE) sequences rephase the dephasing spins not by using a 180º pulse, as in SE sequences, but by using magnetic gradients, Firstly a magnetic gradient is briefly switched on, thereby introducing large magnetic field inhomogeneities and thus causing significant signal decay. This is then switched off and then back on again, but in the opposite direction. This latter action has a similar effect to the 180º refocusing pulse used in SE sequences. A gradient echo is thus produced. These gradient echoes can be achieved in a shorter time than the comparatively lengthy application of a 180º. GRE sequences are sensitive to magnetic field inhomogeneities and therefore produce contrast which is T2*-weighted.

1.5 Imaging Techniques

1.5.1 Diffusion Weighted Imaging

1.5.1.1 Theoretical Background

Diffusion weighted imaging (DWI) is now an essential part of any acute stroke MR imaging protocol. Such sequences measure the motion of water molecules in the brain and are modifications of the basic SE sequence. Not only is there a 90° radiofrequency pulse followed by a 180° pulse, as with the SE sequence, but there are two gradient pulses, one on each side of the 180° pulse i.e. 90° pulse – gradient pulse - 180° pulse – gradient pulse – echo, the sequence often being referred to as the Stejskal-Tanner sequence(45). The gradient pulses are equal in magnitude but opposite in direction to each other. The first pulse has the effect of increasing the dephasing of spins which subsequently increases signal decay. In tissues where spins are not moving (i.e. they are static) the equal and opposite second gradient pulse will reverse this action ensuring that there is no net dephasing. An echo can be produced and a strong signal can therefore be acquired. Where spins are moving however, the phase change following the

second gradient pulse will be less, owing to spins being in a different spatial location from the position they were in during the first pulse. This means the resulting echo and subsequent signal will be less. In what situations do spins move? Blood vessels containing flowing blood is an obvious example. However the natural tendency of molecules at temperatures above absolute zero is a continuous random motion, often termed Brownian motion or diffusion. In this situation the signal decay is even greater than in the example of blood flow as not only will all spins within a particular voxel be in a different position during the second gradient echo compared to the first, but the position of each spin will change in a random direction. The refocusing pulse of the SE sequence does not reverse the loss of phase coherence as the motion is random. Therefore in tissues with restricted diffusion there is strong signal intensity, and in those with greater (e.g. normal) molecular motion the signal intensity is weaker. A standard stroke protocol 'diffusion weighted image' can be produced by averaging the diffusion weighted images performed in three orthogonal directions - x, y and z directions.

Images from DWI are typically reviewed qualitatively but provide little quantitative information because of their dependence of gradient characteristics and the influence of T1 and T2 weighting. The quantification of diffusion is instead expressed as an apparent diffusion coefficient (ADC) which is calculated when a number of diffusion weighted images are acquired (at least two) for a given direction at different b values, and signal intensity is fitted to the diffusion equation by linear regression on a voxel-wise basis – the slope of the line is the ADC.

1.5.1.2 Changes on DWI in Stroke

So how does the theory discussed above relate to acute stroke? The diffusion of molecules in a gas or liquid is totally random – it is isotropic. In tissues with normal physiology, however, there is always a baseline degree of anisotropy, where molecules exhibit a directional preference for diffusion owing to tissue structures. The first studies using DWI in acute stroke were performed in 1990 by Moseley et al who, using an MCA occlusion model in the cat, demonstrated acute

hyperintense lesions on DWI which appeared rapidly and preceded changes on conventional T2 weighted images(46) i.e. there was restricted diffusion of water. Such changes were associated with metabolic abnormalities demonstrated by concomitant MR spectroscopy(47). Therefore in acute stroke there is restricted diffusion. The cause of these changes has still not been fully elucidated and is likely to be multifactorial. The explanation given by the authors was that this represented cytotoxic oedema which has been experimentally confirmed(48). The cell swelling in acute stroke is likely to be due to dysfunction of Na^+/K^+ATPase pumps(49) which not only reduces extracellular water but may cause mechanical impediment of diffusion in the extra-cellular space. Breakdown of intracellular structures may create a similar impediment intra-cellular diffusion of water.

In summary, acute stroke can manifest as hyperintense lesions appearing within minutes after vessel occlusion and is likely to be due, at least in part, to cytotoxic oedema. The time course of changes on DWI and ADC maps will be discussed in a later section.

1.5.1.3 Significance of DWI Lesions

The findings of DWI hyperintensity and ADC hypointensity have been confirmed in human studies, most of which now employ echo-planar imaging (EPI) in order to image the whole brain and improve insensitivity to patient motion(50). In human studies it is often concluded that such lesions represent irreversibly infarcted tissue(51) and this is indeed a premise upon which the PWI-DWI mismatch concept(52) is based (this will be discussed later). However, a number of both animal and human studies have shown reversal of the DWI lesion, particularly when reperfusion therapy has been instituted(53), consistent with the finding that parts of the DWI lesion fit the PET criteria for penumbra(54). Therefore, at early time points, parts of the DWI lesion, although highly compromised, may represent potentially salvageable tissue. At present there is no reliable mechanism to predict which parts of the DWI lesion are reversible(55) although some studies have shown an intermediate value of ADC in tissue which is potentially salvageable compared to infarct core(56, 57).

Nonetheless, despite the potential for reversibility, a number of studies, many of which were performed at later time points, indicate that the lesion on DWI is a good predictor of final infarct size(58, 59). Therefore DWI should be viewed as an invaluable tool which can detect either ischaemia or infarction at early time points.

1.5.1.4 Reliability of Detection of Lesions on DWI

Reported sensitivities and specificities for stroke vary, but sensitivities are usually greater than 80-85% with specificities greater than 90%(60-62). In particular diagnostic accuracy has been demonstrated to be superior to CT in the first 12 hours(60). Figure 1-8 illustrates an axial DWI slice from a subject who presented with a right hemisphere stroke and imaged at 18h.

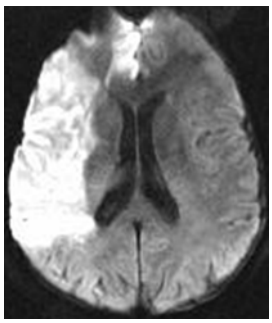

Figure 1-8. Example of a Stroke on Diffusion Weighted Imaging.
A slice from DWI of a subject presenting to the Institute of Neurological Sciences, Glasgow, with a right hemisphere stroke. The image shows that the area of restricted diffusion in the right hemisphere MCA and ACA territories is illustrated with high contrast to noise ratio.

The areas of high signal are readily apparent and DWI is easily interpretable; even studies from hyperacute acute stroke patients (<6h) show excellent interobserver reliability superior to CT(63). DWI is also superior to CT for making a positive diagnosis of stroke. Chalela et al(64) prospectively compared DWI (in combination with GRE which reliably detected haemorrhage) to CT in 356 subjects who presented acutely with a possible diagnosis of stroke(217 had a final diagnosis of stroke) and showed the sensitivity of MRI and CT was 83% and 26% respectively for any diagnosis of stroke. Nonetheless, Barber et al(65) argue that if a scoring system known as ASPECTS is used to detect stroke, the

difference in sensitivity between the two modalities is small and is outweighed by the more rapid acquisition and superior tolerability of CT of CT.

1.5.1.5 Predictive Value of DWI

DWI may be predictive in 3 domains; prediction of outcome after stroke, prediction of haemorrhagic transformation after rtPA, and the prediction of stroke after TIA. Acute DWI lesion volumes are predictive of the results yielded by acute stroke scale scores, chronic stroke scale scores and chronic lesion volumes(66). However, acute neurological deficit is likely to represent the DWI lesion plus the penumbra (estimated by the perfusion lesion); studies in the hyperacute phase have shown a better correlation of final infarct volume with perfusion rather than DWI lesion volumes(67) and that it is at time points *beyond* 4 hours when DWI best predicts final infarct volume(59). It has also been suggested that a clinical-diffusion mismatch (CDM – neurological deficit out of proportion to the size of the DWI lesion) may identify subjects with 'tissue' at risk. Although early results have been encouraging(68) with subjects with CDM showing a high rate of neurological deterioration, there are a number of limitations to the concept. These include lack of specificity(69, 70)and bias against subjects with right hemisphere strokes.

The volume of the DWI lesion can also predict the likelihood of haemorrhagic transformation. A small study investigating the value of a number of clinical and radiological parameters in the prediction of haemorrhagic transformation after rtPA showed that only the volume of the ADC lesion was an independent predictor. These findings were also supported by the DEFUSE study(71). The severity of restriction of diffusion, as measured by the ADC, is also likely to be important, with lesions of lower ADC being more likely to experience haemorrhagic transformation(72).

DWI may also have value as an investigation performed after TIA. Kidwell et al(73) showed that in a cohort of TIA patients nearly half had lesions on DWI, and it is thought such lesions predict a higher risk of future stroke(74, 75), although whether such lesions are truly independent predictors of future stroke remains unclear. Nonetheless it is clear that DWI has the potential to predict a number of clinically relevant end points.

In conclusion, DWI is a rapid and sensitive technique giving an insight into the pathophysiological processes underlying stroke related symptoms, namely bioenergetic failure, which aids the treating clinician to make diagnoses, decisions, and estimates of prognosis.

1.5.2 FLAIR Imaging

The FLAIR sequences used in acute stroke protocols are usually heavily T2 weighted and are often used in preference to standard T2 weighted sequences because the nulling of CSF allows better visualisation of hyperintense lesions, particularly in periventricular regions(76). This may also allow for more accurate volumetric measurements in a research setting.

The most widely assessed stroke sign on FLAIR is the detection of ischaemic changes which appear as parenchymal hyperintensity suggesting vasogenic oedema. Initial investigations suggested that less than a third of cases of unselected stroke show such parenchymal changes within the first 6h following stroke(77). Any lesions which do appear during this time window are generally subtle. Thomalla and colleagues(78) assessed FLAIR images from 120 strokes within 6h and showed that the absence of FLAIR changes with a positive DWI lesion (DWI-FLAIR mismatch) had a high specificity (0.94) for an onset time <3h, albeit with lower sensitivity. A follow up study from Ebinger and colleagues(79) suggested that the specificity was only 0.79 for allocation to the <4.5h time window, but this increased to 0.90 when excluding lesion less than 0.5ml from analysis. The assessment is therefore the subject of ongoing study into ‘wake up’ stroke in studies such as the ‘ Multi-Center Safety Trial of IV rt-PA in Patients With Unwitnessed Stroke Onset’ (MR WITNESS).

The detection of the leukaraiosis may be important in the assessment of the risk of intra-cerebral haemorrhage after thrombolytic therapy(80). The severity of such changes can be graded using rating scales such as the Fazekas scale(81). However at present no data exist as to a precise threshold of the volume or grading of leukoaraiosis which is acceptable in the context of the administration of thrombolytic therapy.

Other early ischaemic signs include the hyperintense vessel sign (HVS) which describes arterial hyperintensity in vessels seen both proximally (e.g. within and proximal to the sylvian fissure) and distally, and is seen in the presence of acute ischemia due to large artery occlusion. Proximal HVS is likely to represent to represent thrombus, whilst distal HVS is likely to reflect either slow flow, static flow, or retrograde flow distal to the site of the thrombus(82-84). Patients presenting with distal HVS have lower NIHSS scores and a trend towards lower subacute infarct volumes(85), suggesting this may be a marker for collateral flow. Interobserver reliability for the detection of HVS has been demonstrated to be very good(86). The HVS sign is shown below (Figure 1-9).

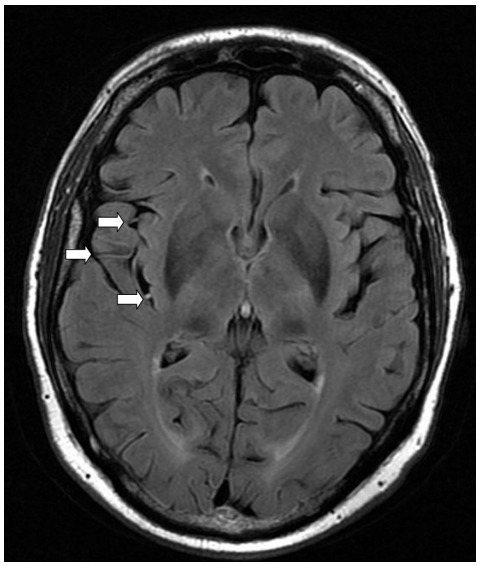

Figure 1-9. Demonstration of the Distal Hyperintense Vessel Sign.
Arrows demonstrate this sign.

FLAIR imaging may also be of use in the assessment of the permeability of the blood brain barrier (BBB). The hyperintense acute reperfusion marker (HARM) reported by Warach and Latour(87, 88) describes enhancement of the CSF with gadolinium, causing the CSF to appear bright. (Figure 1-10). It is hypothesised to occur in those subjects with breakdown of the BBB and is associated with reperfusion and haemorrhagic transformation. It has also been shown to be associated with thrombolytic therapy distinct from other reperfusion strategies, suggesting a direct toxic effect of rtPA(89). Further investigation of this sign is required in order to determine its influence on treatment strategies.

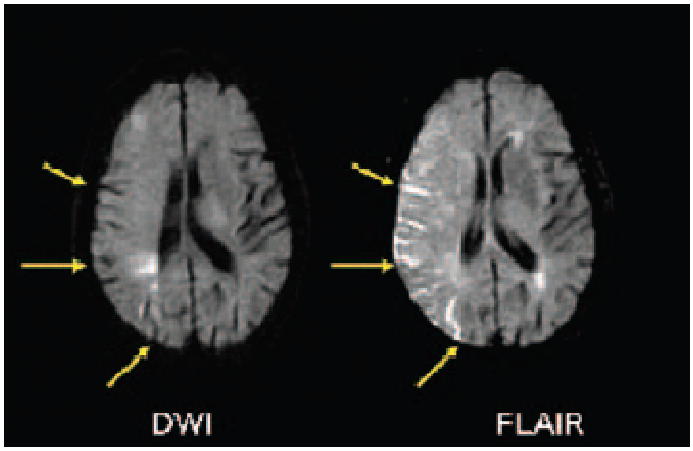

Figure 1-10. The Hyperintense Acute Reperfusion Marker.
Diagram showing HARM on FLAIR (b) which is associated with acute stroke shown on DWI (a). Figure produced from ' Warach S, Latour LL, Warach S, Latour LL. Evidence of reperfusion injury, exacerbated by thrombolytic therapy, in human focal brain ischemia using a novel imaging marker of early blood-brain barrier disruption. Stroke. 2004;35:2659-2661' with permission from Wolters Kluwer Health.

In summary, although FLAIR images are not sensitive for the detection of ischaemia in the first hours of stroke, the detection of other signs such as DWI-FLAIR mismatch, HVS and HARM provide potentially useful information regarding individual pathophysiological status.

1.5.3 Gradient Echo Sequences

The Gradient Echo T2* weighted sequence (GRE) forms an integral part of the acute stroke MR protocol, primarily on the basis of its ability to detect haemorrhage. T2*-weighted sequences are sensitive to paramagnetic compounds which precipitate signal dephasing, and subsequent signal loss. Most conventional GRE sequences produce images which use data concerning the *magnitude* of signal change but newer alternative post processing algorithms also exploit phase information and offer enhanced tissue contrast over conventional methods(90).

After intracranial haemorrhage (ICH) the blood oxyhaemoglobin converts to deoxyhaemoglobin which is then auto-oxidised to methaemoglobin. At later stages, activation of reticuloendothelial cells results in the scavenging of methaemoglobin and its storage of haemosiderin in macrophages and astrocytes. All of these breakdown products of oxyhemoglobin are paramagnetic and can

therefore be detected on GRE images. The sensitivity for haemorrhage on GRE was tested by Fiebach and colleagues(91) who conducted a prospective multi-centre study by recruiting 62 subjects with, and 62 subjects without primary ICH (<6h) and compared the detection of ICH on GRE to the gold standard of CT. The group showed that for experienced stroke physicians the sensitivity and accuracy was 100%. Even for inexperienced observers (medical students) the sensitivity was over 95%. Any fears that GRE cannot detect ICH as early as CT have been allayed by findings that ICH has been detected as early as 23 minutes in one study(92). Subsequently, a single centre prospective comparison of CT and MR in the acute setting has shown that the detection of haemorrhage between the two modalities was approximately the same. GRE sequences have also been compared to other MR sequences. In the absence of a GRE image the B=0 image from the DWI acquisition performs reasonably well in the detection of large haematomas(93) but will not detect small haemorrhages or small cortical microbleeds.

Unlike CT, GRE sequences are also able to detect chronic haemorrhage (haemosiderin). In particular GRE can detect cerebral microbleeds (CMBs) which are variably defined small round regions of signal loss which represent perivascular haemosiderin accumulation and are a marker of underlying microangiopathy. In particular they have been associated with hypertensive microangiopathy when seen in deep structures and cerebral amyloid angiopathy in lobar locations. Accurate stratification of risk for post thrombolytic haemorrhage in those with CMBs is not yet possible. Small studies have reported conflicting results regarding the risk of post-rtPA haemorrhage(94, 95). The Bleeding Risk Analysis in Stroke Imaging Before ThromboLysis (BRASIL)(96) study included 86 subjects with microbleeds who were treated with intravenous rtPA within 6 hours. Although there was a trend towards an increased risk of haemorrhage after rtPA in those with CMBs compared to those without (5.8% vs 2.7%), this did not reach statistical significance. However only 6 subjects had more than 5 CMBs and therefore no conclusions can be made on how to treat subjects with multiple CMBs.

GRE sequences also have the ability to detect intra-arterial thrombus, which also causes signal dephasing and appears dark on GRE images. This finding has been termed the hypodense MCA sign(97) and is more commonly found in strokes of

cardioembolic aetiology compared to those from large vessels. Such occlusions were also noted to be a positive predictor of recanalisation. However, a recent small cohort study suggested that if this sign was seen in the M1 segment of the MCA, this was a poor predictor of recanalization(98).

Finally, as with all MR sequences, the possibility of imaging of potentially salvageable tissue has been raised. Morita and colleagues(99) hypothesised that the hypodense appearance of dilated cortical vessels, the presence of dilated veins in deep white matter (termed the 'brush' sign) and a generalised hypodensity of the ischaemic hemisphere all reflect an increased oxygen extraction fraction in the affected hemisphere. Consistent with this, visual correlation was good between regions of dilated vessels and regions of hypoperfusion. This suggests the possibility of being able to detect potentially salvageable tissue on routine stroke MR sequences but issues such as the sensitivity and specificity and the prognostic significance of such findings requires to be investigated further. The signs are illustrated below (Figure 1-11)

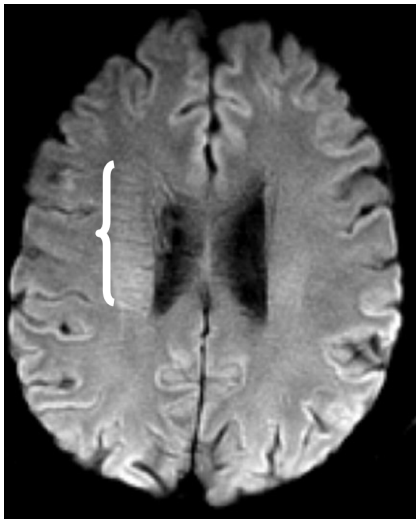

Figure 1-11. Early Ischemic Findings on GRE.
GRE image following acute stroke showing the 'brush' sign (rightwards of the bracket [{] sign).

In conclusion, GRE sequences have become an indispensable part of the MR acute stroke imaging protocol. Not only can they detect acute and chronic haemorrhage but early ischemic signs also provide a wealth of information regarding pathophysiology. Further research on GRE sequences is likely to focus on improved sensitivity with susceptibility weighted imaging, and on the detection of early ischemic signs.

1.5.4 Magnetic Resonance Angiography (MRA)

Magnetic resonance angiography (MRA) may be acquired without contrast (time-of-flight [TOF] and phase contrast [PC[MRA) or with gadolinium based contrast.

The main function of MRA in the assessment of acute stroke is identification of occlusion. The degree of occlusion can be rated using numerous scales. Although the TIMI scale (Thrombolysis in Myocardial infarction){, 1985 #288} has attracted popularity in stroke studies it has been suggested that the TICI (thrombolysis in cerebral infarction) scale(100), which incorporates additional measures of perfusion, is more appropriate. Can angiographic assessment provide a surrogate marker of penumbra? Support comes from the demonstration of occlusion on MRA of acute stroke has been strongly associated with the presence of a PWI-DWI mismatch(101). More proximal occlusions are associated with larger DWI, PWI and mismatch lesions on pretreatment MRI and are more common when mismatch is detected beyond 9h(102). Moreover, results from the DIAS-2(103) trial, which randomised subjects to either desmoteplase thrombolytic therapy or placebo in patients presenting with stroke between 3 and 9h noted that 57% of placebo treated subjects who had no occlusion demonstrated clinical improvement, compared to only 18% of subjects who had occlusion. The premise that arterial occlusion on either MRA or CTA may help to increase the specificity of imaging definitions of ‘tissue at risk’ is being employed in the follow up DIAS 3 and 4 studies. A similar concept is that a discrepancy between the location of occlusion and the size of the DWI lesion may indicate the presence of penumbra and therefore predict the response to thrombolytic therapy – the MRA-DWI mismatch hypothesis. Although yet to be validated in a large data set, preliminary analysis(104) using the DEFUSE data set suggests the presence of partial or complete occlusion in the presence of a small lesion on DWI (<15ml) is highly predictive of a favourable response to thrombolysis.

1.5.5 Perfusion Weighted Imaging (PWI)

The term ‘perfusion’ refers to the haemodynamic state of the microcirculation, the very circulation which serves as the final common pathway for nutrient and oxygen delivery to cerebral parenchyma. Therefore, imaging this component of the circulation in acute stroke patients with perfusion weighted imaging (PWI) is highly relevant

1.5.5.1 Procedure and Theory of Susceptibility Weighted Contrast

Modern PWI utilises high power injector pumps to assist the rapid delivery of gadolinium ion based contrast agents to peripheral veins in the antecubital fossa. MR scanning of the brain at consecutive time points detects changes in signal intensity – a marker of changes in gadolinium concentration - from vessels. The MR sequences employ Susceptibility Weighed Imaging(105) which relies on the paramagnetic gadolinium based contrast causing spin dephasing of adjacent protons, thereby leading to a reduction in T2 and T2*. EPI is usually employed with either SE or GRE sequences to detect T2 and T2* changes respectively.

1.5.5.2 Determining Cerebral Blood Volume and Blood Flow Measurements

Raw data from PWI will demonstrate the changes in signal intensity within tissue. In vivo studies have shown a linear relationship between the concentration of the contrast agent within the tissue and ΔR_2, the change in T_2 relaxation rate ($1/T_2$)(106). However, this relationship may vary depending upon the properties of the contrast agent and the architecture of the microcirculation(107). The relationship between ΔR_2 and measured signal intensity, however, is exponential. By knowing this, and assuming that the concentration of contrast agent is distributed uniformly throughout the cerebral vasculature, the CBV can be calculated by integrating the area under the concentration-time curve. A number of subtly different methods do exist but the

resulting volume of CBV lesion has been shown not to be significantly affected(108).

The relationship between CBF and tissue concentration is rather more complex. For the theoretical case where the injection of contrast agent is instantaneous and the concentration of contrast agent within the cerebral arteries is maximal from the outset, the concentration of contrast agent within tissue ($C_t[t]$) may be defined as the product of arterial concentration of contrast ($C_{[a]}$), the rate of its delivery to the tissue (CBF), and the fraction of contrast agent that remains within the tissue at any given time (residue function - (R[t])), as described below:

$$(C_t[t]) = C_{[a]} \times CBF \times R[t]$$

However, the injection of contrast agent is usually delivered over the course of approximately 4 seconds(s), and therefore the ($C_{[a]}$) becomes dispersed in time; this phenomenon is represented by the concentration-time curve within a particular cerebral artery and described as the arterial input function (AIF). For the purposes of calculation this can be thought of as a series of measurements of instantaneous boluses, occurring throughout the time period of the injection. Therefore at any particular time point the concentration within tissue is equal to the product of CBF and the arterial concentration and residue function measured at that time point, as described by the equation above. Therefore the total concentration of contrast agent within the tissue can be calculated as the sum (integral) of all of these contributions i.e. the AIF curve becomes mathematically convolved with the residue function as represented by

$$C_t[t]) = CBF \times AIF(t)*R[t]$$ where * denotes convolution

Therefore, a measure of CBF may be derived if the concentration curves from the feeding artery and the tissue are measured, and assumptions are made regarding the residue function – this process of ‘deconvolution’ is now discussed.

Deconvolution methods can be broadly classified as model dependent and independent. In the former, an assumption is made about the microvascular architecture which is used to predict the residue function. However, the

accuracy of model dependent approaches may suffer when applied to stroke patients since the residue function may not be uniform throughout the brain. Model independent measures assume that both the residue function and CBF are unknown. Approaches using transforms (e.g. Fourier Transforms) and algebraic methods using matrices solved by either regularization or singular value decomposition, have been used. Singular value decomposition was shown to be superior when an accurate reproduction of values of flow is required. The desirable quality of insensitivity to vascular structure or blood volume was demonstrated through simulations. Model-dependent approaches were shown to be susceptible to producing large errors, particularly when areas of disturbed blood flow exist(109, 110). In light of these results SVD has become the most widespread technique used in the clinical literature. Its drawback in terms of being sensitive to the effects of tracer delay and dispersion will be discussed. Once CBV and CBF have been determined, mean transit time (MTT - time taken to transit through the tissues by the contrast agent) can be determined using the central volume theorem; MTT = CBV / CBF

1.5.5.3 Determining Other Haemodynamic Parameters

As discussed, measurements of CBF and MTT depend on the accurate measurement of an AIF and subsequent deconvolution. A further parameter T_{MAX} defines the time to the peak of the residue function, and therefore also relies on the analysis of the deconvolved curve. However, the identification of an AIF and deconvolution are processes which are time consuming and could in theory lead to a delay in the administration of rtPA. Therefore a number of summary measures of cerebral haemodynamics have been produced; time to peak of the tissue concentration-time curve (TTP), bolus arrival time (BAT), first moment MTT, and the measurement of the full width of the curve at half the maximum signal change (FWHM). The disadvantage of these parameters is that accurate physiological correlates are hard or impossible to define, and they can be affected by other factors such as poor cardiac output. Furthermore, parameters such as TTP can, in theory, be affected by both delay and dispersion, and therefore a prolonged value may theoretically be derived in the context of a normal CBF.

1.5.5.4 Limitations of Current Methodologies – Relaxivity

As discussed both $C_t[t]$ and $C_{[a]}$ are not measured directly, but are inferred from the relaxivity. van Osch et al showed that the relationship between concentration of contrast agent and relaxivity is entirely different in tissues and in blood, being linear in the former and exponential in the latter(111).Therefore, assumptions that relaxivity is the same in all tissues may lead to overestimation of blood flow.

1.5.5.5 Limitations of Current Methodologies – AIF

The selection of an AIF may be from the internal carotid artery (ICA), the proximal or distal middle cerebral artery (MCA), and from the ipsilateral or contralateral hemisphere. The AIF derived from each of these locations is different(112). During AIF selection a 'partial volume' effect almost inevitably occurs since voxels selected for the AIF often contain signal from both tissue and vessel. This problem may lead to underestimation or overestimation of the concentration of the contrast agent(113). Although these effects can be corrected(113) such algorithms require the AIF to be measured from the ICA (parallel to the magnetic field), and measurement at such a proximal vessel will only increase the problems of tracer arrival delay and dispersion (see next section). In the setting of acute stroke the selection of AIF in the contralateral MCA yields hypoperfusion lesions which most closely match the final infarct volume(114). When considering the use of the contralateral MCA as the AIF, a further study(115) showed that the highest variability of perfusion maps occurred if the M1 division was used, and recommended that the M3 division be used preferentially on the basis of having the highest SNR.

1.5.5.6 Limitations of Current Methodologies - Delay and Dispersion

Finally, a further complicating issue in the accurate assessment of CBF is the effect of tracer delay and dispersion. The following equation assumes that the measured AIF is identical to the input to the tissue of interest.

$C_t[t]) = CBF \times AIF(t)*R[t]$ where * denotes convolution

However, the AIF is measured in a large artery, usually the MCA or ICA, which is not always in close proximity to the tissue of interest, and therefore when compared to the AIF the input to the tissue may be delayed, or dispersed across time, as compared to the 'true' AIF. Delay may be particularly problematic in the presence of ICA stenosis(116). The widely used deconvolution technique, SVD, is susceptible to the effects of both delay and dispersion which precipitate underestimation of CBF(117). This may be in the order of 50%. Such miscalculation will lead to an overestimation of any PWI-DWI mismatch. The problem of delay may be theoretically circumvented by the selection of an AIF in closer proximity to the tissue of interest. However, as discussed, selection of an AIF from such smaller arteries increases the problem of partial volume effects and consequently still requires to be validated. However, other techniques such as circular SVD(118) have been shown to be relatively insensitive to tracer delay. In any case, where delays do occur, their effects can be corrected by taking into account the 'bolus arrival time', but only when the SNR is sufficient to allow this. Dispersion of the tracer on the other hand is more difficult to correct for, although, as discussed, model dependent techniques have shown potential(119).

1.5.6 Perfusion-Diffusion Mismatch - A Potentially Viable Option for Penumbral Imaging?

Of the MR defined surrogate markers of the penumbra, the PWI-DWI mismatch hypothesis (the difference between the larger PWI lesion and smaller DWI lesion)(52) has been the most extensively studied. Five different trials have tested this hypothesis in a population receiving either standard alteplase or desmoteplase, an alternative thrombolytic.

Trials using desmoteplase were the phase II DIAS (Desmoteplase In Acute Ischemic Stroke)(120) and DEDAS(121) (Dose Escalation of Desmoteplase For Acute Ischemic Stroke) trials and the Phase III DIAS 2 trial(103). The DIAS trial recruited subjects with a PWI-DWI mismatch of at least 20% and 2cm diameter at 3-9h post ictus. It had a randomised controlled design and initially used high

fixed doses of desmoteplase which caused excessive rates of ICH. However a modified dose of 125μg/kg of desmoteplase administered to 15 patients showed a beneficial effect on reperfusion and clinical outcome when compared to all patients who received placebo. In addition, the rates of symptomatic ICH were low (2.2% in those who received any 62.5-125μ/kg of desmoteplase). The DEDAS trial had a similar design and confirmed the safety profile of desmoteplase which was demonstrated by DIAS. The follow on phase III DIAS-2 used a similar design, again recruiting subjects 3-9h and randomising them to placebo, 90 μg/kg desmoteplase and 125 μg/kg desmoteplase. The inclusion criteria differed from DIAS and DEDAS in that CT perfusion could also be used to include subjects, and mismatch definitions were based on visual assessment concordant with local practices. The DIAS-2 trial failed to show benefit of desmoteplase in mismatch patients at 3-9h post ictus with respect to a composite clinical endpoint. In addition there was a high mortality rate in treated patients. Possible explanations of the negative end point have been the low rate of visible arterial occlusion in this cohort, the relatively small absolute volumes of core and penumbra observed in this study, and the relatively mild stroke in the placebo group(122).

Two phase II trials have tested PWI-DWI mismatch imaging in the context of alteplase. The DEFUSE (Diffusion and Perfusion Imaging Evaluation for Understanding Stroke Evolution) Study(71) was a single arm study of 74 subjects who all received alteplase between 3 and 6h post ictus. A post-hoc analysis of subjects who had a PWI-DWI mismatch defined by a threshold of TMAX plus 2s (54% of the cohort) reperfusion was associated with an improved clinical outcome compared to subjects in whom there was absence of reperfusion. Although strengthening the concept of PWI-DWI mismatch, this was a single arm study and therefore could not assess the efficacy of rtPA. On the other hand, EPITHET (Echoplanar Imaging Thrombolytic Evaluation Trial) was a randomised trial (between alteplase and placebo) and using similar mismatch criteria to DEFUSE, also recruited subjects 3-6h post ictus. Although it was negative for its end point of attenuation of geometric infarct growth in the alteplase group, there was an increased rate of reperfusion in the alteplase group and reperfusion was in turn associated with less infarct growth and better clinical

outcome compared to those subjects who had no reperfusion. These signals of efficacy have prompted a follow up phase III study in this regard (EXTEND).

The disappointing failure of EPITHET and DIAS 2 to provide statistically positive results may be due to the nature of definitions of mismatch. For example, In EPITHET a TMAX threshold of only 'plus 2s' was employed, which is much less stringent than that suggested by back to back MR and PET studies(123). Indeed there is still controversy as to which modality and its subsequent threshold best identifies penumbra(124). The DIAS 2 definitions of penumbra are likely to have varied between centres, and the physiology of tissue compartments may have been different in those subjects recruited by MR compared to CT. In the trials which specified a minimum mismatch ratio, this was 20% (1.2). Recent observations from the DEFUSE study using receiver operator curves to predict favourable clinical response with reperfusion on the basis of mismatch ratio, suggest that far larger mismatch ratios may be required – 2.6 was the optimal mismatch ratio in this data set(125). In addition the methods by which ratios are calculated may be important. Both DEFUSE and EPITHET used a simple subtraction of the DWI volume from PWI volume to calculate mismatch; it has been suggested that co-registration of PWI and DWI images may provide a more clinically relevant measure for mismatch(122). Indeed, re-analysis of the EPITHET data using a co-registration technique yielded a positive result(126).

Recently, a meta-analysis of the five clinical trials discussed here failed to demonstrate a higher rate of favourable clinical outcome after mismatch based delayed thrombolysis, although it was noted that all of the studies apart from DIAS II showed a non-significant trend towards an improved outcome(127). However, reperfusion/recanalization was more common in thrombolysed patients, and in those who reperfused/recanalised, favourable outcomes were more common.

Despite the lack of clear validation of the PWI-DWI mismatch hypothesis, it is also important to note that the presence of a perfusion deficit per se may provide valuable information. For example, a study using CT perfusion suggested that reperfusion rather than recanalization is the better predictor of infarct growth and penumbral salvage(128). Some centres use the absence of a perfusion deficit as a contra-indication to thrombolysis. The DEFUSE study

identified a ‘malignant profile’ of stroke which is unlikely to benefit from the thrombolysis, which included a PWI deficit of 100ml or more and a TMAX > 8s(71). In a similar fashion, it has also been suggested that ‘very low cerebral blood volume’ is a better predictor of haemorrhagic transformation than DWI lesion volume (129). Therefore, even without using the PWI-DWI mismatch concept, PWI provides data which may be used for clinical decision making.

In summary, the signals of efficacy in phase II studies of thrombolysis for patients with PWI-DWI mismatch beyond 3h have not yet been observed in phase III studies. Whilst this could theoretically reflect the inefficacy of thrombolysis after 4.5h, it perhaps more likely represents the currently heterogeneous and perhaps inadequate definitions of PWI-DWI mismatch.

1.5.7 Arterial Spin Labelling

Although not used routinely in MR stroke protocols, Arterial spin labelling (ASL) constitutes the main non-invasive MR technique used in stroke cerebral blood flow studies. The absence of exogenous contrast media means that it can be performed repeatedly without technical or clinical detriment. The basic principle of ASL involves the labelling of arterial blood by inverting its magnetization upstream of a predefined region of interest (ROI). Signal acquisition is then performed in the region of interest. The magnitude of change in magnetisation in the region of interest is dependent on blood flow, and therefore measures of CBF expressed in units of ‘ml/100g/min’ may be derived from the difference between signal acquisition from labelled blood, and from unlabelled blood during a reference scan. ASL sequence designs include pulsed arterial spin labelling (PASL)(130) and continuous arterial spin labelling (CASL)(131).

How well do CBF measurements by ASL compare with other techniques? Although this issue has not been studied extensively, in general values compare well between different modalities. A human volunteer study comparing CASL and PET(132) showed a non-significant overestimation of CBF by ASL compared to PET in grey matter. In white matter, however, ASL significantly underestimated

CBF by 30%. This was hypothesized to be due to failure to account for differences between arterial transit times between gray and white matter. A study of ischaemic stroke patients(133) showed good agreement between PASL (EPISTAR) and dynamic susceptibility (DSC) PWI with regards to the quantitative comparison of the degree of hypoperfusion in the DWI lesion compared to the contralateral side. However qualitative analysis showed that in 4 of 18 patients with hypoperfusion shown on DSC PWI images, ASL erroneously showed no flow, thus highlighting the need for an inversion time (TI) sufficiently long to be able to image collateral flow; a longer TI of 2400ms was able to do this(133). A further study demonstrated that CASL was effective in demonstrating regions of hypoperfusion in acute stroke patients including regions of PWI-DWI mismatch(134).

In summary, until now there has been relatively little investigation of ASL in acute stroke patients. Rather, the emphasis has been on technical improvements in sequence developments. However, with ever improving sequence design ASL offers potential as a clinical and research tool in human acute ischemic stroke, with the ability to measure CBF non-invasively, and repeatedly. Further validation in stroke patients is needed. In the mean time, DSC PWI predominates in both clinical and research settings.

1.5.8 Non-contrast CT

Despite extensive research activity into the potential role of multi-modal MR, NCCT remains the ‘work horse’ of acute stroke imaging in many centres world wide. This reflects its ease of access, relatively short imaging times, and its relatively modest cost.

CT gives anatomical rather than functional information with signal intensity values reflecting the density of tissues which is expressed in Hounsfield units (HU). The first role of CT is to exclude ICH, which appears as parenchymal hyperintensity. It is likely that the signs of ICH are evident instantaneously(135). Unlike GRE however, CT is poor at distinguishing old ICH from old infarct, and cannot demonstrate microbleeds. The focus of attention in acute stroke,

however, has been the identification of early ischaemic signs. Many of these are illustrated in (Figure 1-12) and include tissue hypoattenuation which may manifest as obscuration of the caudate and lentiform nuclei, or frank parenchymal hypoattenuation.

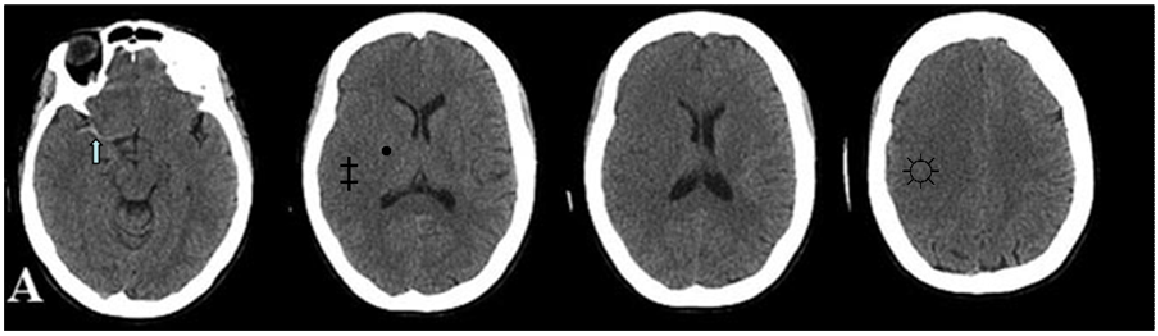

Figure 1-12. Early Ischaemic Signs of MCA Stroke.
Adapted from images shown by 'Vahedi et al. Sequential-Design, Multicenter, Randomized, Controlled Trial of Early Decompressive Craniectomy in Malignant Middle Cerebral Artery Infarction (DECIMAL Trial). Stroke 38 (9); 2506-17' with permission from Wolters Kluwer Health. Vertical open arrow illustrates the hyperdense MCA sign, ‡ indicates sulcal effacement and hypodensity, • illustrates the disappearing basal ganglia, ☼ shows hypodensity and sulcal effacement at higher slices.

The disappearing ‘basal ganglia’(136) suggests MCA occlusion at a location proximal to the branching of the lenticulostriate arteries, causing a reduction in the signal intensity in the basal ganglia. Both basal ganglia and other parenchymal hypodensity is likely to reflect cytotoxic oedema, and therefore be predictive of infarct core, an assertion supported by PET studies(137). In contrast, sulcal effacement represents swelling, and in the absence of hypodensity may represent ‘penumbral’ tissue. Muir and colleagues(138) showed that the CBV measured in regions of ‘isodense’ swelling by CT perfusion was elevated, consistent with penumbral tissue. This reflects the understanding that elevated CBV in acute stroke occurs in the context of vasodilatation in viable tissue(24). In contrast, regions of hypodensity were associated with a ‘core’ perfusion pattern. The authors noted that although these signs were specific, they were not sensitive. Therefore it is unlikely that non-contrast CT can ever be used to accurately identify penumbra. Hyperdense vessels are also frequently reported and typically reflect the thrombus location(139) as demonstrated on angiography. The values of Hounsfield Units in thrombus are higher with increasing haematocrit(140) making it more likely to see erythrocyte rich ‘red’

thrombi than fibrin rich ‘white’ thrombi which may explain why sensitivity is poor at around 30%(139) for proximal MCA occlusion. For MCA stroke, vessel hyperdensity may manifest as the hyperdense MCA sign (HMCAS) of the proximal MCA, the sylvian ‘dot’ sign within the sylvian fissure (M2 or M3 occlusion)(141), or the recently reported hyperintense internal carotid artery sign (HICAS)(142). The HMCAS is associated with severe strokes and a poor functional outcome. Leys and colleagues(139) demonstrated a prevalence of 30.5% in MCA stroke scanned within 12h. Although this sign provided a gain in the prediction of death or bad outcome, multivariate regression analysis did not reveal it as an independent factor of death or recovery. Indeed, patients with this sign still benefit from rtPA(143). Disappearance of this sign after rtPA is associated with hemorrhagic transformation but a higher rate of functional outcome and improved mortality(144), consistent with reperfusion. It has been suggested that its persistence of this sign after rtPA may be an indication for more aggressive interventional therapeutic strategies(144). The sylvian dot sign is generally associated with severe strokes but with a high rate of functional independence measured at 3 months, in those who receive rtPA(141). The HICAS is also associated with severe strokes but also with poor outcome.

A systematic review of the reporting of early ischemic signs showed a widely reported range of interobserver reliability, sensitivity and specificity(145). The number of years of observer experience was thought to influence performance. Many of these studies however were based on imaging with early generation CT scanners which had a poorer performance compared to modern day scanners. A comparison of different types of doctor suggests neuroradiologists are better able to detect subtle signs compared to clinicians in other stroke related specialties(146). In view of the variability of interpretation of early ischemic signs a rating scale known as the Alberta Stroke Programme Early CT Score (ASPECTS)(147) has been proposed. This scale identified early ischaemic signs in 75% of subjects presenting within 3h of stroke onset.

Finally, it is important to note that prognostic data is also available from unenhanced CT. The significance of proximal artery hyperdensity has already been discussed. In addition, a re-analysis of the CT scans acquired as part of the ECASS-1 trial demonstrated that in those subjects who had hypodensity greater than a visually estimated ‘one third’ of the MCA territory volume, or who had

diffuse swelling, rtPA had no beneficial effect but had a detrimental effect with regards to intracerebral haemorrhage(148). The increased haemorrhagic risk in those with strokes more than one third of the MCA territory has been replicated(147). However Patel and colleagues(149) re-examined data from the NINDS trial and after adjusting for baseline variables and assessing interaction between early ischaemic signs and treatment, found different findings with respect to functional outcome; rtPA was found to be beneficial even in those with early ischaemic findings greater than one third of the MCA territory. Other prognostic information may be derived from an ASPECTS rating. A score of 7 or less discriminated outcome defined by death or dependence in a cohort of subjects who received rtPA. The rate of post-rtPA ICH for those with a score of 7 or less is predicted to be 14 times that of a subject with an ASPECTS score greater than 7. In addition, in those who receive rtPA, higher ASPECTS scores are shown to have a higher rate of complete recanalisation(150).The use of ASPECTS in selecting and excluding subjects from thrombolytic therapy remains to be prospectively tested.

In conclusion, unenhanced CT imaging in acute stroke is fast and accessible. It can reliably exclude ICH and can variably define early ischemic signs which help to establish a positive diagnosis and give some prognostic information. It is unlikely, however, to reliably distinguish normal tissue from penumbra and infarct within the first few hours after stroke onset.

1.5.9 CT Angiography

Unlike MRA which can provide flow information, CT angiography (CTA) provides predominantly anatomical information regarding the cerebral vasculature. Modern multi-slice CT scanning can image both extra-cranial and intra-cranial vasculature, whereby multi-detector row CT acquires a large number of thin slices; data can be viewed as either reformatted thick slice source images, or as reconstructed images such as maximum intensity projection (MIPs).

The value of detection of intracranial occlusions has also been discussed. Reassuringly studies comparing CTA and digital subtraction angiography (DSA)

yield excellent sensitivity and specificity for the detection of intracranial occlusion(151, 152). Stenosis of the internal carotid artery can also be assessed in the same examination. Although the literature suggests CTA is a sensitive and specific technique for the diagnosis of carotid artery stenosis(153) two systematic reviews suggest that CTA is not as sensitive as contrast enhanced MRA(154, 155). However, these reviews included relatively old studies of CTA. Although CTA yields primarily anatomical information – the presence or absence of contrast within vessels – some information regarding collateral circulation may be obtained. For example, the presence of contrast within lepto-meningeal vessels, despite the presence of an internal carotid artery occlusion, suggests lepto-meningeal collateral circulation(5, 152). Poor collateralisation demonstrated by CTA can predict a worse clinical outcome and more lesion growth compared to those with good collateral circulation(156).

Knauth and colleagues(152) also demonstrated that regions of tissue without parenchymal enhancement on CTA source images always became hypodense on follow up CT, suggesting that such regions represented reduced CBV and therefore infarct core. Further studies have shown good correlation between DWI volume, and the volume of lesion of CTA source images, although DWI is more sensitive(156, 157). However caution in the interpretation of CTA source images is advised by a back-to-back study of CTA and PET which suggested that the CTA source images are inaccurate in determining the size of critical cortical perfusion.

1.5.10 CT Perfusion

Just as stroke MR examinations employ the use of PWI, CT perfusion (CTp) can also image the circulation at the tissue level. Whilst some studies(158) have used a slow injection of contrast to produce maps of ‘total perfusion’, the majority of studies have focussed on the assessment of the first pass bolus of contrast delivered using a rapid injection, in a manner analogous to PWI in MR imaging. These studies typically inject 40-50ml of iodinated non-ionic contrast material at a rate of 4-5ml/s using a power injector, with assessment of the first pass of contrast. The spatial coverage of the brain is more limited than with PWI, and is

dependent on scanner technology; most current scanners image 1-4 slices of the brain. In an effort to increase coverage of the brain, some acute stroke protocols have either performed two rounds of CT perfusion examinations, each at different anatomical levels(159) or have used a 'jog mode' whereby two different sections of the brain are scanned during the same examination as a result of the scanner table moving back and forward(160). Although the temporal resolution is decreased to the order of about 5s using the latter technique, the acquired data is still sufficient to produce meaningful maps of perfusion relative to the contra-lateral side.

Unlike MR however, there is a linear relationship between the change in signal intensity on CT and the concentration of contrast material within the imaged circulation, making quantification more straightforward(161). As with PWI, CTp processing can involve both non-deconvolution and deconvolution techniques. Non-deconvolution techniques use the maximum slope method where TTP is calculated as the time difference between the peaks of the arterial and tissue time-concentration curves. The predominant deconvolution technique is SVD. The CBV may be calculated as the integral of the residue function but may alternatively be derived by comparing tissue to a region of interest in the superior sagittal sinus. Given that MTT can also be derived from the curves directly, CBF can be calculated by the central volume theorem (CBV/MTT). Many commercial software packages therefore require the user to define both arterial input and venous outflow functions. Unlike in MR, the choice of AIF is not critical, and the default ACA AIF is therefore sufficient(162). The AIF should however, be orthogonal to the plane of imaging. In a similar fashion to MR PWI, CTp programs usually produce maps of CBV, CBF, MTT and TTP.

Given the relative infancy of CTp compared to PWI, justification of its use must include demonstration of its accuracy and reliability. Firstly, after elimination of vascular pixels, CBF values from CT perfusion in normal volunteers are accurate as compared to PET(163). Although the accuracy compared to PET values has also been validated in subjects with chronic carotid occlusion(164), such validation in stroke patients is yet to be performed. Findings on CTp also correlate well with PWI. In particular, regions of low CBV correlate well with DWI lesions and suggest infarct core, and there is a good correlation between CTp and PWI defined penumbra(165). In addition, when values for the same

parameter derived from both modalities are compared there is also a significant correlation(166).

Given that there is good correlation between CTp derived CBV lesions and MR derived DWI lesions, CTp studies have assessed the mismatch between either CBF or MTT and CBV in order to image penumbra (Figure 1-13) in a manner analogous to the PWI-DWI mismatch. The largest study which aimed to derive a threshold was reported by Wintermark and colleagues in 2006(159). This group recruited 130 patients presenting within 12h of acute ischemic stroke and compared baseline CTp findings to baseline DWI when available, and to follow up MR scans performed in the first week in all subjects. Rigorous analysis identified that the optimal penumbral threshold was MTT of >145% of the contralateral side. For the core, the threshold was a CBV of 2.0ml/100g (if DWI was used to define core, or if final infarct in those who recanalised with a small infarct was used) or 2.3ml/100g (if final infarct in those who recanalised with large lesions was used to define core). Of note however, this study did not analyse differential thresholds for GM and WM, and did not analyse whether threshold in those stroke patients with carotid stenosis need to be adjusted.

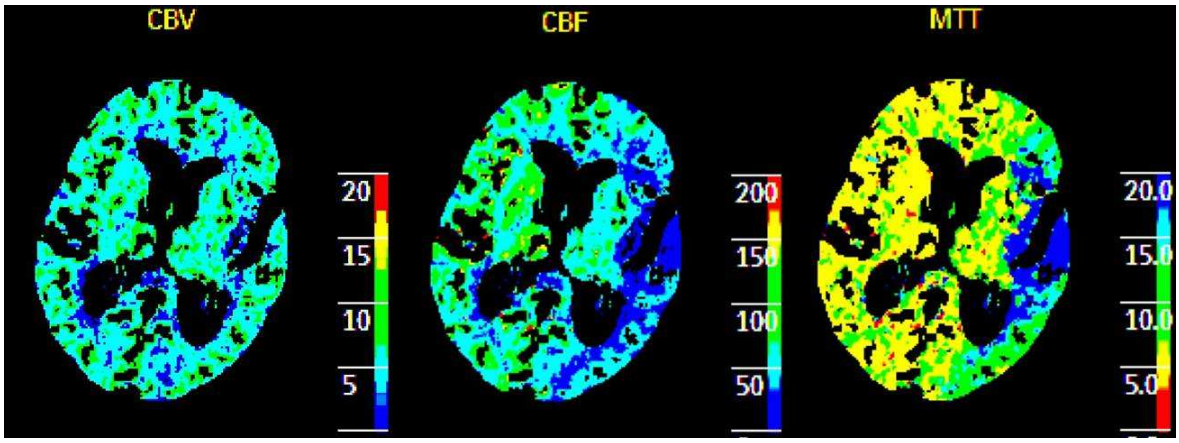

Figure 1-13. Illustration of CT Perfusion Maps.
CT perfusion maps form a subject with MCA territory stroke within 6h of onset scanned as part of a separate study at the Institute of Neurological Sciences Glasgow. CBV = cerebral blood volume map (units in ml/100g), CBF = cerebral blood flow map (units in ml/100g/min), MTT = mean transit time map (units in seconds). There is hypoperfusion (darker blue in CBF and MTT maps) and a smaller area of decreased CBV. The difference between these regions is theoretically the 'penumbra'.

The advantages of CTp include the fact that it can be performed in approximately 5 mins, and can be combined with CT and CTA in a 'multi-modal' stroke assessment(167). It is also useful when subjects cannot tolerate the

longer imaging times of MR or when there is an absolute contraindication to MR. Disadvantages include the limited brain coverage although this is likely to change with improving technology. In addition, although there is a risk of contrast induced nephropathy, 'real life' studies suggest this is rarely a problem if contrast is given to acute stroke patients, particularly if intravenous fluid is adminisered and those with a history or renal disease are excluded(168-170). Finally, radiation exposure is a concern; a multi-modal CT examination for acute stroke is approximately 10 milli-sieverts on a 64 slice scanner(171); when compared to an annual environmental exposure of 3mSv a year this may be deemed acceptable as an isolated acute investigation.

In conclusion, CT perfusion can identify regions of tissue which are at risk of infarction. The procedure is rapid and straightforward to perform in the acute setting. However, the clinical utility of this technique remains to be rigorously tested in randomised controlled trials.

1.5.11 ^{15}O Positron Emission Tomography

Positron Emission Tomography derives data by measuring pairs of photons emitted after the annihilation of a positron emitted from a decaying radioligand, with an electron. ^{15}O multitracer PET can measure oxygen consumption (cerebral metabolic rate of oxygen - $CMRO_2$) and oxygen extraction fraction (OEF) as well as provide quantitative measures of CBF and CBV. Therefore it remains the gold standard imaging technique for the ischaemic penumbra. Although logistic limitations such as arterial puncture, relatively long imaging time (about 1 hour) and scarce PET scanner availability have precluded its use as the standard acute stroke imaging technique, the insights provided from PET have been invaluable. Early PET studies suffered from a number of technical limitations, including low resolution PET scanners(172, 173), patients imaged moderately late after stroke(172) and lack of exact topographical correlation with structural imaging(21). Nonetheless it was appreciated that if a pattern of extensive irreversible damage was identified, the outcome was poor, if there was reperfusion of still metabolising tissue the outcome was good, and if there was continued ischemia the outcome was variable(174). The latter observation

suggested that this pattern may represent the target population for therapies. Moreover, potentially viable tissue could be detected up to 48h post ictus(21).

In a rigorous study, Marchal and colleagues(175) performed a voxel-by-voxel analysis of subjects within 17h after onset, with follow up PET scanning and structural CT. In the eight subjects included, $CMRO_2$ declined between the acute and chronic PET scan. The authors also confirmed a $CMRO_2$ threshold for infarction (approximately 1.4ml/100g/min), and that a substantial proportion of tissue (10-52%) which ultimately infarcted had a $CMRO_2$ above this threshold in the acute phase even when imaged far later than the current reperfusion window. In these penumbral voxels the CBF was in the accepted penumbral range as suggested by previous studies, and the OEF was between 0.7 and 1.0 in all but one subject. A study by the same group strengthened the notion that this tissue could be genuinely salvaged with clinical benefit, by showing that the volume of salvaged penumbral tissue was correlated to clinical improvement(25). These findings are consistent with other observations that the pattern of pathophysiology identified by PET helps to predict neurological evolution independent of baseline neurological status(175). Therefore, PET studies not only confirmed that penumbra could be detected in man, but suggested that reperfusion therapies may offer a clinical benefit in human acute stroke. Moreover, they shaped currently accepted PET criteria for penumbra which include a preserved $CMRO_2$, OEF >0.7 and CBF in the penumbra range of approximately 7-22ml/100g/min(27).

Not only has PET given us insights regarding stroke pathophysiology but it has also proved useful in the validation of other acute stroke imaging techniques, such as the identification of PWI-DWI mismatch. For example, it has identified some penumbral tissue in the DWI lesion (previously hypothesised to be infarct core) and has suggested that TTP-DWI mismatch represents a variable metabolic state(176). In summary ^{15}O multitracer PET imaging in acute stroke has to date exclusively been a research tool and has offered invaluable insight into stroke pathophysiology.

1.5.12 Other Techniques

Although not directly relevant to this project, there are a number of techniques which should be mentioned in brief. MR spectroscopy exploits the principle of 'chemical shift' in order to ascertain the chemical composition of the environment of interest. Although changes in metabolites have been well characterised in the subacute and chronic phase after stroke (177-181) there is very little data to describe the acute phase. Based on their data from subjects imaged less than 7h Nicoli et al(182) hypothesised that areas of PWI-DWI mismatch correlated with areas where there was hypoperfusion, subnormal or normal ADC, normal NAA, and elevated lactate. Indeed such findings have been proposed to represent the penumbra(181). Singhal et al(183) showed lactate levels were present, but in a lesser concentration, in PWI-DWI mismatch areas compared with DWI bright areas. The precise penumbral signature on MRS, however, remains to be elucidated. In particular there is no data for the threshold of the core/penumbral and penumbra/oligaemic borders.

Transcranial Doppler ultrasound (TCD) can image cerebral vasculature by directing an ultrasound probe through the temporal 'window' in the skull. Identification of arterial occlusion is performed with reasonable accuracy as compared to MRA or DSA(184). However, the real advantage of the technique is the ability to monitor vessel status in real time and the ability to determine parameters such as the speed(185, 186) and timing(187) of recanalisation. In a manner analogous to the TIMI scale(188) for myocardial infarction, the Thrombolysis In Brain Ischemia (TIBI) (189) scale can be used to document the degree of recanalisation.

Single Photon Emission Tomography (SPECT) involves the injection of a radioactive tracer and subsequent detection of the gamma emissions by a gamma camera, in an examination which takes 20 to 30 minutes. Since it can measure blood flow it has been suggested to have the potential to identify stroke(190), monitor reperfusion therapies(191), identify subjects at risk of post-thrombolytic haemorrhage(192) and even identify intact viable neurons(193). However, it is unlikely that SPECT imaging will become routine in acute ischemic

stroke. Not only are imaging times relatively long, but examinations are not easily combined with other modalities such as in multi-modal CT or MR.

1.5.13 Emerging Techniques for Metabolic Imaging

Owing the complex nature of ^{15} O PET, a number of other PET techniques have been developed which are potentially less burdensome. One of these is ^{18}F-fluormisonidazole (FMISO) PET imaging. FMISO is a nitroimidazole and it is proposed that it is trapped intracellularly exclusively by hypoxic, yet still metabolising tissue. It is retained in tissue with continuing hypoxia, but binding does not occur after effective reperfusion(194). Animal studies suggest that FMISO binding is greatest in the early hours after stroke and declines with time(195), consistent with the concept of the penumbra. Human studies have given support to these findings, as binding can be detected in the first 48h but not after 1 week(196). Other studies have confirmed a changing topography of such tissue with time(197), and that spontaneous survival of hypoxic tissue is associated with improved neurological outcome(198). Recent attempts to validate this technique in animals have proven encouraging. In a small pilot rodent study using 18F-FMISO tracer uptake was only seen early after stroke, and not when either early reperfusion or tissue necrosis had(199) developed. However, issues remain as to the optimal threshold with respect to timing of imaging; a recent study suggested that imaging at less than 90 mins would underestimate tissue at risk, and at 24h after permanent ischaemia would overestimate final infarction(200). Indeed, given that tracer needs to circulate in the presence of ischaemia for 2h negates this technique as a useful pre-rtPA scan. Nonetheless, this technique remains an attractive candidate for penumbral imaging.

Just as FMISO may image hypoxic tissue at risk, PET imaging with radiolabelled flumazenil (FMZ), which binds central benzodiazepine receptor, proposes to identify infarct core. Indeed, data from a small cohort suggests that it appears to predict final infarct volume with similar accuracy as DWI, but with a lower false positive rate(201). In a study by Heiss and colleagues(202) the 95% confidence intervals for cortical infarction were calculated for FMZ binding and

CBF, and in a manner analogous to the PWI-DWI mismatch, tissue with low blood flow (<14ml/100g/min) and preserved FMZ binding could be identified, tissue which the authors proposed as penumbra. It has been suggested that if reperfusion of tissue without decreased FMZ binding occurs, the tissue will be salvaged. Although data from a small cohort supports this(203), it requires to be validated by a larger data set. Additional limitations to this technique include long imaging time and imaging of grey matter only.

1.6 Which Modality to Image Acute Stroke?

Previous discussions have considered the use of NCCT, multimodal CT and multi-modal MR. To date there has not been a head-to-head study comparing clinical outcomes of patients with acute ischaemic stroke who were evaluated with all three of these modalities. However, in a head-to-head study of NCCT to multi-modal MR in patients receiving rtPA(204), the rates of ICH and mortality were worse in the NCCT arm compared to the MR arm. In addition, time-to-treatment was not a significant predictor of outcome in univariate or multi-variate analyses, prompting the authors to conclude that patient selection is more important than time to treatment when administering rtPA. In a separate comparison of NCCT to MRI (DWI and GRE), the MR sequences yielded a significantly greater sensitivity for a positive diagnosis of acute ischaemic stroke (83% vs 26%) and the detection of chronic haemorrhage was more frequent with MRI(64). In addition, as discussed previously, it has been shown that GRE is as sensitive as CT for the detection of acute haemorrhage(91). However, whilst the argument for MR over CT in acute stroke is building, these issues have to be countered by the high rate of intolerance of MR in acute stroke patients and the longer time to imaging(65) in a scenario where ‘time is brain’. In addition, when using the ASPECTS scoring system the differences in stroke detection become much less(65) than observed in studies not employing this system(64). In conclusion, controversy still remains as to which modality is best in acute stroke.

2 Oxygen Challenge MRI: Evaluation of Signal Changes in Different Tissue Compartments

2.1 Introduction

In Chapter 1, the need for a clinically applicable penumbral imaging technique was discussed. The perfusion-diffusion (PWI-DWI) mismatch concept is potentially useful, although studies to date have proven disappointing. Although refinements to the PWI-DWI mismatch hypothesis are promising, there may still be an additional role for alternative imaging techniques. The 'gold standard' imaging modality for the penumbra is Positron Emission Tomography, on the basis that it measures tissue perfusion and metabolic activity. Operational criteria for the penumbra defined by PET include reduced blood flow, preserved cerebral metabolic rate for oxygen ($CMRO_2$) and also, relevant to this Chapter, an increased oxygen extraction fraction (OEF) - more oxygen extracted from the blood and therefore a decreased ratio of oxyhaemoglobin : deoxyhaemoglobin. Therefore, although PET is logistically unfeasible for acute stroke imaging, it hints at potential future directions for other imaging techniques. Given that perfusion can be measured on MRI, the additional ability to measure metabolic indices such as $CMRO_2$, OEF, or deoxyhemoglobin, may prove invaluable. This chapter and those which follow consider a novel application of an MRI sequence which is sensitive to a phenomenon termed the 'Blood Oxygenation Level Dependent' ('BOLD') effect, and is thus in turn sensitive to changes in deoxyhemoglobin, and therefore metabolic activity.

2.1.1 T2-, T2'-, T2-Weighted MRI and the 'BOLD' Effect*

To understand the BOLD effect it is useful to review the basic principle behind magnetic resonance. Chapter 1 considered the decay in transverse magnetisation as an influence on MRI signal. The relaxation of transverse magnetisation occurs

in part due to the effects from other spins (spin-spin relaxation) with a time constant T2. However, magnetic field inhomogeneities also contribute to the decay of the transverse magnetisation, according to the time constant T2'. The additive effects of T2 and T2' contribute to the constant T2* according to the equation;

$1/T2^* = 1/T2 + 1/T2'$.

Although T2 weighted contrast may be detected by a standard spin echo sequences, T2* weighted contrast may be obtained using a 'gradient echo' sequence(205) which is sensitive to magnetic field inhomogeneities. The influences of magnetic field inhomogeneities on transverse magnetisation decay have been described as 'macroscopic, 'mesoscopic' or 'microscopic'(206, 207). The macroscopic effects of background field variation, which occur over distances larger than the imaging voxel, are related to local scanning conditions and not physiological processes. Such effects may be seen around the nasal sinuses for example and generally present a 'nuisance' factor. 'Microscopic' fluctuating magnetic field inhomogeneities which occur on a molecular level contribute to the T1 and T2 effects, as previously discussed. Of additional interest, however, is the mesoscopic effect (larger than microscopic but smaller than the resolution of the imaging voxel) of the microcirculation which also influences the relaxation of transverse magnetisation which can be measured by T2' and T2*–weighted MRI sequences – the BOLD effect.

The BOLD effect was first described by Ogawa and colleagues in 1990(208) who observed veins in the mouse and rat brain as dark lines on gradient-echo images. Whilst such delineation of veins was striking when animals were breathing only 20% oxygen, the contrast disappeared when the oxygen concentration was increased to 100%. Ogawa and colleagues subsequently showed that increased oxygenation due to an increase in cerebral blood flow also increased signal (209). After concluding that the effect was entirely due to blood oxygenation, the term 'Blood Oxygen Dependent' (BOLD) MRI was coined. Although the discovery of BOLD gave birth to a new form of investigation - functional magnetic resonance imaging (fMRI)(210)- which will not be considered further, the principles behind BOLD may be relevant for a variety of imaging purposes(211).

The signal changes observed by Ogawa and colleagues are explained by a change in the balance between oxyhemoglobin and deoxyhemoglobin within the vasculature. Deoxyhemoglobin molecules, with their unpaired electrons, are paramagnetic(212) and therefore generate magnetisation (susceptibility) when placed in a static magnetic field, such as that of an MRI scanner. Oxyhemoglobin on the other hand, is diamagnetic, and therefore does not exert such a susceptibility effect. Intra-vascular deoxyhaemoglobin therefore creates a magnetic susceptibility difference between blood and tissue parenchyma. Increases in deoxyhaemoglobin will therefore increase magnetic susceptibility between vessels and tissue, which may in turn be detected as a reduction in signal intensity on SE or GRE MRI sequences measuring T2 or T2* respectively. Although less common, multi-echo sequences sensitive to T2' may also be employed. Signal changes due to paramagnetic deoxyhaemoglobin are detected by T2 and T2*/T2' by separate mechanisms (213, 214). The T2 effect predominates in the intra-vascular compartment and is partly diffusion dependent; the high intra-vascular rate of diffusion of water past deoxyhaemoglobin molecules leads to loss of phase coherence (spin-spin effects) which can be detected by changes in T2 as measured using a SE sequence. However, dense packing of haemoglobin molecules in the intravascular compartment means that the magnetic field inhomogeneities of individual erythrocytes, on average, cancel each other out (there is no net phase shift) and therefore changes in T2*-weighted signal are not apparent. On the other hand, when local field inhomogeneities are relatively large compared to the rate of diffusion, such as in the proximity of a large vessel, T2*/T2' would be influenced to a greater degree than T2, a phenomenon which can be measured by GRE sequences. For example, in tissue surrounding capillaries both T2 and T2*/T2' effects may be elicited. In tissue surrounding larger venules and veins the phase shift between blood and tissue due to deoxyhaemoglobin induced magnetic field inhomogeneities is even greater compared to the diffusional effects, and therefore the T2*/T2' effect predominates. Therefore deoxyhaemoglobin causes dephasing of spins and a reduction in T2/T2* weighted signal - the BOLD effect. The magnitude of signal is larger on T2*- compared to T2-weighted images(215).

Does the enhancement of transverse relaxation by the BOLD effect, predict deoxyhemoglobin concentration? In 1981, Thulborn and colleagues(216)

conducted a test tube study and demonstrated a quadratic relationship between the fraction of deoxygenated blood in a sample, and the T2, while also demonstrating a dependence on haematocrit. The dependence of transverse relaxation on deoxyhemoglobin concentration has since been replicated(216, 217) including in volunteers and swine models(218) using T2*-weighted signal, again confirming the quadratic relationship, although a linear fit seems to offer a reasonable alternative at deoxyhemoglobin fractions greater than '0.2'.

In summary, as the fraction of deoxyhemoglobin increases, the T2*-weighted signal intensity (and to a lesser extent T2-weighted signal intensity) decreases, an effect due to magnetic susceptibility differences(213) which is dependent on deoxyhaemoglobin concentration.

2.1.2 The BOLD Effect for Detection of Potentially Salvageable Tissue

The observations that MR sequences which are sensitive to the BOLD effect can detect changes in deoxyhemoglobin, a metabolic by-product of oxidative metabolism, give rise to the attractive possibility that they may potentially aid detection of the ischemic penumbra. This could be achieved by 1) qualitative assessment of MR sequences which provide static measurements of the BOLD effect, 2) modelling BOLD MR data to derive quantitative measures of metabolic activity, or 3) deriving semi-quantitative measures of metabolic activity based on induced dynamic changes in the BOLD effect. These three approaches will be considered in the following sections

2.1.2.1 Assessment of Static BOLD Signal Intensity; Animal Studies

The most intuitive method to detect the BOLD effect after stroke is to approach BOLD-sensitive sequences in a manner analogous to the conventional evaluation of other stroke MR sequences such as DWI and Fluid Attenuated Inversion

Recovery (FLAIR) – to perform a simple, often visual assessment, of signal intensity.

Animal studies have thus far proven encouraging in this regard. In 1991, Turner and colleagues demonstrated a reduction in T2*-weighted signal intensity in the feline brain after applying a short period of anoxia. Furthermore, after restoration of normoxia they noted a subsequent rise in signal intensity with a temporary overshoot(219). A year later, de Crespigny and colleagues(220) demonstrated a similar reduction in T2*-weighted signal in a feline model of transient focal middle cerebral artery occlusion (MCAO) model. Although the decline in signal intensity plateaued after approximately 60 seconds, the magnitude of the decrease was greater following longer periods of focal ischemia, consistent with the known dependence of transverse relaxation on deoxyhemoglobin concentration. A temporary overshoot in T2*-weighted signal increase after reperfusion was also seen in this study and tended to be larger following longer periods of ischemia. Consistent with these findings, Roussel and colleagues(221) noted that following MCAO in the rat, there was an acute reduction in T2*-weighted signal intensity which extended beyond the limits of the lesion seen on Diffusion Weighted Imaging (DWI) and which could therefore represent increased OEF. A recent study(222) of further validation using seven rodents to assess T2'-weighted signal in the DWI lesion 90 mins after reperfusion after MCAO yielded varying degrees of success of reperfusion. However, in the single rat with hyperperfused DWI lesion, the T2'-weighted signal was significantly increased, rather than decreased. Therefore, the available animal data suggest that BOLD sensitive sequences may distinguish between misery perfusion and luxury perfusion.

However, despite the simplistic concept, animal studies have also highlighted potential complexities in interpretation of findings. For example, Dunn and colleagues demonstrated regional heterogeneity of the BOLD response to anoxia of the rat brain(223). In particular the change in T2*-weighted signal intensity was less in the CA1 region of the hippocampus compared to cortical regions during the same period of anoxia. The authors reasoned that such differences could be accounted for by a higher baseline oxygen extraction fraction (and therefore less capacity for change), differences in baseline blood volume between regions, differences in blood flow changes due to anoxia, or even

differences in the local architecture of the vasculature. Similarly, clear differences in BOLD response to hypoxia have been consistently observed between grey and white matter(219, 224) which could also confound interpretation of the BOLD response unless tissue segmentation is performed. Therefore, qualitative interpretation of BOLD changes may not be straightforward.

2.1.2.2 Assessment of Static BOLD Signal Intensity; Human Studies

The encouragement from the animal studies of signal intensity has been broadly reflected by findings in human stroke. In 2002 Tamura and colleagues(225) examined the pre-contrast images from the T2*-weighted series of dynamic susceptibility weighted perfusion images in subjects with large vessel occlusion imaged less than 4 hours post ictus. Qualitative analysis showed reduced signal intensity in the ipsilateral compared to the contralateral hemisphere. Although the images were of insufficient quality for accurate volumetric analysis, this study validated the principle of using deoxyhaemoglobin-weighted imaging in acute stroke. Using a T2*-weighted sequence, Wardlaw and von Heijne(226) reported a case of a subject imaged less than two hours post stroke onset where the region of hypointensity could be clearly delineated in the ischaemic regions, and which was substantially larger than the lesion on DWI. Although such findings were not consistently detected in the cohort from which the case reported was derived, subsequent analyses of Gradient Echo (GRE) images acquired from hyperacute subjects, primarily for the purpose of excluding intracerebral haemorrhage (ICH) have demonstrated more consistent findings(99, 227, 228). Using a cohort of 48 subjects imaged less than 6 hours on a 1.5T scanner, Hermier(227) showed that subjects with hypointense leptomeningeal vessels presented with smaller acute DWI lesions compared to those without, suggesting that such findings represent a marker of collateral circulation. Hypointensity on GRE has been shown to manifest only in those who have large vessel occlusion and has been subdivided into hypointensity of cortical vessels, hypointensity of the deep white matter vessels (brush sign), and hypointensity of the parenchyma(99). In one cohort of 24 subjects with large vessel occlusion imaged less than 6 hours by a 3.0T scanner these findings were frequently detected; cortical vessels (100%), brush sign (92%) and hypointense parenchyma (58%)(99) and such findings disappeared after reperfusion.

Geisler and colleagues (229) focussed on the T2' parameter. Thirty-two subjects were imaged less than 6 hours on a 1.5T scanner, and signal intensities from the lesion on Apparent Diffusion Coefficient (ADC), ultimately salvaged PWI-DWI mismatch, and the region of lesion growth were measured. Reassuringly, hypointense regions were observed and differences in signal intensity between tissue compartments were noted. However, wide confidence intervals precluded the determination of thresholds for tissue compartments. Interestingly, the lowest signal intensity was observed in the 'infarct' region defined by the lesion on ADC images. Possible explanations for this were the persistence of penumbral activity within the ADC lesion, and reduced washout of deoxyhaemoglobin under conditions of low CBF. This study gave rise to a larger systematic analysis of 100 stroke subjects (< 6 hours) who were evaluated for the presence of a T2'-ADC mismatch, in a manner analogous to the PWI-DWI mismatch concept(230). For the prediction of infarct growth, the T2'-ADC mismatch was sensitive (0.78/0.87 for two readers) and more specific than the PWI-DWI mismatch (0.42/0.46) when perfusion was measured using 'time-to-peak'. In subjects without recanalization the positive predictive value of infarct growth was good (0.63/0.80). The agreement for detecting T2'-ADC mismatch was moderate (kappa=0.53). Again, these results were encouraging, but the T2'-ADC mismatch has yet to find a precise clinical role.

Finally, a word of caution regarding the evaluation of static T2*-weighted signal intensities. In a back-to-back study of MR and PET imaging in 5 subjects imaged 7-21 hours after stroke Donswijk and colleagues(231) found no correlation between static T2*-weighted signal intensity and oxygen extraction fraction. Whilst these findings require serious consideration, they do not spell the end of deoxyhaemoglobin sensitive imaging techniques. Firstly the population studied was imaged later than the time window in which rtPA has shown to be effective. In addition, at these late time points, the T2*-weighted signal intensity will be affected by the inevitable rise in T2-weighted signal due to oedema occurring after about 6 hours, a phenomenon unrelated to deoxyhaemoglobin. Finally prospectively acquired BOLD sensitive imaging techniques may provide better results compared to the pre-contrast images from PWI used in this study. These data do, however, raise an important question; perhaps what is needed is more

formally modelled data, or assessment of dynamic signal changes in order to reduce other influences on the T2*-weighted signal?

*2.1.2.3 Modelling the BOLD Effect; Exploiting T2**

A theory of proton dephasing in the presence of magnetic field homogeneities has been comprehensively described by Yablonskiy and Haake(232). They refer to the 'static dephasing regime' to describe proton dephasing due to local variations in spin frequencies which predominate over the effects from diffusion of water. The Yablonskiy and Haake(206) theory states that below a particular echo time (TE) the T2' decay is a linear function of the TE. In contrast, when TE exceeds this particular 'characteristic time' of TE, the R2' relaxation rate (with time constant T2') instead becomes a linear function of the volume of the signal perturbers (e.g. deoxyhaemoglobin), susceptibility differences between tissues, and static magnetic field. Therefore for modelling a randomly orientated vessel network the *extravascular* T2' signal intensity may be expressed as dependent on oxygen extraction fraction, the magnetic susceptibility of blood, venous CBV, haematocrit and static magnetic field (see equation below).

$$R2' = \lambda * \gamma * (4/3) * \Delta X_0 * Hct * (1 - CBOS)$$

where R2' = 1/T2', λ = venous CBV, assuming arterial blood is fully saturated, γ = gyromagnetic ratio (2.68 x 10^8 rad/s/Tesla), ΔX_0 is the difference in magnetic susceptibility between fully oxygenated and fully deoxygenated blood (0.18ppm per unit Hct(233), Hct = haematocrit and CBOS = cerebral blood oxygen saturation and thus (1-CBOS) = oxygen extraction fraction.

The investigators Hongyu An and Weili Lin who are based in research groups in St Louis and North Carolina have exploited this model in order to provide estimates of MR derived cerebral oxygen saturation, oxygen extraction fraction (OEF) and ultimately the cerebral metabolic rate of oxygen ($CMRO_2$). An and Lin(234) employed a type of MR sequence which combined features of gradient echo and spin echo sequences and has been termed a multi-echo gradient and spin echo sequence (MEGESE). In this sequence a spin echo was acquired between 10 gradient echoes on either side. Given that signal intensity measured using different TEs varies and may be dependent on different factors, as stipulated by

Yablonskiy and Haake(232), differences between the MR signal measured at spin echoes and gradient echoes were used to provide estimates of R_2' and λ (venous CBV), and therefore CBOS (venous oxygen saturation) and OEF. The authors used asymptotic signal behaviour by extrapolating signal intensity measured at the spin echo, by using a logarithmic scale. MR signal data which was measured at long periods before or after the spin echo can measure R2' and data collected at shorter time scales with respect to the spin echo was used to distinguish effects of venous CBV and OEF. In their seminal study using this technique the authors estimated a normal OEF of 41.6%(234). Despite being highly encouraging a number of limitations were acknowledged. Firstly, venous CBV was calculated to be 16% which was much larger than expected (usually <5%). In addition, a large inter-subject variability was noted and this was attributed to noise. A number of assumptions were also acknowledged. For example, only extravascular effects are measured and therefore assumptions may be violated under conditions of increased CBV, such as in the ischaemic penumbra. Other potential errors may be introduced by local magnetic field variations and by the assumption that the model does not take into account effects of intravascular diffusion.

The authors developed the original concept by exploring the surprisingly (and erroneously) large venous CBV value attained by the first study. Variation in non-physiological macroscopic magnetic field inhomogeneities was investigated. Field maps were acquired from 12 healthy subjects so that variations in local magnetic field attributed to non-physiological effects could be modelled and their effects eliminated(235). Correction of such variations reduced the estimates of venous CBV down to just below 3%, a value which is in good agreement with the literature. A further investigation in human volunteers reported a ratio of the 'venous' CBV measured by this technique to total CBV as being '0.77' a value broadly similar to those from PET studies.

After the original report in rodents, their next task was to validate the technique in human volunteers(236). In doing so, measurements of OEF were combined with CBF measurements generated from conventional PWI using the standard SVD technique to produced a measure of MR derived $CMRO_2$ (which they have since termed 'cerebral metabolic oxygen index - MR-COMI), according to the following equation:

MR $CMRO_2$ (COMI) = CBF * OEF

The group claimed to demonstrate a uniform OEF across hemispheres, which would be expected from PET literature and therefore in keeping with current physiological understanding. Moreover, MR-COMI was greater in grey versus white matter, again a reassuring finding. Although the ratio of MR-COMI in grey versus white matter was 2.37, a higher value than quoted in the PET literature (~2.0(237)), differences were explained on the basis of higher CBF measurements systematically measured by MR compared to PET.

Since then, MRI COMI has been tested under different oxygen saturations and in both animal and human stroke. A study of healthy rats(238) has confirmed an increase in MRI derived cerebral oxygen saturation values after hyperoxia, and moderate and severe decreases after moderate and severe hypoxia respectively. Moreover there was excellent correlation between the oxygen saturation directly measured from the jugular vein and MR derived oxygen saturation in the superior saggital sinus. Application of MR COMI to rodents with MCA occlusion revealed lowest values in the MR defined infarct core compared to any other region. Over time there was a shift in the number of ipsilateral voxels with MR COMI values within the inter-quartile range (38-70% of normal) to those in the lowest quartile (<38% of normal), suggesting MR COMI is capable to detecting the metabolic evolution of tissue after stroke.

In 2003(239), the group produced the first report of the application of their technique in human acute stroke subjects. Measurements of MR-COMI were made in seven patients imaged at an average of 7.5h post ictus. As expected, values for MR-COMI were lower in operationally defined infarct 'core' compared to the PWI-DWI mismatch region, thus helping to validate results. Interestingly, a gradient of MR-COMI deficit was observed in a region of matched PWI-DWI abnormality, a region which, by conventional MRI parameters, would be considered as homogeneous. These preliminary results were encouraging although it was acknowledged that haematocrit levels may not remain stable under ischaemic conditions, thus introducing potential errors in the estimations. Further work in human acute stroke was presented at the International Stroke Conference 2010(240). Nine acute ischaemic stroke patients were imaged at an average of 2.9 hours post ictus. It was found that measures for MR COMI

predicted grey matter infarction better than MTT or ADC. However, such an effect could not be demonstrated for white matter.

He and Yablonskiy(206) have argued that modelling should also incorporate signal from intra-vascular compartments and should also account for the fact that the brain is composed of multiple tissue compartments (grey matter, white matter, CSF). The group called their 'model-based multivariable curve-fitting approach' quantitative BOLD (qBOLD), and applied it to nine healthy volunteers scanned on a 3T MR scanner. The group measured deoxygenated blood volume (DBV – a term coined to acknowledge that the relevant blood volume is not just from venous compartments but also from part of the capillary bed) as being 1.56% and 0.62% from grey matter and white matter. OEF was calculated to be 32.9% and 33.1% from grey and white matter respectively. Deoxyhaemoglobin concentration was 12.4 μM and 4.4μM for grey and white matter respectively. A further validation study(241) in rodents demonstrated an excellent correlation (R^2 = 0.92) between MR measured venous oxygen saturation and directly measured oxygenation of venous blood drawn from the superior saggital sinus.

Finally, a noteworthy concept from Peter Jezzard and colleagues(242) from the University of Oxford should be discussed. BOLD data were collected from six healthy volunteers who were imaged on a 3T MR scanner. A method using hyperoxic contrast was employed whereby T2* signal intensity was measured from the saggital sinus (pure blood compartment) and the tissue (CBV = unknown variable) under normoxic and hyperoxic conditions. By assuming the venous oxygen saturation was constant between tissue and saggital sinus venous blood, the change in signal intensity in the tissue parenchyma was used to calculate tissue CBV by using the change in saggital sinus signal intensity as a reference. This is another example of the T2* effect being exploited to derive physiological information, although in this case it was not strictly a metabolic parameter.

2.1.2.4 Modelling the BOLD Effect; Exploiting T2

Other groups have argued that because the T2*-weighted signal intensity may be affected by a wide variety of influences which include sources other than deoxyhemoglobin such as regional field variations and perturbation at air-tissue interfaces, analysis of the T2 effect may provide more reproducible results. An advantage of using T2 is that there is generally little inter-individual variation. Peter van Zijl and colleagues(243) from Johns Hopkins University produced maps of CBV by developing a theoretical model of the physiological contributions to signal loss (T2) *within* the vessel (c.f. An and colleagues(234) who examined the *extra-vascular* signal loss of T2*). The group modelled the contributions of different deoxyhaemoglobin containing tissue compartments and applied their theory to data acquired using a spin echo sequence in the context of hypoxic hypoxia in cats. It was shown that the predominant contribution to intra-vascular signal was intra-vascular water exchange between tissue with different magnetic susceptibilities (erythrocytes and plasma) and the contribution to signal from water diffusion through field gradients and from water exchange between tissues and capillaries was small. Building on the theory proposed by van Zijl(243), magnetic properties of different vascular compartments were modelled with respect to haematocrit, gas exchange properties and transit time(244). The major influences on T2 were reported to be CBV and OEF. Simulations demonstrated that at 1.5T there appeared to be a linear relationship between OEF and T2. However, at 4.7T, venous T2 was decreased at higher OEFs, and therefore total venous signal contributed very little to the total T2 signal at such OEFs i.e. the relationship between T2 and OEF is not linear at higher field strengths. In experimental hypoperfusion using absolute single spin echo images acquired at 4.7T the reduction in T2 was U-shaped with respect to CBF reduction and a maximal reduction in T2 was seen at 15-60% of normal. It was postulated that the partial reversal of the reduction in T2 at very low blood flows may have reflected the inhibition of $CMRO_2$. Using a model of transient forebrain ischaemia in the rodent, the group went on to show that T2 reduction could also be demonstrated at 1.5T(245). Moreover, with restoration of perfusion a transient overshoot in the T2 increase was observed. Simulations have suggested that increases in CBF and CBV only partially explain the increase in T2 seen with luxury perfusion, with reductions in OER and depressed $CMRO_2$

also contributing(246). A recent clinical application of this technique was demonstrated on subjects with carotid artery steno-occlusive disease where it was shown that OEF was elevated in 8/22 subjects, not all of whom had elevated CBV(247).

An alternative method of exploiting the BOLD effect to give measures of $CMRO_2$ was proposed by Davis and colleagues(248). They used a spin echo sequence to detect the BOLD effect, and combined it with arterial spin labelling (ASL) to derive the additional measure of blood flow. By applying hypercapnia as a calibration tool, the group exploited the Fick principle to derive measures of $CMRO_2$. Using the application of CO_2 which was theorised to increase blood flow but not change $CMRO_2$, the expected increase in the BOLD signal was calculated for a given change in CBF. After next performing photic stimulation with concomitant measures of BOLD and CBF, the contribution of the change in $CMRO_2$ to the BOLD signal was calculated on the basis of the change in CBF. The group expressed the 'calibration factor' as 'M' which represented the ceiling of BOLD change which could be achieved due to metabolic activity and represented the baseline BOLD signal, a function of deoxyhaemoglobin. Image maps of 'M' allowed the definition of three tissue compartments; M = large, where large veins were included in the voxel and these areas were excluded; M= medium, where the parenchyma was termed 'reactive' and ; M=small, where parenchyma was termed 'non reactive'. The differences in these three areas were postulated to represent differences in microvessel density and according to the 'M' maps shown, appeared to show the grey matter as more 'reactive' than the white matter. Although exciting, this technique may be inappropriate for application to acute stroke patients, owing to the side effects associated with CO_2. Of perhaps greater suitability, however, would be calibration of the BOLD signal not by CO_2 but by O_2, as recently proposed(249).

2.1.3 Oxygen; a Naturally Occurring Contrast Agent

It has been suggested that oxygen may be used as a natural intravascular contrast agent. Its potential benefits and limitations include having relatively few contra-indications, ease of access, and rapid washout times allowing

repeated investigations(250). From the very first seminal paper on the BOLD effect (208), oxygen has been used to alter the balance of oxyhaemoglobin : deoxyhaemoglobin ratio and thereby derive physiological information. The use of hyperoxia to probe cerebral blood volume has already been discussed. Rostrup and colleagues(251) precipitated hypoxia and hyperoxia by varying the degrees of inspired oxygen in healthy volunteers. Increases in T2*-weighted signal intensity were observed after hyperoxia. It was speculated that this observation could be explained by increased venous oxygen saturation, which increased the venous oxyhaemoglobin : deoxyhaemoglobin ratio thereby altering intra-vascular magnetic susceptibilities. It was also concluded that hyperoxia induced haemodynamic changes could not have explained the signal changes. Such increases in T2*-weighted signal intensity after hyperoxia in normally metabolising tissue have been replicated(252, 253). Kennan and colleagues(253) developed this theme in rodents at 2.0T. After administration of an iron based contrast agent to probe blood volume, the influence of CBV to the total T2*-weighted signal was assessed at varying oxygen concentrations. Reassuringly, it was found that, at most, 12% of the T2*-weighted signal change noted with varying oxygenation was due to changes in CBV, with the major influence being the change in magnetic susceptibility. Moreover, the authors also concluded that very large changes in CBV, unlike those typically seen with respiratory challenges, would be needed to dominate the influence of change in T2*-weighted signal intensity. However, regional heterogeneity has been noted(254).

In summary these findings are encouraging and suggest that the application of hyperoxia during BOLD sensitive imaging may probe local tissue oxygenation without a major influence from hyperoxia induced haemodynamic changes.

2.1.4 Proposed Technique

The hypothesis of the proposed technique is that it is sensitive to deoxyhaemoglobin and therefore OEF. Deoxyhaemoglobin sensitive imaging, if successfully implemented, may help to differentiate tissue compartments following acute ischaemic stroke. It is based on the following key aspects which have been previously discussed and referenced in this thesis.

1) OEF (and therefore vascular deoxyhaemoglobin) increases in misery perfusion, a condition which has been associated with potentially salvageable tissue. OEF is reduced or absent in infarct 'core' and increased in the penumbra (please see Discussion section for exceptions to this rule). Vascular deoxyhaemoglobin will therefore vary between tissue compartments following acute ischaemic stroke

2) 'Blood Oxygenation Dependent' (BOLD) MRI is sensitive to deoxyhaemoglobin concentration, which possesses paramagnetic properties. BOLD sensitive sequences include T2, T2' and T2*-weighted imaging. T2*-weighted imaging provides the greatest signal-to-noise ratio.

3) Hyperoxia has shown potential to serve as a contrast agent. Application of hyperoxia during T2*-weighted imaging precipitates a signal increase in healthy volunteers. This has been attributed to increased venous oxygen saturation and therefore altered magnetic susceptibilities; extra administered oxygen combines with paramagnetic deoxyhaemoglobin, a by-product of oxidative metabolism, to form oxyhaemoglobin. Therefore the oxyhaemoglobin : deoxyhaemoglobin ratio increases, precipitating a signal increase, thus indicating metabolising tissue.

The proposed technique involves the application of hyperoxia as a contrast agent during T2*-weighted imaging in order to probe relative deoxyhaemoglobin concentrations and therefore tissue metabolism. The rationale for using this approach is to provide a simpler technique with less assumptions than the other approaches which use complex modelling to derive quantitative physiological values, but which have still not been completely validated. T2* rather than T2-weighted imaging was chosen for its greater signal to noise ratio.

Hypothesis for the Technique: It is hypothesised here that following acute ischaemic stroke, the application of hyperoxia during T2*-weighted imaging will produce different changes in T2*-weighted signal intensity in different MRI-defined tissue compartments. It is hypothesised that in penumbral tissue, where $CMRO_2$ is maintained and OEF is high, the signal increase will be greater than in normal tissue, indicating a large deoxyhaemoglobin pool. In hypoperfused infarct core, it is hypothesised that signal intensity increases will be diminished or absent. In perfused infarct core where there is an excess of paramagnetic

oxygen dissolved in plasma, signal decreases may be seen. These hypotheses are summarised in .

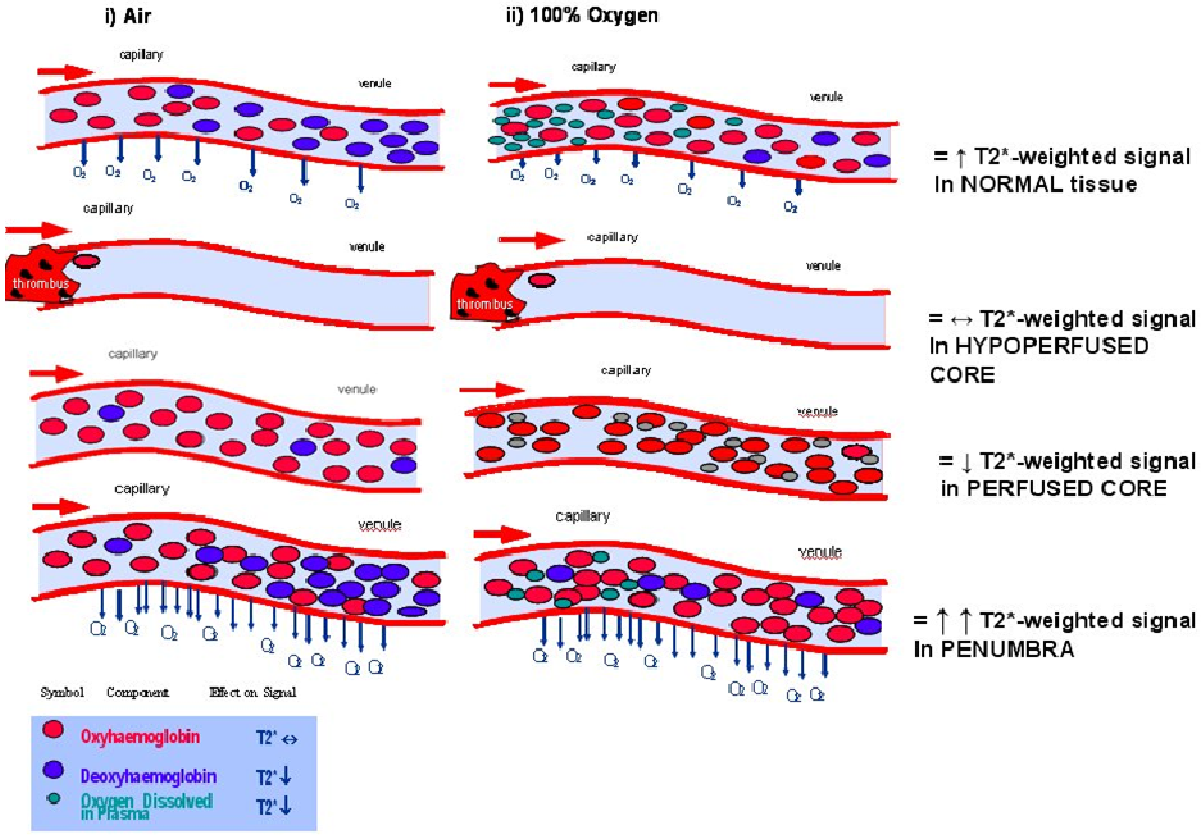

Figure 2-1. Hypotheses for the Oxygen Challenge Technique.
This figure has been adapted from a more simplified diagram received from Dr David Brennan, Institute of Neurological Sciences, Glasgow (Personal Communication). The cartoons on the left and right show the state of oxygen extraction from the blood under normoxic (i) and hyperoxic (ii) conditions, respectively, in the stroke brain. In normal tissue (top) the Oxygen Extraction Fraction (OEF) is ~0.3-0.40. Therefore after oxygen administration the paramagnetic deoxyhaemoglobin in the capillary and venous beds will be replenished with oxygen, reducing magnetic susceptibility, and leading to an overall signal increase. Distal to blood vessel occlusion, where there is no perfusion (2nd top), no such change will occur. If there is reperfusion into a region of little or no remaining metabolism (e.g. luxury perfusion, 3rd top), the OEF will be low and there will be little dynamic contribution of supplementary oxygen to the deoxy/oxyhaemoglobin ratio. Administered molecular oxygen will simply remain dissolved in the plasma, exerting its paramagnetic effect and causing a decrease in T2*-weighted signal intensity. In penumbra where the OEF is high, there will be an abundance of deoxyhaemoglobin to combine with oxygen (bottom). Therefore we would expect a large signal increase, greater than in 'normal' tissue. The legend at the bottom right of the diagram illustrates the effect of each relevant blood component on the direction of signal change.

This technique as been tested in rodents as part of an 'animal pilot study' by the Brain Ischaemia group, University of Glasgow(255). The hypotheses above were partially validated; signal increases in the PWI-DWI mismatch region, contralateral 'normal' region, and operationally defined infarct 'core' were 3.7%, 1.8%, and 0.24% respectively. The aim of this current study was to apply the new technique (termed Oxygen Challenge MRI) to subjects with acute ischaemic stroke.

2.2 Methods

The following figure illustrates the main methodological steps pertaining to this part of the study (Figure 2-2). These steps are described in further detail in the following sections.

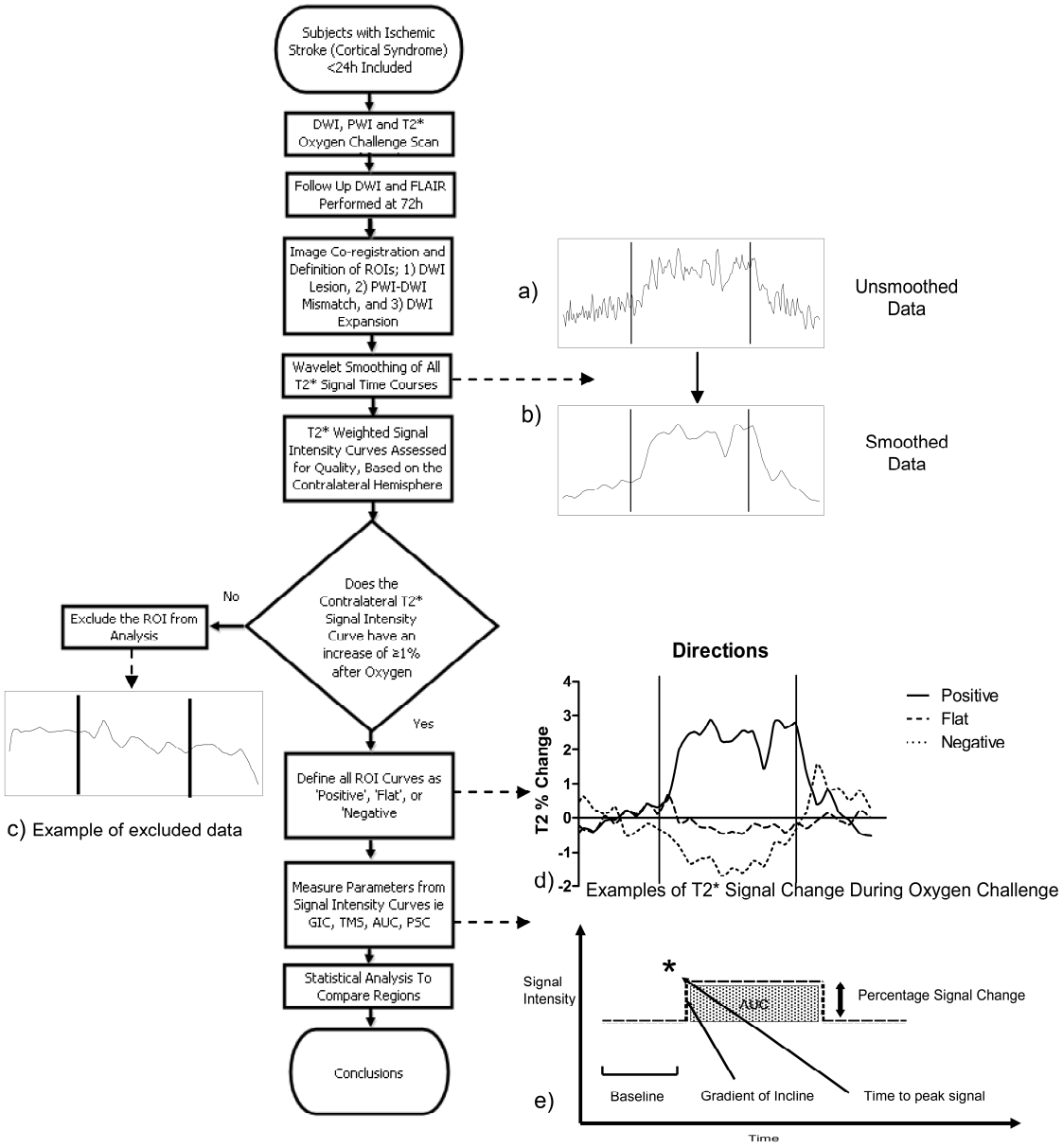

Figure 2-2. Summary of Main Methodological Steps
NIHSS = National Institutes of Health Stroke Scale, DWI= diffusion weighted Imaging, PWI= perfusion weighted imaging, FLAIR = Fluid attenuated inversion recovery, ROI = region of interest, GIC = gradient of the incline of the curve, TMS = time to maximum signal, PSC = percentage signal change. Reproduced with permission John Wiley and Sons from 'T2*-weighted magnetic resonance imaging with hyperoxia in acute ischemic stroke: Annals of Neurology: 2010'.

2.2.1 Ethical Approval

Ethical approval for this single centre study was granted by the Multi-centre Research Ethics Committee for Scotland A (MREC A); project reference *05/MRE00/37*.

2.2.2 Subject Recruitment

Recruitment of subjects to the study was performed between 1st August 2006 and 1st June 2008. Patients who were admitted to the Acute Stroke Unit at the Institute of Neurological Sciences Glasgow, and fulfilled the inclusion criteria for the study, were considered. Institutional scanning hours were between 8am and 8pm on weekdays.

Subjects were recruited by direct informed consent or, if incapacitated by written assent from the nearest available family member. Assessment of capacity to consent was made using clinical judgement, in addition to discussion with the receiving clinical stroke team.

2.2.2.1 Inclusion Criteria

Inclusion Criteria for subjects were as follows:

- Clinical diagnosis of acute ischaemic hemispheric stroke <24h after onset
- Clinical evidence of cortical involvement i.e. evidence of a partial anterior circulation syndrome (PACS) or total anterior circulation syndrome (TACS) as defined by the Oxford Community Stroke Project (OCSP)(2)
- Exclusion of primary intra-cerebral haemorrhage by baseline scanning (usually Computed Tomography [CT]) requested for clinical purposes
- Informed consent from patient or assent from relatives

2.2.2.2 Exclusion Criteria

Exclusion Criteria were as follows;

- Incompatibility with 3 Tesla (3.0T) MR scanners (e.g. cardiac pacemaker, metallic implants, some coronary stents)
- Coma or other concomitant condition making survival to one week unlikely
- Known type II respiratory failure
- Patients requiring continuous oxygen support
- Pregnancy
- Evidence of acute non-cortical stroke on prior imaging
- MRI scanner unavailable

2.2.3 Imaging Protocol

2.2.3.1 Standard of Care

All subjects received baseline brain scans (usually CT) requested for clinical reasons prior to study specific scanning procedures. Most patients also had intra-cranial and extra-cranial vessel imaging by CT angiography at some point during their clinical course. Clinical management decisions e.g. administration of thrombolytic therapy, were also made and implemented prior to study procedures. Therefore clinical management was unaffected by this study.

2.2.3.2 Clinical Observation

A supervising clinician was present in the MR magnet room throughout the duration of scanning. Subjects were monitored with a combination of visual inspection and continuous heart rate and oxygen saturation monitoring (Schiller MagLife C. Plus).

2.2.3.3 Scanning Protocol

Scanning was performed at baseline (as soon as possible after consent and within 24 hours of ictus) and at follow up - as near to 72 hours as practically possible.

The following table (Table 1) gives details of the MRI sequences which were performed on a 3.0 Tesla (3T) scanner (General Electric Signa® Excite™) at baseline and at follow up.

Examination	Sequence Details	Duration	Repetition Time [TR] (ms)	Echo Time [TE] (ms)	Field of View [FOV] (cm)	Slice Thickness (mm)	Interslice gap (mm)	Resolution (frequency x phase)	NEX	Flip Angle (degrees)
3 plane localiser	-	-	-	-	-	-	-	-	-	-
Saggital T1	Fast SE	91s	2500	8.9	24	5	2	320x224	1.0	-
DWI	SE EPI	61s	7600	30	26	4	1	256x256	2.0	-
T2*	GRE EPI	672s	3000	30	24	4	1	128x128	1.0	90
PWI	GRE EPI	68s	2000	21.6	26	4	1	128x128	1.0	60

a)

Examination	Sequence Details	Duration	Repetitio n Time [TR] (ms)	Echo Time [TE] (ms)	Field of View [FOV] (cm)	Slice Thickness (mm)	Interslice gap (mm)	Resolution (frequency x phase)	NEX	Flip Angle (degrees)
3 plane localiser	-	-	-	-	-	-	-	-	-	-
Saggital T1 FLAIR	Fast SE	91s	2500	8.9	24	5	2	320x224	1.0	-
T2 FLAIR	Fast SE	100s	10 000	140	24	5	1.5	384x256	1.0	-
DWI	ASSET calibrate d SE EPI	182s	7600	64.9	26	5	1.5	256x256	6.0	-

b)

Table 1 Parameters of the MR Protocols
Acquisition Parameters are shown for the baseline and follow up protocols in Tables a) and b) respectively. Abbreviations; TR= repetition time, TE = Echo time, FOV = field of view, ms = milliseconds, cm = centimetres, mm = millimetres, FLAIR = fluid attenuated inversion recovery, DWI = diffusion weighted imaging, PWI = perfusion weighted imaging, SE = spin echo, EPI = echoplanar imaging, GRE = gradient echo, NEX = number of excitations, s = seconds

Baseline imaging comprised of DWI, PWI, and T2*-weighted sequences with transient hyperoxia. At follow up a DWI and T2-weighted Fluid Attenuated Inversion Recovery (FLAIR) sequence was performed. DWI was performed with diffusion gradient b values of 0 and 1000 s/mm^2 (to give b0 and b1000 maps). For PWI a Medrad Spectris Solaris® injection system delivered 0.1mmol/kg of the gadolinium based contrast agent Magnevist® through an intravenous catheter (18

gauge) to an antecubital vein at a rate of 5ml/s, with a 10s delay after the initiation of the sequence. This was followed by a 20ml saline flush. Preceding the T2*-weighted acquisition there were 12 seconds of lead in scans to allow for stabilisation of magnetisation and T1 equilibrium, followed by 220 volumes, each with a duration of 3s. Oxygen was transiently administered during the T2*-weighted scanning as detailed in the section entitled 'Oxygen administration'. A second T2*-weighted MR sequence with transient hyperoxia was acquired in cases where it was practically possible (i.e. when there was no pressing time issue for the scanning staff and the subject was stable and settled in the scanner). The DWI at follow up was acquired with an ultrafast sequence using a commercial modification of sensitivity encoding (SENSE)(256) known as ASSET (GE, Milwaukee, USA). Clinical examination at baseline and at day 7, when possible, was performed using the National Institutes of Health Stroke Scale (NIHSS)(257).

2.2.4 Oxygen Challenge

Oxygen was administered via a standard 'Hudson' face mask (Lifecare Clear View Adult Mask) at a rate of 15 litres per minute (l/min) for a period of 5 minutes during the middle segment of the T2*-weighted EPI sequence, which lasted for 11 minutes in total, as demonstrated graphically below (Figure 2-3). In subjects who were scanned with a second T2*-weighted MR sequence, the oxygen was administered at 7l/min. This application of oxygen will be referred to as an 'Oxygen Challenge' throughout the remainder of the text.

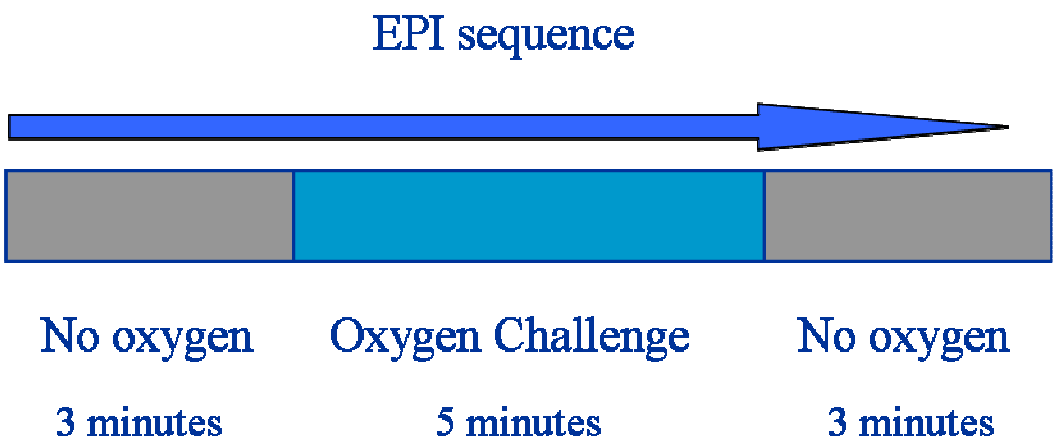

Figure 2-3. Graphical Representation of the Timing of the Oxygen Challenge during the T2*-weighted EPI Sequence.
The Oxygen Challenge was administered during the middle segment of the T2*-weighted EPI sequence. Medical air was administered at other times ie no oxygen = no additional oxygen = FiO_2 = 0.21

At all times when oxygen was not being administered, air was delivered at the same rate as the Oxygen Challenge (i.e. 15l/min). Both oxygen and air were sourced from a gas point located within the MR magnet room (Ohmeda Flowometer, Columbia, USA). Both gases were administered through a common tubing system in order avoid a change of mask or tubing during the sequence. The total length of the tubing (gas point to mask) was 6m for each subject.

2.2.5 Image Processing

Image data were processed on a PC workstation (assembled 'in house') which used a 'Windows™' platform, with a Intel Pentium 4 processor and on a 'Windows™' based laptop computer (Dell Precision M6300, Intel Centrino processor).

2.2.5.1 Processing of Diffusion Weighted Imaging

Delineation of the DWI lesion was performed in 'Stroketool' (Version 2.3, Digital Image Solutions, Germany). Firstly, manual tracing around the hyperintense lesion on the b=1000 image was made. The resulting DWI lesion 'mask' was coregistered to the T2*-weighted EPI data and saved as an 'object map' which

could then be overlaid onto the T2*-weighted EPI, to define the DWI lesion. This process is depicted below (Figure 2-4). When assessing both PWI and DWI data, lesions less than 1cm^3 were excluded from analysis in order to minimise the impact of potential measurement errors and coregistration errors. In addition, in order to avoid susceptibility artefact from the nasal sinuses, segments of lesions which were found anterior to the lateral ventricles at the level of the nasal sinuses were excluded from analysis.

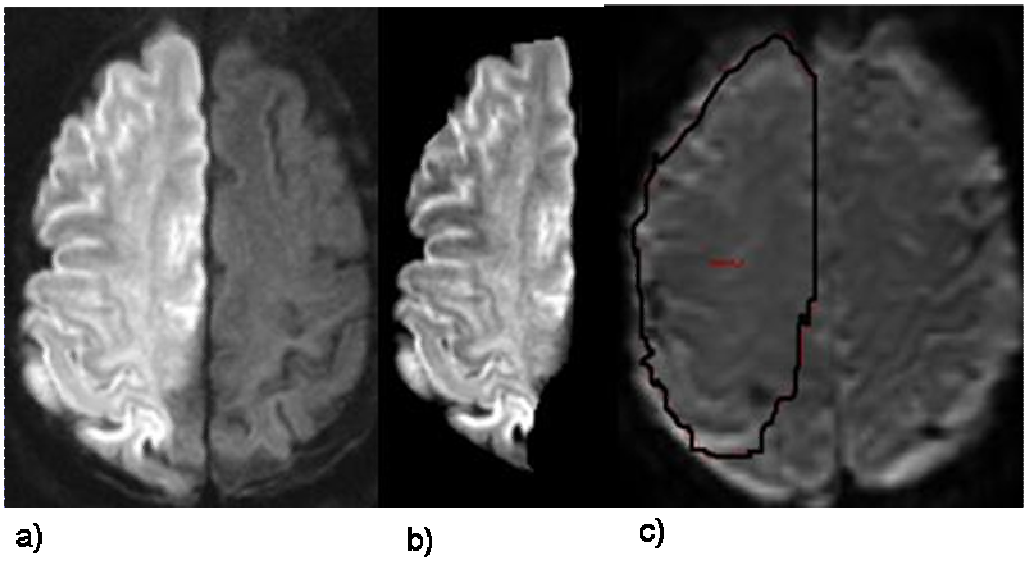

Figure 2-4. Post Processing of the DWI Lesion.
Firstly the raw DWI image (a) was manually segmented (b) and the resulting image was saved as a map, interpolated to the structural space of the T2*-weighted EPI, and overlaid on the EPI (c) so that Oxygen Challenge data for the DWI lesion region could be derived.

2.2.5.2 Processing of Perfusion Weighted Imaging

Thresholded perfusion maps were generated using 'Stroketool' (Version 2.3, Digital Image Solutions, Germany). This package uses the standard Singular Value Decomposition (SVD) methods suggested by Ostergaard(109). An arterial input function (AIF) was selected by identifying multiple voxels from the M1 segment of the contralateral middle cerebral artery (MCA) which exhibited an early and steep decrease in signal intensity. Spatial smoothing using a 3x3 Gaussian kernel was applied, and maps showing delays in TMAX - the peak of the deconvolved tissue concentration curve - were subsequently created on a pixel-

by-pixel basis. Thresholded TMAX maps showing regions with a TMAX of ≥4s were then produced. TMAX values were chosen because of the widespread use in ongoing clinical trials.

2.2.5.3 Processing of T2-weighted Echo Planar Imaging*

Realignment to correct for head motion was performed using SPM2 software (Statistical Parametric Mapping version 2, Wellcome Trust Centre for Neuroimaging, University College London, UK) which was run using the Matlab suite (Version 6.5.1, The MathWorks, Inc. Natick, MA, USA). Firstly, for each image, 6 realignment parameters – in x-, y-, and z-translations and x-y, x-z, and y-z rotations -were determined using 'rigid body transformation'. In SPM2, the highest density of voxel sampling was chosen ('1.00 – Slowest and most accurate'). The original data were then resampled to give true signal changes, corrected for motion, using Fourier interpolation.

2.2.6 Determination of Tissue Compartments

2.2.6.1 Determination of PWI-DWI Mismatch Compartments

The software package 'Analyze' (Version 8.1, Mayo Clinic, and Rochester, USA) was used in order to define tissue compartments and subsequently generate data describing time courses of signal intensity from each predefined compartment.

Four classes of tissue compartment were defined; 1) The DWI lesion, 2) the PWI-DWI Mismatch region, 3) the DWI expansion region and 4) the contralateral 'mirror' region. Definition of the 'DWI lesion' was straightforward and was described in the previous 'Processing of Diffusion Weighted Imaging' section.

Subjects with PWI-DWI mismatch were identified by first reviewing the PWI and DWI together, side by side, and excluding cases where a PWI-DWI mismatch clearly did not exist. For the remaining cases, definition of the PWI-DWI

mismatch tissue compartment required the PWI and DWI data to be in the same structural space. Therefore, coregistration of the raw PWI data to the raw DWI data was performed using 'windowed sinc' interpolation and application of additional manual refinement in the coronal, transverse or saggital directions was performed if necessary. The transformation matrix derived from this step was applied to the thresholded TMAX maps so that they too were transformed into DWI structural space. Next, the thresholded TMAX and DWI maps were reviewed together, in the same structural space. If the deficit on TMAX was greater than on DWI, a mismatch existed, and this was manually delineated to create a map which defined the PWI-DWI mismatch region.

2.2.6.2 Determination of DWI Expansion Compartments

In order to determine areas which were initially normal on DWI, but which subsequently became abnormal on the 72h examination, an identical approach was used to that described above but this time the follow up DWI data was co-registered to the baseline DWI data.

2.2.6.3 Determination of 'Penumbral' Compartments

Tissue compartments representing the 'ischaemic penumbra' were defined as the PWI-DWI mismatch regions, or, if these were unavailable, regions of DWI expansion.

2.2.6.4 Determination of the Contra-lateral 'Mirror' Region

The contralateral T2*-weighted signal intensity-time curve was used as internal control. Using 'Analyze', the object map delineating the region of interest was reflected 180°, and manually placed on the contra lateral hemisphere in the T2*-weighted image in a symmetrical region.

2.2.7 Generation of Signal Intensity Time Series

Next, it was necessary to produce a time series of signal intensity measurements (which we will call the 'T2*-weighted signal intensity-time curve') from the specific tissue compartments detailed above

To do this the 'map' representing the tissue compartment of interest e.g. PWI-DWI mismatch area identified in the previous steps, was co-registered onto the realigned T2*-weighted EPI data. The coregistration method used was identical to that used to coregister PWI to baseline DWI data, and follow up DWI to baseline DWI data, and is detailed in section entitled 'Determination of Tissue Compartments'. After the co-registration step, the tissue compartment of interest was saved as an 'object map' and overlaid onto the T2*-weighted EPI (Figure 2-4). Analyze software then produced a time series for the T2*-weighted signal intensity from regions defined by the object map (i.e. the tissue compartment). These were then saved into a Microsoft Excel™ spreadsheet (Microsoft Office 2003).

2.2.8 Derivation of Measurements

Graphical illustration of the measurement of the curve parameters is illustrated below (Figure 2-6). Measurements were performed on data smoothed using the previously determined wavelet transform scale. Only 'good quality' curves were assessed. The criterion for quality of a T2*-weighted signal intensity-time curve for any given region of interest was that at least a 1% T2*-weighted signal change after Oxygen Challenge should have been observed in the contra-lateral 'mirror' region.

2.2.8.1 Area Under the Curve (AUC)

In order to measure the magnitude of signal change induced by the oxygen challenge, measurements of the area under the T2*-weighted signal intensity-

time curve were made using the software package 'GraphPad Prism version 5.00 for Windows' (GraphPad Software, San Diego California USA, www.graphpad.com). Each individual time series was normalised to its own baseline, so that any signal change was expressed as a percentage change from baseline (100*[value-baseline]/baseline) [Graphpad v5.00].The baseline was defined as the mean signal intensity of the first 60 time points (180s) (i.e pre-oxygen challenge). The trapezoid rule was used for the AUC calculation (Graphpad v5.00). The time points for which AUC measurements were made were those corresponding to oxygen challenge i.e. 181s to 480s.

The overall 'direction' of change in T2*-weighted-signal intensity after oxygen challenge was classified by identifying a clear predilection for a change in one particular direction while accounting for the possibility that there may have been minor fluctuations in the opposite direction due to noise. Therefore, the direction was classified as 'positive' if the combined AUC value for the negative peaks was <25% of the combined AUC value for the positive peaks during the period of the OC, and vice versa for a 'negative' direction. Curves fulfilling neither of these definitions were classified as 'flat'.

2.2.8.2 Gradient of Incline of the Curve (GIC)

Graphpad Prism was also used for this analysis. The gradient of the incline of the curve (GIC) was measured to derive a measure of the rate of increase of signal intensity. In order to determine which section of the incline of the curve to measure, the first time point of measurement was chosen by the calculation of the hypothetical time of first arrival (FAT) of hyperoxic blood to the brain. Determination of this point was calculated as 21 seconds by the following method based on values quoted for the standard adult male.

Time Taken to flow through oxygen tubing = 1.90s

$$= \frac{\text{Rate of oxygen flow}}{\text{Area of tubing}}$$

$$= \frac{15\text{l/min}}{\pi r^2 * h}$$

$$= \frac{250\text{cm/s}}{3.146 * 0.5*0.5*600}$$

= 1.9 seconds

where π = Pi, r= radius of tubing, h = length of tubing, cm =centimetres, s=seconds

Time from oxygen mask to small airways = 1.85s

- derived from values suggested by Gast et al(258), with the upper limits reference ranges

Time for oxygen to diffuse across alveolus = negligible = rounded to 0s

Time taken from lungs to left ventricle = 3.25s

$$= \text{Pulmonary circulation time(259)} * 0.5$$

$$= \frac{\text{volume of blood in pulmonary circulation}}{\text{Cardiac output}} * 0.5$$

$$= \frac{0.83l}{2 * 6.48l/min}$$

$$= 3.25s$$

Time Taken from Left Ventricle to Carotid artery *= 1.5s(259)*

Time to Traverse Cerebral Circulation *= 8.5s(259, 260)* (artery to vein)

Perfusion Delay typically seen in Stroke Subjects *= 4s*

Total Time *= 21s*

Next, the second point was defined arbitrarily as the duration of 2 FATs i.e. 42 seconds, equivalent to 14 measured time points. This broadly coincided with the plateau point of the averaged T2*-weighted signal intensity curve from the contralateral hemisphere of included subjects. Linear regression analysis of the data values between the two defined points was performed to derive a value for the 'slope' (Graphpad) which was termed the 'gradient of the incline' (GIC). An assessment of other final time points was made in order to ensure that results of comparative statistical tests did not vary with a change of final time point.

2.2.8.3 Time to Maximum Signal (TMS)

The time taken between the onset of the oxygen challenge and the time at which maximum signal was derived was measured.

2.2.8.4 Percentage Signal Change (PSC)

Percentage signal change (PSC) was calculated using the data normalised to the individual baseline as described in the section entitled '*Area Under the Curve)*. This was defined as the maximum value of signal measured after the onset of oxygen.

2.2.9 Data Smoothing

Data smoothing using wavelet transforms was performed on the premise that high frequency noise may impair the ability to accurately measure certain components of the T2*-weighted signal intensity-time curve. Wavelet transforms aim to reduce meaningless noise in data whilst retaining genuine physiological information. They simultaneously assess not only the frequency of signals forming the time series, as is done by the Fast Fourier Transform, but also the temporal location within the time series where such signals are present.

The statistical package 'R: A Language and Environment for Statistical Computing, Austria' (version 2.6.1) was used to run 'Waveslim' (version, 1 .6.1, Brandon Whitcher, UK) and a code written 'in house' (supplied by Martin Shaw, University of Glasgow, see Acknowledgements), in order to apply basic discrete wavelet transforms. This package allows 5 degrees of smoothing (scales of wavelet transform) to be implemented.

The particular scale of wavelet transform to be used in this study was determined. The ideal degree of wavelet smoothing was pre-specified to be one which allowed measurement of parameters which may otherwise be affected by high frequency noise, whilst having minimal effect on parameters which should be less sensitive to high frequency noise. We used the gradient of the incline of the T2*-weighted signal intensity-time curve as the 'noise sensitive' parameter, and the area under the T2*-weighted signal intensity-time curve (AUC) as the 'noise insensitive' parameter (see the following 'Derivations of Measurements' section for definitions of these parameters). Therefore, the ideal scale was defined as the one which demonstrated the gradient of incline of all curves to be

different from zero, but with no statistical differences between the measured AUC values on smoothed and unsmoothed data.

To determine the scale, the T2*-weighted signal intensity-time curves from the ‘mirror’ regions contralateral to the DWI lesion region were assessed (n=17). Analysis was performed in two phases (Figure 2-5).

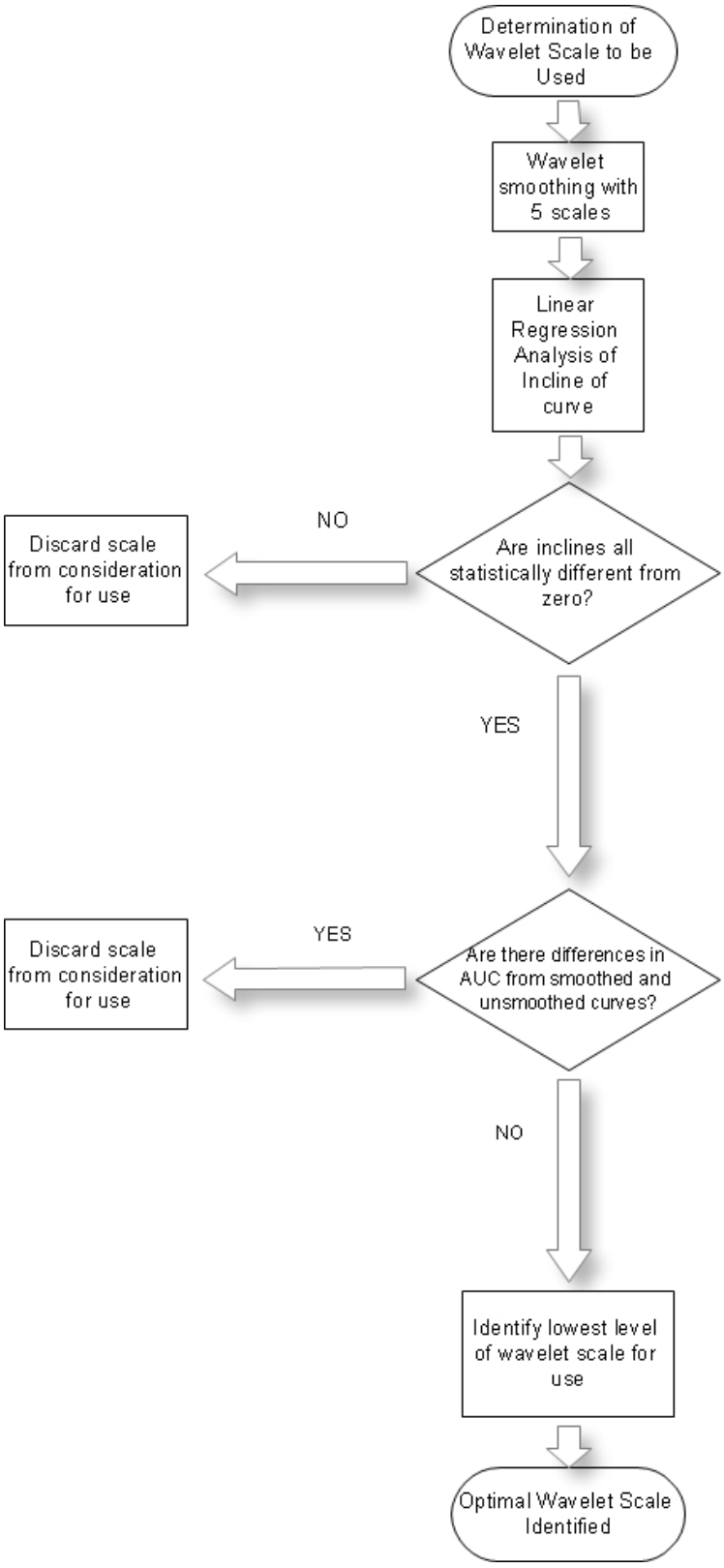

Figure 2-5. Determination of the Wavelet Scale to be Used.
AUC = area under the curve

1) **Which wavelet scales smooth sufficiently to demonstrate a signal increase?** Firstly, it was assumed that there would be an increase in T2*-weighted signal intensity after Oxygen Challenge in all 'mirror' regions. Therefore, the scale which gave rise to the most number of T2*-weighted signal intensity-time curves which had gradient of incline statistically different from zero, was identified. Statistical significance of linearity was determined by the application of linear regression ('GraphPad Prism version 5.00 for Windows' ,GraphPad Software, San Diego California USA, www.graphpad.com), with statistical significance denoted by $p<0.05$.

2) **Which wavelet scales do not alter 'Area Under the Curve' measurements**? Next, using the wavelet scales identified from step 1, the AUCs from smoothed curves were compared to the AUCs from the unsmoothed curves using a one way analysis of variance (ANOVA) with post hoc testing using a Dunnet's analysis(StatsDirect Ltd. StatsDirect statistical software. http://www.statsdirect.com. England: StatsDirect Ltd. 2008. Assessment of normality was performed using a Shapiro-Wilk analysis.

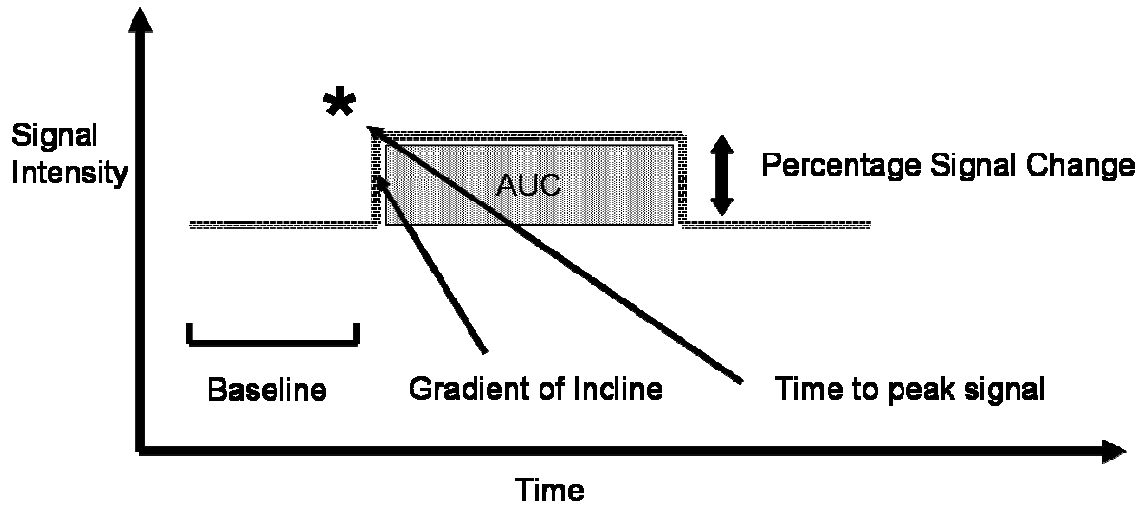

Figure 2-6. Definition of Measured Parameters.
A hypothetical signal-time curve illustrating the measurement of the parameters previously discussed. Broken line = hypothetical T2* signal-time curve, arrows = annotation, *=time to peak signal. AUC = area under the curve

2.2.10 Statistical Analysis

Statistical testing was performed using Statsdirect (StatsDirect Ltd. StatsDirect statistical software. http://www.statsdirect.com. England: StatsDirect Ltd. 2008). Statistical significance was set at $p<0.05$. The parameters measured from the signal-time curves generated from the tissue compartments of interest were compared to those from normal tissue using paired t-tests if data was of normal Gaussian distribution, or using the Wilcoxon signed ranks test if data was non-parametric. Non-normality was determined using a Shapiro-Wilk test.

2.3 Results

2.3.1 Data Acquisition and Completeness

Thirty three subjects with a provisional clinical diagnosis of acute ischaemic stroke were recruited by KD (thesis author) in the 23 month time period previously specified. An additional 2 subjects (Subjects 1 and 2) were recruited by the preceding Research Fellow giving a total of 35 subjects (Table 2). Subject 1 also participated in a separate clinical trial(261) with imaging end points. Baseline clinical data were available for all subjects at the time of recruitment. T2*-weighted Oxygen Challenge data were acquired in 32/35 subjects. The remaining three subjects (9%) did not tolerate the MRI procedure for reasons unrelated to the Oxygen Challenge (subjects 3, 7, 15). Twenty five subjects underwent PWI successfully. Reasons for not performing PWI were those of technical or logistical problems (subjects 8, 11, 21, 27), non completion of the T2* weighted oxygen challenge scan (subjects 3, 7 and 15), and impaired renal function of subjects (subjects 17, 23, 30). Follow up imaging was performed in 26 subjects as near as possible to 72h (Days 2-4). Nine subjects did not achieve this for the following reasons; non-completion of the baseline oxygen challenge T2*-weighted scan (Subjects 3, 7, 15), death prior to the follow period (Subject 9), access to the scanner (Subjects 11, 24), non stroke diagnosis being made between baseline and follow up periods (Subject 27) and transfer to a geographically distinct treatment facility prior to the follow up period (Subject

29, 34). Follow up NIHSS for subject 1 was not performed at day 7, but a day 3 NIHSS was collected for this subject for another study. Three subjects died before the day 7 NIHSS clinical assessment (Subjects 3, 7, 9), one subject did not complete baseline oxygen challenge T2* weighted scan (Subject 15), and one subject was subsequently judged to have a non-stroke diagnosis (Subject 27). Six other subjects did not under go NIHSS follow up for reasons of geographical inaccessibility, owing to either hospital discharge or transfer to the referring district hospital. One of these (Subject 29) however had an NIHSS of 0 on Day 1. Therefore NIHSS assessment at follow up (at some point) was performed for 25 subjects.

	Subject	Gender	Age	OCSP	Time to Imaging (hrs)	NIHSS (arrival)	NIHSS (Day 7)	rtPA Given?	Scanned Day 1 & 3?	PWI Performed
*	1	Female	55	TACS	30	14	17 (Day 3)	Yes	Yes	Yes
*	2	Male	79	PACS	24	1	0	No	Yes	Yes
	3	Male	86	TACS	24	15	Deceased	No	No	No
*	4	Male	64	PACS	4.25	8	0	Yes	Yes	Yes
*	5	Female	67	TACS	22.25	20	6	Yes	Yes	Yes
*	6	Male	68	TACS	26	20	20	Yes	Yes	Yes
	7	Male	58	TACS	26.5	18	Deceased	No	No	No
	8	Female	73	TACS	21.25	10	0	Yes	Yes	No
	9	Male	76	TACS	18.5	19	Deceased	No	No	Yes
*	10	Female	75	PACS	25	5	0	No	Yes	Yes
	11	Male	52	PACS	18.5	6	*	No	No	No
*	12	Male	64	TACS	18	5	0	Yes	Yes	Yes
*	13	Female	61	PACS	18	2	2	No	Yes	Yes
*	14	Male	89	PACS	23	2	0	Yes	Yes	Yes
	15	Male	73	TACS	21	22	*	Yes	No	No
*	16	Female	67	PACS	18	16	*	No	Yes	Yes
	17	Male	85	TACS	5	21	13	No	Yes	No
*	18	Male	52	TACS	5.5	20	15	Yes	Yes	Yes
*	19	Female	53	TACS	5.5	21	1	Yes	Yes	Yes
*	20	Male	54	PACS	4.75	4	0	Yes	Yes	Yes
	21	Male	79	TACS	6.5	17	18	Yes	Yes	No
*	22	Male	64	PACS	27	9	8	No	Yes	Yes
	23	Female	75	TACS	23	18	18	No	Yes	No
	24	Female	79	PACS	21	3	0	Yes	No	Yes
*	25	Male	67	PACS	5.75	6	0	Yes	Yes	Yes
*	26	Female	95	TACS	6.25	20	0	Yes	Yes	Yes
	27	Male	72	PACS	8.5	2	n/a	No	No	No
*	28	Male	78	PACS	24	13	*	No	Yes	Yes
	29	Male	54	PACS	13.5	3	0 (Day 1)	No	No	Yes
	30	Male	78	TACS	4.5	20	20	Yes	Yes	No
*	31	Male	67	TACS	20	6	*	No	Yes	Yes
*	32	Male	85	TACS	18	17	32	Yes	Yes	Yes
	33	Female	60	TACS	6.75	21	19	Yes	Yes	Yes
	34	Female	70	PACS	7	7	*	Yes	No	Yes
*	35	Male	69	PACS	7.5	3	1	No	Yes	Yes

Table 2 Basic Clinical and Demographic Data for All Recruited Subjects
OCSP = Oxfordshire Community Stroke Project (2) classification. TACS = total anterior circulation stroke, PACS = partial anterior circulation stroke. LACS =lacunar stroke syndrome. NIHSS = National Institutes of Health Stroke Scale(257), rtPA = recombinant tissue plasminogen activator, PWI = perfusion weighted imaging. * indicated subjects in whom the entire imaging protocol was completed.

2.3.2 Basic Clinical and Radiological Data

There were 23 males and 12 females, whose mean age was 70yrs (range 52-95 years). A 'Total Anterior Circulation Syndrome' (TACS) was seen in 19 subjects and a 'Partial Anterior Circulation Syndrome' (PACS) in 16 subjects. Median time to imaging was 18h (interquartile range [IQR] 6.5-23h) with 13 subjects imaged at less than 9 hours post ictus. Five subjects (Subjects 1,6,7,10 and 22) were

imaged marginally beyond 24h; although these subjects were consented in anticipation of scanning before 24h there were practical difficulties associated with access to the scanner. rtPA was administered in 18 (51%) of subjects (all prior to study specific procedures). Median NIHSS on admission and at the time of scanning was 13 (IQR 5-20, n=35) and 8 (IQR; 2-18, n=31) respectively. Of the 23 subjects for whom NIHSS was measured at both the time of the baseline scan and at 7 days, 15 demonstrated an improvement, 5 were static, and 3 deteriorated. Of those who improved, 9 subjects improved by 4 or more units on the NIHSS. When DWI lesion volume was assessed, it was too small to attempt measurement in 2 subjects, and did not represent stroke in one subject (subject 27). When the remaining 32 subjects were considered, the median lesion volume was 12cc (IQR 3.4 – 280cc). Basic clinical data are summarised (Table 2).

Of the 35 subjects recruited, data from 25 were analysed. A summary for these twenty five subjects is presented separately in Appendix E. Cases which were not analysed were those where there was stroke related patient agitation necessitating scan termination (Subjects 3,7,15), lack of a confluent lesion >1ml (Subjects 4,10,13,14,20,25), and final non-stroke diagnosis (Subject 27). Based on the thresholded TMAX maps, 7 of these 25 subjects had PWI-DWI mismatch, 3/25 had no demonstrable perfusion deficit, even on unthresholded maps (Subjects 24,28, and 31), and the remainder had matched PWI-DWI deficits. Eighteen out of 25 subjects provided baseline data which met the stipulated quality criteria. The proportion of ROIs included was 17/25 for DWI lesions, 6/7 for mismatch regions, and 3/4 for DWI expansion regions. Evaluable possible regions of penumbra (PWI-DWI mismatch or, if unavailable, regions of DWI expansion) were detected in 8 subjects (subjects 1,5,16,18,22,30,33,35).

2.3.3 Determination of Optimal Wavelet Scale to be Used

An illustration of data smoothing with different wavelet scales is shown below (Figure 2-7) using the T2* signal intensity curve in normal tissue from subject 11 as an example. It is clear that the time series become smoother as the scale of wavelet transform is increased.

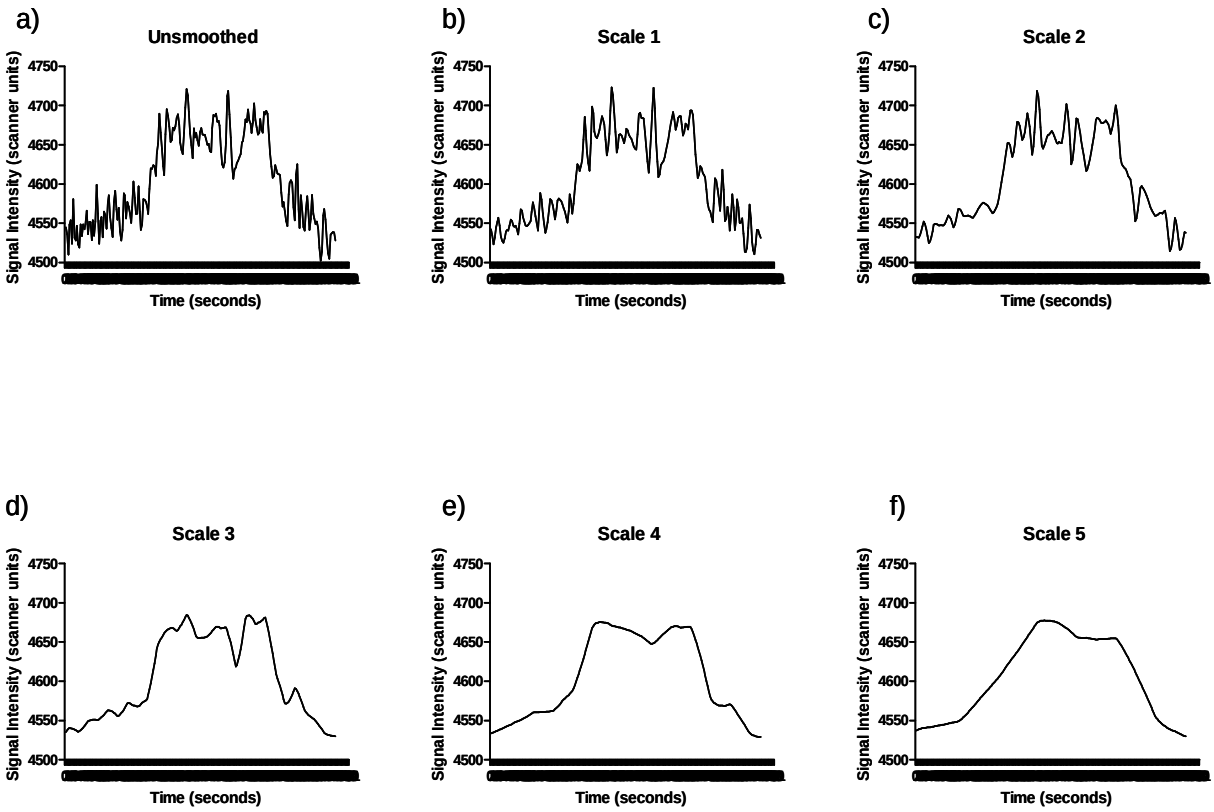

Figure 2-7. Illustration of Smoothing of T2*-Weighted Signal Intensity-Time Curves by Wavelet Transforms
Graphs a) through f) demonstrate progressively increasing degrees of smoothing by wavelet transforms (unsmoothed, and wavelet scales 1-5)**.** The signal time curves are derived from normal tissue in Subject 11. The Y-axis of the graphs represents signal intensity in scanner units, and the X-axis denotes time. The time points of the application of hyperoxia are not illustrated in this example.

2.3.3.1 Gradient of Incline Assessment

At wavelet scale 3 and greater, all subjects demonstrated a GIC of the T2* signal intensity curve in normal tissue which was statistically different from zero (Table Y). Therefore wavelet scales 3, 4, and 5 were considered further.

Wavelet Scale	No. of Subjects with a GIC with no statistical difference from zero
No smoothing	6
First scale	3
Second Scale	3
Third Scale	0
Fourth Scale	0
Fifth Scale	0

Table 3 Effect of Smoothing by Wavelet Transform on Gradient of Incline Assessment
GIC = gradient of the incline of the time –signal curve

2.3.3.2 Area Under the Curve Assessment

Calculation of the AUC was performed for T2* signal intensity curves smoothed with wavelet scales 3, 4, and 5. One way ANOVA and post hoc testing with Dunnet's analysis, comparing smoothed to unsmoothed data, did not reveal any statistical difference between the AUC from data smoothed with any of the wavelet scales used, from the AUC from unsmoothed data ($p \geq 0.99$ for each of scales 3, 4, and 5).

2.3.3.3 Optimal Wavelet Scale for This Study

Given that data sets smoothed with wavelet scales 3, 4, and 5 showed a significant GIC for all subjects, and AUC was not significantly different from that from the unsmoothed data sets, all 3 of these scales could be used, according to the predefined criteria for selection. In order to use the scale with least attenuation of the data, a **third scale wavelet** was chosen as the preferred wavelet scale in this study.

2.3.4 Assessment of the Optimal Length of Curve for Measurement of GIC

Analysis by one way ANOVA with post hoc testing using a Tukey's test for multiple comparisons did not reveal any statistical differences between the values for the GIC when measured for a duration of 21s, 31s and 42s (equivalent to 1, 1.5 and 2 FATs). These results were applicable for each wavelet scale. Therefore the longest duration was arbitrarily chosen [**a duration of 42s** (2 FATs)] was used to measure GIC in this study.

2.3.5 T2*-weighted Signal Intensity Curves in DWI Lesions

2.3.5.1 Direction of T2-weighted Signal Intensity Time Curves from the DWI Lesion*

According to the arbitrary definitions of 'positive', 'flat' and 'negative' curves which were stipulated in the 'Methods' section, T2* signal intensity curve AUC values were 'positive' from the DWI lesions of 10 subjects, 'negative' in 3 subjects, and 'flat' in 4 subjects. The AUC of T2* signal intensity curves from normal tissue was positive in all subjects. The figure below (Figure 2-8) shows the AUC for curves in areas of normal tissue and DWI lesions. The AUC is stated as a vertical vector to indicate the predominant direction of change, where the value of the AUC given is that of the 'positive' value minus that of the 'negative' value compared to the baseline. The AUC value of the T2*-weighted signal intensity curve from the DWI lesion was greater than that from normal tissue in one case (Subject 28). In every other case the AUC was substantially greater in normal tissue compared to that in the DWI lesion.

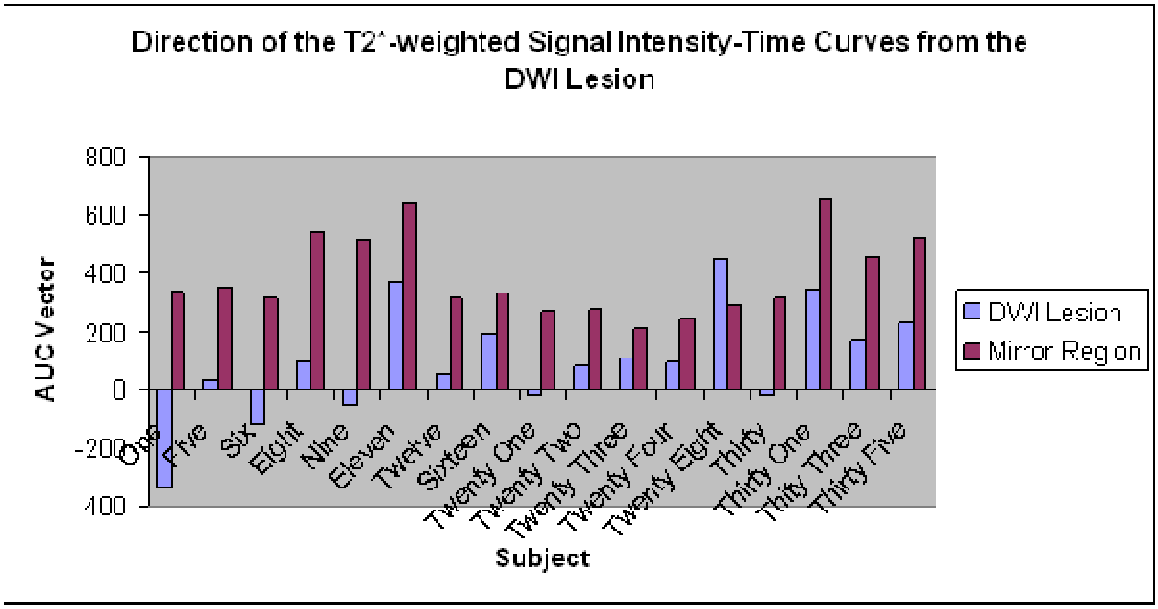

Figure 2-8. Direction of the T2*-weighted Signal Intensity-time Curve from DWI Lesions. Individual subjects are described on the x-axis, and the AUC is described on the Y axis. The AUC value given is that of the 'AUC of the positive curve' minus 'AUC of the negative curve' in order to give a summary of the vertical vector of the direction of change. Maroon bars represent the AUC with regards to signal intensity curves in normal tissue, and the blue bars correspond to the DWI lesion. Bars above the x axis indicate that the predominant direction of signal change with oxygen was positive (i.e. an increase), and those below the x-axis a negative change (i.e. a decrease). The 'positive' curves were seen from Subjects 11,12,16,22,23,24,28,31,33,35. The 'negative' curves were seen in subjects 1,9, and 30. The 'flat' curves were seen from subjects 5,6, 8, and 21.

2.3.5.2 Measurement of Parameters of the T2-weighted Signal Intensity Time Curves from the DWI Lesion*

Individual T2*-weighted signal intensity-time curves from the DWI lesion are illustrated in and summary averaged curves presented in . Raw data for T2*-weighted signal intensity PSC and for GIC/AUC/TMS are given in and respectively.

Compared with contralateral tissue, the T2*-weighted signal intensity-time curves from DWI lesions of 17 subjects exhibited smaller AUC (p=0.0001, Wilcoxon), less steep GIC (p=0.0032, Wilcoxon), later time to maximum signal (TMS; p=0.04, Wilcoxon) and smaller percentage signal change (PSC; p=0.0008, Paired t-test). From this group there were 3 evaluable ROIs with no demonstrable perfusion deficit (subjects 24, 28, 31); the curve from two of these small DWI lesion regions (subjects 24 and 31) also had this pattern of lesser AUC, lesser GIC, longer TMS and smaller PSC.

When only curves with non-negative AUC were analyzed, these differences remained significant for all but TMS (p=0.1). When only positive curves were analysed, there were still differences between hemispheres for AUC (p=0.003, paired t-test) and TMS (p=0.008 Wilcoxon). However such differences did not reach significance for PSC (p=0.08, Wilcoxon, less in 9/10 cases) and GIC (p=0.08, paired t-test, less in 9/10 cases).

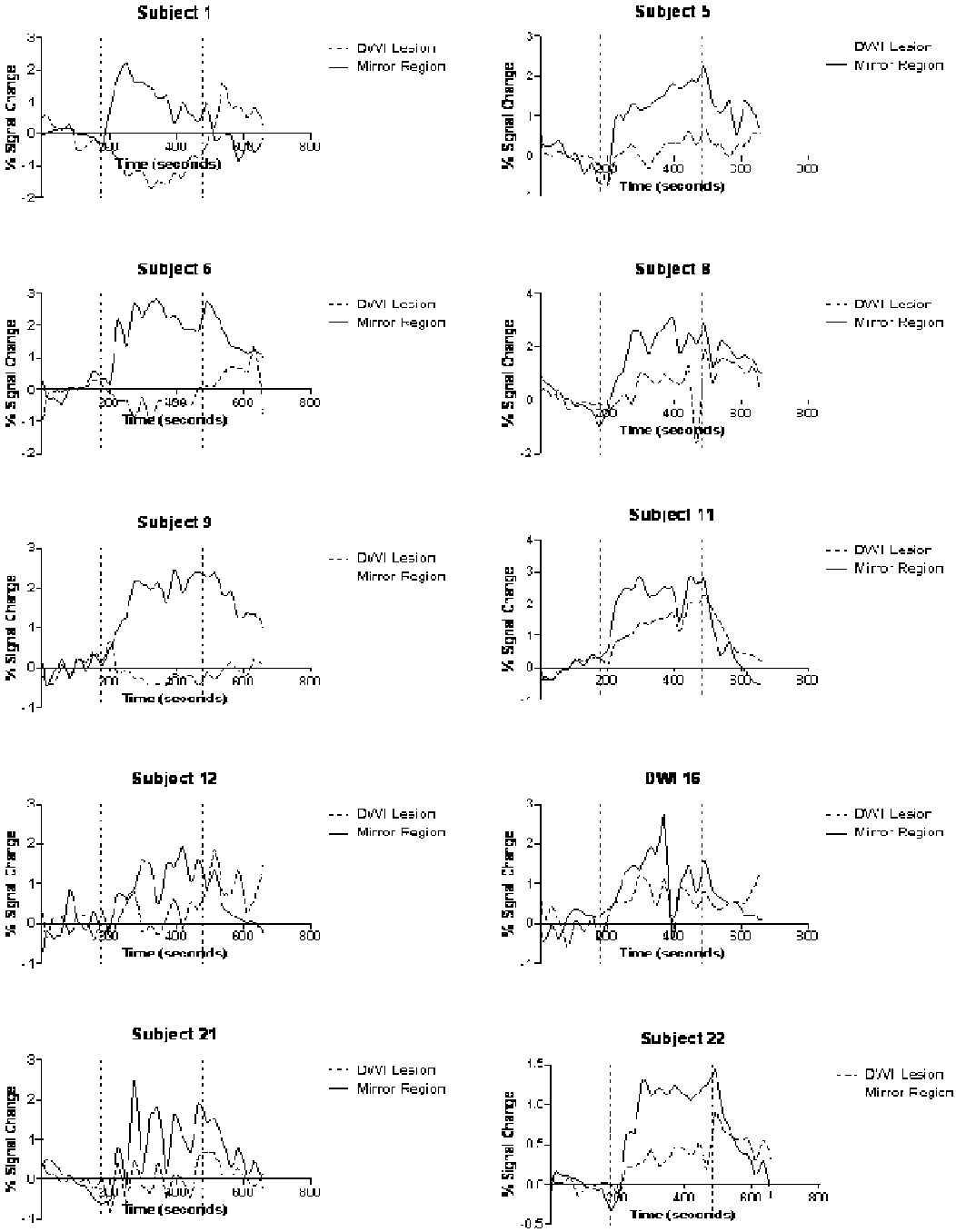

Figure 2-9. T2*-Weighted Signal Intensity-Time Curves from the DWI Lesion of Individual Subjects

The x-axis represents time (seconds) and the y-axis represents % T2*-signal change from the baseline. Vertical broken lines represent the onset and cessation of the oxygen challenge. The solid and broken lines represent the T2*-weighted signal intensity-time curve from the contra-lateral mirror region and the DWI lesion respectively. Reproduced with permission John Wiley and Sons from 'T2*-weighted magnetic resonance imaging with hyperoxia in acute ischemic stroke: Annals of Neurology: 2010.

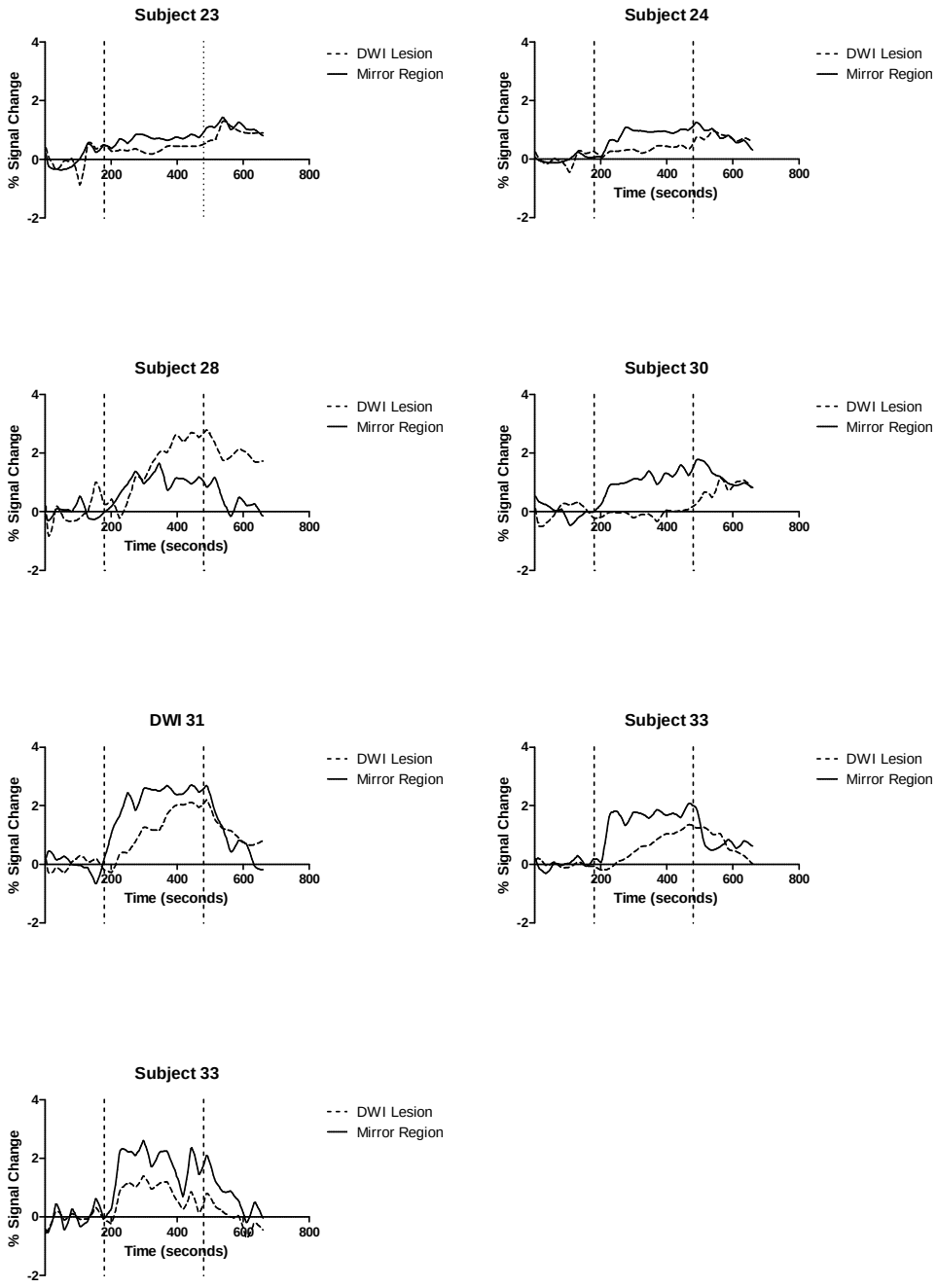

(cont.)

The x-axis represents time (seconds) and the y-axis represents % T2*-signal change from the baseline. Vertical broken lines represent the onset and cessation of the oxygen challenge. The solid and broken lines represent the T2*-weighted signal intensity-time curve from the contra-lateral mirror region and the DWI lesion respectively.

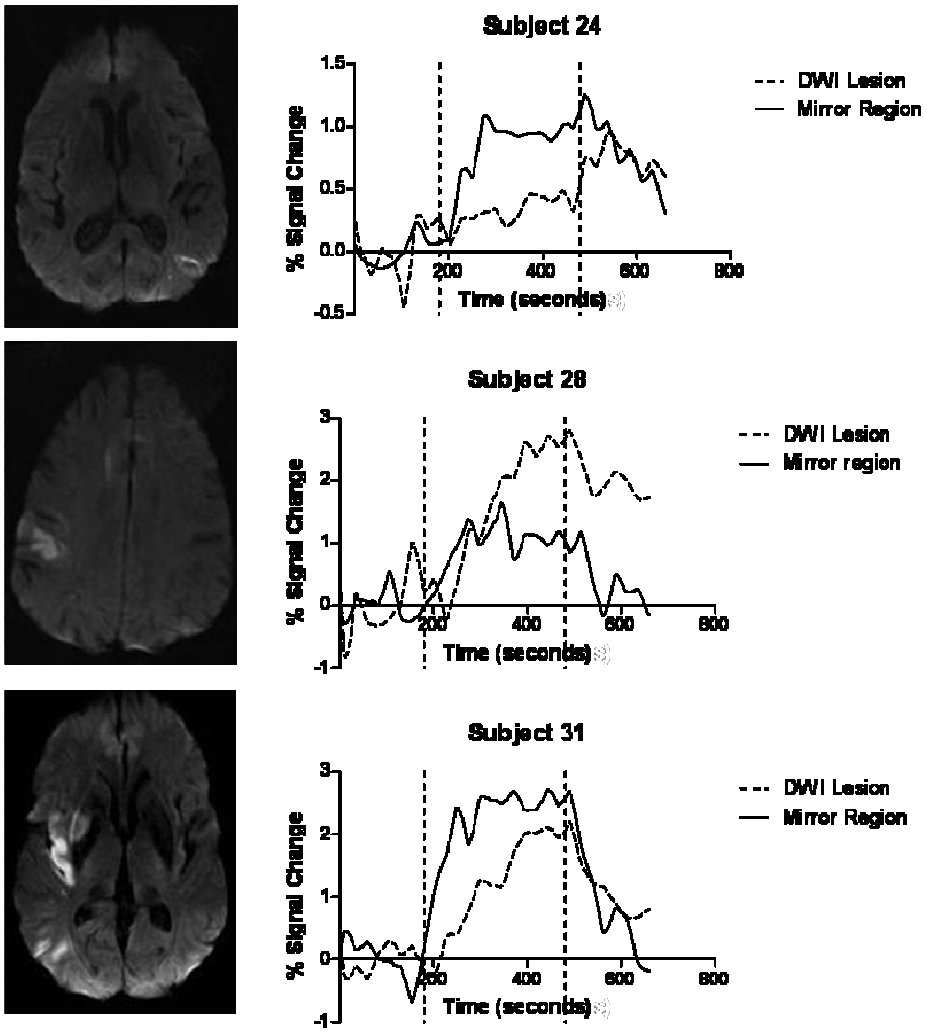

Figure 2-10. T2*-weighted Signal Intensity-Time Curves from DWI Lesions without Demonstrable Perfusion Deficit.
Images on the left hand side are from Diffusion Weighted Imaging (DWI). For the graphs, the x-axis represents time (seconds) and the y-axis represents % T2*-signal change from the baseline. Vertical broken lines represent the onset and cessation of the oxygen challenge. The solid and broken lines represent the T2*-weighted signal intensity-time curve from the contra-lateral mirror region and the DWI lesion respectively.

2.3.5.3 Measurement of Parameters of the T2-weighted Signal Intensity Time Curves from the 'Penumbral' Region*

Whole group analysis revealed no statistical differences between hemispheres with respect to AUC, GIC, TMS and PSC for 'penumbral' ROIs. However, when considering only the ROIs from subjects imaged in the hyperacute phase (<8h), 1 curve had a negative AUC (subject 30, lesion-growth ROI), and 3 had positive AUCs (subject 18 lesion-growth ROI, subject 33 and 35 mismatch ROIs). Positive

signal change was greater in the mismatch region compared to the contralateral side in all 3 of these hyperacute, positive AUC subjects: (Subject 18 Lesion Growth ROI; 1.8 vs 1.1%, Subject 33 Mismatch ROI; 2.6 vs 2.1%, Subject 35 Mismatch ROI; 5.1 vs 1.8%). Individual T2*-weighted signal intensity-time curves are illustrated in and summary curves in . Raw data for T2*-weighted signal intensity PSC and for GIC/AUC/TMS are given in and respectively.

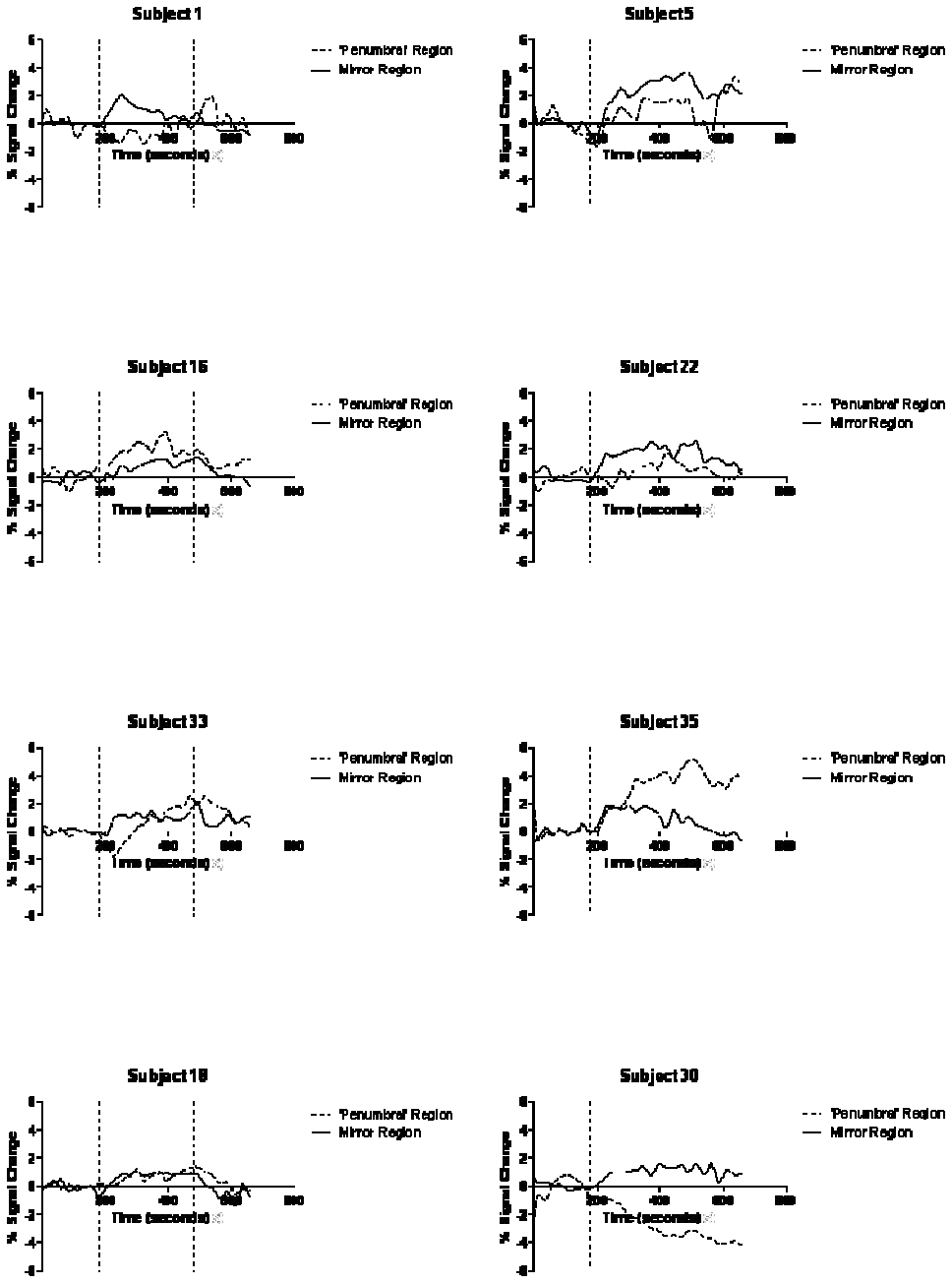

Figure 2-11. T2*-weighted Signal Intensity-Time Curves from the 'Penumbral' Region of Individual Subjects

The 'penumbra' region was that of DWI expansion for Subjects 18 and 30 (bottom row) and was 'PWI-DWI' mismatch for the remainder. The x-axis represents time (seconds) and the y-axis represents % T2*-signal change from the baseline. Vertical broken lines represent the onset and cessation of the oxygen challenge. The solid and broken lines represent the T2*-weighted signal

intensity-time curve from the contra-lateral mirror region and the DWI lesion respectively. Reproduced with permission John Wiley and Sons from ‘T2*-weighted magnetic resonance imaging with hyperoxia in acute ischemic stroke: Annals of Neurology: 2010.

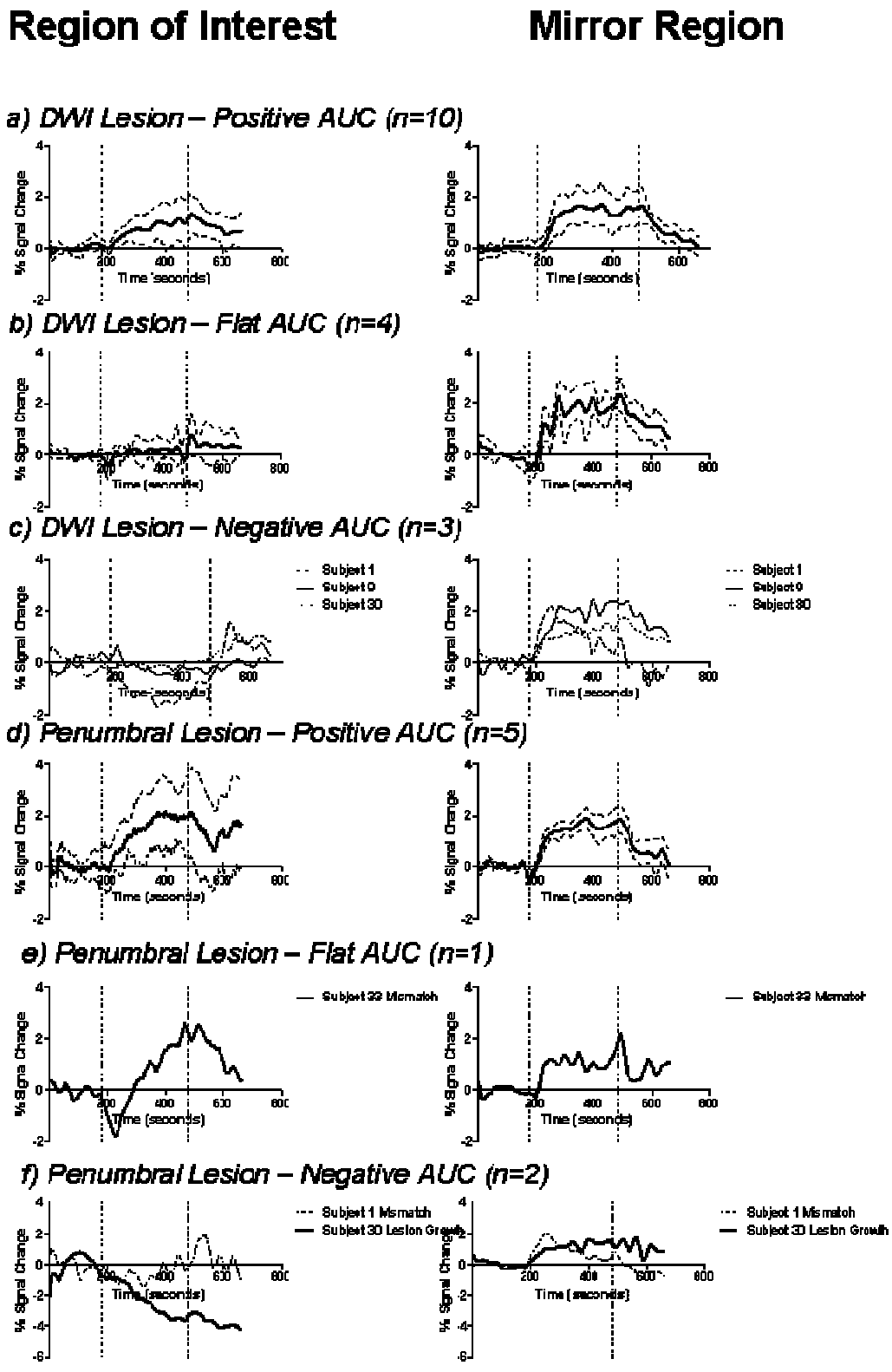

Figure 2-12. Summary T2*-Weighted Signal Intensity Time Curves Categorised by Predominant Direction of Signal Change and by tissue Compartment.

In Panels (a), (b), and (d) the solid line represents the T2*-signal intensity-time curve and the broken lines represent the error (standard deviation) bars. The x-axis represents time (seconds) and the y-axis represents % T2*-signal change from the baseline. Vertical broken lines represent the onset and cessation of the oxygen challenge. Reproduced with permission John Wiley and Sons from 'T2*-weighted magnetic resonance imaging with hyperoxia in acute ischemic stroke: Dani et al Annals of Neurology: 2010.

	DWI Lesion			Mismatch Region			DWI Expansion Region		
Subject	**Lesion Vol. (ml)**	**PSC (%) T2* (ipsi/contra)**		**Lesion Vol. (ml)**	**PSC (%) T2* (ipsi/contra)**		**Lesion Vol. (ml)**	**PSC (%) T2* (ipsi/contra)**	
Subject 1	103	-1.7	2.21	14	-1.45	2.1			
Subject 2	6	u/e	u/e						
Subject 5	106	0.71	2.26	12	3.3	3.7	10	1.93	2.32
Subject 6	102	-1	1.9				24	u/e	u/e
Subject 8	56	1.88	3.14						
Subject 9	244	0.67	2.46						
Subject 11	25	2.27	2.88						
Subject 12	44	1.84	1.96						
Subject 16	88	1.23	2.81	17	3.2	1.5			
Subject 17	3	u/e	u/e						
Subject 18	17	u/e	u/e	u/e	u/e	u/e	21	1.77	1.1
Subject 19*	6	u/e	u/e						
Subject 21	142	0.68	2.46						
Subject 22	62	0.91	1.43	19	1.8	2.6			
Subject 23	12	1.3	1.43						
Subject 24	3	0.95	1.25						
Subject 26	2	u/e	u/e						
Subject 28	22	2.79	1.65						
Subject 29	7	u/e	u/e						
Subject 30	55	-0.33	1.79				10	-4.15	1.75
Subject 31	13	2.2	2.71						
Subject 32	60	u/e	u/e						
Subject 33	81	1.36	2.08	5	2.6	2.1			
Subject 34	6	u/e	u/e						
Subject 35	14	1.4	2.61	6	5.1	1.8			
Mean (SD)	**51 (57)**	**1.0 (1.2)**	**2.2 (0.6)**	**12.2 (5.7)**	**2.4 (2.2)**	**2.3 (0.8)**	**16 (7)**	**-0.15 (3.5)**	**1.7 (0.6)**

Table 4 Raw Data for T2* Percentage Signal Change for Each Tissue Compartment
Negative values indicate a signal decrease. PSC = percentage signal change, ipsi = ipsilateral hemisphere, contra = contra-lateral hemisphere, Vol. = volume, DWI = diffusion weighted imaging, ml = millilitres, SD = standard deviation, u/e = unevaluable. Reproduced with permission John Wiley and Sons from 'T2*-weighted magnetic resonance imaging with hyperoxia in acute ischemic stroke: Annals of Neurology: 2010.

	DWI Lesion								Mismatch Region								DWI Expansion Region							
Subject	AUC - Positive (Ipsi/contra)		AUC - Negative (Ipsi/contra)		GIC (Ipsi/contra)		TMS [s] (Ipsi/contra)		AUC - Positive (Ipsi/contra)		AUC - Negative (Ipsi/contra)		GIC (Ipsi/contra)		TMS [s] (Ipsi/contra)		AUC - Positive (Ipsi/contra)		AUC - Negative (Ipsi/contra)		GIC (Ipsi/contra)		TMS [s] (Ipsi/contra)	
Subject 1	0	337	336	2	-0.015	0.035	510 (321)	219	0.6	257	205	0	-0.016	0.031	537 (321)	252								
Subject 2	u/e	u/e	u/e	u/e	u/e	u/e	u/e	u/e																
Subject 5	54	373	29	19	0.025	0.05	489	489	283	663	47	21	0.059	0.064	636	489	188	297	15	13	0.047	0.041	354	384
Subject 6	33.17	589	13.87	0	-0.001	0.051	198	315									**u/e**	u/e	u/e	u/e	u/e	u/e	u/e	u/e
Subject 8	132	555	38	16	0.013	0.036	192	390																
Subject 9	18	519	72	0	-0.025	0.018	201 (369)	396																
Subject 11	373	643	0	0	0.023	0.05	189	397																
Subject 12	70	314	17	4	0.018	0.022	513	417																
Subject 16	193	337	0	7	0.3	0.019	660	369	574	232	0	2.7	0.022	0.001	393	489								
Subject 17	u/e	u/e	u/e	u/e	u/e	u/e	u/e	u/e																
Subject 18	u/e	u/e	u/e	u/e	u/e	u/e	u/e	u/e	u/e	u/e	u/e	u/e	u/e	u/e	u/e	u/e	220	206	1	10	0.007	0.017	204	297
Subject 19*	u/e	u/e	u/e	u/e	u/e	u/e	u/e	u/e																
Subject 21	27	285	50	16	0.028	0.034	495	273																
Subject 22	86	282	3	6	0.012	0.024	492	480	175	515	20	0	-0.016	0.033	420	513								
Subject 23	105	207	0	0	0.002	0.009	540	537																
Subject 24	95	247	0	0	0.006	0.017	540	489																
Subject 26	u/e	u/e	u/e	u/e	u/e	u/e	u/e	u/e																
Subject 28	152	200	0	0	-0.013	0.017	189	315																
Subject 29	u/e	u/e	u/e	u/e	u/e	u/e	u/e	u/e																
Subject 30	4	311	25	0	0.005	0.02	564 (369)	495									0	309	673	0	0.001	0.018	183 (660)	561
Subject 31	356	657	/	0	0.02	0.025	489	444																
Subject 32	u/e	u/e	u/e	u/e	u/e	u/e	u/e	u/e																
Subject 33	171	155	9	0	0.001	0.051	168	168	238	200	104	4.0	-0.014	0.042	480	489								
Subject 34	u/e	u/e	u/e	u/e	u/e	u/e	u/e	u/e																
Subject 35	231	521	4	0	0.037	0.059	297	297	816	379	0	0	0.044	0.041	510	297								
Mean (SD)	141 (138)	407 (146)	35 (80)	4 (7)	0.026 (0.072)	0.031 (0.016)	475 (109)	405 (84)	349 (294)	388 (170)	63 (80)	5 (8)	0.013 (0.03)	0.04 (0.02)	494 (88)	422 (116)	129 (115)	271 (56)	230 (384)	8 (7)	0.018 (0.026)	0.025 (0.014)	277 (87)	414 (135)

Table 5 Raw Data for Gradient of Incline / Area Under Curve / Time to Maximum Signal for Each Tissue Compartment.
Negative values indicate a signal decrease. PSC = percentage signal change, ipsi = ipsilateral hemisphere, contra = contra-lateral hemisphere, Vol. = volume, DWI = diffusion weighted imaging, ml = millilitres, SD = standard deviation, u/e = unevaluable. Reproduced with permission John Wiley and Sons from 'T2*-weighted magnetic resonance imaging with hyperoxia in acute ischemic stroke: Annals of Neurology: 2010.

2.4 Discussion

2.4.1 Findings

To the author's knowledge, this study is the first to report the use of oxygen as a dynamic contrast agent during BOLD sensitive T2*-weighted MRI in acute human ischaemic stroke. Evaluation of static BOLD sensitive sequences has previously suggested an increased deoxyhaemoglobin concentration in potentially salvageable tissue which may be reversed with reperfusion. Other groups have reported T2*-weighted signal increases after respiratory challenge in healthy volunteers and have postulated such changes to be dependent on baseline deoxyhaemoglobin concentration in the context of ongoing metabolic activity. However, this is the first study to combine the application of transient hyperoxia (Oxygen Challenge) during BOLD sensitive (T2*-weighted) MRI in the context of acute human stroke.

In the contra-lesional 'mirror' region which was assumed to represent 'healthy' tissue, a signal increase after Oxygen Challenge was consistently observed. In the operationally defined infarct core (DWI lesion) the response was more varied. On the basis of the observed morphology of the T2*-weighted signal intensity-time curves, three different categories of direction of change were observed; single increases from baseline ('positive' curve), very little overall change ('flat') and signal decreases after Oxygen Challenge ('negative' curve). Overall, measurements for each parameter were attenuated in the DWI lesion, with a lesser magnitude of signal increase being observed compared to the contra-lesional hemisphere. Even when signal increases were observed to give 'positive' T2*-weighted signal intensity-time curves from the DWI lesions, the magnitude of signal increase (as measured by 'area under the curve') was still diminished compared to the contra-lateral side. Finally, the time to achieve maximum signal was longer, and the gradient of incline of signal increase was less in the DWI lesion compared to the contra-lesional side. The exact physiological significance of these parameters is, at present, unclear. The gradient of incline of signal increase may reflect the rate of contribution of deoxyhemoglobin to the total pool, but the influence of impaired perfusion requires to be examined. The latter factor is likely to have played a large role in

determining the ‘time to maximum signal’. In addition, it should be noted that in subject 28, the response in the DWI lesion was greater than in the mirror region. However, whilst this could theoretically be due to a greater OEF, this cannot be established until maps of CBV are evaluated. This case is considered further in Chapter 6.

The number of subjects with regions of possible’ penumbra’ was small in this cohort – only eight subjects from thirty five patients initially recruited. Of the penumbral regions examined in this study, six had PWI-DWI mismatch and 2 had DWI expansion. The regions of interest for these ‘penumbral’ tissues were also generally small and many of these subjects were imaged late. Therefore, when taken as a whole group, the hypothesised increase in T2*-weighted signal after Oxygen Challenge was not observed with any statistical effect. However, closer consideration of the subjects who were imaged <8h showed that the three ‘positive’ curves from ‘penumbral’ regions were all of greater magnitude than those form the contra-lesional side. Although these numbers are not large enough for statistical analysis, it is reassuring that a dramatically large signal increase of 5.1% above baseline was seen from one mismatch region.

2.4.2 Interpretation of Results / Context in Literature

2.4.2.1 Comparison to Animal Pilot Study

The results of this current study broadly reflect the pilot animal study(255). In the preceding animal study which used a rodent model of permanent MCA occlusion, the increase in T2*-weighted signal after Oxygen Challenge was less in the DWI defined core compared to the ‘normal’ tissue (0.24% vs 1.8%), which is consistent with the results of this study. However, in the pilot animal study the signal changes seen in the infarct core were universally negligible; although a signal increase of 0.24% was reported, it is generally accepted that signal changes below an arbitrary value of 0.5% are not reliably detected by fMRI studies, and thus the same would be expected here. Examination of the animal pilot study T2*-weighted signal intensity-time curves shows very little change in the infarct (Figure 2-13).

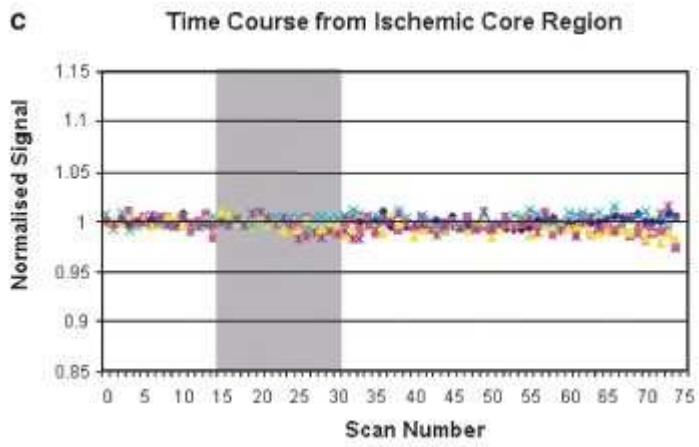

Figure 2-13. T2*-Weighted Signal Intensity-Time Curves from Operationally Defined Infarct Core from the Animal Pilot Study(255)
The x-axis denotes time and the y-axis denotes normalised signal intensity. The vertical grey bar indicated the duration of the Oxygen Challenge. Very little signal change is observed with Oxygen Challenge in the infarct core in this study. Reprinted by permission from Macmillan Publishers Ltd: 'Santosh C, Brennan D, McCabe C et al. Potential use of oxygen as a metabolic biosensor in combination with T2(*)-weighted MRI to define the ischemic penumbra. J Cereb Blood Flow Metab. 2008'.

Although broadly similar, those results do differ from the results from this current study. Firstly, although in this study there were cases where very little signal change was seen (panel [b] in), there were also cases from within the DWI lesion where clear signal increases were observed (in one case this was even greater than the signal increase seen in the contra-lesional 'mirror' region). Such signal increases are, however, not surprising. Firstly the operational definitions varied between studies. The animal study defined infarct core as the 'center of the zone of the ADC abnormality'(255) after permanent MCA occlusion using an intra-luminal filament technique. This study considered the mean signal change from the whole of the DWI lesion. In fact, using the DWI lesion as a surrogate of core is inaccurate – the DWI lesion can represent a heterogeneous tissue region with areas of both core and penumbra scattered throughout(54) and all patients in this study were scanned within a time window where penumbral tissue may exist(21). Secondly, although not consistently measured, the occlusion status of the cohort from this study is likely to have been variable with respect to occlusion site, recanalisation status and collateral blood flow. Even in critically hypoperfused tissue, some residual flow is usually seen in human stroke MR examinations. On the other hand, the intra-luminal filament technique used in the animal pilot study is effective in generating a marked reduction in CBF with little residual blood flow. Therefore differences in residual CBV and therefore the residual deoxyhaemoglobin pool may explain the reduced

but persistent signal increases in the DWI lesion after oxygen challenge. This hypothesis is in keeping with results from a human stroke study using T2'-weighted imaging which suggested a large deoxyhaemoglobin pool exists within the acute DWI lesion(229).

The second difference from the animal study is the observation of signal decreases after Oxygen Challenge (panel C,) which were seen in three subjects. Given the small number of cases from which this phenomenon was seen, it is useful to examine whether this effect is genuine. In Subject 9 there was indeed a decrease in T2*-weighted signal intensity which had a good temporal association to the Oxygen Challenge. Although only a single case, it is tempting to speculate that this is a genuine reduction in T2*-weighted signal intensity due to Oxygen Challenge. If so, this may be explained by, 1) haemodynamic changes or, 2) changes in magnetic susceptibilities directly related to the Oxygen Challenge. Haemodynamic changes will be considered in more detail later in this Discussion. However, it should be noted that to cause decreases in T2*-weighted signal intensity due to haemodynamic changes, one would expect Oxygen Challenge to cause a decrease in CBF. Although this is possible and is the response seen in healthy tissue(262), such changes would need to be extremely large to override the overall effects of changes in magnetic susceptibilities related to changes in oxyhaemoglobin : deoxyhaemoglobin ratio(253). In addition, unlike healthy tissue, decreases in CBF in 'core' after hyperoxia are not generally expected(263, 264). A pure haemodynamic effect as an explanation for signal decreases after Oxygen Challenge is therefore not particularly attractive. Another possibility is that the effect may be explained by molecular oxygen dissolved in plasma, which is paramagnetic on the basis of having two unpaired electrons(265). Under physiological conditions hyperoxia causes only a modest increase in venous oxygen tension(266) and therefore this is unlikely to contribute significantly to MRI signal in the absence of physiological disturbance. However, using an ocular model, Berkowitz(267) showed that when arterial oxygen tension is elevated after hyperoxia (PO_2 of >350 mmHg), the venous haemoglobin can no longer buffer excess haemoglobin and the excess oxygen is dissolved in plasma and may affect MRI signal (T1-weighted signal was evaluated in their case). It is possible that under conditions of low or absent oxygen extraction fraction, the venous side of the vasculature has less capacity

to buffer the excess oxygen (less deoxhaemoglobin available to buffer) and therefore oxygen is offloaded more readily. The threshold to affect MRI signal may be reached more easily and therefore a decrease in signal intensity may be seen as a result of molecular oxygen dissolved in plasma. To the author's knowledge there are no precise data describing the effects of molecular oxygen dissolved in plasma on T2* at 3.0T under conditions of low oxygen extraction fraction, and therefore the precise magnitude of these effects is uncertain and this hypothesis remains speculative.

In other cases the 'negative' signal change may have been due to 'non-physiological' causes. For Subject 30 the apparent decrease in signal intensity after Oxygen Challenge may have simply been due to a variable baseline. In Subject 1 there appears to be a downward drift starting approximately half way through the pre-Oxygen Challenge baseline and continues to a nadir (indicated by * in). After this nadir, which is approximately half way through the Oxygen Challenge, T2*-weighted signal intensity starts to increase. Therefore, in this case it is difficult to conclude that the true effect of the Oxygen Challenge is to precipitate a decrease in T2*-weighted signal intensity in this case. Rather, Oxygen Challenge may simply have reversed a downward drift. The cause of the decrease in T2*-weighted signal intensity is unclear but may be due to scanner drift or physiological factors such as 'low frequency fluctuations' due to vasomotion(268).

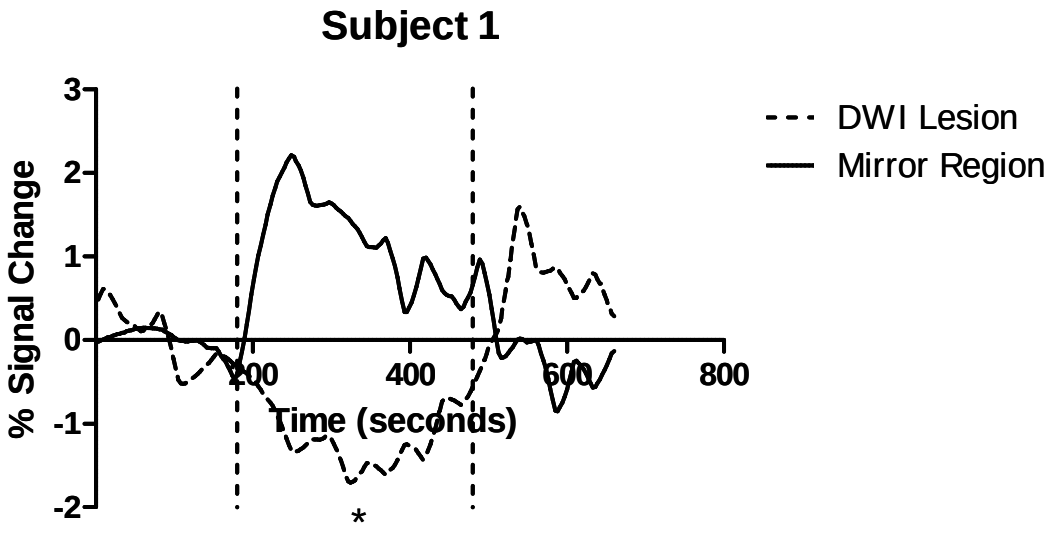

Figure 2-14. 'Negative' Signal Change - T2*-Weighted Signal Intensity-Time Curve Derived from the DWI Lesion of Subject 1
The x-axis represents time (seconds) and the Y axis represents percentage change from baseline. The broken line represents the T2* signal curve from the region defined by the DWI lesion, and the continuous line represents the respective curve from normal tissue. The broken vertical lines show the time of onset and cessation of hyperoxia. The time point at which signal intensity increases in the curve from the DWI lesion is denoted by *.

Finally, the animal study observed large increases in T2*-weighted signal in operationally defined 'penumbra' regions compared to normal tissue(255). That study defined penumbra in two ways; 1) PWI-DWI mismatch, and 2) a histologically defined border zone (55% normal neuronal morphology from a region at the ADC lesion boundary). The observation in this study that, at least in some cases, a large signal increase compared to normal tissue was seen in the 'penumbral' regions is consistent with this. It should be noted that the penumbral regions in this current study were generally small and imaged late and therefore may not all be genuinely 'penumbral'. The limitations of comparing Oxygen Challenge to a technique (PWI-DWI mismatch) which is not the gold standard are therefore clearly highlighted.

2.4.2.2 Comparison to Other Studies – 'Normal' Tissue

The magnitude of observed signal changes in this study was consistent with the results from previous studies. In this study the mean percentage signal change

from the contra-lateral hemisphere in the 'mirror' regions of the DWI lesion was 2.2% (range 1.25-3.14). The variability may be explained by 1) variability in the actual FiO_2 administered and 2) the variable anatomical locations of the regions of interest. Interestingly, however, the mean percentage signal change in 'normal' tissue reported by the pilot animal study(255) was 1.8% - remarkably similar given the differences in magnetic field (pilot animal study performed at 7.0T) and the inevitably larger proportion of grey matter in rodents. Results from other studies reported average signal changes 1.29-3.17%(249, 252, 269) in healthy tissue and have also highlighted the importance of underlying tissue type on results, with differences in percentage signal change reported between basal ganglia, cortical grey matter, and white matter. Again, the use of the mirror region for comparison to the pathological regions of interest will have eliminated most of the confounding effect of variation of tissue type in the current study.

2.4.2.3 Comparison to Other Studies – 'Penumbral' Tissue

The limited data for penumbral tissue in this study limits discussion of this aspect. However, the occasionally observed exaggerated T2*-weighted signal increase after Oxygen Challenge is consistent with an increased oxygen extraction fraction. The penumbral correlate for studies of static signal intensity is a decrease in BOLD sensitive signal intensity and, as previously mentioned numerous studies have demonstrated this phenomenon in tissue likely to be 'penumbral'(99, 219-221, 225-229, 270, 271).

The only comparison of changes in T2*-weighted signal intensity to PET data after acute stroke was made by Donswijk and colleagues(231). In 5 subjects imaged 7-21h post ictus the pre-contrast T2*-weighted images from PWI were compared to OEF data from PET data acquired immediately following PWI. There was no correlation between T2*-weighted signal intensity (relative to the contra-lesional side) and OEF. There are two explanations for this. The first is that BOLD signal intensity simply bears no relationship to oxygen extraction fraction. This, however, is contrary to the evidence previously discussed. The second is that refinements of the measurement of the BOLD effect are required before inferences of the OEF can be made. Firstly, the study by Donswijk and

colleagues examined patients who were 7-21h post ictus. However, the T2-weighted signal intensity has been shown to increase as a result of oedema after 3h post ictus(78) and therefore these subjects almost certainly had a rise in T2 independent of the BOLD effect, thus confounding results. This phenomenon is not an issue in this current study as the normalised change in T2*-weighted signal intensity was examined, thus ignoring the absolute baseline signal intensity value. Secondly, assessment of static T2*-weighted signal intensity needs to account for the cerebral blood volume as well as OEF(206). Finally, the T2*-weighted sequences used in this study were not optimised for the detection of OEF and were designed to collect PWI data. Therefore, it is very possible that these limitations alone may explain the failure for correlated the T2*-weighted MRI findings with PET data.

2.4.2.4 Comparison to Other Studies – 'Infarct Core'

Geisler and colleagues specifically examined T2' –weighted signal intensity from within the infarct core, as defined by the ADC lesion. They specifically found that the lowest T2'-weighted value (and by implication the highest deoxyhaemoglobin concentration) was found in the infarct core. This was in contrast to this current study's observation that the lowest Oxygen Challenge induced signal increase was from the DWI lesion. Potential explanations are multiple. Firstly, the DWI lesion was examined at less than 6h post ictus by Geisler and colleagues, and could well have had penumbral tissue(54) within it. This would be less likely in this current study's cohort which was imaged at a median of 18h post ictus. Secondly, in the early hours OEF may still be elevated(272) in infarct core, again potentially explaining results from the Geisler study. Finally, the group hypothesised that there may be reduction in the wash out of deoxyhaemoglobin from tissue under conditions of low CBF, and therefore the increase in deoxyhaemoglobin may be a remnant of previously metabolic activity(229). If this last hypothesis is true, the Oxygen Challenge technique may detect this as failure of the T2*-weighted signal intensity to return to baseline at the same rate as 'healthy tissue after oxygen cessation. In summary, therefore, the differences in signal intensity observed in operationally defined infarct core between this and the Geisler study may reflect both methodological and biological differences between studies.

2.4.3 Evaluation of the Theory of the Technique

2.4.3.1 General Considerations

Although the rationale of the technique has been stated, it is useful to consider the mechanisms behind the T2*-weighted signal changes after Oxygen Challenge. Firstly, oxygen was delivered at 15l/min using a simple face mask. Under physiological conditions arterial haemoglobin is almost (≥95%) completely saturated with oxygen, and therefore hyperoxia generally has little effect on arterial haemoglobin saturation and the magnetic susceptibilities thereof. Even under hyperoxic conditions, haemoglobin will remain the majority oxygen carrier but there will also be a small increase in plasma dissolved oxygen. The increase in the arterial partial pressure leads to an increase in cerebral venous haemoglobin saturation. Under normal conditions cerebral tissue extracts 30-40% (OEF =0.3-0.4) of oxygen content in the blood(273). Extraction occurs by diffusion, predominantly along the first third of the capillary bed although some extraction proximal to this does occur across arterioloes(274). The oxygen is extracted by diffusion(275) along a gradient from high capillary oxygen tension to low tissue oxygen tension(276). The majority of oxygen which is extracted is dissolved in the plasma, with only a negligible amount being extracted directly from haemoglobin(277). Very little unmetabolised tissue oxygen re-enters the blood from tissue after the initial extraction(278). Therefore, with a normal OEF (~30%) the cerebral venous oxygen saturation will be approximately 70%. This represents a potential for a much larger change in venous haemoglobin saturation compared to arterial saturation after hyperoxia is given (~30% vs ~5%). Administered oxygen will combine with venous deoxyhaemoglobin, increasing venous oxygen saturation(266, 279). The increase in cerebral venous oxygen saturation occurring as a result of increased oxyhaemoglobin : deoxyhaemoglobin ratio will thereby increase T2*-weighted signal intensity(253). The effect of oxygen challenge is therefore weighted towards capillaries and veins rather than arteries and arterioles. The basis for this technique is that in regions where the deoxyhaemoglobin pool is increased as a result of increased oxygen extraction fraction, there will be more deoxyhaemoglobin to combine with the extra administered oxygen and therefore larger signal changes will be produced after Oxygen Challenge.

In the DWI lesion therefore, where OEF may be expected to be low, T2*-weighted signal increases were small or absent. In contrast, contra-lesional tissue (assumed OEF = 0.3-0.4) consistently gave rise to T2*-weighted signal increases. In some regions of PWI-DWI mismatch (where OEF was assumed to be elevated) there were T2*-weighted signal increases greater than in contra-lesional tissue. However, an immediate conclusion that the results are a direct effect of underlying $CMRO_2$ and OEF would be premature and other influences on the capacity of increase in T2*-weighted signal intensity must be evaluated. It is therefore useful to return to the following equation original derived from Yablonskiy and Haake(232) which was also stated in an earlier section.

$$R2' = \lambda * \gamma * (4/3) * \Delta X_0 * Hct * (1 - CBOS)$$

where R2' = 1/T2', λ = venous CBV, assuming arterial blood is fully saturated, γ = gyromagnetic ratio (2.68 x 10^8 rad/s/Tesla), ΔX_0 is the difference in magnetic susceptibility between fully oxygenated and fully deoxygenated blood (0.18ppm per unit Hct(233), Hct = haematocrit and CBOS = cerebral blood oxygen saturation and thus (1-CBOS) = oxygen extraction fraction.

After excluding static variables which will not change with oxygenation, we are left with a number of variables; venous CBV, haematocrit, and haemoglobin saturation for oxygen. The hypothesis for the Oxygen Challenge Technique explicitly acknowledges the effect of hyperoxia on haemoglobin saturation for oxygen (CBOS). It does not however, deal directly with influences from haematocrit (Hct) and cerebral blood volume. Each of these influences will be considered in turn in the following sections. Finally, when evaluating results from this technique, it should be remembered that OEF may be high in core and in oligemia as well as in penumbra, and this may confound results.

2.4.3.2 Cerebral Venous Oxygen Saturation

Firstly the effect of hyperoxia on cerebral venous oxygenation should be considered. Oxygen was administered via a simple face mask which may be considered 'variable' performance. Therefore the inspired concentration of oxygen is likely to have been variable between subjects(280). It is often erroneously assumed that such delivery of high flow oxygen via a standard face

mask delivers '100%' oxygen. In fact, as applied in this study, it is unlikely that inspired oxygen extraction fractions (FiO_2) would have exceeded much more than 50-60% (FiO_2 = 0.5-0.6) at most (281). What effect do such oxygen concentrations have on cerebral venous oxygen saturations? Chiarrelli(249) and colleagues applied simple equations defined by Severinghaus(282) which were based on theoretical analyses of oxygen exchange between tissues. They showed that in six volunteers, even a FiO_2 of 1.0 (100% O_2) only gave rise to an approximately 10% increase in cerebral venous oxygen saturation. Applied FiO_2s of 0.4 and 0.6 (assumed to be in the range of the applied hyperoxia in this study) gave rise to increases in cerebral venous oxygen saturation of 3-4% and 6-7% respectively. Such small increases in cerebral venous oxygen saturation mean that there is equal scope between blood volume compartments associated with healthy tissue (venous saturation 60-70%) and penumbral tissue (venous saturation <30%) for such a magnitude of increase in venous saturation. If these data are applicable to the cohort examined in this study, they argue against a dependence of the Oxygen Challenge induced signal increases on OEF, when the OEF is normal or increased i.e. 6-7% increases in cerebral venous oxygen saturation could occur in both penumbra and normal tissue, meaning the change in magnetic susceptibility would be no different in either tissue compartment. However, a counter argument to this is that the venous oxygen saturation increase described by Chiarelli and colleagues(249) referred to a measure of global venous oxygen saturation. The actual increase in regional venous oxygen saturation is likely to depend to the underlying CBV and rate of delivery of oxygen to the tissue. The signal change detected in one voxel is related to the absolute quantity of deoxyhaemoglobin within that voxel, rather than the venous oxygen saturation per se. Therefore results for healthy 'whole brain' from Chiarelli and colleagues(249) are not directly applicable to stroke tissue compartments such as the 'DWI lesion' and the 'PWI-DWI mismatch' region. Furthermore, under conditions of high OEF, the relationship between T2*-weighted signal intensity and deoxhaemoglobin concentration becomes non-linear, thereby complicating interpretation(218). Nonetheless, it is necessary to consider other influences.

2.4.3.3 Cerebral Blood Flow (CBF) and Cerebral Blood Volume (CBV)

The previous equation acknowledges CBV as an undoubtedly large influence on the magnitude of T2*-weighted signal intensity increases after Oxygen Challenge. In particular, it is venous CBV which is influential on T2*-weighted signal intensity and this entity contributes approximately 70-80% of total CBV(207, 283). One issue is whether haemodynamic changes due to hyperoxia, including those relating to CBF and CBV, occur with a sufficient magnitude to influence the signal change. This is important as increases in CBV are proportional to increases in CBF(284) and both affect T2*-weighted signal(285).

Indeed, hyperoxia precipitates a plethora of haemodynamic effects including a reduction in heart rate, cardiac index and an increase in mean arterial blood pressure, systemic vascular resistance and baroreflex sensitivity(286, 287). A multitude of human volunteer studies have investigated the CBF response to hyperoxia and these are summarised in Appendix F(251, 262, 288-295). Early studies using the N_20 technique in young healthy volunteers(262, 288) demonstrated a 12-15% reduction in CBF in response to hyperoxia. More recent studies using MRI have shown a reduction in CBF of up to 32%(295) and the effect is perhaps more pronounced in younger subjects(292). Most studies have also demonstrated a concomitant reduction in arterial CO_2 which is often statistically significant and can be explained by the Haldane effect. Although induced hypocapnia could theoretically account for all of the reduction in CBF, it has been demonstrated that hyperoxia has a statistically independent effect(295). Changes in CBF after the application of hyperoxia occur fairly rapidly. A reduction within 2-4 minutes of hyperoxia, with restoration of flow within 6 minutes of subsequent normoxia is typical of time courses quoted in the literature(292). Could these changes have affected results? The direct effect of the reduction in CBF seen in healthy tissue would lead to a decrease in T2*-weighted signal intensity, if any effects were indeed present. This would have only served to attenuate the positive signal increase observed in the contra-lesional hemisphere. Therefore, such changes cannot be explained by haemodynamic effects. Moreover, any influence of CBV changes after respiratory challenge on the T2*-weighted signal has been shown to be, if present, relatively small(253). Therefore haemodynamic changes are unlikely to significantly confound results from this technique in normal tissue.

What about stroke regions? In an animal study, Shin and colleagues(264) showed an increase in CBF after hyperoxia applied to isofluorane anaesthetised mice. Animals were subjected to permanent middle cerebral artery occlusion and blood flow was monitored continuously with laser doppler flowmetry. In a human study using the xenon inhalation technique Nakajima and colleagues(263) examined patients recruited both less than, and more than, 15 days after non-lacunar anterior circulation stroke acute stroke. CBF in the ipsilateral hemisphere and in some areas of contra-lateral hemisphere was increased after hyperoxia in the <15 day group, despite a concomitant decrease in pCO_2. Although precise values were not given in this study CBF increases of >30% were seen in some areas on the hemisphere ipsilateral to the lesion. However, this study was performed at late time points and therefore could not assess penumbra. Nonetheless it suggests that the loss of autoregulation in stroke influences the effect of hyperoxia on CBF. The mechanisms of CBF increases are unclear and may relate to an increase in systemic mean arterial blood pressure (MAP) or could even be due to an 'inverse steal' effect whereby the reduction of CBF in adjacent normal tissue which demonstrates vasoconstriction in response to hyperoxia allows a compensatory increase in CBF where in the stroke regions with autoregulatory vasoconstriction is abolished. With respect to Oxygen Challenge results, positive signal increases observed from within the DWI lesion could have in theory been due to increases in CBF. Only concomitant CBF monitoring, such as with ASL, can resolve this issue.

Importantly, in addition to the effect of a *change* in haemodynamic parameters after Oxygen Challenge, it is also vital to consider the effect of such parameter at baseline. The total quantity of deoxyhaemoglobin in the measured pool is not only dependent on the underlying metabolic activity and oxygen extraction fraction, but also the total volume of the pool itself – venous cerebral blood volume. In this study the differential effects of baseline CBV and OEF were not distinguished. This will be required before inferences about underlying metabolic activity can be made and should be the subject of further investigation. The influence of baseline CBV is likely to be of far greater importance than any minor changes in T2*-weighted signal occurring as a result of hyperoxia induced haemodynamic change.

2.4.3.4 Haematocrit

The haematocrit (fractional volume of erythrocytes of the total blood volume) will clearly influence the absolute concentration of deoxyhaemoglobin within a given volume of vessel, and therefore T2*-weighted signal intensity. Although the haematocrit varies according to the size of the cerebral vessel(296) the use of a 'mirror' region from the contra-lesional hemisphere should minimise the influence of this variation between individual regions of interest. However, the haematocrit may decrease after cerebral ischaemia(297), particularly under conditions of decreased blood flow and increased oxygen extraction fraction. Therefore the use of mirror regions in this situation may introduce minor errors.

2.4.4 Limitations of the Technique

2.4.4.1 Theory

The limitations of the theory of the technique have previously been discussed.

2.4.4.2 Application of the Technique

There are a number of additional limitations imposed by the manner in which the technique was applied. Firstly a T2*-weighted sequence was chosen, in order to provide a superior signal-to-noise ratio compared to T2-weighted sequences. Limitations imposed by this sequence include vulnerability to susceptibility artefacts. These are typically most pronounced at tissue interfaces. In this study, the circulation of administered oxygen in the nasal sinuses created a large signal artefact with pronounced signal drop out observed around the nasal sinuses. For this reason, all tissue which was anterior to the lateral ventricles was discarded from analysis. Although uncommon, a stroke lesion predominantly affecting the frontal lobes around the paranasal sinuses would be not be reliably analysed using this technique. Secondly, the sequence was employed in a continuous fashion, in a similar manner to that employed in fMRI studies. While this allowed novel analyses of the T2*-weighted signal intensity-time curve such as 'Area Under the Curve' and 'Gradient of Incline', it rendered the data

susceptible to low and high frequency ‘noise’ and thus the signal-to-noise ratio, as judged by inspection of the T2*-weighted signal intensity-time curves, was generally poor in this study. As a result, additional smoothing was required as a post-processing step. The acquisition of two BOLD sensitive images for approximately 5 minutes each (one pre- and the other peri-Oxygen Challenge) may have provided better signal-to-noise ratios than those seen in this study.

It is also important to appreciate that as a result of using a sequence used in fMRI studies, signal changes during the Oxygen Challenge sequence may have occurred due to sensory stimuli. For example, the change in sound of the T2*-weighted sequence which followed other sequences potentially introduced an auditory stimulus, despite the application of ear plugs. The use of a glass mirror system to allow subjects to see out of the scanner into the control room was employed to reduce claustrophobia, but potentially introduced visual stimuli. Finally, medical air was administered either side of the Oxygen Challenge so that the sensation of Oxygen Challenge administration was limited. However, the possibility that subjects ‘sensed’ the change of gas administration cannot be excluded and this again could have provided a stimulus. The full effect of these potential stimuli on the acquired data is unclear but is unlikely to have produced any systematic bias. Only the change in gas mixture was correlated to the Oxygen Challenge and could potentially confound comparisons of baseline to Oxygen Challenge, and even this effect is unlikely to have lasted the entire duration of Oxygen Challenge (5 minutes).

There are a number of issues pertaining to the application of hyperoxia in this study. Firstly, a variable performance simple ‘Hudson’ mask was used. Whilst the use of such masks reflected their low cost and availability, it is likely that the FiO_2 administered during both a single Oxygen Challenge and also between patients was variable. Measurement of inspired oxygen concentration would have been helpful. However, this limitation is somewhat overcome by comparison of the data to the contra-lesional hemisphere. Therefore comparison between subjects is still possible by normalising data to the contra-lesional hemisphere. In addition, the recording of the end tidal CO_2 and repeated blood pressure measurements would have been helpful for calibration of the T2*-weighted signal intensity and determining the likely effect of Oxygen Challenge on haemodynamic parameters. These data could also potentially be applied as

regressors to the T2*-weighted data in an effort to improve signal-to-noise ratio. Similarly, continuous monitoring of SaO_2 was not performed. This will be important in future studies since if baseline oxygen saturations are low, there may be a signal change due to c xvhanges in arterial oxygen saturation, which is separate from the effect from venous oxygen saturation. Finally, it should be noted that it takes at least 1 minute for measurements of oxygenation to equilibrate after the onset of hyperoxia(252) and may take as long as 3 minutes for full denitrogenation of the alveoli. The analysis of the T2*-weighted signal intensity curves could therefore have been performed using only the last minute (5^{th} minute) of Oxygen Challenge data when equilibrium had been reached. However, given that all subjects had the same protocol applied, it is unlikely that any systematic bias was introduced by using the data acquired throughout the whole period of the Oxygen Challenge.

Finally, limitations of this technique also relate to the direct use of oxygen. Firstly, a small proportion of stroke subjects inevitably have type II respiratory failure due to other co-morbid conditions such as chronic obstructive pulmonary disease (COPD). In such subjects the application of hyperoxia is relatively contra-indicated. Secondly, concern has been raised about the potential toxicity of oxygen with respect to free radical generation(298). Such an occurrence in the brain after acute stroke could theoretically exacerbate ischaemic damage. However, this is not generally considered to be an issue for short periods of hyperoxia, and studies suggesting detriment have studied prolonged hyperoxia(298). In fact, in the acute phase of acute stroke, hyperoxia may prolong the duration of existence of the penumbra(299, 300) and has therefore been suggested as a potential neuroprotectant(301). Indeed, clinical trials are currently investigating oxygen as stroke therapy(302). The next issue pertaining to the use of oxygen as a contrast agent is its biological activity. An ideal contrast agent should highlight biological features of interest without altering the very function which is purports to measure. In healthy tissue, hyperoxia has been shown not to affect $CMRO_2$. However, in stroke tissue, hyperoxia may precipitate a shift from anaerobic to aerobic metabolism as suggested by a reduction in lactate concentration(183). This suggests that oxygen is not a purely inert contrast agent by affects metabolic activity – the very parameter we are using it to measure. This constitutes a minor limitation of this technique.

2.4.4.3 Post –Processing

Fairly extensive post-processing was necessary for this study. Firstly, owing to the relatively low signal-to-noise ratio of this technique, the data was temporally smoothed using wavelet transforms. This reduced the influence of high frequency noise on measurement of parameters of the T2*-weighted signal intensity-time curves. Although wavelet transforms are designed to reduce meaningless noise whilst preserving physiological data, demonstrates that with progressive smoothing the T2*-weighted signal intensity-time curve changes morphology, especially using a fifth scale wavelet. In this study a third scale wavelet was used since this was the least amount of smoothing required to allow distinction of a gradient of signal increase in normal tissue without significantly changing the area under the curve. However, it should be noted that no particular wavelet transform scale is accepted and validated as optimal, particularly for the application in this study. Further work to improve signal-to-noise ratio may eliminate the need for such smoothing.

Secondly, there are limitations to the measurement of parameters on the T2*-weighted signal intensity-time curves. Measurement of area under the curve (AUC) is likely to be fairly robust and insensitive to high frequency noise. Therefore, this parameter is likely to be a reproducible measure of the magnitude of signal change. Percentage signal change on the other hand may be more susceptible to high frequency noise if artefacts manifest as ‘spikes’ on the T2*-weighted signal intensity-time curve. The same issue will therefore apply to the ‘time to maximum signal’ parameter. Despite this potential problem, however, the percentage signal changes reported by this study are remarkably consistent with other work, as previously discussed. The measurement of the ‘gradient of incline’ is likely to be the least reproducible parameter. In order to avoid biased ‘data driven’ analyses the same segment of the T2*-weighted signal intensity-time curve was measured for ‘gradient of incline’ in each patient. However, there were inevitably variations between individuals as to when the signal intensity increase occurred and therefore it is possible that the true gradient of incline of signal increase was not captured for all T2*-weighted signal

intensity-time curves. Therefore data for this parameter should be interpreted with caution.

Next, it should be noted that the parameters of the T2*-weighted signal intensity-time curves were made with reference to the baseline signal. This was calculated as the mean of all pre-Oxygen Challenge measurements. Therefore the measurement of baseline was made over 3 minutes, during which time signal baseline variation could have occurred due to physiological(268) or artefactual processes. The quality selection criteria most likely excluded those T2*-weighted signal intensity-time curves with significant variation since a 1% signal increase compared to baseline in contra-lesional tissue was required. However, baseline variations have the potential for two problems. Firstly, if there is substantial change in the baseline over time, then the ability to produce accurate measurements of magnitude of change is limited. Secondly, if baseline variation for T2*-weighted signal intensity-time curves derived from the stroke and 'normal' tissue are inherently different, then the same *actual* magnitude of change between regions will produce different *measured* magnitudes of change, potentially introducing an inherent bias. This issue requires further investigation.

Thirdly, it should be noted that contra-lesional 'mirror' regions were used as an internal reference. This had the advantage of limiting the confounding effect of variations between subjects for factors such FiO_2 and anatomical location. However, due to brain asymmetries the contra-lesional region of interest will never have been an exact mirror. However, any errors due to this are likely to have been minor and unbiased.

Fourth, there were potential limitations in the definition of tissue compartments. The gold standard imaging technique to define penumbra and infarct core is PET. However, because this modality was unavailable, other MRI parameters (PWI-DWI), which are acknowledged to be inaccurate for defining the physiological tissue compartments(303), were used. For example, the DWI lesion does not represent pure infarct core but may include penumbra(54). In addition, PWI-DWI mismatch is of limited accuracy in defining the penumbra. In this study a TMAX threshold of 4s was chosen to define the outer border of the penumbra. While not unreasonable, more recent studies have suggested a more

conservative threshold may be more appropriate(123, 304), while other studies suggest that no threshold can accurately define the penumbra(305). Finally, the standard SVD method of deconvolution was chosen for this study due to the availability of software, but it is now acknowledged that the circular SVD method of deconvolution is more accurate(123). In addition, while the concept of retrospectively defining DWI expansion as representing the penumbra is robust, accurate delineation of this region at day 3 (when there is significant swelling) means that it is difficult to distinguish between regions of genuine DWI expansion and regions which have simply swollen. Following up imaging after a longer interval would help to circumvent this problem in future studies.

2.4.4.4 Recruited Cohort

A limitation of this study is that treatment decisions were made on the basis of non-contrast CT scan and these were made prior to study specific MR procedures. This resulted in a substantial proportion of subjects receiving rtPA prior to MR scanning. This, combined with the relatively late imaging time (median time = 18h post ictus), meant that the number of subjects with possible penumbra was small, and the volumes of such regions of interest tended to be small when present. The late imaging time resulted from access issues to MRI and constitutes a challenge for MR imaging studies of acute stroke throughout the UK.

2.4.5 Conclusions

This study reports different magnitudes of Oxygen Challenge induced T2*-weighted signal change in different tissue compartments after acute ischaemic stroke. The results are consistent with differences in oxygen extraction fraction between tissue compartments, although results from the PWI-DWI mismatch region are dissappointing. Further work should investigate more subjects with larger volumes of tissue which is likely to be penumbral and which proceeds to infarction as this would help define thresholds for predicting tissue viability.

Further work is required to determine the influence of baseline CBV on the Oxygen Challenge results. Until these issues have been resolved this technique remains promising but not ready for clinical use.

3 Results from Oxygen Challenge Depend on Tissue Type

3.1 Introduction

In order to understand the results of a cerebral imaging technique, an understanding of the 'normal response' of tissue unaffected by the pathology of interest is required to fully understand and quantify changes in pathological regions. However, it is important to appreciate that there is widespread regional heterogeneity for a number of physiological parameters, even in normal tissue, which inevitably influences results of cerebral imaging. For example, despite the observation that OEF is relatively constant, there are substantial differences between cortical grey matter and subcortical white matter with respect to $CMRO_2$, CBF, and CBV(273); the values in grey matter are approximately double those in white matter for these three parameters. Moreover, of especial relevance to imaging techniques such as PWI and Oxygen Challenge which are dependent on vascularity, large vessel and capillary density varies between normal tissue types(306). In addition, there are differences in the mechanisms of infarction between grey and white matter(307, 308) which result in different thresholds for infarction determined by both MR-PWI(309) and CT perfusion(310, 311).

Only a limited number of studies have compared the results of hyperoxia induced T2*-weighted signal changes in different normal tissue compartments such as grey and white matter(242, 248, 249, 251, 252, 269). Davis and colleagues(248) suggested that the greatest 'BOLD sensitivity', a term which may be translated to having the 'largest capacity of signal increase after Oxygen Challenge', was seen in voxels with the highest cerebral blood volume such as the venous sinuses, and cortical grey matter. Other studies(242, 249, 251, 252, 269) have confirmed that the largest signal increases may be in the venous sinuses, followed by cortical grey matter, and then white matter. Although very helpful, such studies may not be completely generalised to results from the brain of an older subject, for example a patient with stroke. These studies have exclusively assessed volunteers and, where reported(242, 249, 251, 252), have

examined subjects with a mean age of no more than 29yrs. However, a number of changes in the brain occur with aging. These include a decline in $CMRO_2$, CBF and CBV of about 0.5% per year(273), deposition of iron within the basal ganglia(312), and possibly some degree of volume loss and atrophy(313). These data suggest that validation of novel imaging techniques should not be limited to healthy volunteers, but should also target the population for which the technique is likely to be applied.

In this study, results for the Oxygen Challenge were investigated in tissue types with different haemodynamic and metabolic properties. Data from the segmented contra-lesional brain of stroke subjects, and also within the DWI lesion segmented into grey and white matter were examined, since these tissue types have inherently different metabolic rates. Therefore, distinction of these tissue types by Oxygen Challenge would help to validate the technique. This approach also allowed comparison of the Oxygen Challenge data set to studies from the literature (grey and white matter data from healthy tissue), another necessary step in the validation of this technique.

3.2 Methods

Firstly, the T2*-weighted signal responses in contra-lesional cortical grey matter and white matter were compared. Next, the results from contra-lesional cortical grey matter were compared to those from subcortical grey matter (lentiform nucleus). In order to validate the hypothesis that the magnitude of T2*-weighted signal intensity changes is dependent on deoxyhaemoglobin concentration in a given region of interest, the signal from the saggital sinus, which represents a pure ‘blood’ pool, was also assessed. Finally, differences between T2*-weighted signal intensity changes from grey and white matter within large DWI lesions was investigated.

3.2.1 Subjects

The standard Oxygen Challenge data set which was used in Chapter 2 was used for these analyses. All Oxygen Challenge data which were analysed were acquired using oxygen flow rates of 15l/min. In order to include the maximum

possible number of subjects, there was no quality threshold for inclusion of scans to this part of this study. The contra-lesional hemisphere was used for most of the following analyses. Therefore all acute ischaemic stroke subjects from whom Oxygen Challenge data were acquired were used for these analyses, regardless of lesion size (i.e. n=31; Subjects 1, 2, 4, 5, 6, 8, 9,10, 11, 12, 13, 14, 16, 17, 18, 19, 20, 21, 22, 23, 24, 25, 26, 28, 29, 30, 31, 32, 33, 34, 35). All subjects were used for analysis of the region of interest from superior saggital sinus, and contra-lesional grey matter, white matter, and subcortical grey matter. For analysis of the regions of interest from grey and white matter from within the DWI lesion, only subjects with large (≥80ml) DWI lesions were considered, in order to minimise the effects of segmentation errors (n=7; subjects 1,5,6,9,16,21,33).

3.2.2 Segmentation Procedure

3.2.2.1 Contra-lesional Grey and White Matter

The software package SPM8 (Functional Imaging Laboratory, Wellcome Trust Centre for Neuroimaging, UCL, UK) was used for these analysis. Traditional segmentation techniques have used one of two methods(314). The first involves registering the brain images of study subjects to a template and the second involves tissue classification based on signal intensity. SPM8 uses a method developed by Ashburner and Friston(314) which combines both elements to form a ‘unified segmentation’ procedure in a ‘single probabilistic framework’. This incorporates both co-registration to a tissue probabilistic map (based on 452 subjects International Consortium for Brain Mapping {ICBM 452, www.loni.ucla.ed, Figure 3-1) and secondly on voxel intensity.

Figure 3-1 Example of the International Consortium for Brain Mapping (ICBM) probabilistic tissue maps.
Grey matter and white matter maps are shown on the left and right respectively. These maps have been thresholded to indicate probabilities of ≥70% of being the tissue class represented by the map.

The requirement for voxel intensity differences between tissue compartments emphasises the need to use images with obvious contrast between grey and white matter. This may typically be a T1 weighted image. However, the standard Oxygen Challenge data set acquired from acute stroke patients set did not include a T1 weighted image. Therefore, the T2*-weighted EPI data, which did demonstrate tissue contrast between the tissue types, were used for these analyses and provided reasonable results.

Firstly, the series of T2*-weighted MR images were realigned to the mean image in order to correct for head motion, using the algorithms described in Chapter 2. Next, segmentation was performed using SPM8. In the modelling, the number of Gaussians chosen to represent the intensity distribution of grey matter: white matter : cerebrospinal fluid (CSF) : other tissues was 2:2:2:4. This accounts for the fact that, in practice, any given individual voxel may not be solely comprised of only one tissue type e.g. may be comprised of both grey and white matter. Other SPM default settings were used. After segmentation, SPM8 produced tissue probability maps for grey and white matter. These were manually inspected. Occasional there were minor errors in distinguishing grey matter from CSF in the ventricles. In the event that CSF was misclassified as grey matter, CSF regions

were manually edited out of the grey matter map. After the generation of an optimal grey matter tissue probability map, regions of subcortical grey matter were also manually edited out, to create a map of cortical grey matter. Editing of this fashion was not required for the white matter map. For both grey and white matter maps, regions from anterior to the lateral ventricles were manually edited out in order to avoid susceptibility artefact from the nasal sinuses.

The following steps were performed using Analyze (Version 8.0, Mayo Clinic Rochester, MT). Firstly, the grey and white matter tissue probability maps were thresholded using a fairly stringent value of '0.7'. The maps were then binarised so that any 'positive' voxel (assigned a value of 1.0) had at least a 70% probability of being from the tissue type indicated by the respective map. Next, a 'mask' of the contra-lesional hemisphere was generated manually. This mask was also binarised, with voxels within the mask being assigned a value of '1.0'. This allowed the use of an image calculator to identify the regions in the contra-lesional hemisphere which were of grey matter and which were white matter (i.e. voxels with the value '2.0' in the image produced by the addition of the contra-lesional hemisphere mask and the grey matter or white matter tissue map). The resulting image was saved as a region of interest (termed 'object map' in the Analyze software) and applied to the original realigned T2*-weighted EPI. These object maps delineated the region of interest from which the time series data were acquired.

3.2.2.2 Contra-lesional Lentiform Nucleus

In order to create a region of interest map to indicate the lentiform nucleus (to generate a map representing subcortical grey matter which could be compared to cortical grey matter), the unthresholded grey matter map was overlaid onto the T2*-weighted EPI data. The use of an unthresholded map allowed better delineation of this region compared to the use of a thresholded map. The lentiform nucleus was then manually segmented. The resulting image was also saved as a region of interest 'object map'.

3.2.2.3 Superior Saggital Sinus

In order to derive measures signal changes from within the saggital sinus, this region was manually segmented. The region of interest was selected from the superior saggital sinus, using the lateral ventricles as an anatomical guide.

Examples of segmentation of the aforementioned tissue compartments are given in Figure 3-2.

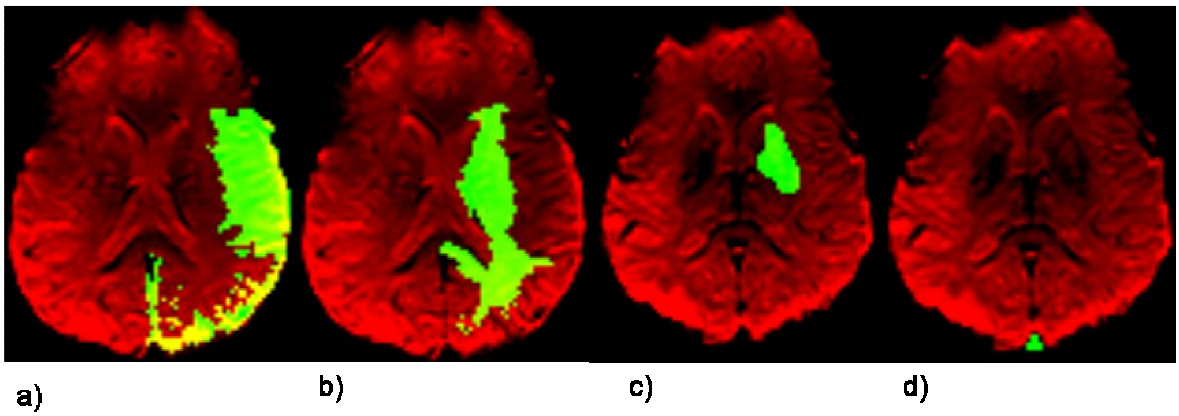

Figure 3-2 Example of Segmented Regions of Interest
a) segmented contra-lesional grey matter, b) segmented contra-lesional white matter, c) segmented contra-lesional lentiform nucleus, and d) segmented superior saggital sinus. The example was taken from Subject 9 but is typical of the results from all other subjects. All regions of interest spanned across multiple slices. Red voxels indicate brain, green voxels indicate the segmented regions of interest. Regions anterior to the lateral ventricles were manually edited out.

3.2.2.4 Intra-lesional Grey and White Matter

Next, the grey matter and white matter from within the lesion was segmented. Routine application of the 'unified segmentation' algorithm may result in misclassification errors if applied to lesioned areas where the voxel intensity is changed{Seghier, 2008 #37}. Visual evaluation suggested that these errors were indeed present when the algorithm was applied to the standard Oxygen Challenge data set. In particular, lesioned white matter was occasionally misclassified as grey matter, owing the bright signal seen on the images which was caused by the stroke. Attempts to circumvent this problem by adjusting the number of Gaussians prior to segmentation did not provide satisfactory results. For example modelling the grey matter with only one Gaussian and the white matter with 3 Gaussians led, in some cases, to overestimation of the white matter, as judged by qualitative visual inspection. Therefore, for segmentation

of lesional grey and white matter, the unified segmentation technique was not applied.

Instead the grey and white matter maps generated for the normal hemisphere were reflected onto the lesioned hemisphere. This was achieved by applying a transformation matrix in 'Analyze' software package, which corrected for asymmetries introduced by a rotated head position within the scanner. Next, the binarised map of the DWI lesion generated for the Chapter 2 study was added to the new ipsi-lesional tissue probability map, again using an image calculator, to create maps of grey matter and white matter within the DWI lesion.

3.2.3 Generation of T2-weighted Signal Intensity-Time Curves*

Using Analyze in a similar manner to Chapter 2, the 'object maps' representing the regions of interest for the above named tissue compartments were overlaid onto the EPI data to derive time series data. The resulting time series data representing the T2*-weighted signal intensity-time curves were smoothed by Wavelet Transforms using the algorithm described in Chapter 2. Calculation of the following parameters was also performed using the previously described procedure; 'Area Under the Curve' (AUC), 'Percentage Signal Change' (PSC), 'Time to Maximum Signal' (TMS) and Gradient of Incline' (GIC) of the signal increase. Curves were classified as 'positive', 'negative' and 'flat', as previously.

3.2.4 Statistical Analysis

Values for the parameters measured from the T2*-weighted signal intensity-time curves derived from the various tissue compartments were compared. Firstly, the distribution of the data was assessed using the Shapiro Wilk test (StatsDirect). If there was no evidence of non-normality and no evidence of unequal variances detected by the application of an Analysis of Variance (ANOVA), a paired t-test was applied. If the statistical assumptions were not met, data were compared using a Wilcoxon Signed Ranks test. Statistical significance was considered at $p<0.05$.

3.3 Results

3.3.1 Contra-lesional Grey and White Matter

T2*-weighted signal intensity-time curves from contra-lesional cortical grey matter were classified as being in the 'positive' direction in all 31 cases. In those from white matter, 2 cases were 'negative' and 2 cases were 'flat', and 27 were 'positive'. Fifteen curves from the lentiform nucleus were 'positive', 8 were 'negative' and 8 were 'flat'. Signal differences in T2*-weighted signal intensity-time curves were noted between tissue types (please see Figure 3-3 and Table 6).

When results from cortical grey matter were compared to white matter the following were noted; AUC in grey matter was larger ($p<0.0001$), PSC in grey matter was larger ($p<0.0001$) and the GIC in grey matter was steeper ($p<0.0001$). There was no difference between tissue types with respect to TMS. The magnitude of signal changes was therefore larger in cortical grey matter compared to white matter.

When results from cortical grey matter were compared to subcortical grey matter (lentiform nucleus) the following were noted; AUC in cortical grey matter was larger ($p<0.0001$), PSC in cortical grey matter was larger ($p<0.0001$) and the GIC in cortical grey matter was steeper ($p<0.0001$). There was no difference in between tissue types with respect to TMS. The magnitude of signal changes was therefore larger in cortical grey matter compared to lentiform nucleus.

When results from lentiform nucleus were compared to white matter the following were noted; AUC in white matter was larger ($p=0.001$), there was no statistically significant difference in PSC ($p=0.6$), TMS ($p=0.07$), or GIC ($p=0.6$).

The signal from the lentiform nucleus appeared to be noisy. Although no significant differences in the variance of the baseline (pre Oxygen Challenge) data were noted between cortical and subcortical grey matter ($p=0.3$), the

variance of baseline data was considerably smaller in white matter compared to cortical grey matter ($p<0.0001$) and lentiform nucleus ($p=0.0005$).

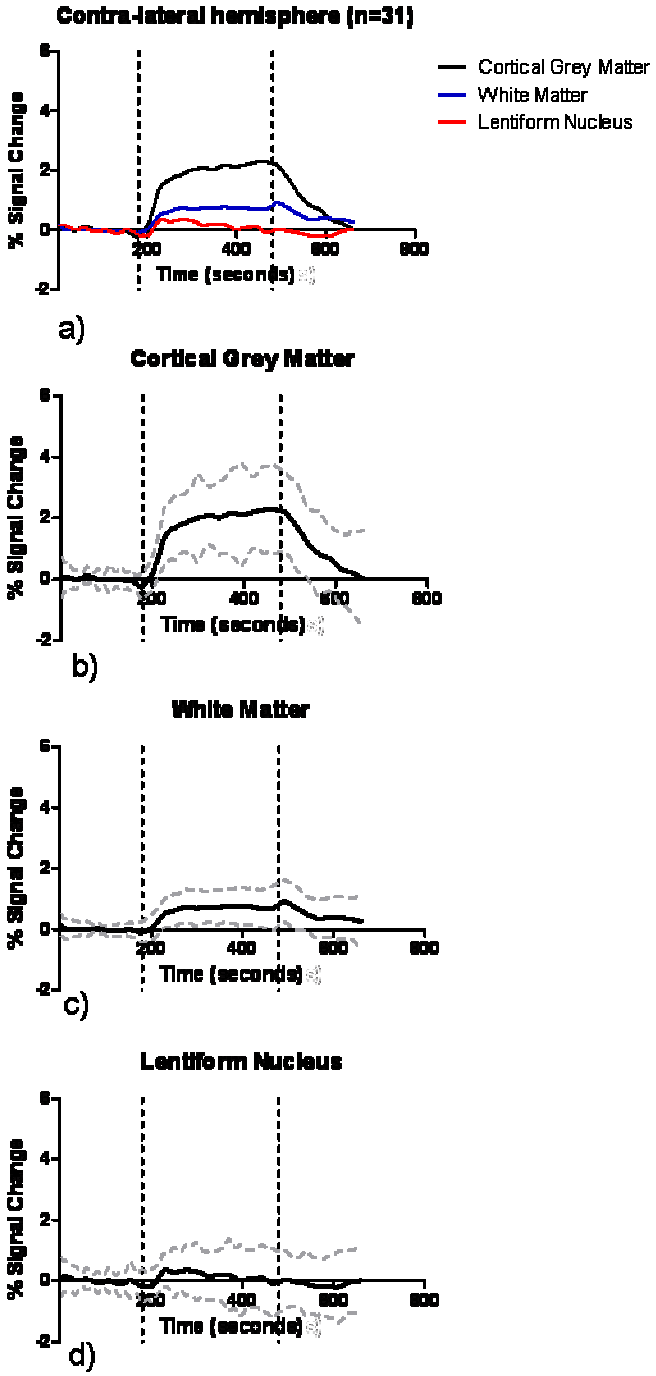

Figure 3-3 T2*-weighted signal intensity-time curves from different tissue compartments from the contra-lesional hemisphere (n=31)
In panel (a) the mean (n=31) signal from each tissue compartment is shown on the same graph. Each curve is shown with error bars in panels (b), (c) and (d). In these panels the solid line represents the T2*-signal intensity-time curve and the broken lines represent the error (standard deviation) bars. The x-axis represents time (seconds) and the y-axis represents % T2*-signal change from the baseline. Vertical broken lines represent the onset and cessation of the oxygen challenge.

Parameter / Tissue Type	Cortical Grey Matter		White Matter		Lentiform Nucleus	
	Value	s.d.	Value	s.d.	Value	s.d.
Area Under Curve (% units)	556	300	195	146	43	201
Percentage Signal Change (%)	2.02	0.48	0.57	0.43	1.3	0.8
Time to Maximum Signal (s)	411	90	441	107	383	160
Gradient of Incline	1.3	0.02	0.48	0.02	0.51	0.02

Table 6 Values for parameters from the T2*-weighted signal intensity-time curves derived form contra-lesional tissue compartments.
The arbitrary values for Area Under Curve was calculated using units of % signal change on the y-axis of the T2*-weighted signal intensity-time curve plots. s.d. = standard deviation. s = seconds.

3.3.2 Superior Saggital Sinus

The direction of the T2*-weighted signal intensity-time curves from the superior saggital sinus was 'positive' in all but two cases (Subjects 10 and 23). The respective curve from Subject 10 showed very little signal change and was classified as 'negative' according to the 'direction' criteria stipulated in Chapter 2. The curve from Subject 23 did show a signal increase but owing to a variable (pre oxygen challenge) baseline (standard deviation = 6.7%) the curve was classified as 'flat.

The magnitude of signal changes from within the superior saggital sinus was substantially larger compared to those from tissue parenchyma. Median percentage signal change was 24.26% (range 1.6-113.7%) and median area under curve was 5054 (range 30.4-15357).

3.3.3 Intra-lesional Grey and White Matter

Segmentation of cortical grey and white matter was performed for 7 subjects with DWI lesion volumes ≥80mls (Subjects 1,5,6,9,16,21,33). The T2*-weighted signal intensity-time curves from cortical grey and white matter are shown in Figure 3-4. There was no statistical difference for AUC (p=0.06, Wilcoxon) or PSC (p=0.94, Wilcoxon) between intralesional grey matter and intralesional white matter. Results from qualitative analysis are as follows. The T2*-weighted signal intensity-time curves from the DWI lesion demonstrated varied morphology. The curves from Subject 1 and Subject 6 were similar when derived from grey and white matter. In both cases there was a downward drift until approximately half way though the Oxygen Challenge and both curves were 'negative'. The T2*-

weighted signal intensity-time curve from white matter DWI lesion showed very little response to Oxygen Challenge in Subject 5. The respective curve from grey matter DWI lesion demonstrated a small and slow signal increase corresponding to the duration of Oxygen Challenge. Unlike the typical morphology of the T2*-weighted signal intensity-time curves from ‘normal’ contra-lesional regions, the signal intensity did not fall after cessation of Oxygen Challenge. A similar response was observed in grey matter for Subject 9, but in this case the mean signal from the white matter DWI lesion demonstrated a signal decrease. The curves from grey matter and white matter were both ‘positive’ in Subjects 16 and 33, and in both cases the magnitude of signal increase was marginally greater in grey matter. In Subject 21 there was very little signal change in response to Oxygen Challenge in grey matter and white matter.

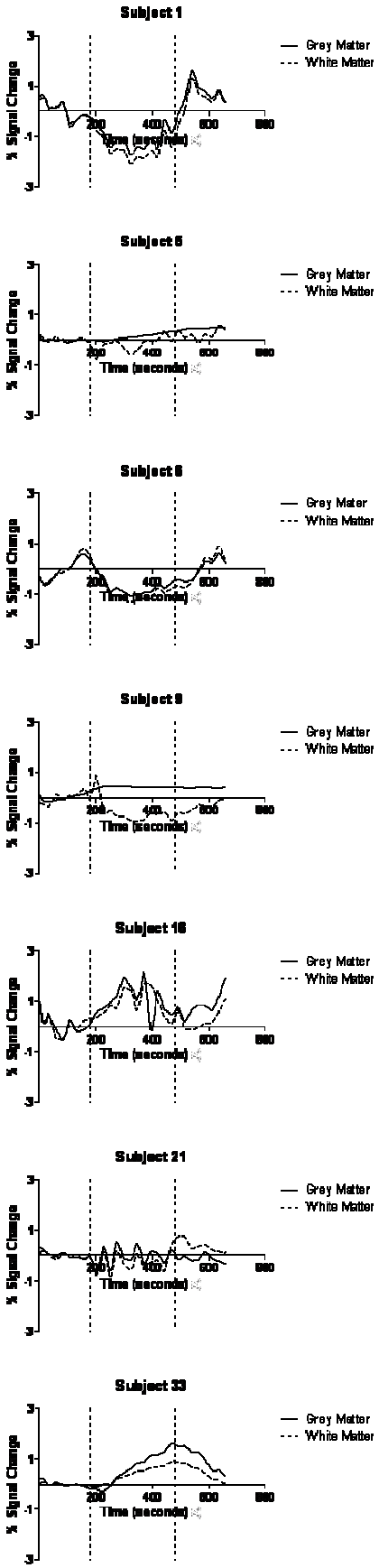

Figure 3-4 Segmented T2*-weighted signal intensity-time curves from grey and white matter within the DWI lesion.
The x-axis represents time (seconds) and the y-axis represents % T2*-signal change from the baseline. Vertical broken lines represent the onset and cessation of the oxygen challenge.

3.4 Discussion

This is the first study to assess hyperoxia as a MRI contrast agent in subjects older than those in their third decade, and secondly, to assess findings within the DWI lesion segmented for grey and white matter. In this study there was a marked difference in the magnitude of signal increase in grey matter compared to white matter. The signal in the basal ganglia was noted to be noisy, with a large standard deviation relative to the observed signal increase. Therefore, the calculated signal changes in this tissue were small. Conversely, the signal increases in the saggital sinus were extremely large. In addition to the assessment of the contra-lesional hemisphere, the DWI lesion was also segmented for grey and white matter. Whilst the T2*-weighted signal intensity-time curves from DWI lesion grey and white matter were concordant with respect to the direction of signal change in most cases (e.g. when the DWI lesion grey matter curve was 'positive', so too was the DWI lesion white matter curve), data from DWI lesional grey and white matter were discordant in one case (subject 9). This case was interesting for two reasons. Firstly, whilst there was a small positive increase in DWI lesion grey matter, there was a small signal decrease in DWI lesion white matter. Secondly, the signal in DWI lesion grey matter did not fall back to baseline after the cessation of Oxygen Challenge, suggesting failure to replenish the deoxyhaemoglobin to the measured tissue compartment.

These results were generally consistent with the literature. Firstly, responses from the saggital sinus were greater than those from contra-lesional grey matter which were in turn where greater than those from contra-lesional white matter, a pattern which has previously been reported. Berthezene and colleagues(269) reported signal increases of 14.7% / 4.23% / 1.92% in the longitudinal sinus / grey matter / white matter respectively, after administering 10l/min of Oxygen to healthy volunteers. Similarly, Losert and colleagues(252) reported signal increases of >30% /3.41% / 0.82% in the superior saggital sinus / grey matter / white matter respectively, after administering 22l/min oxygen to healthy volunteers. The pattern of change in R2* reported by Rostrup and colleagues(251) was consistent with these findings. Similarly, Bulte and colleagues(242) reported an approximately 2.5% signal increase in grey matter

compared to a 120% increase in the saggital sinus. In this study, the 24% /2%/ 0.6% signal increases in superior saggital sinus / grey matter / white matter were consistent with these findings. The small disparities in exact values between studies is likely to be due to the combination of disparities in the following factors; method used to calculate percentage signal change, FiO_2, respiratory function of subjects, cerebral blood flow / cerebral blood volume of subjects, inherent noise, and MRI sequence parameters including 'flip angle'. Given these potential confounds it is not surprising that the subjects in this cohort, who were older and more likely to have impaired respiratory function, had a slightly smaller PSC in grey matter compared to the respective values for volunteers reported in the literature.

The most significant disparity between findings from this study and the other studies comes from data from the basal ganglia. Other studies reported the signal increase from basal ganglia to be midway between that of white matter and grey matter(251, 252). In this study, although there was no statistical difference between the PSC for white matter and basal ganglia, there was a highly statistically significant difference between the AUC from the two regions. In addition, the signal responses from the basal ganglia were noisy with large standard deviations. The reason for this is unclear. However, a possible explanation comes from the differences in clinical characteristics between cohorts. There is a iron deposit related susceptibility induced decline in T2*-weighted signal of the basal ganglia with increasing age(312). Therefore, subjects in this cohort are likely to have had greater iron content in the basal ganglia compared to the volunteers in their third decade from other studies. Therefore the hyperoxia induced dynamic susceptibility differences between blood and surrounding basal ganglia tissue are likely to be different between cohorts, thus potentially explaining the disparities between studies. This highlights the importance of validating novel imaging techniques, such as Oxygen Challenge, in subjects who are representative of the patient group of interest.

What is the explanation for the difference between white matter and grey matter? Are the differences due to metabolic or haemodynamic factors? It has previously been discussed that there are differences between grey and white matter with respect to $CMRO_2$, cerebral blood flow and cerebral blood volume. It is well established that under physiological conditions there is coupling between

CBF and $CMRO_2$ which allows OEF to stay constant(315). Therefore, given that the contra-lesional regions of interest are unaffected by the stroke, one would expect the CBF and $CMRO_2$ to be coupled in both contra-lesional grey and white matter, providing a similar OEF in both tissue types(273). It thus follows that for a given unit of cerebral blood volume, the amount of oxygen extracted from haemoglobin should be the same in grey and white matter. Therefore, assuming a constant OEF, the concentration of deoxyhaemoglobin in a given imaging voxel is therefore dependent predominantly on cerebral blood volume. This is consistent with findings by Davis and colleagues which showed that the greatest capacity for BOLD signal changes was in the venous sinuses, and also the cortical grey matter(248). In this study, the largest signal increase was seen in the saggital sinus, a 'pure' blood compartment where the CBV is 100%. Therefore, differences between saggital sinus, grey matter, and white matter, can be attributed to differences in CBV.

What is the explanation for the divergent response of T2*-weighted signal from grey and white matter from the DWI lesion in subject 9? Whilst differential blood flow changes between tissue compartments could explain results, the negative signal seen in white matter could reflect the lesser amount of deoxyhaemoglobin to combine with oxygen in white matter compared to grey matter, thus forcing oxygen to dissolve in plasma. This issue is discussed in greater detail in Chapter 4 (section 4.4). A further interesting observation was that in this case, where there was a small positive increase in T2*-weighted signal intensity in grey matter, the signal did not return to baseline. This could suggest that there was little or no ongoing oxygen extraction in this region to contribute deoxyhaemoglobin pool, and therefore the usual decline in T2*-weighted signal intensity was not seen.

What are the implications of this study? The first is that when assessing a stroke lesion for signal changes, a contra-lesional mirror region should be used as a reference. Although this cannot provide an exact representation of the proportion of grey and white matter and sulcal veins from within the lesion, it still provides the best available estimate. The second conclusion is that for accurate thresholds to be determined for the distinction of stroke tissue compartments, particularly in white matter, an improvement in signal-to-noise ratio will be required. The standard deviations reported by this study are

relatively large compared to the magnitude of signal changes seen. Next, caution should be exercised when assessing the signal changes from the basal ganglia form older subjects, and the artefacts seen in this study constitute a limitation of the technique. Finally, it should be noted that this study serves as a demonstration of how novel techniques should not simply be tested in young healthy volunteers, but the cohort used for validation must be clinically relevant.

A number of limitations should be acknowledged. Firstly, in future studies the segmentation procedure could be improved by the use of a high quality T1-weighted structural scan. It should be acknowledged that errors of spatial normalisation due to distortions on the T2*-weighted imaging were inevitable in this study, and these likely led to some errors in segmentation.Unfortunately, for reasons of scan duration, T1-weighted imaging was not acquired in this study at the time of imaging. Although this could also have been performed at a follow up visit, geographical and practical constraints mitigated against this. Nonetheless, the segmentation procedure provided by the SPM 8 software provided a reasonable result, as shown in Figure 3-2. One potential approach to validating the technique adopted could be to apply the same technique to volunteers from whom T1-weighted images were acquired. However, there was no specific ethical approval or funding available to do this. Next, for the thresholding of grey and white matter maps, a probability of ‘0.7’ was applied. Therefore the tissue maps used in this study only had a specificity for the purported tissue type of 70%. For the calculation of grey matter signal changes, for example, this may have resulted in a slight attenuation of percentage signal change. A threshold of value of ‘0.7’ may be viewed as fairly stringent. This inevitably led to a substantial number of voxels being exluded from analysis. Next, it should be noted that there is no ideal method to segment DWI lesions for grey and white matter. Although changing the parameters of the ‘unified segmentation’ procedure was attempted, this did not provide a satisfactory result in the absence of a T1-weighted image. A limitation of simply flipping contra-lesional regions of interest in the mid-saggital plane is that the effects of tissue oedema are unaccounted for. In addition, brains are never symmetrical and therefore the mix of grey and white matter will never be exactly matched in the homologous contra-lateral region. Next, accurate and consistent definition

of the superior saggital sinus using the T2*-weighted EPI data was limited by the nature of the data. One problem was that artefact on T2*-weighted images is seen at tissue interfaces. Secondly, such regions of interest are inevitably very small and therefore susceptible to errors imposed by measurement error and partial volume effects. Nonetheless, in order to derive an estimate of the data from within the saggital sinus, this region was manually segmented. Finally, it should be acknowledged that this study was limited by small numbers, especially for the segmentation of grey and white matter from within the DWI lesion.

In summary, this study demonstrated differences between grey and white matter with respect to Oxygen Challenge results. These differences are likely to be mediated by a difference in cerebral blood volume. The influence of cerebral blood volume on signal from the DWI lesion should be investigated. Finally, an age related artefact from the basal ganglia has been demonstrated.

4 Results from Oxygen Challenge Depend on Flow Rate of Applied Hyperoxia

4.1 Introduction

When considering the use of a tracer in any medical imaging technique, attention should be paid to optimising the administered concentration of the tracer. For example, for perfusion MRI the optimal concentration of gadolinium based contrast has been investigated(316) and there is now a consensus as to which dose of gadolinium to use in stroke(317, 318). The optimal tracer concentration may be considered as the one which safely and effectively provides the largest signal-to-noise ratio, for the signal of interest.

For the Oxygen Challenge technique, the optimal concentration (or flow rate) of administered oxygen has yet to be determined. However, it is proposed here that it may be the one which maximally increases venous oxygen saturation, but at the same time the one which minimises the 'spill over' of paramagnetic molecular oxygen to plasma, as has been observed beyond a particular tissue specific threshold(267).

Studies investigating hyperoxia as a contrast agent for MRI(242, 249, 250, 252, 269) have inevitably used different concentrations or and flow rates of oxygen but most have aimed to administer concentrations of '100%'. However, studies to date have been performed using healthy volunteers and the interplay between different tissue compartments (e.g. normal grey matter, normal white matter, stroke lesions) with different concentrations or flow rates of oxygen has not been investigated. This is important to appreciate since the change in R2* (the relaxivity component describing T2*) is dependent on underlying tissue characteristics such as cerebral blood volume (CBV), oxygen extraction fraction and venous oxygen saturation(232, 238, 249, 319). What is clear, however, is that for cortical grey matter, despite a decrease in cerebral perfusion(250), there is a linear relationship between T2*-weighted signal intensity and concentration of administered hyperoxia(249).

In studies aiming to determine the optimal concentration or flow rate of oxygen for Oxygen Challenge, the tissue type of interest needs to be considered. The optimal oxygen concentration or flow rate to distinguish a specific tissue type / tissue compartment from the remainder of the brain may not be the same for all tissue types. An appreciation of the magnitude and direction of the signal changes after different concentrations or flow rates of hyperoxia is important in moving towards determining the optimal concentration or flow rate of hyperoxia from the Oxygen Challenge. In this study, the effect of two flow rates of Oxygen Challenge is considered in different contra-lesional and stroke tissue compartments.

4.2 Methods

The influence of oxygen flow rate was investigated, primarily by analysing the T2*-weighted signal intensity time-curves in the contralateral hemisphere. Changes within the DWI lesion were also investigated where possible.

4.2.1 Subjects

In a subgroup of subjects included in the standard Oxygen Challenge data set, two Oxygen Challenge data acquisitions were performed, each using a different flow rate of oxygen. Performance of two Oxygen Challenges was considered after the first 2 subjects were scanned (recruited by a previous Research Fellow). After patient 20 was recruited, dual oxygen challenges were no longer considered following a decision to minimise scanning time in an effort to reduce head motion artefacts. In subjects 3-20, dual Oxygen Challenge was performed if the subject was deemed to be able to tolerate the additional scanning time required. This decision was taken jointly by the supervising radiologist and KD (thesis author). In these cases, the first Oxygen Challenge acquisition was always performed using an oxygen flow rate of 15l/min. The second was always performed using an oxygen flow rate of 7l/min. Apart from oxygen flow rate, all aspects of data acquisition were the same between Oxygen Challenges. The duration between the first and second applications of hyperoxia was a minimum of 4 minutes.

Dual oxygen challenges were performed in the following subjects (n=7); Subjects 4, 6, 8, 10, 13, 14, 17. The T2*-weighted signal intensity-time curves were analysed from the contra-lesional hemisphere in all these cases. Curves were also analysed from the DWI lesion where this was large enough (≥1ml, as determined in Chapter 2; n=3, subject 6, 8, and 17).

4.2.2 Post Processing

T2*-weighted signal intensity-time curves were generated for the following regions of interest for the higher and lower flows of oxygen; contra-lesional grey matter, contra-lesional white matter, and contra-lesional lentiform nucleus. The segmentation procedures were described in detail in Chapter 3 (3.2.2.1), and all other aspects in Chapter 2.

4.2.3 Statistical Analysis

In a similar manner to the previous description, AUC, PSC, TMS, and GIC from contra-lesional grey matter and white matter were compared. Again, the Wilcoxon signed ranks test was employed for this purpose after failure to suggest normal distribution. Qualitative comparisons were also performed. For data from the DWI lesion, only qualitative analysis was performed owing to small numbers.

4.3 Results

4.3.1 Qualitative comparisons of T2-weighted signal intensity-time curves from contra-lesional grey and white matter for different oxygen flow rates*

Figure 4-1 and Figure 4-2 (overleaf) show the T2*-weighted signal intensity-time curves associated with both flow rates of oxygen from grey matter and white matter respectively. A signal increase was generally observed throughout the duration of the Oxygen Challenge. However, very little change was seen in Subject 10, and the T2*-weighted signal intensity-time curves derived from

Subject 17 appeared noisy. Inspection of the graphs in Figure 4-1 (grey matter) shows that the area under the curve was generally greater with the use of 15l/min Oxygen Challenge compared with the use of 7l/min Oxygen Challenge. In one case this difference was marked (Subject 6) whilst in others the differences were more subtle (e.g. subject 13).

For white matter (Figure 4-2), there were three cases where there was a larger signal increase after the higher flow rate of oxygen compared to the lower oxygen flow rate, consistent with the responses seen in grey matter (Figure 4-1). However, in Subjects 4, 8, and 13, there was a larger signal increase (albeit sometimes subtle) after the lower flow rate of Oxygen Challenge. In Subjects 4 and 8 this difference was fairly marked.

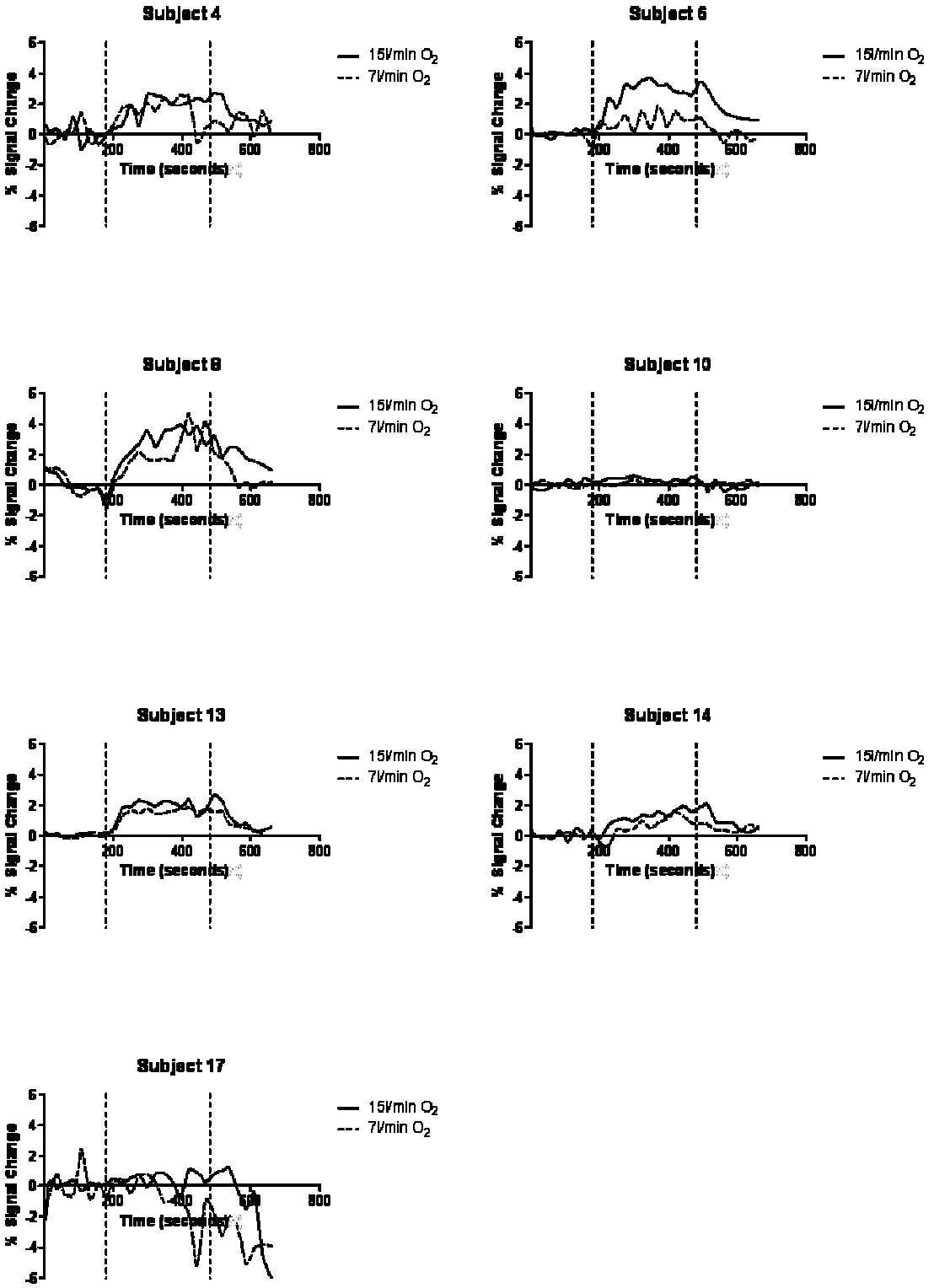

Figure 4-1 Grey matter T2*-weighted signal intensity-time curve s acquired from Oxygen Challenges administered using 15l/min and 7l/min oxygen
The x-axis represents time (seconds) and the y-axis represents % T2*-signal change from the baseline. Vertical broken lines represent the onset and cessation of the oxygen challenge.

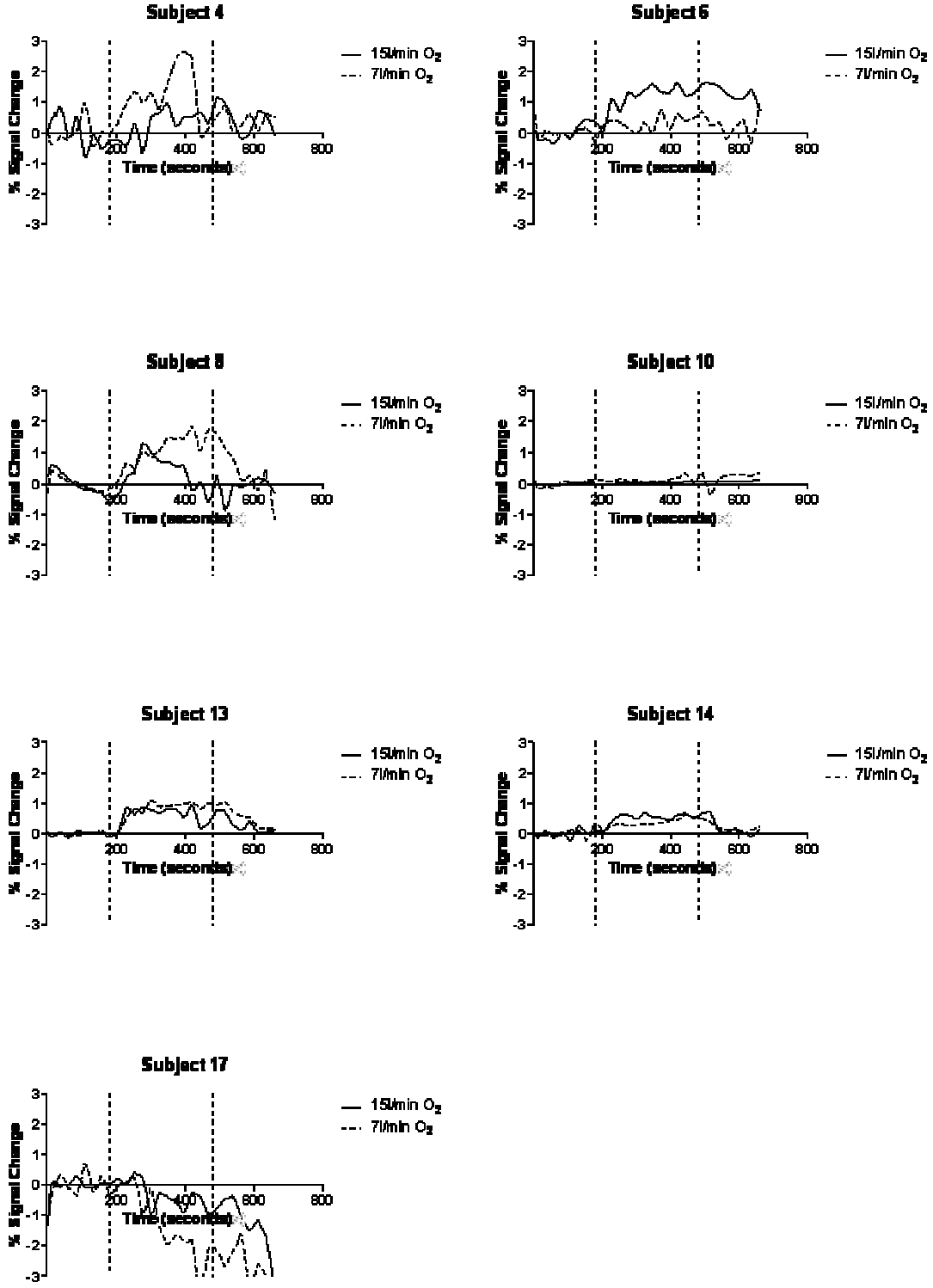

Figure 4-2 White matter T2*-weighted signal intensity-time curve s acquired from Oxygen Challenges administered using 15l/min and 7l/min oxygen
The x-axis represents time (seconds) and the y-axis represents % T2*-signal change from the baseline. Vertical broken lines represent the onset and cessation of the oxygen challenge.

4.3.2 Statistical comparisons of T2*-weighted signal intensity-time curves from contra-lesional grey and white matter for different oxygen flow rates

4.3.2.1 Grey Matter

The AUC of the T2*-weighted signal intensity-time curve derived from contra-lesional grey matter with 15l/min Oxygen Challenge was significantly larger than that derived by 7l/min Oxygen Challenge (p=0.020, n=7). The differences in 'percentage signal change' did not reach statistical significance in this small cohort (2.4% [15l/min] vs 2.0% [7l/min], p=0.2). Similarly there were no significant differences in the 'gradient of incline' (p=0.2) of signal increase or the 'time to maximum signal' (p=0.2).

4.3.2.2 White matter

No differences in the curves from white matter between the two oxygen flow rates were seen with respect to 'area under curve' (p=0.6), 'percentage signal change' (p=0.12), 'gradient of incline' (p=0.44) and 'time to maximum signal' (p=0.7). In a similar fashion, no differences between oxygen flow rates were seen in the lentiform nucleus.

4.3.3 Qualitative comparisons of T2*-weighted signal intensity-time curves from DWI lesion grey and white matter for different oxygen flow rates

Figure 4-3 shows the T2*-weighted signal intensity-time curves from the DWI lesion from the 3 subjects who had a measurable DWI lesion (>1ml) and Oxygen Challenge acquired with two flow rates of oxygen. Owing to the small number of subjects available in this subgroup, no formal statistical analysis was performed.

The baseline data from Subject 6 was variable but there appeared to be a decrease in the T2*-weighted signal intensity after the application of the

hyperoxia. This decrease appeared to be more pronounced after the higher (15l/min) than the lower (7l/min) flow rate of oxygen. In Subject 8, there was a positive increase in T2*-weighted signal intensity after the 15l/min Oxygen Challenge, but very little change was observed after the 7l/min Oxygen Challenge. In subject 17, the application of the 15l/min Oxygen Challenge was associated with a transient decrease in T2*-weighted signal intensity, but no such change was seen after the 7l/min Oxygen Challenge.

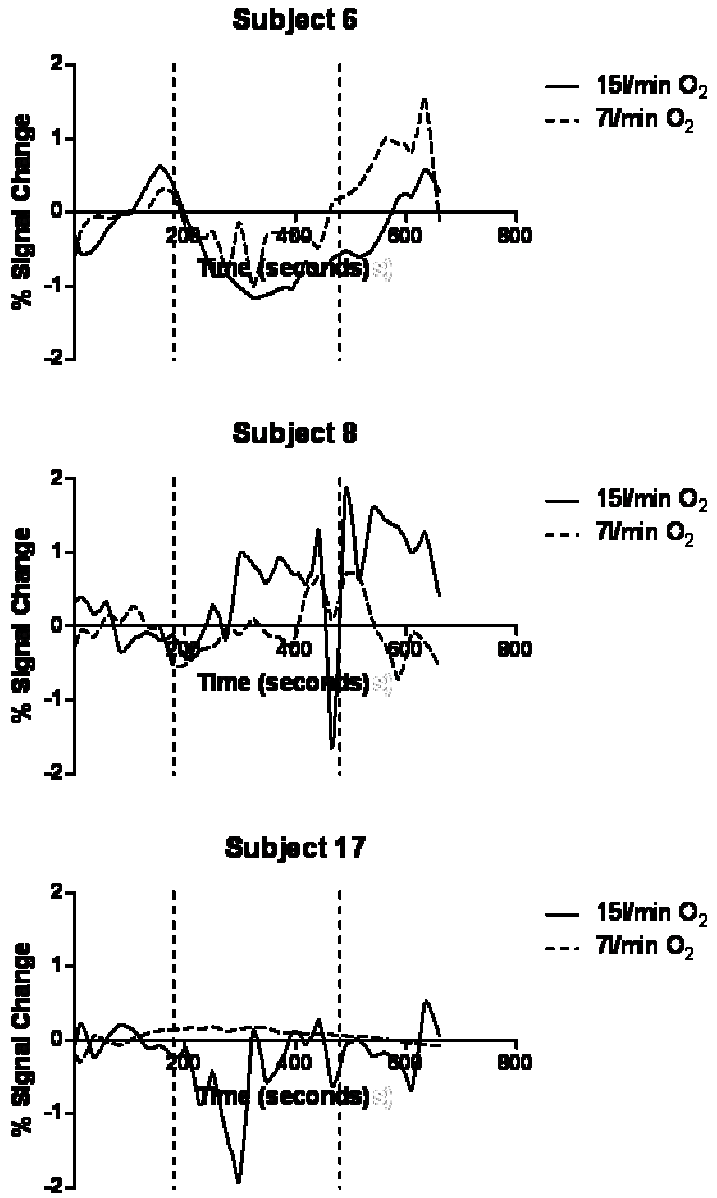

Figure 4-3 DWI Lesion T2*-weighted signal intensity-time curves acquired from Oxygen Challenges administered using 15l/min and 7l/min oxygen
The x-axis represents time (seconds) and the y-axis represents % T2*-signal change from the baseline. Vertical broken lines represent the onset and cessation of the oxygen challenge.

4.4 Discussion

This study not only examined two different flow rates of oxygen, but also considered multiple tissue types. In contra-lesional grey matter there was a larger T2*-weighted signal increase after Oxygen Challenge with 15l/min hyperoxia compared to 7l/min hyperoxia. In the white matter there was no statistical difference in the magnitude of signal change between 15l/min and

7l/min Oxygen Challenge. However, this may simply be a result of small numbers since it was observed that in 3/7 cases the signal increase was paradoxically greater after 7l/min Oxygen Challenge compared to 15l/min Oxygen Challenge. Of the subjects who had separate Oxygen Challenges (15 and 7l/min), three had a measurable DWI lesion (>1ml). Two of these subjects showed a decrease in signal in the DWI lesion after Oxygen Challenge, and in these cases the magnitude of the decrease was greater with the higher (15l/min) compared to the lower (7l/min) Oxygen Challenge flow rate. For the case with the positive signal increase in the DWI lesion, the magnitude of signal increase was larger with the higher flow rate of Oxygen Challenge. Taking these data together, it appears that in contra-lesional grey matter, which has relatively high CBV(242), low (~70%) venous oxygen saturation(249), and thus high deoxyhaemoglobin pool, the higher flow rate of oxygen produced the largest signal increases. This is consistent with the possibility that the higher flow rate of hyperoxia used in Oxygen Challenge produces the largest increase in venous oxygen saturation. In tissues which would be expected to have a lower total deoxyhaemoglobin pool due to either a lower CBV (white matter) or higher venous oxygen saturation (DWI lesion), this response was not seen. In fact, in many cases the converse was true.

Results from this study are consistent with previous studies. Firstly, as discussed in the previous chapter, the magnitude of signal increase of 2-3% in healthy cortical grey matter is similar to that reported in the literature(242, 249, 250, 252). Secondly, in cortical grey matter, the higher oxygen flow rate produced the largest increase in T2*-weighted signal intensity. It has previously been shown from group averaged data that there is an approximately linear increase of BOLD signal with increasing concentrations of oxygen(249). In the same study it was shown that an FiO_2 of 0.4 / 0.6/ 0.8 /1.0 was associated with increases in venous oxygen saturation of approximately 5% / 7% / 9%/ 10%(249). A similar study of oxygen enhanced MRI in volunteers(269) investigated oxygen delivered at 5l/min and 10l/min during T2*-weighted MRI, and showed a global signal increase of 2.12% and 3.17%, consistent with the findings from Chiarelli and colleagues(249). Despite often noisy signal, this current study confirms these previous findings from cortical grey matter. The explanation for these findings is simple, and has been outlined in Chapter 2. In brief, an increase in FiO_2 allows

extra administered oxygen to combine with venous deoxyhaemoglobin, increasing venous oxygen saturation and at the same time reducing the paramagnetic effect of deoxyhaemoglobin of T2*-weighted signal. Based on previous data(249), it is likely that, even despite hyperoxia, the venous haemoglobin is still incompletely saturated with oxygen. It should be noted that in addition to human studies, oxygen concentration has been investigated in animal models of Oxygen Challenge. Baskerville et al(320) compared 40% oxygen to 100% oxygen concentration Oxygen Challenge in a rodent model of stroke. Consistent with this study, it was also found that the higher concentration of oxygen gave rise to the largest changes in T2*-weighted signal. Interesting this phenomenon was seen in the penumbra (4.56% vs 8.65% in FiO_2 0.4 vs 0.6) but not for contra-lateral cortex. The differences in penumbra were also accompanied by differences in CBF and pO_2 and systemic blood pressure. Although the haemodynamic changes in penumbra could explain the differences between oxygen concentrations in this tissue compartment, changes in these parameters are unlikely to explain the differences precipated by different oxygen flow rates in T2*-weighted signal in this study, since autoregulation was likely to have been intact in healthy tissue.

Next, why was the response in contra-lesional white matter, and in DWI lesions, not always consistent with this? To the best of the author's knowledge, no study has focussed the investigation of varying oxygen concentrations or flow rates in these tissue compartments. One possible explanation for the findings in this study is that this is a chance finding due to small numbers of subjects analysed combined with noisy data (unlike the analyses reported in Chapter 2, there were no quality inclusion criteria for this study, owing to small numbers). However, compared to cortical grey matter regions, contra-lesional white matter and the DWI lesions were likely to have been associated with a smaller deoxyhaemoglobin pool. Both the contra-lesional white matter and the DWI lesions in this study were likely to have had an intrinsically lower $CMRO_2$ and cerebral blood volume(242) compared to grey matter. In addition, the OEF in the DWI lesion was likely to have been lower than in grey matter. Therefore the absolute quantity of oxygen molecules required to increase venous haemoglobin to full saturation was likely to have been less in these regions compared to grey matter. Therefore, it is possible that at higher concentrations of oxygen, a

greater concentration of paramagnetic oxygen was dissolved in plasma associated with these regions, a factor which would have attenuated the usual increase in T2*-weighted signal intensity, or even precipitated a decrease in signal intensity.

The results of this study suggest that the optimal concentration or flow rate of oxygen may vary between tissue types. For example, to distinguish regions of penumbra (where the venous oxygen saturation may be less than 10%) from 'healthy' tissue (where venous oxygen saturation is ~70%), one should administer sufficient oxygen to increase the venous oxygen saturation by greater than 30%. By doing this, one may precipitate differences in signal increase based on differences in venous oxygen saturation in the respective tissue compartment. Conversely, to distinguish infarct core (where venous haemoglobin may be near fully saturated) from healthy tissue, one will need to administer very little extra oxygen to achieve a difference in percentage signal change between tissue compartments. However, in this case, administering too much oxygen could blur the distinction between white matter and infarct core. It should be noted that these examples are intentionally simplistic in order to demonstrate the issues, and elsewhere in this thesis the issue of baseline cerebral blood volume (Chapter 6 and Chapter 8), which potentially confounds the interpretation of signal changes, is discussed.

How should 'dose' findings be performed? Firstly, the ideal scenario would be to perform such studies for subjects with acute stroke (both penumbra and infarct core) and also analyse changes in contra-lesional grey and white matter. Whilst varying the levels of administered hyperoxia within the same sequence is a logical approach, and one which could potentially be fairly time efficient, studies have suggested that such paradigms produce different results, at least with respect to perfusion changes, than would be obtained by performing separate, temporally distinct, Oxygen Challenges(250). Therefore, another possibility would be to evaluate different concentrations or flow rates of oxygen in different subjects using a latin square design in order to reduce the number of subjects required.

Whilst the responses in grey matter were fairly clear, it should be noted that conclusion made for the effects of hyperoxia in tissue compartments of low

metabolism remain tentative owing to the limitations associated with this study. Such limitations include small numbers and, probably most importantly, often noisy data. In addition, oxygen administered at the two flow rates used in this study was 'uncontrolled'; it has previously been discussed that oxygen flow rates through standard oxygen masks do not directly translate into precise values for FiO_2. In addition, it has been previously acknowledged that end tidal CO_2 was neither measured nor corrected for. Finally, it has been shown that the duration of administered oxygen is also important in determining the percentage signal change(252). Although this has been observed in healthy tissue, this phenomenon is likely to be even more of an issue in stroke tissue where it has been demonstrated that there is a longer time to maximum signal (Chapter 2), possibly due to hypoperfusion. The duration of administered oxygen was constant in this study, but differed from other previous studies.

In summary, the higher oxygen flow rate produced a greater signal increase in cortical grey matter, compared to the lower oxygen flow rate investigated. However, such findings were not consistently observed in the white matter, or the DWI lesion. Further investigation to investigate the optimal flow rate to delineate different tissue compartments would be valuable.

5 The Oxygen Challenge Technique May Detect Crossed Cerebellar Diaschisis

5.1 Introduction

In previous chapters, the Oxygen Challenge technique was applied to subjects with acute ischaemic stroke. In order to validate the technique, regions where substantial metabolic derangements were likely to exist were examined on a 'regions of interest' basis. Such regions included the 'DWI lesion', the 'PWI-DWI mismatch' region, and regions of 'DWI expansion'. Characteristics of these regions determine, at least in part, the potential relative benefit and harm from reperfusion therapies. However, there are other potential metabolic consequences from stroke. The term 'diaschisis' describes loss of excitation (and consequent hypometabolism) in regions anatomically remote from areas of damage. Although this phenomenon has been reported as being caused by non-stroke aetiologies such as cerebral tumours(321), much of the emphasis on the literature has been on stroke disease. Crossed cerebellar diaschisis (CCD) is one such form of diaschisis, and describes hypometabolism of a cerebellar hemisphere secondary to a lesion in the contra-lateral cerebral hemisphere, and is thought to be due to the destruction of the corticopontocerebellar tract. It was first described by Baron and colleagues in an abstract to the American Neurological Association. Using steady state ^{15}O-labelled PET, a matched reduction in blood flow and metabolism was seen in the contra-lesional cerebellar hemisphere when subjects were imaged within 2 months of stroke(322)(323). Further results suggested that findings tended to be more pronounced in those subjects with large cortical stroke or lesions affecting the internal capsule(324). More recently it has been shown that those subjects without CCD tend to have a good outcome(325).

Studies of CCD have conventionally used steady state PET (assessing cerebral metabolic rate for oxgen(322) or glucose metabolism(321)), Xenon CT(326) or other nuclear medicine techniques(327) and have usually imaged subjects predominantly beyond the hyperacute phase of stroke. These studies have suggested that the incidence of CCD after stroke is approximately 50%(328).

However, there are only a few studies which have focussed on acute stroke(329-332)(325) and only three which have used MRI to demonstrate the phenomenon(332, 333)(334). The MRI studies have only imaged haemodynamic changes and not the metabolic changes.

Given that the 'Oxygen Challenge' technique aims to provide an index of metabolic activity, the ability to demonstrate asymmetry of response between cerebellar hemispheres could potentially achieve two things. The first would be to provide further validation of the Oxygen Challenge technique itself, demonstrating that Oxygen Challenge has the required sensitivity to changes in metabolic activity, which are less dramatic than those changes seen between infarct core and healthy tissue. The second gain to be had is the introduction of a rapidly available technique for the further investigation of CCD in future studies.

In this study, the potential for the Oxygen Challenge technique to detect CCD was examined by comparing the asymmetries between cerebellar hemispheres using the Oxygen Challenge technique and maps of 'cerebral blood volume generated from conventional DSC-MRI data.

5.2 Methods

5.2.1.1 Subjects

In order to target a population likely to have CCD, only subjects with DWI lesions ≥50ml were considered for this part of the study. These were Subjects 1,5,6,8,9,12,16,21,22,30,32,33 (n=12). All of these subjects had suffered strokes within the middle cerebral artery territory. There were no T2*-weighted data quality inclusion criteria for this part of the study.

5.2.1.2 Post Processing

Using the software package 'Analyze' (Version 8.0, Mayo Clinic, Rochester, MT), regions of interest were manually delineated in the ipsi and contra-lateral cerebellar hemisphere. Regions were drawn to define a volume as large as possible, which spanned multiple slices (Figure 5-1). Different parts of the

cerebellar hemisphere were not distinguished. Regions from each hemisphere were drawn separately, but were drawn to match the 'region of interest' from the other hemisphere as close as possible. Values for the 'Percentage Signal Change' (PSC) and 'Area Under the Curve' (AUC) were from the defined regions of interest, as described in Chapter 2.

Figure 5-1 Example of manually defined regions of interest from the ipislateral and contralateral cerebellar hemisphere.
The example was taken from Subject 9 but is typical of the results from all other subjects. All regions of interest spanned across multiple slices. Red voxels indicate brain, yellow voxels indicate the segmented regions of interest.

5.2.1.3 Perfusion Imaging

The perfusion imaging was analysed for subjects included in this study. This was available from Subjects 1,5,6,9,12,16,22,32,33 (n=9). The software package 'Stroketool' (Digital Image Solutions, University of Dusseldorf) was used to generate images for 'relative cerebral blood volume' (relative CBV). Maps were generated automatically by the software, and were then smoothed using a 3x3 Gaussian kernel. The regions of interest for the ipsilateral and contralateral cerebellar hemispheres which were applied to the T2*-weighed imaging data were then co-registered to the relative CBV maps in 'Analyze'. Values for the ipsilateral and contralateral relative CBV in cerebellar hemispheres were recorded.

5.2.1.4 Statistical Analysis

Values for relative CBV were compared between cerebellar hemispheres using a 'Wilcoxon Signed Ranks Test (StatsDirect).. Values for the 'percentage signal change' and 'area under the curve' parameters were also compared between cerebellar hemispheres using the non-parametric Wilcoxon signed ranks test.

5.3 Results

5.3.1 T2-weighted Data*

A graphical representation of the T2*-weighted signal intensity-time curves from each subject is presented in Figure 5-2. This illustration shows that the magnitude of signal change was clearly greater in the ipsilateral cerebellar hemisphere, compared to the contralateral cerebellar hemisphere in Subjects 1,8,9,16, 22,30 and 33. An example of the percentage signal change map seen in Subject 8 is given in Figure 7-7. The T2*-weighted signal intensity-time curves from each cerebellar hemispheres appeared very similar to each other in Subjects 5,6,12, 21 and 32. In no case was the PSC or AUC greater in the contra-lateral hemisphere compared to the ipsilateral hemisphere. Interestingly, after Oxygen Challenge cessation, the T2*-weighted signal intensity increased in the cerebellar hemispheres of Subject 16 and Subject 32.

When considering the whole cohort for this study, the mean percentage signal change in the ipsilateral cerebellar hemisphere (5.1%, standard deviation = 2.7%) was significantly greater ($p=0.027$) than the corresponding value in the contralateral cerebellar hemisphere (3.7%, standard deviation = 3.1%). Again, when considering the whole cohort, the area under curve was significantly greater in the ipsilateral cerebellar hemisphere than the contralateral cerebellar hemisphere ($p=0.0015$).

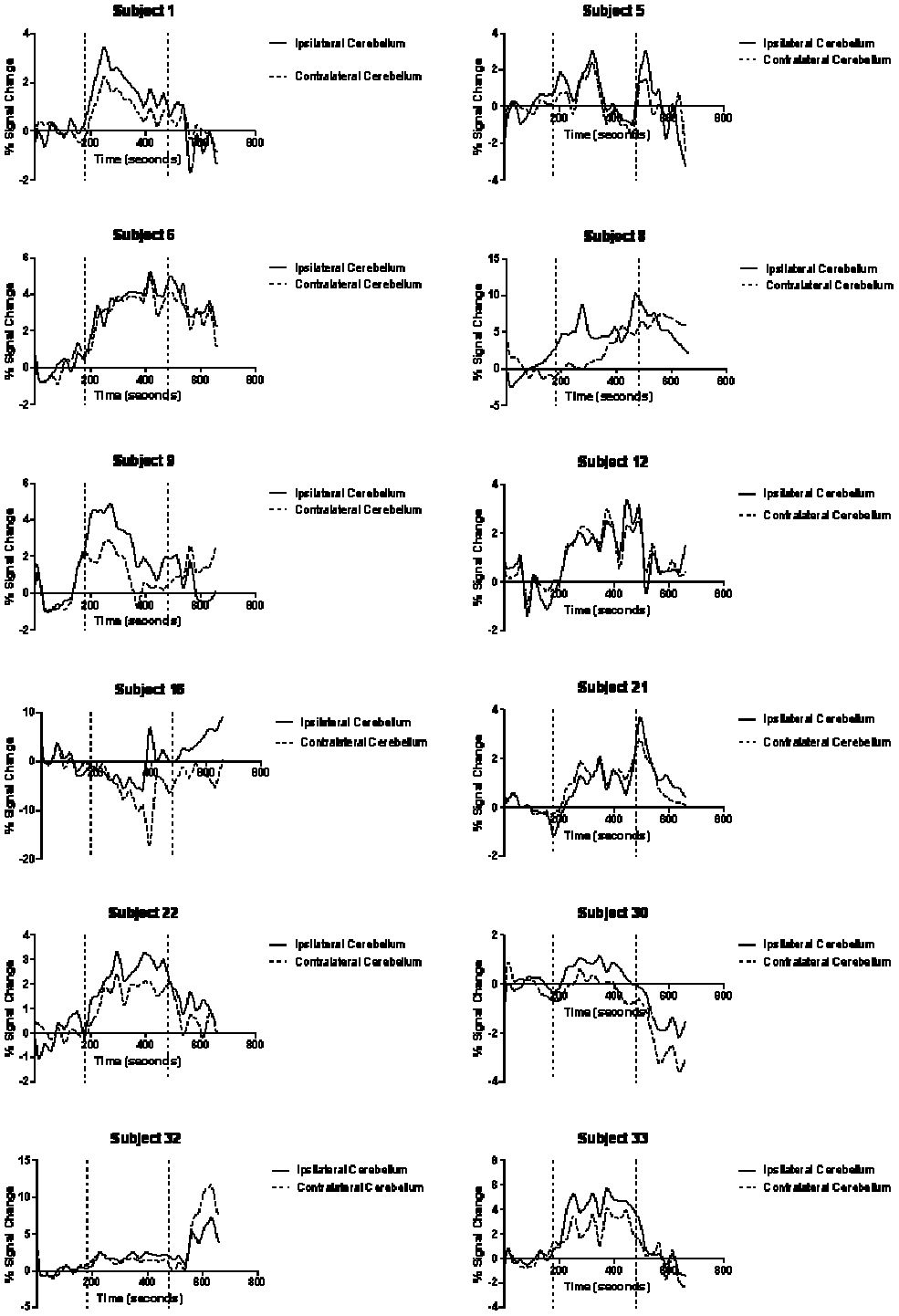

Figure 5-2 T2*-weighted signal intensity-time curves from ipsilateral and contralateral cerebellar hemispheres from subjects with large stroke lesions
The x-axis represents time (seconds) and the y-axis represents % T2*-signal change from the baseline. Vertical broken lines represent the onset and cessation of the oxygen challenge.

5.3.2 Perfusion Data

Values for relative CBV were less in the contralateral cerebellar hemisphere compared to the ipsilateral hemisphere (p=0.039, n=9). A greater than 10% reduction in CBV in the contralateral hemisphere was seen in subjects 1,5,9,16,22,33 (i.e. 6/9 CBV scans).

5.4 Discussion

This study examined the potential for the 'Oxygen Challenge' technique to detect crossed cerebellar diaschisis (CCD). In this cohort of subjects who had a large DWI lesion within the middle cerebral artery territory within the first day after stroke, PWI data were available in 9/12 (75%) of cases. Consistent with results from previous studies of CCD using MR-PWI after acute stroke(332, 333), a reduction in perfusion values (CBV in this study) was seen in the contralateral cerebellar hemisphere. A greater than 10% reduction in CBV was seen in 6/9 subjects with PWI data available. In addition, in 58% of cases (7/12), the magnitude of T2*-weighted signal intensity response to Oxygen Challenge was diminished in the contra-lesional cerebellar hemisphere compared to the ipsilesional hemisphere. This proportion is consistent with the oft quoted incidence of CCD as detected by PET studies(328). In all 6 cases with significantly reduced CBV (subjects 1,5,9,16, 22,33), there was also a clear reduction in T2*-weighted signal intensity in the contralateral cerebellar hemisphere.

How should these results be interpreted? Firstly, there are several potential explanations for the observation of significant differences between cerebellar hemispheres demonstrated by Oxygen Challenge. These include 1) that the Oxygen Challenge results were a chance finding, 2) that the Oxygen Challenge results were a manifestation of a stroke related phenomenon unrelated to metabolic activity and 3), the changes were due to CCD. Firstly, it is possible that the results from the Oxygen Challenge are a chance finding. This study used a relatively small group of subjects from the recruited cohort which was

presented in Chapter 2 in order to target a population most likely to manifest CCD. Twelve subjects with large strokes were considered and the use of such small numbers inevitably increases the chances of producing statistically significant chance findings. In addition, visual assessment of the T2*-weighted signal intensity-time curves shows that the signal derived from the cerebellar hemispheres was often noisy. For example, there appeared to be a drift in the signal in some subjects (e.g. subjects 16 and 30) which may have been due to scanner drift. Some subjects demonstrated T2*-weighted signal intensity-time curves which did not conform to the standard 'box-car' morphology expected from time series data generated from healthy tissue. For example, in the T2*-weighted signal intensity-time curve derived from subject 9, an initial rise in signal intensity was apparent after the onset of Oxygen Challenge, but this was not maintained throughout the duration of the Oxygen Challenge. This may have been due to noise artefacts which may be particularly prominent at the skull base due to air in the paranasal sinuses and mastoid air cells. Therefore there is a chance that the combination of small numbers and noisy signal led to a chance finding of a statistically significant positive result. However, it should be noted that in no case was the magnitude of the T2*-weighted signal intensity response greater in the contra-lateral cerebellar hemisphere, a finding in favour of the observed response being a genuine finding.

The second aspect to consider is the possibility of a technical confound. It is appreciated that subjects with large stroke exhibit a predilection for head tilt. One potential problem introduced by this phenomenon is the unequal proximity to the MRI radiofrequency coils for the two cerebellar hemispheres. A head tilt could potentially reduce the magnitude of signal detected from one hemisphere compared to the other. If this was the case, one would expect a similar morphology between the T2*-weighted signal intensity-time curves for the two cerebellar hemispheres, with only differences in absolute signal change being apparent. In five of the six cases where differences were detected, such findings were indeed seen. However, data from subject 8 does show two very different curve morphologies derived from ipsi- and contra-lesional hemispheres. In this case at least, the differences were unlikely to due simply to head tilt. In addition, in this study the potential for head tilt was reduced by secure foam padding surrounding the cranium within the MRI coil.

The final, most likely possibility, is that the observed changes were indeed genuine. Indeed, studies which have reported metabolic changes of CCD have also reported concurrent haemodynamic changes, and previous studies using perfusion weighted MRI have examined and reported haemodynamic changes(332, 333)(334). In this study there was a statistically significant reduction in T2*-weighted signal intensity and CBV in the contralateral cerebellar hemisphere. Moreover, the cases with reduced CBV in the contra-lesional hemisphere were those with the reduced T2*-weighted signal change in the same region. These findings, taken together, are strongly supportive of the possibility that the changes are due to hypometabolism due to CCD. The reduction in contralateral cerebellar T2*-weighted signal intensity can be explained by haemodynamic changes, since the hypometabolism in CCD is associated with decreased CBF and CBV with constant OEF. This means that CCD could be used to further understand the effect of baseline CBF and CBV on Oxygen Challenge result, without the confounding effect of changes in OEF. Further validation of this observation could be performed using steady state ^{15}O-labelled PET which may provide the definitive diagnosis of CCD and back-to-back Oxygen Challenge

This study is only the fourth MRI study to report changes consistent with CCD, and the only one to do so not using PWI. Yamada and colleagues(116) used a T2-weighted PWI sequence with a temporal resolution of one second to examine a cohort of 10 stroke subjects (both ischaemic and haemorrhagic stroke) from between 6 and 120 days since onset. In all ten cases, there was a reduced cerebral blood volume in the contra-lesional hemisphere. In addition to the cohort examined, differences between studies include a greater temporal resolution and less sensitivity to susceptibility artefacts (use of T2- weighted rather than T2*-weighted sequence) in the study by Yamada and colleagues compared to this study. Next, Lin and colleagues(332) studied 301 subjects within 5 days of anterior circulation ischaemic stroke. They showed that 15.6% of subjects had a delay TTP in the contra-lesional compared to the ipsi-lesional cerebellar hemisphere. The median delay in TTP was 1.6s, with differences of as little as 0.38s being reported. More recently, in a PET and MR study, Madai and colleagues showed that the degree of hypometabolism in CCD is poorly predicted by all perfusion parameters when applied at 1.5T(334).

A number of limitations of this study should be acknowledged. Firstly, the Oxygen Challenge measurements from the cerebellar hemispheres were potentially vulnerable to susceptibility artefacts from the paranasal sinuses and mastoid air cells. In addition, there was no T1-weighted image available for precise anatomical delineation of regions of interest. Therefore, it is clear that the regions of interest used in this study were suboptimal. Next, as previously acknowledged, only small numbers of subjects were considered in these analyses, potentially allowing statistically significant chance observations to be made. There is no measure available to guide how much inter-hemispheric variation may be expected in the cerebellum. A study of Oxygen Challenge in healthy volunteers could easily answer this question. In addition, this study focussed on all subjects with at least moderately large (>50mls) stroke. A larger number of subjects would allow more an even more homogenous cohort e.g. large lesions affecting both the internal capsule and the frontal lobes may identify subjects most likely to have CCD(335).

In conclusion, the observation that there is diminished Oxygen Challenge response in the contralateral cerebellar hemisphere, and that this is associated with decreased CBV, further validates the Oxygen Challenge technique. In this case Oxygen Challenge likely detected changes in $CMRO_2$ associated with haemodynamic changes only, since OEF is constant in CCD.

6 Oxygen Challenge Results are Dependant on Tissue Cerebral Blood Volume

6.1 Introduction

In earlier sections of this thesis it has been suggested that evaluation of cerebral blood volume may be important when interpreting Oxygen Challenge results from a stroke lesion compared to the contra-lesional side. There are a number of theoretical and practical reasons for believing why this may be important. To briefly recap, the signal model termed the 'static dephasing regime' which was described by Yablonskiy and Haake(232) and which modelled the BOLD signal intensity, emphasised venous cerebral blood volume as one of the key components in influencing the BOLD signal intensity. Considered simplistically, one can think of the total BOLD signal from a given voxel as dependent on the total measured pool of deoxyhaemoglobin. Two determinants for the absolute amount of deoxyhaemoglobin in this pool are the amount of deoxyhaemoglobin which enters the pool (OEF) and the volume of the pool at baseline (intrinsic CBV). Therefore, interpreting the total signal as dependent on OEF without considering CBV is likely to be incorrect. This is all the more pertinent when considering the sequence of patho-physiological events which is illustrated in Chapter 1 (Figure 1-4), and emphasises that in penumbral regions the rise of OEF is associated with a rise in CBV. Similarly, in the regions of infarct core, low OEF may be associated with a low CBV. However, although these parameters may be associated with each other, and often move In the same direction, they are independent in their influence on /the amount of deoxyhaemoglobin within the measured pool, and therefore both should be accounted for.

Data presented in this thesis thus far have also suggested that CBV is critical in determining T2*-weighted PSC. For example, selection of a region of interest from the saggital sinus (where the CBV is '100%') provided the greatest signal increase. Moreoever, signal increases were greater in cortical grey matter compared to subcortical white matter. This is reflected by findings from Davis(248) which suggested that the regions with the greatest capacity for T2*-

weighted signal increases after hyperoxia (a parameter they termed 'BOLD sensitivity') had the highest CBV. In addition, when Chiarelli and colleagues(249) gradually ramped up the concentration of administered oxygen, the first regions to be 'activated' on statistical maps were the venous sinuses (greatest cerebral blood volume), followed by grey matter in the cortex (intermediate cerebral blood volume) and followed thereafter by subcortical white matter (lowest cerebral blood volume).

With respect to investigating the influence of cerebral blood volume on the Oxygen Challenge results, the data from the animal pilot study cannot be interrogated since no measure of cerebral blood volume is provided by the ASL sequence used. However, measures of cerebral blood volume may be derived from MR-PWI. Therefore this study investigated the relationship between relative cerebral blood volume and the observed T2*-weighted signal changes in the stroke compartments for those subjects for whom PWI data were acquired.

6.2 Methods

6.2.1 Subjects

Analysis of the relationship between CBV and Oxygen Challenge results from grey and white matter was performed using data from the contra-lesional hemisphere of subjects for whom both PWI and T2*-weighted data were available, regardless of stroke lesion volume. After exclusion of PWI data from one subject owing to excessive noise artefact precluding accurate quantitative measurements (subject 34) and another owing to a highly anomalous intra-cranial circulation which would have yielded AIF selection inconsistent with other subjects (subject 19), data from 23 subjects were considered for this analysis.

Assessment of CBV in stroke tissue compartments was performed for subjects in whom PWI data were acquired and who had a measurable lesion (≥1ml) on DWI or PWI (for DWI lesion, n=12; subjects 1,5,6,9,12,16,22,24,28,31,33,35; for PWI-DWI mismatch region, n=7, subjects 1,5,16,18,22,33,35).

6.2.2 Image post-processing

6.2.2.1 Generation of Perfusion Maps

Maps of whole brain quantitative cerebral blood volume (CBV, ml/100g) were calculated using Stroketool (version 2.4, Digital Image Solutions, University of Dusseldorf). The arterial input function was defined using the contra-lateral proximal MCA. Deconvolution was performed using the standard singular value decomposition (sSVD)(109, 110). In addition to the generation of perfusion maps using an AIF, maps of relative cerebral blood volume were also generated using 'Stroketool' for comparison to the quantitative CBV maps. In a similar fashion, maps of unthresholded TMAX were also produced. Stroketool software allowed the specification of the time window for analysis. This was specified to start from the point of deflection of the AIF curve, and the last point being 2-5 volumes after the return to baseline.

6.2.2.2 Definition of Regions of Interest

Regions of interest from which values for CBV were derived were 1) the DWI lesion (n=12) and its mirror region from the contra-lesional side, 2) the PWI-DWI mismatch region (n=6) and its associated mirror region, and 3) the contra-lesional grey and white matter (n=23). A ratio of CBV values was subsequently expressed for each region ([DWI lesion : mirror], [PWI-DWI mismatch region : mirror], [contra-lateral grey-matter : contra-lateral white-matter]).

The 'regions of interest' maps defining DWI lesions and PWI-DWI mismatch regions were the same as used for the analyses stated in Chapter 2. The regions of interest maps used for contra-lateral grey and white matter delineation were the same as used in Chapter 3 (section 3.2.2), where a detailed description of their generation was provided.

6.2.2.3 Derivation of values for CBV for each tissue compartment

Using Analyze software (version 8.0, Mayo Clinic, Rochester, USA), maps of CBV were co-registered to the T2*-weighted EPI data using 'windowed sinc' interpolation. Next, maps of previously defined regions were overlaid on the transformed CBV maps and values for CBV for the different tissue compartments were subsequently derived automatically by the software.

The values for the Oxygen Challenge results (AUC, PSC, TMS, and GIC) from the DWI lesion and PWI-DWI mismatch regions, and from contra-lesional grey/white matter were the same as those generated from the analyses stated in Chapters 2 and 3 respectively.

6.2.3 Statistical analysis

All statistical analyses were performed using the software 'StatsDirect' (version 2.7.8. www.statsdirect.com). Statistical significance was set at $p<0.05$. Owing to the predominantly non-normal distribution of the data, non-parametric tests were used unless otherwise stated.

Firstly, in order to determine which CBV data were to be used, data from 'relative CBV' and deconvolved 'quantitative CBV' maps were compared using a Wilcoxon signed ranks test and a Spearman's rank correlation. To do this, the [DWI lesion : mirror region] CBV ratios were compared, since it was assumed that this would allow a range of CBV values to be assessed.

Next, the relationships of perfusion parameters (CBV and TMAX) to Oxygen Challenge results (PSC and AUC of of the T2*-weighted signal intensity curves) were assessed. To do this the correlation of the ratio of perfusion parameters in a region of interest : reference region was correlated with a ratio of Oxygen Challenge results in the region of interest : reference region i.e. data were 'normalised' with respect to a reference region. These [regions of interest : reference regions] were 1) [DWI lesion : mirror], 2) [PWI-DWI mismatch region : mirror] and 3) [grey matter : white matter]. Correlations between CBV values

(DWI lesion : mirror region) with values for T2*-percentage signal change (T2*-PSC) and area under the curve of the T2*-weighted signal (T2*-AUC) (DWI lesion : mirror region) were assessed using a test of Spearman's rank correlation. Similar analyses were performed to assess the relationship between TMAX and T2*-weighted data. In addition, these same analyses were performed for values derived from PWI-DWI mismatch regions (ratio of mismatch : mirror region) and grey and white matter (data expressed as 'grey matter : white matter' ratios).

In order to quantify the percentage variance of T2*-weighted signal changes as dependent on CBV a simple regression analysis was performed for CBV (DWI lesion : mirror) and T2*-PSC data (DWI lesion : mirror). Where data were not normally distributed they were transformed using a 'natural logarithmic' function to achieve normal distribution as defined by the 'Shapiro Wilk' test.

Finally, the CBV ratio (DWI lesion : mirror region) was assessed in the three cases of 'reperfused DWI lesion' in order to seek any relationship between CBV and the observed T2*-PSC in these regions.

6.3 Results

6.3.1 Comparison of 'relative' to 'quantitative' CBV values

There was a strong correlation (*Rho*=0.92, p=0.0001), between relative CBV (DWI lesion : mirror region) and quantitative CBV (DWI lesion : mirror region). However, the quantitative CBV ratio (median =0.29) was lower than the ratio derived using relative cerebral blood volume (median =0.53) by a difference which was statistically significant (p=0.005). Figure 6-1 shows an example from subject 22, where the CBV in the region of the DWI lesion was lower (relative to the contra-lesional side) on the quantitative CBV map compared to the relative CBV map. This example also shows that under conditions of low flow, there appears to be reduced CBV in the region of the PWI-DWI mismatch on the CBV map derived using deconvolution. This was due to some voxels being assigned a 'zero' value where flow was very low. Therefore, due to concerns about inaccurate quantification due to poor modelling of the arterial input function

(AIF) for the deconvolved quantitative CBV maps, relative CBV maps were used for subsequent analyses. Maps of relative cerebral blood volume are simpler to perform and compute, require lesser assumptions, and are more automated requiring less user input.

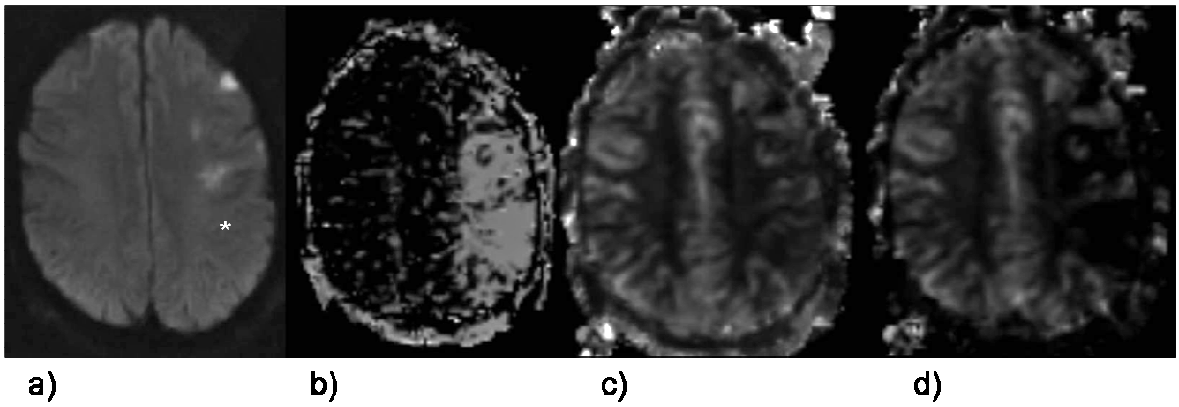

Figure 6-1 Demonstration of the difference in CBV maps which show 'relative' values and those which are 'quantitative'
a) shows the lesion on diffusion weighted imaging, b) shows the perfusion lesion as defined by the unthresholded TMAX parameter, c) shows the map of relative cerebral blood volume, and d) shows the map of cerebral blood volume derived with deconvolution. All images are from subject 22. The deconvolved CBV map shows a lower CBV relative to the contra-lateral side compared to the relative CBV map. This difference is also apparent in the region of PWI-DWI mismatch (*).

6.3.2 Perfusion parameters in the stroke tissue compartments : influence on Oxygen Challenge results

6.3.2.1 DWI lesion

A statistically significant correlation between CBV ratio (DWI lesion : mirror region) and the percentage T2*-weighted signal change (DWI lesion : mirror region) was noted (*P*=0.68, p=0.01, Spearman's rank correlation). Next, a simple linear regression was performed in order to determine how much of the variance of the T2* percentage signal change was explained by the CBV. Although the data for T2*-weighted PSC were likely to be normally distributed (p=0.35, Shapiro-Wilk test), normal distribution for the CBV ratio for DWI lesion : mirror data could not be definitively proven (p=0.06, Shapiro-Wilk). Data for CBV were therefore transformed using a natural logarithmic function to achieve a distribution likely to be normal (p=0.7). As expected, there was a positive

correlation between PSC ratio (DWI lesion : mirror) and transformed CBV ratio (DWI lesion : mirror) (*P*=0.62, p=0.03, r^2=0.39, Figure 6-2). These results suggest that 39% of the variance of PSC ratio (DWI lesion : mirror) is explained by the CBV ratio (DWI lesion : mirror). A similar result was attained when assessing data for AUC for the T2*-weighted signal data (DWI:mirror), which were also log transformed, for a correlation with CBV ratio (*Rho* =0.64, p=0.03, r^2=0.40).

There was a negative correlation between the TMAX value derived from the DWI lesion and the T2*-PSC (DWI lesion : mirror) which was statistically significant (*P*=-0.61, p=0.04). The correlation was stronger when the absolute T2*-PSC value was considered, rather than being normalised to the contralateral hemisphere ((*P*=-0.74, p=0.008). Similarly, correlations with TMAX were observed when the AUC of T2*-weighted signal was considered (*P*=-0.87, p=0.003 for AUC ratio [DWI:mirror]; *P*=-0.9, p<0.0001 for non-normalised (absolute) AUC).

Finally, there was no correlation between either CBV or TMAX values and the gradient of incline or time to maximum signal (P>0.05 for all analyses).

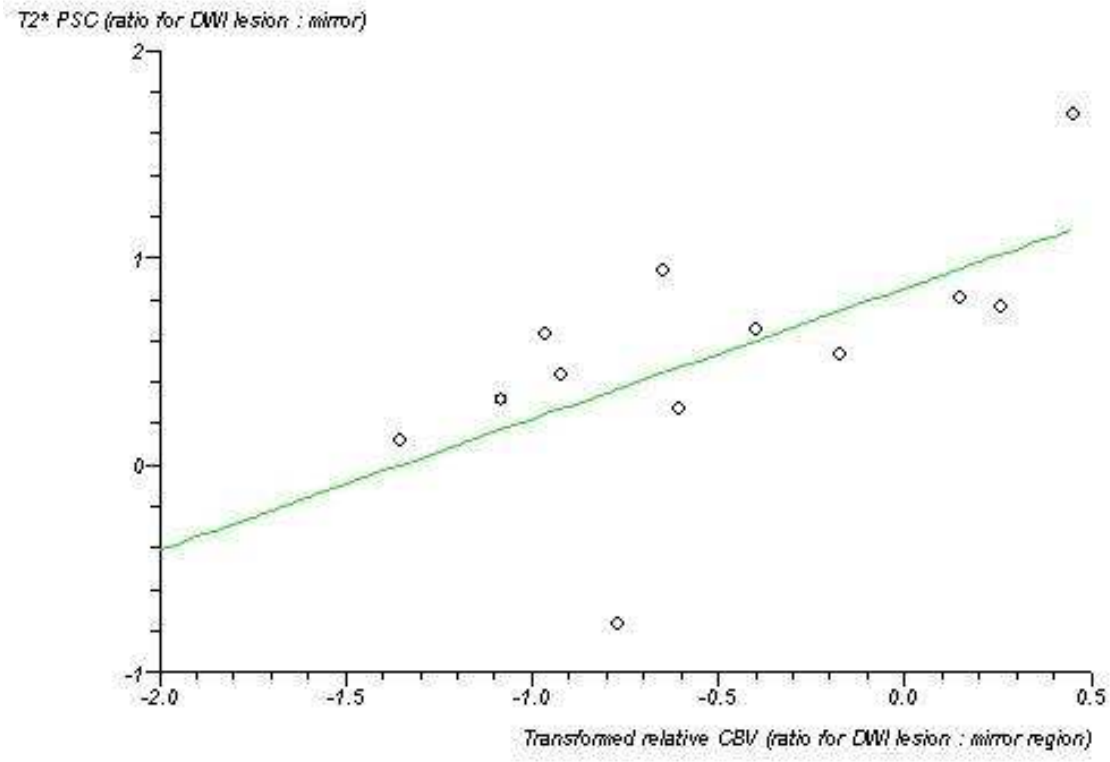

Figure 6-2 Scatter plot of CBV and percentage signal change
The x-axis shows the CBV ratio (DWI lesion : mirror) and the y-axis shows the percent signal change ratio (DWI lesion : mirror) . The open circles show individual data points. The solid line shows the regression line. PSC = percent signal change, CBV = cerebral blood volume, DWI = diffusion weighted images.

Results from Chapter 2 showed that in regions of reperfused DWI lesion, one case had an elevated T2*-PSC compared to the contra-lesional side. In two other cases the T2*-PSC response was diminished in regions of reperfused DWI lesion. The figure has been adapted to show the CBV ratios in these regions. The case where the response of the reperfused DWI lesion was exaggerated had the higher relative CBV value (ratio = 1.56).

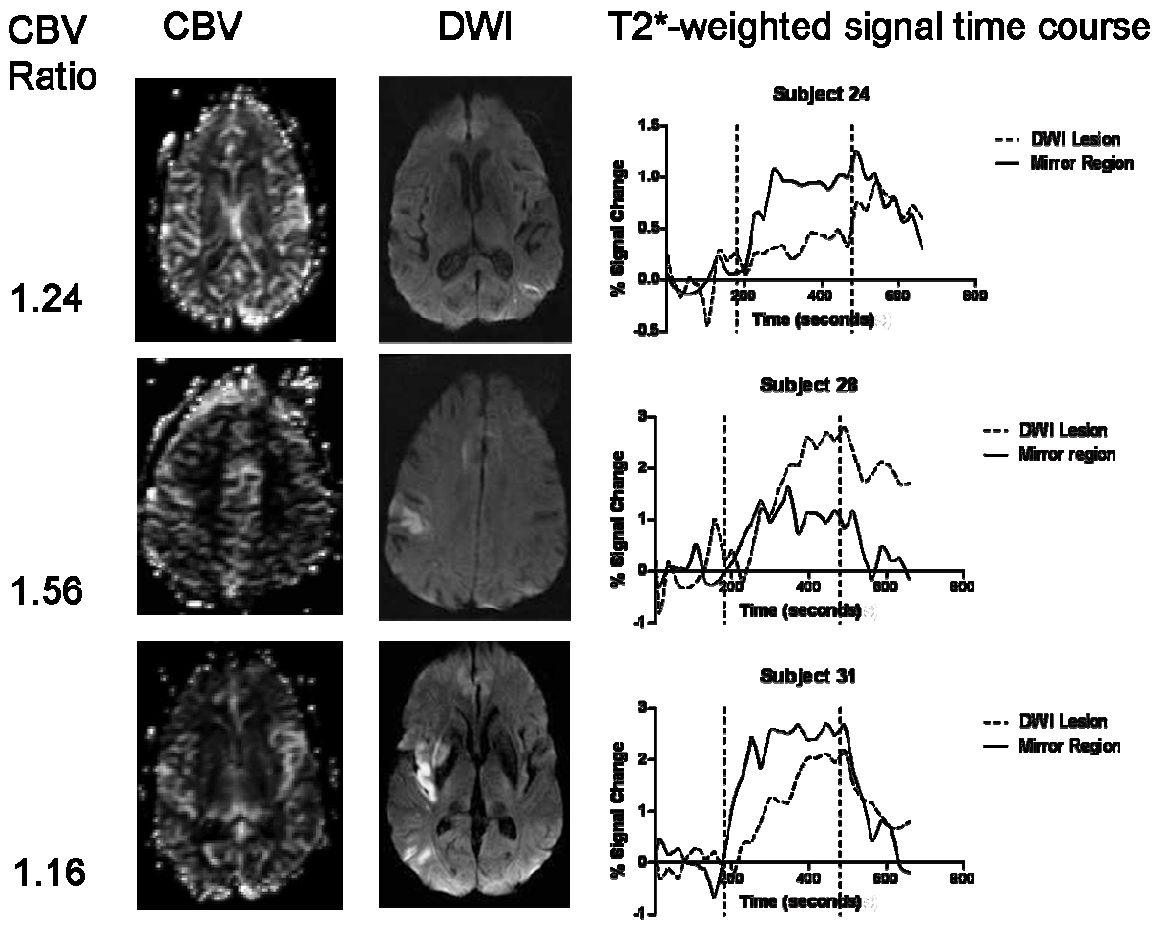

Figure 6-3 CBV in regions of reperfused DWI lesion
Figure adapted from Chapter 2. CBV = cerebral blood volume. DWI = diffusion weighted imaging

6.3.2.2 PWI-DWI mismatch region

There was no statistically significant correlation between T2*-PSC ratio (mismatch region : mirror) or AUC ratio (mismatch : mirror) and CBV ratio(mismatch : mirror) ($p>0.05$ in each case). No region of PWI-DWI mismatch was found to have an elevated CBV ratio (mismatch : mirror) and in some cases there appeared to be a reduction in CBV in the mismatch region compared to the contralateral side . Despite this, PSC was increased in mismatch region compared to the contra-lateral side, for 3 cases.

Subject	Relative CBV ratio	PSC ratio MM
1	1.12	-0.69
5	0.64	0.89
16	0.79	2.13
22	0.54	0.69
33	0.87	1.24
35	0.55	2.83
Median	0.78	1.24

Table 7 Percentage signal change and cerebral blood volume in regions of PWI-DWI mismatch.
CBV = cerebral blood volume, PSC = percentage signal change, MM = mismatch

6.3.3 Cerebral blood volume in contra-lesional grey and white matter : influence on Oxygen Challenge results

There was no correlation between CBV (grey : white matter ratio) and T2*-weighted percentage signal change (grey : white matter ratio) (*P*=-0.018, p=0.93) and area under curve (*P*=-0.1, p=0.65). There was also no correlation between the percentage difference in CBV between grey and white matter, with either the PSC ratio (p=0.92) or percentage difference in PSC between grey and white matter (p=0.67). Figure 6-4 shows that the CBV ratio in grey : white matter was clustered around 2.0 and within this narrow range of CBV ratio values there was substantial variation in the percentage signal change ratio.

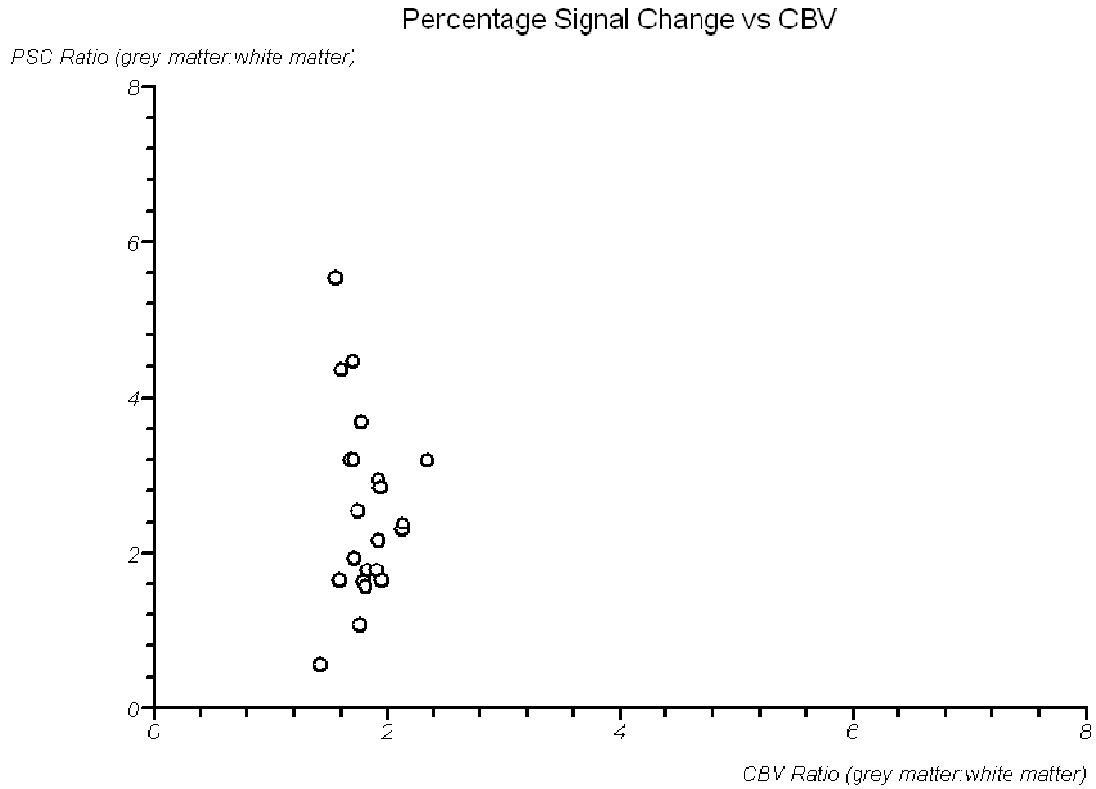

Figure 6-4 Scatter plot showing of CBV versus percentage signal change
Values are expressed as a ratio between grey and white matter. PSC = percentage T2*-weighted signal intensity. CBV = cerebral blood volume. Please note that one outlier was excluded from this graph; the PSC ratio for this subject was ‘878 owing to a negligible signal change in white matter.

6.4 Discussion

This study was performed on the background of theoretical and ‘results driven’ suggestions that CBV is likely to play a major influence in the determination of the magnitude of T2*-weighted signal change after hyperoxia. Maps of relative CBV were used in preference to deconvolved maps due to concerns regarding lack of inaccurate quantification. Within the DWI lesion, a moderate positive correlation between ‘normalised’ CBV and ‘normalised’ PSC was observed, suggesting an association between the two parameters. Interestingly, when considering cases of reperfused DWI lesions, the case which showed an exaggerated T2*-weighted signal increase after hyperoxia compared to the contra-lesional side showed an elevated CBV (ratio = 1.56). Although it is possible that this DWI lesion did represent a penumbral region at 24h post ictus(21, 54), a more plausible explanation is that the marked T2*-weighted

signal increase was due to the elevated CBV in this region. The association between CBV and magnitude of signal change was not seen when normalising grey matter data to white matter data, or data from the mismatch region to the contralateral side. Finally, it was demonstrated that there was a negative correlation between TMAX, a perfusion parameter measured in units of 'seconds', and PSC.

There are three possible explanations for why CBV and PSC values were correlated with each other when expressed as [DWI lesion : mirror] but not when expressed as [PWI-DWI mismatch region : mirror] or [contra-lateral grey matter : contra-lateral white matter]. The first possible explanation is that the positive findings from data derived from the DWI lesion are a chance finding. These data were derived from only 12 subjects; correlations for such few data points may be easily influenced by a small number of outliers. However, although possible, this explanation is at odds with the currently accepted theory of the BOLD signal(206) and observations from this thesis which predict a significant influence from baseline CBV. The second explanation is that the observation is genuine, but that the CBV is simply a surrogate marker for metabolic activity and there is no independent influence from CBV. The plausibility of this argument is supported by findings showing a good correlation between low CBV and prediction of infarction(165). The third possible explanation, and in the opinion of the author the one which is most plausible, is that the correlation observed with data from the DWI lesion is genuine, and it represents an independent contribution of CBV to total BOLD signal. This is consistent with other studies which have suggested CBV plays a critical role in determining the 'ceiling' of potential BOLD signal change after hyperoxia(248, 252). It is likely that the large range of normalised CBV in the DWI region (0.26-1.6) enabled the association between CBV and PSC to be demonstrated by a positive correlation. Conversely, the relatively tight range for grey : white matter CBV ratio, which was clustered around a value of approximately 2.0, gave rise to a much more limited spread of data than compared to the DWI lesion, and thus a genuine association may have been masked when simply assessing correlations. Another likely source of potential error comes from the calculation of PSC from white matter. It has previously been shown that there is a relatively low signal-to-noise ratio from this region and thus small errors in the determination of PSC in

this region may have had a strong influence on the grey : white matter PSC ratio.

It should be noted that hyperoxia during BOLD sensitive MRI has been used specifically to calculate CBV. Bulte and colleagues(242) employed a modification of the equation proposed by Newman and colleagues(336) which suggested that CBV was proportional to the ratio of the relative change in signal intensity in tissue compared to the relative signal change from the saggital sinus, the latter representing a voxel of pure blood (CBV = 100%). Whilst this approach is not suitable for use in stroke subjects due to non-uniform OEF through the brain, it highlights the dependence of the signal change on baseline CBV, and does not consider $CMRO_2$. The findings from Bulte and colleagues(242) which were generated using this method were comparable to other studies reporting grey matter : white matter ratios for CBV.

However, in addition to the likely influence of CBV on the observed results, the data also support an argument for an independent influence from metabolic activity. For example, Figure 6-3 shows there is a diminished Oxygen Challenge response from within the DWI lesion despite a CBV which is likely to be within normal limits. In addition, Table 7 demonstrates that an elevated PSC may be observed in the mismatch region in the absence of elevated CBV in this region.

The major implication of this study is that the percentage signal change after Oxygen Challenge should be interpreted with knowledge of baseline cerebral blood volume. This argues the case for using DSC-PWI rather than ASL, as was used by the pilot animal study to measure CBF(255), since the latter only provides a measure of CBF. Secondly, there are two approaches to Oxygen Challenge which may be taken in the future. The first is to assess the Oxygen Challenge using the uncorrected percentage signal change, as was done in this study. Even given the aforementioned dependence on CBV, this is still a potentially viable approach, since the results provide a measure of the total deoxyhaemoglobin pool, which is a combined marker of metabolic and haemodynamic activity and therefore potentially clinically useful. The second potential approach is to correct the percentage signal change for baseline CBV, in order to provide an index which represents OEF in a more specific manner. To do this one could use the CBV ratio and PSC ratio from contra-lesional grey

matter : white matter, to generate a correction factor. However, as was seen in this study, a greater signal-to-noise ratio, particularly for white matter would be required for accurate results. Moreover, such as correction constant would vary according to magnetic strength. In addition, this approach strays from the underlying philosophy of the Oxygen Challenge technique, which should be simple and free from as many assumptions as possible. Perhaps a more appropriate approach is simply to view Oxygen Challenge data side by side to other sequences such as CBV and TMAX, in a manner analogous to the conventional approach to stroke MRI.

A number of limitations of the study should be acknowledged. Firstly, the limitations of small numbers of subjects and poor signal-to-noise ratio have already been mentioned. Secondly, measurement of relative cerebral blood volume using the maps generated in this study may be associated with some inaccuracies. In this study the relative maps of cerebral blood volume were used as they were associated with less signal drop out compared to those maps generated by standard SVD(109). Maps of CBV are not sensitive to the potentially detrimental effects of delay and dispersion since only the peak, but not the area under the curve from which CBV is calculated, is attenuated due to such effects(117). However, it has been shown that after the stipulation of a fixed time window for calculation of the area under the curve, which was performed to limit the effects of tracer recirculation performed for both relative and absolute CBV maps in this study, CBV values may be underestimated since the whole curve may not be analysed in hypoperfused tissue where there is delay(117, 337). This may explain the marked signal drop out on the absolute CBV maps and could explain the surprising low CBV ratio observed in the PWI-DWI mismatch region. It has been suggested that using all data after the arrival of contrast may provide more accurate results(108). This approach may have provided slightly different results. Finally, this study only considered the influence of baseline cerebral volume on T2*-weighted signal. In fact, with changes in CBF which are seen during hyperoxia(262), the CBV may also change dynamically(284). However, at the level inspired FiO_2 which was likely to have occurred in this study (probably no more than ‘0.6’), perfusion changes are likely to have been minimal(250). Finally, when interpreting the results of this study, it should be remembered that the positive correlations demonstrated

here suggest only associations between correlated parameters, rather than causations.

A number of approaches may be adopted by further studies aiming to further investigate the haemodynamic and metabolic influences on Oxygen Challenge results. The ideal method would be to compare Oxygen Challenge data to ^{15}O PET, which could provide measures of OEF and CBV. Using this current data set a voxel based multiple linear regression analysis could be performed using data from across multiple subjects to determine if factors such as CBV, TMAX and ADC provide an independent prediction of PSC from Oxygen Challenge. This is particularly important as both TMAX and CBV correlated with PSC in DWI lesions in this study. To do such an analysis, one would need to generate a map of percentage signal change. Both voxel based and regions of interest analyses may be performed on future data sets similar data sets to this one, but ideally with improvements to signal-to-noise ratio and imaging of a more acute population. In addition, a critical factor in determining the relative influence of baseline CBV and OEF will be the measurement of venous oxygen saturation. Although this could be done from blood sampling from the internal jugular vein, this approach cannot inform with respect to regional heterogeneity. More localised data may be derived from novel emerging MRI techniques such as the multi-echo gradient echo / spin echo sequence which may measure blood oxygen saturation within a region of interest(234).

In conclusion, ‘normalised’ CBV was correlated to ‘normalised’ PSC, from data collected from DWI lesion regions. This suggests CBV influences results from Oxygen Challenge. Therefore CBV maps should be viewed along side the Oxygen Challenge data for accurate interpretation of results. In addition, the results raise the possibility that for interpretation of the metabolic contribution to PSC, results could be corrected for CBV.

7 Oxygen Challenge Results May Be Interpreted as a Brain Image

7.1 Introduction

The work presented in Chapters 2-5 showed that there were differences in the T2*-weighted signal intensity-time curves between different tissue compartments following acute ischaemic stroke. However, the nature of the analysis, which was to assess the T2*-weighted signal intensity-time curves of the mean signal from tissue compartments defined by DWI and PWI, was insensitive to the potential spatial heterogeneity of the Oxygen Challenge data. There was no indication of the spatial correlation of the Oxygen Challenge results to findings from other MRI sequences, there was no evaluation of how Oxygen Challenge results varied throughout the ipsi-lesional and contra-lesional hemispheres, and no appreciation given for how much or little variation there was within tissue compartments defined by conventional MRI sequences. The generation of an image representing the Oxygen Challenge data may help to address these issues.

The importance of image generation for the evaluation of acute ischaemic stroke was discussed to in Chapter 1. The evaluation of images for clinical purposes is primarily qualitative; clinicians make inferences of the underlying patho-physiological state based on morphological appearances(52), before making a dichotomous decision; to administer, or not to administer, thrombolytic therapy. Image generation therefore allows evaluation of all the data across the whole brain for any given sequence, as well as allowing comparison to other sequences; crucially these qualitative evaluations can be performed rapidly before treatment decisions are made. Quantitative thresholding may also be applied to images to allow for further more detailed analyses(123, 159).

Image generation has also proven invaluable in the research setting. For example, co-registration of PET and MR images has allowed comparisons of spatially correlated data and thus enabled new insights into results from MR techniques based on the gold standard PET data(54, 176). From the perspective

of clinical trials, evaluation of the morphology of lesions on MRI has formed the basis of trial end points(26, 338-340) and it is believed that such an approach has the potential to reduce the number of subjects required for adequate power in clinical trials(341). Similarly, imaging based inclusion criteria may also increase the efficiency of clinical trial design(342, 343).

The ability to produce an image of the Oxygen Challenge results would be invaluable for a number of reasons. Firstly it would allow qualitative spatial correlation of whole brain Oxygen Challenge results to other MR imaging modalities such as DWI and PWI, thus complementing the analyses presented in Chapter 2. Secondly, it would allow co-registration of Oxygen Challenge maps to DWI and PWI, thus allowing voxel based analyses to be performed - a natural extension of the evaluation of regions of interest which as presented in Chapters 2-5. Finally, if the Oxygen Challenge technique becomes ready for clinical use, image generation will be essential for making clinical decisions.

Although a number of parameters of the Oxygen Challenge data have been evaluated (percentage signal change, area under the curve, time to maximum signal, and gradient of incline of the signal increase), it is perhaps percentage signal change (PSC) which is most relevant to the initial hypotheses, which considered the magnitude of signal changes in various tissue compartments. Therefore, work presented in this chapter considers the generation of PSC maps. Owing to the limitations imposed by low signal-to-noise ratio, the use of simple 'difference' images, where the baseline data could be simply subtracted from the Oxygen Challenge data to produce maps of percentage signal change, was not possible. Instead, in a manner analogous to the evaluation of functional MRI (fMRI) studies, the data from each voxel was fitted to a pre-specified model using the General Linear Model. This powerful approach, which is commonly employed in studies of psychology, allowed a voxel based mass univariate analysis of the Oxygen challenge data.

7.2 Methods

All percentage signal change (PSC) maps were created using FEAT (FMRI Expert Analysis Tool, version 5.98, part of FSL FMRIB's Software Library,

www.fmrib.ox.ac.uk). The following pre-processing steps were applied by the software: motion correction (MC-FLIRT, FMRIB Centre, Oxford, UK), non-brain removal (brain extraction tool: BET), and spatial smoothing. For the latter, a gaussian kernel of full width at half maximum (FWHM) of 10mm was applied in this study in order to clearly highlight anatomical regions of interest. The usual temporal filtering method applied to fMRI studies is 'high pass filtering', which removes low frequency noise such as that induced by scanner drifts. However, fMRI studies usually examine short lived events, and events of 300s duration, such as the Oxygen Challenge, would be unusual in their length for fMRI. Given the design and duration of the Oxygen Challenge sequence, high pass filtering was therefore not applied for this study. However, a previously acknowledged problem associated with the Oxygen Challenge data was high frequency noise. For the analysis of the T2*-weighted signal intensity-time curves derived from defined regions of interest, much of this high frequency noise was filtered out using wavelet transforms. In order to filter out this high frequency noise in the images, low pass filtering was applied.

After pre-processing, the data were then modelled by the FSL software using the general linear model (GLM). The general principle of GLM is to fit the actual data to a user defined model, on a voxel by voxel basis. The parameter estimates (also termed 'Betas') provide a measure of how well the data fit the model. In order to derive a measure of percentage change, a simple calculation was performed. The parameter estimates generated from the GLM which fitted the Oxygen Challenge data to the pre-specified model were multiplied by baseline / maximum range of the design (in this study these values were equal to '1'). This value was then divided by the mean image of the pre-oxygen time points using an image calculator in 'FSL maths', provided by the FSL software. Although FSL employed the technique of 'grand mean scaling' to enable comparisons between subjects, all images (e.g. parameter estimate and mean images) used in these calculations were scaled by the same value. This procedure provided percentage change maps.

Data were modelled in two fashions. The first approach (Model 1) was simple, used all of the data acquired, and made few assumptions. The model used simply reflected the sequence of gas administration as shown below. It was specified that from 0-180s there was a 'rest'/baseline period, from 181 to 480s

there was ‘activation’ (in this case the Oxygen Challenge) and from 481 to 660s seconds there was a ‘rest’ / baseline period. The second model (Model 2) focussed on data which was deemed to be of highest potential ‘yield’ for the generation of percentage signal change maps. Given the possibility of signal drifts and physiological low frequency fluctuations(268), assignment of the mean of all pre-Oxygen Challenge time points acquired over three minutes as being baseline, may potentially give rise to an inaccurate calculation for percentage signal change. Therefore , in the second model, only the final minute of the pre-Oxygen Challenge time points was used to define the baseline. For the ‘activation time points’, the mean T2*-weighted signal acquired in the final minute of the Oxygen Challenge was used to calculate the maximum signal. This corresponded to the eighth minute of the entire Oxygen Challenge sequence. This allowed time for physiological equilibration after the onset of Oxygen Challenge which may have varied between subjects and therefore introduced potential confounds into Model 1. Finally, the time points following Oxygen Challenge cessation were not considered by Model 2. This removed any confounds of variability between subjects with respect to the decline in T2*-weighted signal seen post Oxygen Challenge. Therefore, Model 1 used all available time points, whilst Model 2 used only 2 minutes of the 11 minutes worth of data acquired.

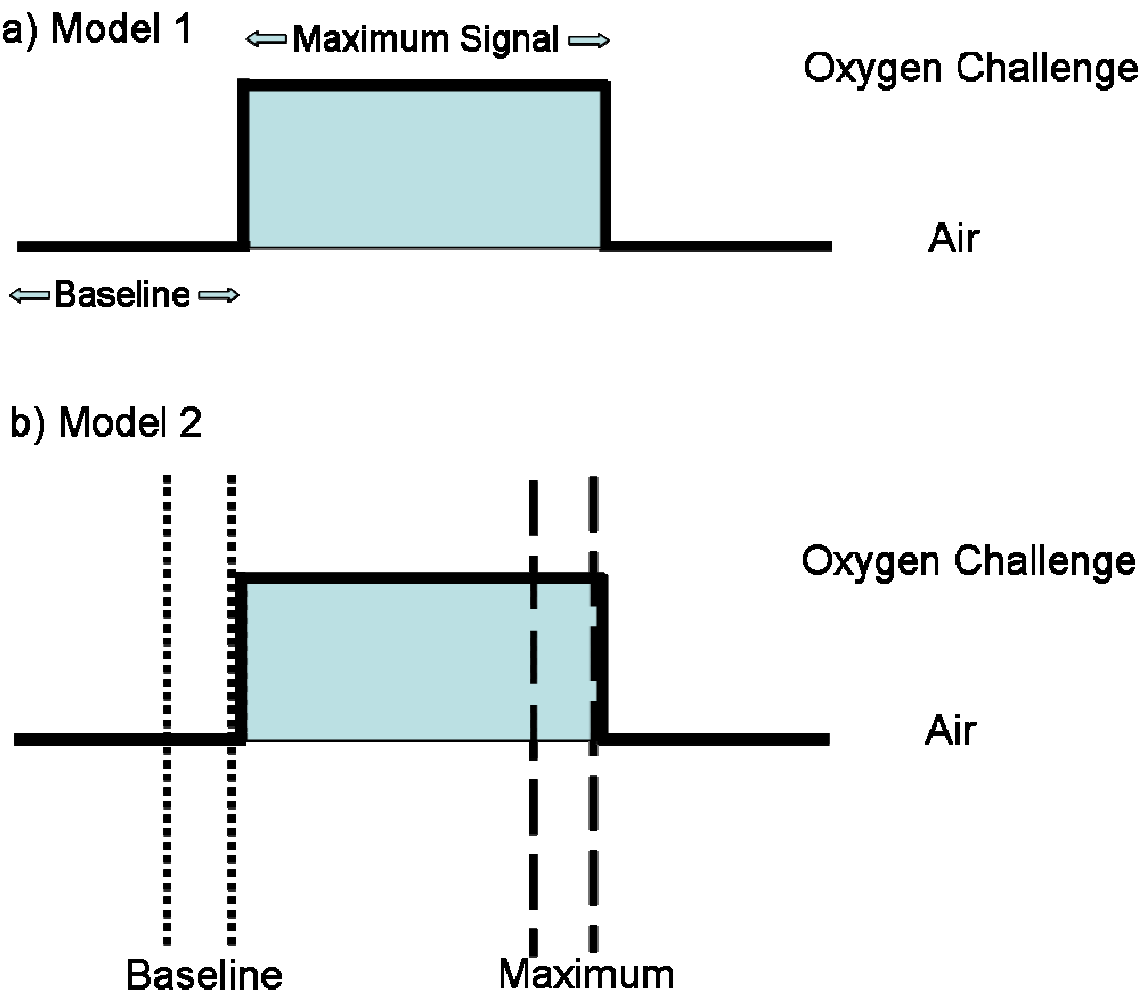

Figure 7-1 Depiction of two models used for the generation of 'percentage change maps' In both sections, the solid lines represent a theoretical T2*-weighted signal intensity-time curve. The lower level of each curve represents the time points where air was administered, and the upper level represents the Oxygen Challenge time points. a) shows Model 1. Here all data from all time points were used. All pre-oxygen time points were operationally considered to represent the baseline signal, and all time points during Oxygen Challenge were used to calculate percentage signal change. b) shows Model 2. Here only the last minute of the pre Oxygen Challenge time points were used to define the baseline, and only data acquired during the last minute of Oxygen Challenge were used to calculate the maximum percentage signal change.

Finally, generation of colour maps was performed using MRIcron (v. July 2009, www.mricro.com), using the 'NIH' colour scale. Qualitative comparison of maps of percentage signal change generated by Model 1 and Model 2 was made, with the T2*-weighted signal intensity-time curve for each subject being available for additional comparison. The regions of interest which were assessed for each subject were 1) the DWI lesion, and 2) the PWI-DWI mismatch. These subjects with these regions of interest were the same as those used in Chapter 2; therefore for the DWI lesion, images of 17 subjects were assessed, and for the PWI-DWI mismatch region, images from 6 subjects were assessed. Finally, the

ability to image the phenomenon of crossed cerebellar diaschisis was also investigated.

7.3 Results

The figures below demonstrate percentage signal change (PSC) maps generated using Models 1 and 2, for both PWI-DWI mismatch (Figure 7-2) and DWI regions (Figure 7-3, Figure 7-4, Figure 7-5, Figure 7-6). Corresponding maps of CBV are given in Appendix C(Figure 13-1 and Figure 13-2). Both models successfully generated PSC maps which were in agreement with the T2*-weighted signal intensity-time curves. In the contra-lesional hemisphere there was a demarcation between grey and white matter regions, with the PSC in grey matter being greater. In the ipsi-lesional hemisphere, regions of 'abnormality' on the Oxygen Challenge PSC maps were not seen beyond the outer limit of the PWI or DWI deficit. However, for some cases there appeared to be a heterogeneous PSC response from Oxygen Challenge in regions conventionally considered by MRI criteria to be a single compartment (DWI lesion - for an example see Figure 7-6q [subject 35]; PWI-DWI mismatch region – for an example see Figure 7-2c [subject 16]).

Two subjects with PWI-DWI mismatch had a PSC which was clearly greater in the mismatch region compared to the contra-lesional mirror regions (see Figure 7-2c Figure 7-2f for subjects 16 and 35 respectively). For subject 16, this region of exaggerated PSC was visible as a small region intense PSC (indicated by the colours of yellow and red) in the PWI-DWI mismatch region. This was seen in maps generated by both models. For subject 35, the region of increased PSC in the mismatch region was detected by the PSC map generated by Model 2, but not by that generated using Model 1. In subject 33 (Figure 7-2e), where there was little difference in percentage signal change derived from T2*-weighted signal intensity time curves between PWI-DWI mismatch and mirror regions, the mismatch region was not clearly delineated by the PSC maps generated by Model 1 or Model 2.

DWI lesions were generally detected by the PSC maps generated using both models, and were apparent as a region of attenuated percentage signal increase.

However, for those subjects with small DWI lesions (Subjects 24, 28, and 31 shown in Figure 7-5 l/m/o), these regions were not readily detected by the maps generated by this study. Finally, regions where the magnitude of signal change in the contra-lateral cerebellar hemisphere was less than in the ipsi-lateral hemisphere (presumed crossed cerebellar diaschisis; CCD) could be visualised using percentage change maps produced by both models.

In general, PSC maps generated by Models 1 and 2 were very similar in appearance. However, there were some important differences which likely contributed to the differences in observed quantitative values. For cases where there was a slow rise in signal intensity throughout the course of the Oxygen Challenge, but where the ultimate increase if signal intensity was similar to the mirror region (e.g. in the DWI lesion of subject 33, Figure 7-6p), Model 1 maps highlighted these regions more clearly than the PSC maps from Model 2. Conversely, in cases where the morphology of the curves from the DWI lesion and mirror regions were very similar, but where there was a marked difference in the magnitude of PSC (e.g. DWI lesion of subject 22, Figure 7-4j), then the DWI lesion region was more clearly delineated by the Model 2 PSC maps.

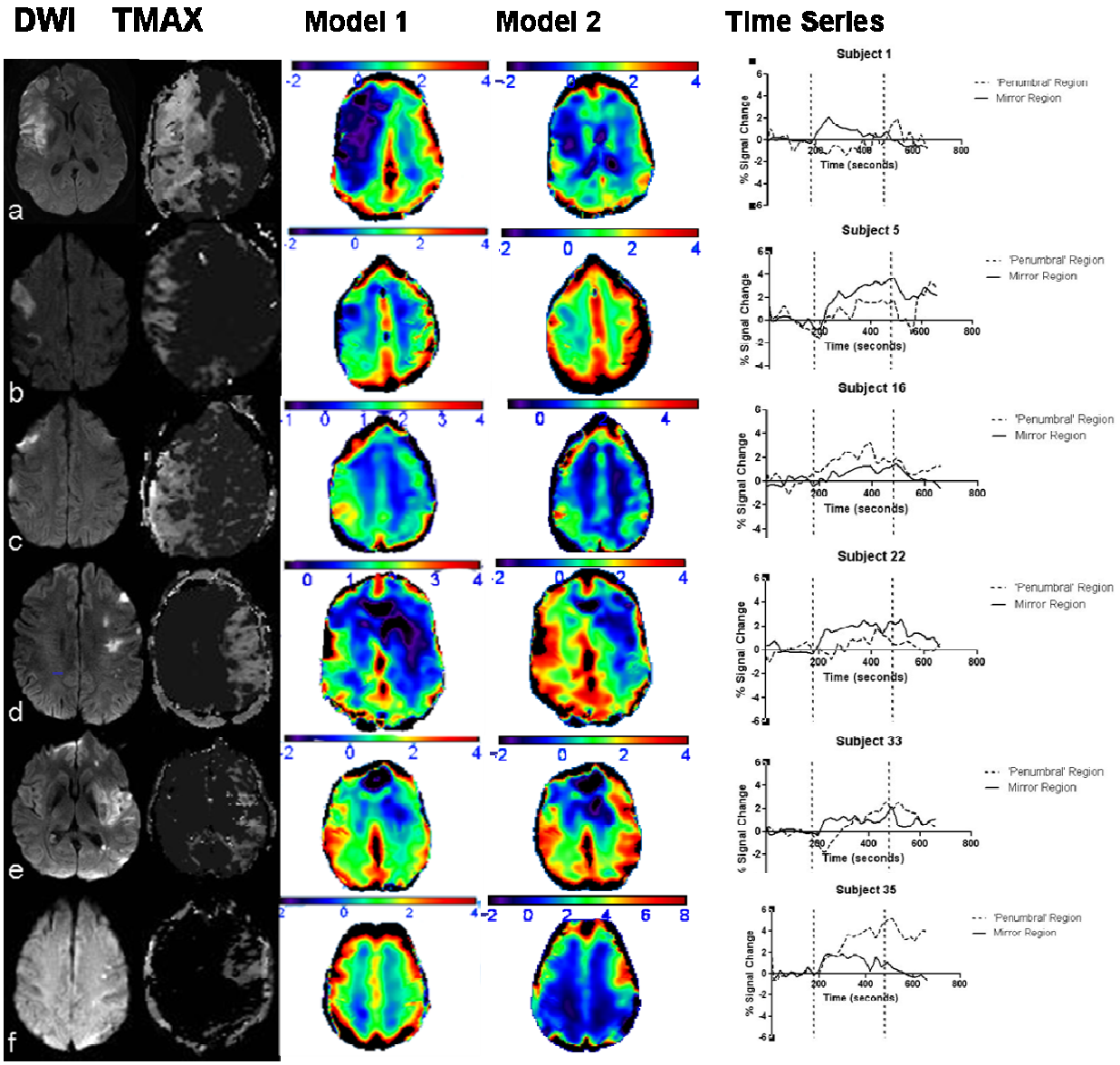

Figure 7-2 Percentage change maps for regions of Perfusion-Diffusion mismatch
The first column shows the diffusion weighted image (DWI), the second column shows maps of unthresholded TMAX, the third column shows images of percentage signal change generated using Model 1, the fourth column shows images of percentage signal change generated using Model 2, and the fifth column shows the T2*-weighted signal intensity-time curves for the regions of perfusion-diffusion mismatch. For the percentage signal change maps, the colour bar above each image is scaled in units of '%'. For the T2*-weighted signal intensity-time curves, the x-axis represents time (seconds) and the y-axis represents % T2*-signal change from the baseline. Vertical broken lines represent the onset and cessation of the oxygen challenge. The solid and broken lines represent the T2*-weighted signal intensity-time curve from the contra-lateral mirror region and the mismatch region respectively. Each row represents data for a separate subject as follows; a = subject 1, b = subject 5, c = subject 16, d = subject 22, e = subject 33, and f = subject 35.

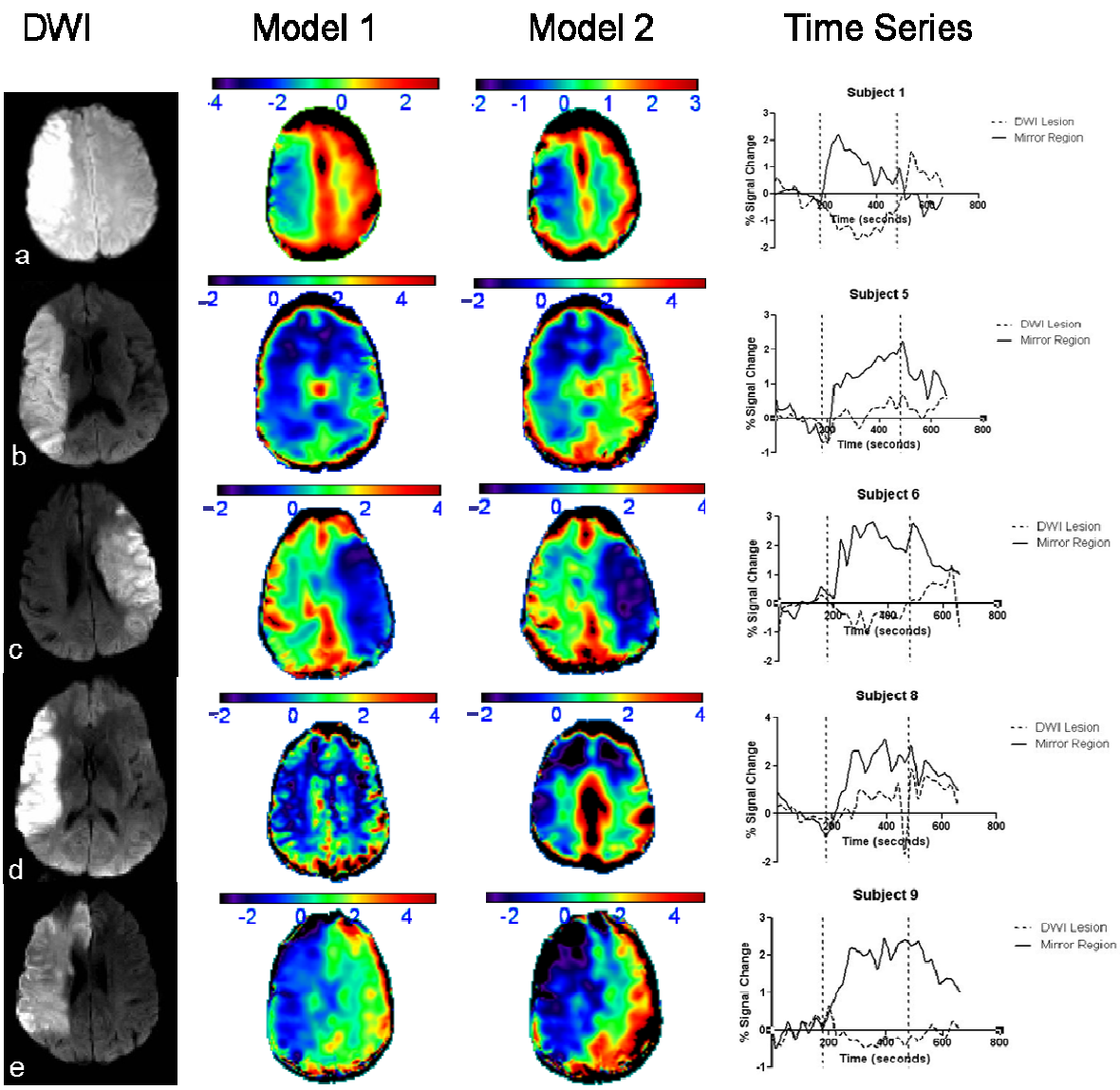

Figure 7-3 Percentage change maps for the DWI lesion
The first column shows the diffusion weighted image (DWI), the second column shows images of percentage signal change generated using Model 1, the third column shows images of percentage signal change generated using Model 2, and the fourth column shows the T2*-weighted signal intensity-time curves for the DWI lesion. For the percentage signal change maps, the colour bar above each image is scaled in units of '%'. For the T2*-weighted signal intensity-time curves, the x-axis represents time (seconds) and the y-axis represents % T2*-signal change from the baseline. Vertical broken lines represent the onset and cessation of the oxygen challenge. The solid and broken lines represent the T2*-weighted signal intensity-time curve from the contra-lateral mirror region and the DWI lesion respectively. Each row represents data for a separate subject as follows; a = subject 1, b = subject 5, c = subject 6, d = subject 8 and e = subject 9.

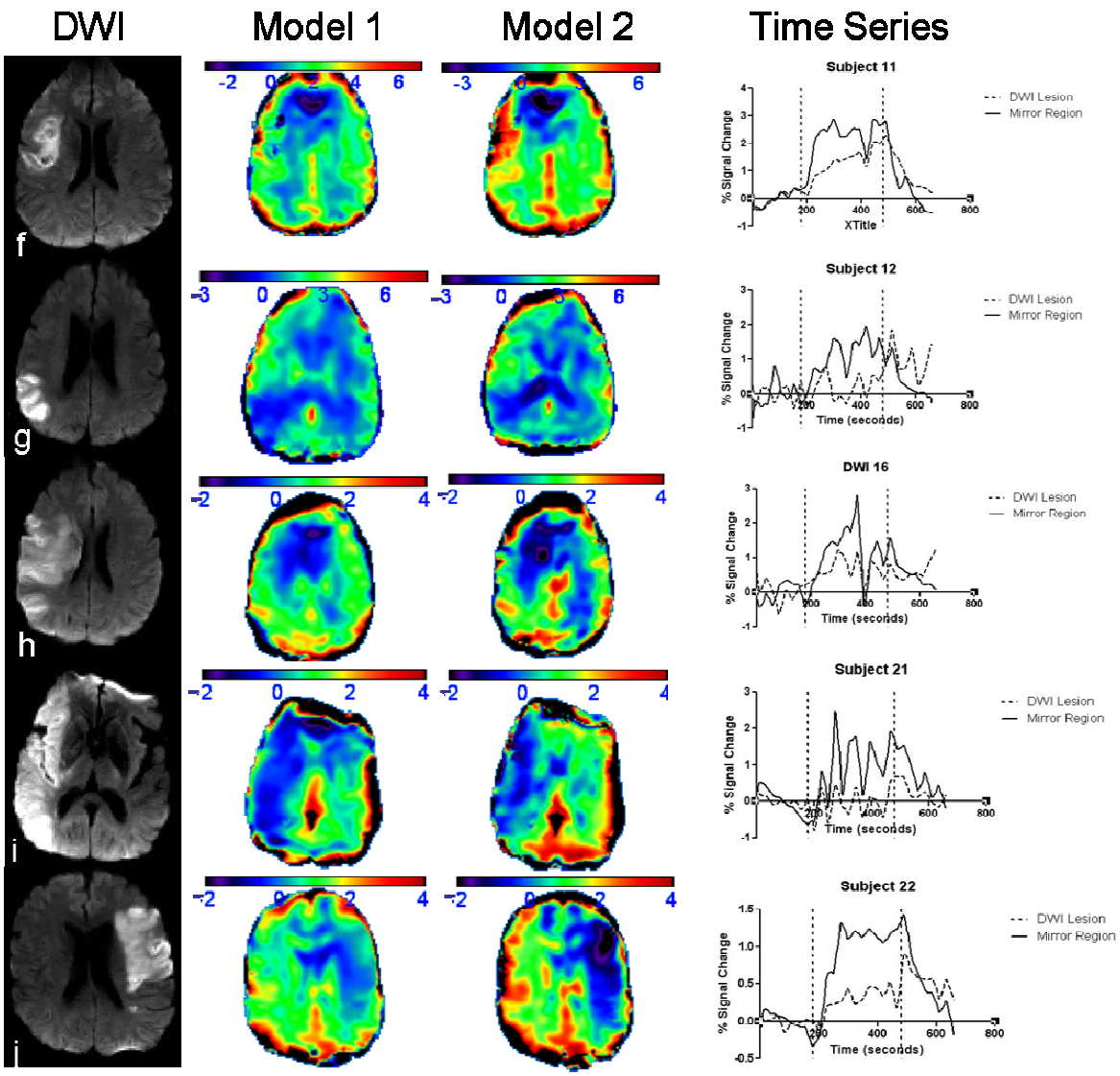

Figure 7-4 Percentage change maps for the DWI lesion (continued, 1)
The first column shows the diffusion weighted image (DWI), the second column shows images of percentage signal change generated using Model 1, the third column shows images of percentage signal change generated using Model 2, and the fourth column shows the T2*-weighted signal intensity-time curves for the DWI lesion. For the percentage signal change maps, the colour bar above each image is scaled in units of '%'. For the T2*-weighted signal intensity-time curves, the x-axis represents time (seconds) and the y-axis represents % T2*-signal change from the baseline. Vertical broken lines represent the onset and cessation of the oxygen challenge. The solid and broken lines represent the T2*-weighted signal intensity-time curve from the contra-lateral mirror region and the DWI lesion respectively. Each row represents data for a separate subject as follows; f = subject 11, g = subject 12, h = subject 16, i = subject 21, and j = subject 22.

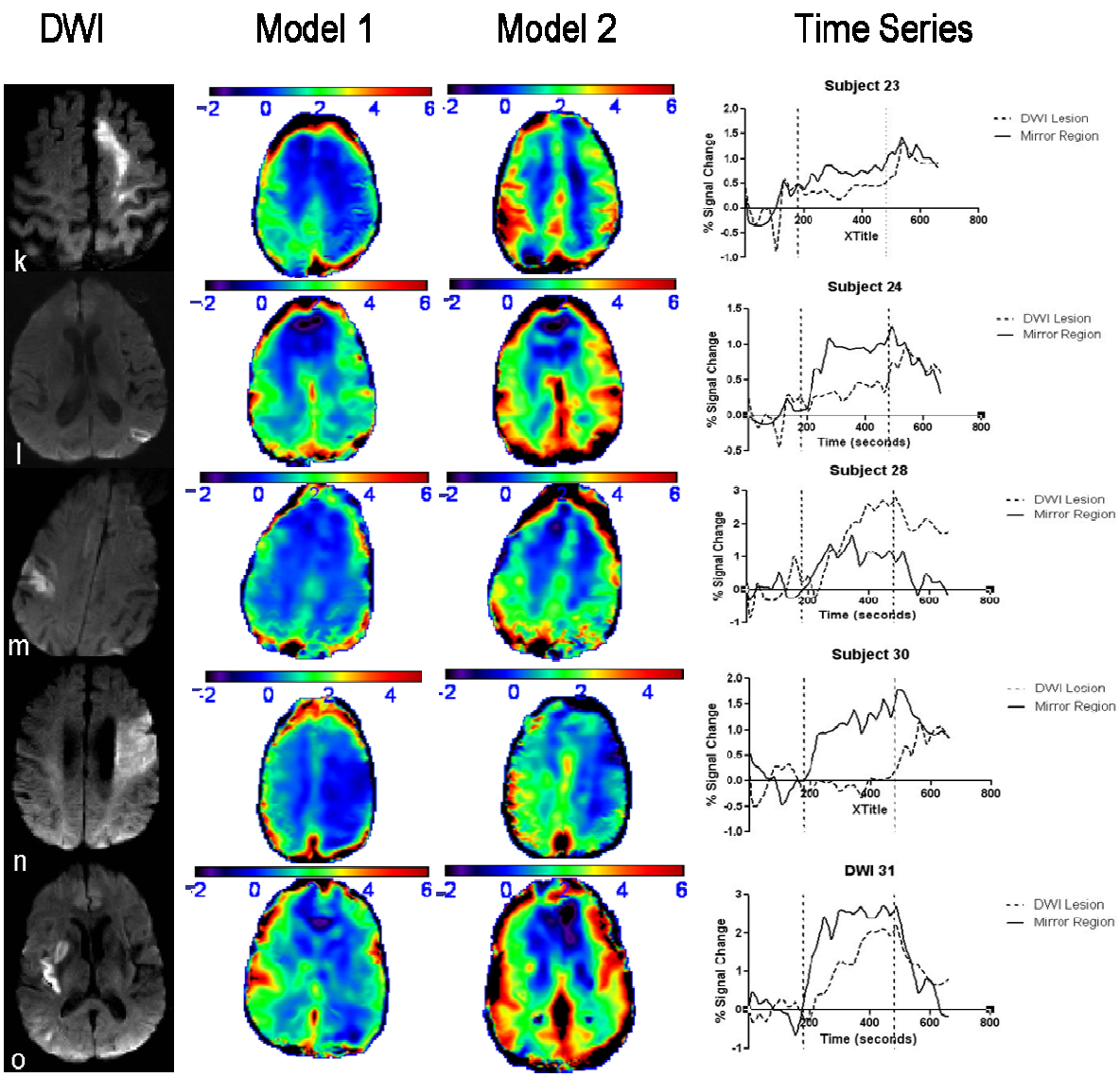

Figure 7-5 Percentage change maps for the DWI lesion (continued, 2)
The first column shows the diffusion weighted image (DWI), the second column shows images of percentage signal change generated using Model 1, the third column shows images of percentage signal change generated using Model 2, and the fourth column shows the T2*-weighted signal intensity-time curves for the DWI lesion. For the percentage signal change maps, the colour bar above each image is scaled in units of '%'. For the T2*-weighted signal intensity-time curves, the x-axis represents time (seconds) and the y-axis represents % T2*-signal change from the baseline. Vertical broken lines represent the onset and cessation of the oxygen challenge. The solid and broken lines represent the T2*-weighted signal intensity-time curve from the contra-lateral mirror region and the DWI lesion respectively. Each row represents data for a separate subject as follows; k = subject 23, l = subject 24, m = subject 28, n = subject 30, and o = subject 31.

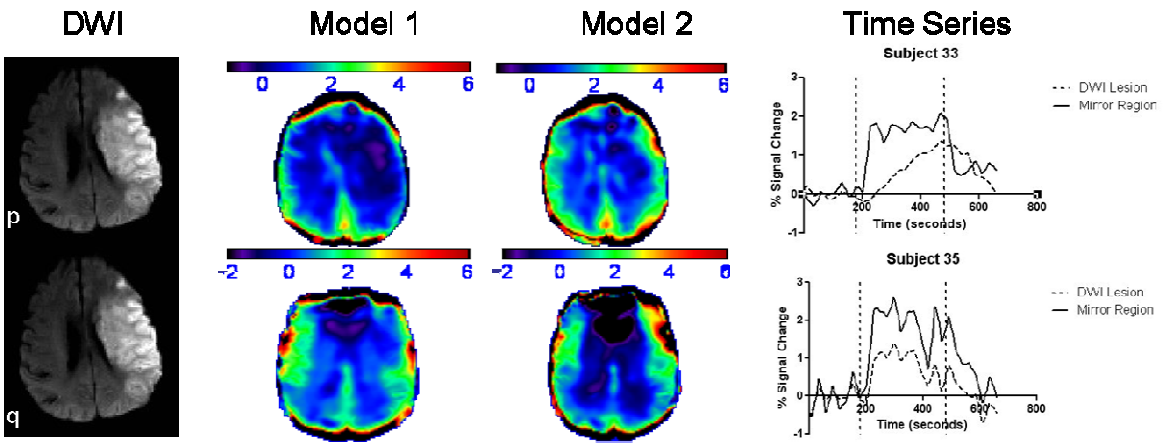

Figure 7-6 Percentage change maps for the DWI lesion (continued, 3)
The first column shows the diffusion weighted image (DWI), the second column shows images of percentage signal change generated using Model 1, the third column shows images of percentage signal change generated using Model 2, and the fourth column shows the T2*-weighted signal intensity-time curves for the DWI lesion. For the percentage signal change maps, the colour bar above each image is scaled in units of '%'. For the T2*-weighted signal intensity-time curves, the x-axis represents time (seconds) and the y-axis represents % T2*-signal change from the baseline. Vertical broken lines represent the onset and cessation of the oxygen challenge. The solid and broken lines represent the T2*-weighted signal intensity-time curve from the contra-lateral mirror region and the DWI lesion respectively. Each row represents data for a separate subject as follows; p = subject 33, and q = subject 35.

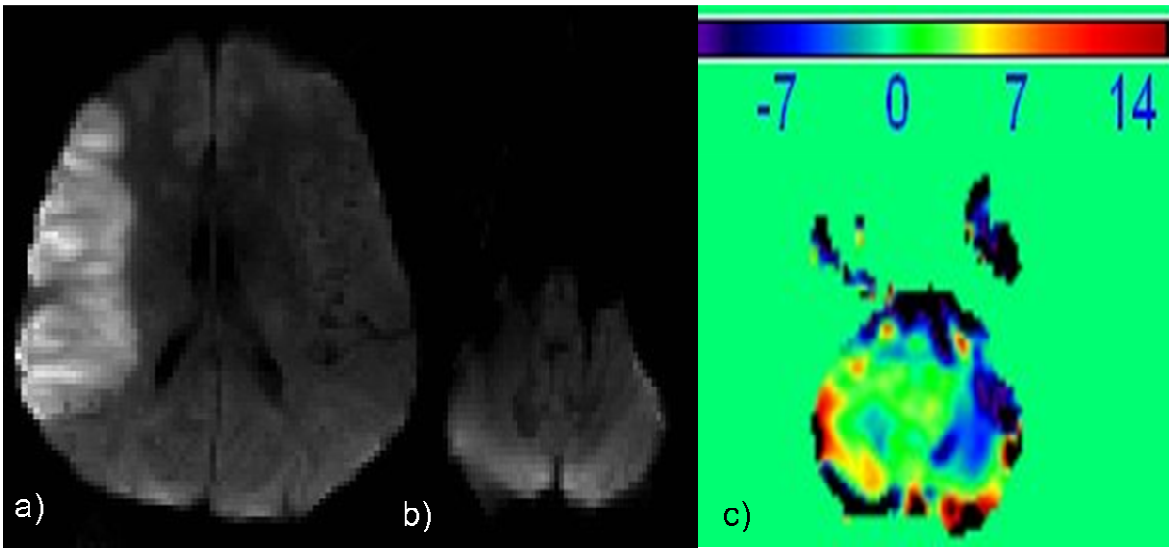

Figure 7-7 Attenuated Oxygen Challenge Response in the Contra-lesional Cerebellar Hemisphere
Images are from Subject 8. a) Diffusion weighted imaging of the stroke lesion, b) normal diffusion weighted imaging in the cerebellum and c) attenuated response in the contra-lesional cerebellar hemisphere on Oxygen Challenge Percentage Change Scan (model 2). The colour scale is in units of percentage signal change.

7.4 Discussion

In this study, the feasibility of producing Oxygen Challenge percentage change maps was demonstrated. Such maps were produced using freely available software and utilised standard image processing techniques. The PSC maps allowed rapid qualitative evaluation of whole brain Oxygen Challenge data. The maps produced in this study showed differences between grey and white matter in the contra-lesional hemisphere, whilst successfully demarcating moderately large DWI lesions in the ipsilateral hemisphere. Regions of exaggerated PSC in PWI-DWI mismatch regions were also demonstrated on the PSC maps. In addition, regions of proposed crossed cerebellar diaschisis were detected by the PSC maps. Finally, the PSC maps appeared to provide additional information to current MRI techniques by showing heterogeneity within the DWI lesion and PWI-DWI mismatch regions in some subjects. This suggests potential additional utility of PSC maps in comparison to PWI-DWI mismatch maps alone. A further aspect of this study was the demonstration of two types of model. Model 1, which used all available data, demonstrated percentage signal change best for the voxels where the T2*-weighted signal intensity-time curve adhered most rigidly to the square wave morphology of a 'box car' design. Model 2, which used only 2/11 of the data sequence, appeared to be more successful in demonstrating a purer measure of absolute percentage signal change.

How does this study inform the validation process for Oxygen Challenge? Firstly, conclusions from this qualitative analysis, based upon visual evaluation of all data voxels from the whole brain, were consistent with the conclusions from the analysis of 'regions of interest' which were reported in Chapter 2 and Chapter 3. Secondly, the generation of PSC maps, which may ultimately be co-registered to DWI and PWI, potentially allows for more detailed quantitative voxel based analyses in future studies. Finally, the feasibility of producing such maps has been demonstrated, suggesting potential clinical utility.

How does the process of map generation in this study compare with other potential methods? In the author's opinion, the simplest, most accurate, and most reliable method, would be to acquire baseline data over a short period of time, subsequently administer the Oxygen Challenge and then, after a delay to

allow for physiological equilibrium, one could acquire more data to define the peak signal. A simple subtraction of the baseline from the peak data would then provide a value for percentage signal change. Unfortunately, owing to a relatively low signal-to-noise ratio, this approach was not deemed to be feasible and therefore modelling techniques were employed. The animal pilot study for Oxygen Challenge(255) employed similar modelling techniques, but instead of expressing data as percentage signal change, data were presented as statistical image maps, which indicated the likelihood of the data from a given voxel fitting the pre-specified model. This approach was not employed in this study for two reasons. The first is that while statistical maps which express t-statistics or z-statistics incorporate measures of 'error' and are therefore potentially more accurate than the approach adopted here, the physiological and clinical meaning of such maps is hard to define. The concept of 'percentage signal change' is simpler and more intuitive. Secondly, and more importantly, there is no ideal model to which the data should be fitted. Specification of a 'square wave' model would have been inaccurate for the Oxygen Challenge data as the morphology of the T2*-weighted signal intensity-time curves did not always adhere to this design. Another possibility was to use the T2*-weighted signal intensity-time curve from the contra-lesional hemisphere as the pre-defined model. However, this would have only been relevant to the anatomical region selected and ignores the possibility of spatial heterogeneity for the morphology of the T2*-weighted signal intensity time curve. Moreover, it assumes that the morphology of the curve, rather than simply the magnitude of signal change, is the most important indicator of metabolic activity. However, this is not certain, and if the only parameter which represents deoxyhaemoglobin concentration is PSC, as was originally hypothesised, then this approach would be less relevant. Finally, it has been suggested that the T2*-weighted signal intensity from the saggital sinus may be used to generate the model (252). Whilst this may work well in healthy subjects(252) where the global OEF should be constant, it would be inherently flawed for use in stroke subjects. This is because the venous oxygen saturation in the saggital sinus, which is likely to influence the T2*-weighted signal intensity-time curve, is dependent not only on the OEF in healthy tissue but also OEF in stroke lesion tissue. The absolute deoxyhaemoglobin concentration in the saggital sinus is therefore dependent on whether there has been a stroke, the overall oxygen extraction fraction within

the stroke lesion, and the volume of the stroke lesion. Since all of these vary between subjects with stroke, and between stroke and healthy subjects, the use of the T2*-weighted signal intensity-time curve to define the 'normal' model may be inaccurate. Therefore, in this study, modelling was not based on data from individual subjects. Instead, the same model (either Model 1 or Model 2) was applied to all subjects, accepting their limitations.

Limitations to the models should be discussed. Two approaches were adopted in this study. Model 1 used data from all time points. Whilst this avoided any bias in analysis, this approach is associated with a number of limitations. Firstly, it assumed no delay in T2*-weighted signal change after the administration of hyperoxia, which is clearly not the case. Next, the baseline was defined as the mean signal from time points for which Oxygen Challenge was not being administered. However, in some cases the pre-Oxygen Challenge baseline was not stable and there appeared to be a sustained drift in the baseline of some T2*-weighted signal intensity-time curves. As an example, consider the case of a sustained downward drift in signal during baseline scanning. In this scenario the actual percentage signal increase after Oxygen Challenge would be greater than the measured percentage signal increase owing to a 'mean' baseline value that may be substantially higher than the signal intensity immediately preceding the Oxygen Challenge. Model 1 is insensitive to such baseline drifts for the calculation of simple 'percentage signal change'. Secondly, all data acquired during Oxygen Challenge time points contributed to the evaluation of peak signal, for PSC calculation. However, in reality, the T2*-weighted signal intensity-time curves did not precisely mirror a 'square wave'. Moreover, the morphology of the T2*-weighted signal intensity-time curves varied between tissue compartments. For example, in the DWI lesion, if a positive signal increase was indeed observed, there tended to be a slow rise in the T2*-weighted signal intensity. This was in contrast to the sharper increase in T2*-weighted signal intensity in the contra-lesional hemisphere. Therefore, even if the same absolute PSC was achieved in both tissue compartments, the T2*-weighted signal intensity-time curve from 'normal tissue' would fit the square wave model better that the curve from the DWI lesion, leading to different parameter estimates and thus different calculated percentage changes. This issue is not only relevant for comparison of different tissue compartments from

the same subjects, but for comparisons between subjects, since inter-subject variations will inevitably exist for physiological equilibration after Oxygen Challenge. As in other studies(252), Model 1 may have benefitted from a fixed delay for this equilibration to occur, but this was not implemented owing to the variations between subjects. Another source of potential 'noise' in Model 1 comes from the post-Oxygen Challenge time points. Since the post-Oxygen Challenge data points were also defined as 'baseline' by Model 1, the inevitable variations in decline in the T2*-weighted signal intensity would again lead to differences in the parameter estimates and therefore the measurement percentage signal change. Considering all of these points, it is clear that if there is a slow increase and decline in T2*-weighted signal intensity before and after Oxygen Challenge respectively, the parameter estimates will be poor and this will affect the measurement of percentage signal change. Therefore Model 1 has the ability to highlight voxels with a T2*-weighted signal intensity-time curve which conforms to the square wave model. Whilst this is potentially advantageous if one is interested in conformance to the model, such assessment could more accurately be achieved using statistical maps which also take into account the 'error' in the data fitting. Nonetheless, the advantage of Model 1 os that it is simple, uses all available data, makes very few assumptions, and is applied in the same manner to all subjects.

In view of the potential limitations of Model 1, a second model was assessed. Model 2 defined only the immediate pre-Oxygen Challenge time points as 'baseline', and examined only the final minute of Oxygen Challenge for calculation of peak signal. Whilst this model should be less sensitive to the issues associated with Model 1, these will not have been entirely eliminated. Nonetheless, despite these theoretical limitations, and some examples of where different results were produced by the different models, the maps produced by the two methods were generally very similar. However, for future voxel based quantitative studies where one may be most interested in absolute signal change, Model 2 is likely to be more accurate.

A final limitation should be discussed. Owing to low signal-to-noise ratio, a heavy smoothing kernel of 10mm FWHM was applied in this study. This was chosen in order to maximise the ability of the maps to highlight 'abnormal' regions. With future refinements to the Oxygen Challenge protocol to address the issue of low

signal-to-noise ratio, the degree of smoothing should be reduced. With a voxel height and width of 1.875mm, the ideal smoothing kernel would be no more than approximately 3-4mm FWHM for clinical use. Future refinements to signal-to-noise ratio may also improve the ability to detect small lesions, which were not detected by this study. In future studies, other approaches to image processing could also be considered to reduce artefact, such as applying independent component analyses which have previously been applied to epilepsy fMRI data sets(344).

In summary, despite data with relatively low signal-to-noise ratio and limitations to the approaches used, the feasibility of producing PSC maps has been demonstrated. These maps showed findings which were consistent with the results produced from the analysis of 'regions of interest' which were presented in Chapter 2. For future studies of voxel based analyses, Model 2 is likely to produce more accurate measures of percentage signal change.

8 A Voxel Based Analysis of the Oxygen Challenge Results

8.1 Introduction

Previous chapters have evaluated the Oxygen Challenge response from within predefined regions of interest. These have included contra-lesional grey and white matter, DWI lesions, and PWI-DWI mismatch regions. These analyses have shown differing responses to oxygen challenge within tissue compartments which have different levels of metabolic activity and cerebral blood volume. Results presented thus far have suggested that the response is dependent on underlying CBV, as indicated by differences in grey and white matter. Results also suggest a potential influence from underlying OEF, as suggested by a diminished or 'negative' T2*-weighted signal change from within the DWI lesion. However, associated with the advantages that the 'region of interest' approach delivered, a number of limitations were also apparent. Firstly, only the mean signal from the different regions of interest was considered. While this allowed general conclusions to be made, there was no account for spatial heterogeneity within lesions. Secondly, the regions of interest / tissue compartments have been defined by other imaging techniques such as DWI and PWI. Whilst these tissue compartments are generally those which have been of interest to other investigators, this approach has limited the volume of data which has been evaluated, and has assumed that tissue not defined by regions of interest provides no valuable information. For example, tissue with mild hypoperfusion (TMAX ≥2-4s) has not been considered thus far. A further limitation of the 'regions of interest' approach, which has been applied to relatively few numbers of subjects, is that although assessment for univariate correlations has been performed, it was not possible to ascertain which variables were independently predictive of the parameter of interest. For example, whilst there were statistically significant positive / negative correlations between PSC and CBV / TMAX respectively, it was not clear whether TMAX was a predictor of PSC independently from CBV.

Therefore, in addition to the 'regions if interest' method, a potential complementary approach method is to consider each voxel as being independent from every other voxel, and examine data from each voxel separately. Such voxel-based analyses have previously proven powerful for the interrogation of data from stroke imaging studies. These have informed with respect to stroke pathophysiology(54, 175) and thresholds for the distinction between tissue compartments(345). The adoption of a voxel-based approach may help to address some of the aforementioned limitations to the previous analyses of the Oxygen Challenge data.

In this study, a voxel based approach was adopted. The aims were to apply univariate and multivariate regression analyses to determine how much the data derived from other MRI sequences predict percentage signal change after Oxygen Challenge. This is important when considering the potential *additional* utility of PSC to current MR stroke protocols – can PSC already be predicted from sequences which are already used in clinical practice? Similarly, the ability of PSC to discriminate DWI lesions from normal tissue (the former being likely to have a lower OEF) and grey from white matter (tissues which have different CBV) was investigated. Finally, in a similar approach to Chapter 2, the ability of PSC to discriminate regions of PWI-DWI mismatch from mirror regions was investigated, this time on a voxel-wise basis.

8.2 Methods

8.2.1 Image post-processing

Maps of apparent diffusion coefficient (ADC) were generated using the software package MIStar® (Appollo Medical Imaging Technology, www.appollomit.com). The B1000 and B0 maps from DWI were loaded to the software and ADC maps were generated automatically. Next, non-brain voxels were removed using a skull stripping technique (Brain Extraction Tool, BET(346)). BET is part of the 'FSL' software package which is part of the FMRIB software library, University of Oxford. This stage was essential to ensure that only voxels corresponding to

tissue parenchyma were included in these analyses. Next, regions anterior to the lateral ventricles were manually removed owing to artefact from the nasal sinuses. In addition, owing to iron deposits in the basal ganglia, signal drop out was seen in these regions giving an artificially low ADC(312). Therefore the basal ganglia regions were also manually removed for all subjects. Next, CSF was removed from the ADC maps. This ensured that voxels from sulci or ventricles were not included in the analyses. To do this, ADC maps were loaded into the software package 'Medical Image Processing, Analysis and Visualisation' (MIPAV, National Institutes of Health, Bethesda, MD, USA). CSF was removed using a simple thresholding algorithm, using an intensity threshold $1.0X10^{-3}$ mm^2/s. All voxels with an ADC value above this threshold were assigned a value zero. Such suppression of CSF leads to lesion ADC values which are more homogeneous and accurate(347). Therefore, in addition to providing physiological data, the ADC maps also served as a tissue mask – all voxels with a zero value corresponded with non-brain material or CSF and were excluded from the statistical analyses in the next stage. Next, maps of TMAX were generated using a method previously discussed in Chapter 2, using Stroketool (v.2.4, Digital Image Solutions, University of Dusseldorf). In brief, an arterial input function (AIF) was selected from the contra-lesional proximal middle cerebral artery, and maps of unthresholded TMAX were generated using standard singular value decomposition(109). These TMAX maps allowed quantitative measures of perfusion. Owing to concerns about the use of standard singular value decomposition(109) as applied in the Stroketool package for the generation of precise CBV measurements, as discussed previously (section 6.4), maps of relative CBV were used for these analyses. These maps were also generated using the Stroketool package. Finally, the 'modified' percentage change (PSC) maps from the Oxygen Challenge were used in these analyses. These maps employed 'Model 2' (Chapter 7) which uses the final minute of pre-Oxygen Challenge data to define the baseline and the final minute of Oxygen Challenge data to define the peak. The degree of smoothing employed for maps used in these analyses was set at 3mm FWHM, in order to match the smoothing kernel applied to the perfusion maps.

Next, the TMAX, CBV and ADC maps were coregistered to the T2*-weighted EPI data so that all maps were aligned with the PSC maps. This procedure was

achieved using 'Analyze' software (version 8.0, Mayo Clinic, Rochester, USA). To achieve the best anatomical resolution while doing this, co-registration was initially performed using the raw images (DWI, PWI, T2*-EPI). In a second step the subsequent transformation matrices which were generated from the first step were applied to the derived maps (i.e ADC/TMAX/CBV/PSC) to ensure that these derived maps were also co-registered to each other. Given that imaging data were already roughly aligned, a non-linear 'windowed sinc' interpolation method was used. Following this, coregistered images were inspected in axial, coronal and saggital planes and very fine manual adjustments were made to the co-registration if required. This meant that all voxels from all of the imaging modalities were of equal dimension, and matched the PSC maps. Therefore the standard voxels dimensions were as follows; depth = 5mm, width = 1.875mm, height = 1.875mm and corresponding voxels from any given anatomical region were aligned between imaging modalities. Only after all of these procedures were followed could voxel based comparisons be performed.

Next, a programming script written using the 'MATLAB' programming envionment(MATLAB 2009b; The Mathwoks, www.mathworks.com) was supplied by Dr Rosario Lopez-Gonzalez, Clinical Physicist, University of Glasgow. This script allowed automated export of values from each imaging modality for each voxel, to a spreadsheet. This could be performed for two consecutive slices. Therefore, visual inspection was performed for each image data set for each subject to determine the two slices with the largest lesions. If a subject had previously been determined to have a region of PWI-DWI mismatch, slices incorporating this region were also included. The voxel-based script was then applied to all included subjects. This generated data for ADC, TMAX, relative CBV and PSC for parenchymal voxels on two axial slices from all subjects. Using previously generated maps for 'regions of interest' (Chapter 2 and 3), individual voxels belonging to the following tissue compartments were labelled: DWI lesion, DWI mirror region, contra-lesional grey matter, contra-lesional white matter, grey matter within the DWI lesion and finally PWI-DWI mismatch and corresponding mirror regions.

Before data could be compared between subjects, some data had to first be 'normalised' for comparison. The TMAX and ADC data are fully quantitative by nature and were therefore not normalised. The values from relative CBV were

normalised to the contra-lesional white matter, using a manually defined 'region of interest' which was applied to the same white matter anatomical region, superior to the lateral ventricle, in each case. Therefore, voxel CBV values were expressed as 'CBV voxel value / mean CBV values from contra-lesional WM voxels). Normalisation to contra-lesional white matter is a commonly applied technique in the field of perfusion weighted imaging. Finally, although PSC values were 'quantitative' they were dependent on technical and physiological values (e.g. FiO_2, baseline venous oxygen saturation) which may have varied between patients. Therefore these values were also normalised to the contra-lateral hemisphere. Since grey matter provided the best signal-to-noise ratio for PSC data, PSC values were normalised to the mean of the contra-lesional grey matter PSC. This value was attained by applying a grey matter region of interest (described in Chapter 3) to each PSC map, and deriving the mean signal intensity in each region of interest, again using 'Analyze' software.

8.2.2 Statistical Analysis

Subjects who had both PWI and Oxygen Challenge data acquired, and for whom there was a measurable lesion (as determined in Chapter 2) were included in these analyses.

Voxel based data for the following parameters from all subjects were entered into a single spreadsheet; normalised PSC, normalised CBV, TMAX, and ADC. Next, values which appeared to be artefactual were excluded. These were as follows; 1) a CBV ratio (voxel : contralateral mean white matter CBV) of >10.0 (557 voxels excluded), 2) PSC >10% or < -10% (1674 voxels), 3) TMAX >25s (896 voxels) and 4) ADC values <20% of normal (0.7×10^{-3} mm^2/s) ie 0.14×10^{-3} mm^2/s, based on previous data(348). By thresholding the ADC values in this way, all 'zero' value voxels were automatically excluded, thereby eliminating CSF, ventricles, areas of artefact and non brain from all subsequent analyses. After exclusion of outlier voxels, data for each imaging parameter were assessed for normality. Rather than using statistical tests for normality (e.g. Shapiro Wilk etc), visual inspection of data using histograms was performed using Minitab software 9v. 15.1). This approach was adopted since, owing to the very large

numbers of voxels examined, data may have been statistically non-normal despite close adherence to 'bell shaped curve' histogram morphology. Therefore, the decision to use a histogram for assessment of normality was a pragmatic one. If data were positively skewed, transformations using square root, natural logarithmic, and reciprocal functions were assessed for the best data transformation.

StatsDirect Software (v2.7.8, www.statsdirect.com) was used for all subsequent analyses. Firstly, univariate assessments for the correlation between normalised PSC and untransformed TMAX / ADC / normalised CBV were performed using the Spearman statistic. Next, after optimal data transformation was achieved, TMAX, CBV and ADC data were entered into a multiple linear regression model to predict PSC. This analysis was performed for all voxels from all included subjects, and subsequently only for voxels which were included in the DWI lesion. Next, the same analysis was performed but this time for each individual subject, using all available voxels.

Finally, the discriminatory utility of PSC maps was assessed using receiver operating characteristic (ROC) curves using voxels from all subjects. The ability of PSC and CBV to differentiate DWI lesion and DWI mirror regions and also grey versus white matter using the 'area under the curve' as measured by the Wilcoxon method (a non-parametric method analogous to the Wilcoxon signed ranks test and Mann-Whitney-U test) was compared. Values for AUC of 0.5-0.69 were considered poor to fair, values of 0.7-0.79 were considered acceptable, and values of 0.8 and above were considered excellent. The decision to investigate the difference between grey and white matter and between DWI lesion and mirror regions was made on the background of previous findings which showed statistically significant differences between these tissue compartments for Oxygen Challenge PSC(Chapter 2 and 3). Finally, although no clear differences between likely penumbral regions and normal tissue were found using region of interest analyses (Chapter 2), these regions were examined by using ROC curves to assess the ability of PSC to discriminate between voxels from the 'mismatch' region from those in the respective mirror region. This time data were not pooled and this was done for individual subjects separately owing to the variable responses to Oxygen Challenge between patients (PSC variably

increased or decreased after Oxygen Challenge in the mismatch regions of this cohort).

8.3 Results

8.3.1 Data characteristics

Data from subjects for whom there was a measurable lesion detectable by imaging and who had PWI and Oxygen challenge acquired were analysed (n=12). These subjects were; subjects 1,5,6,9,12,16,22,24,28,31,33,35. As discussed in Chapter 2, these data incorporated unaffected tissue (all subjects, in both ipsi-lesional and contra-lesional hemisphere), hypoperfused DWI lesion (subjects 1,5,6,9,12,16,22,33,35), reperfused DWI lesion (subjects 24,28,31), and PWI-DWI mismatch tissue (subjects 1,5,16,22,33,35). These data yielded 53 955 separate voxels, all of which were considered in these analyses.

Given that multiple linear regression analyses require that data are normally distributed, the distribution of data was assessed. Data for absolute and normalised PSC satisfied requirements of the appearance of a 'bell shaped curve' (Figure 8-1 [a]), consistent with a normal Gaussian distribution. Data for normalised cerebral blood volume and TMAX were positively skewed (Figure 8-1 [c] and [e]). The application of a 'natural logarithmic' function transformed the data for cerebral blood volume towards a normal distribution (Figure 8-1 [d]). A reciprocal transformation reduced the positive skew of the TMAX data and although it was superior compared to the use of square root and natural logarithmic function, transformation of the data was suboptimal (Figure 8-1 [f]). Data for ADC was bimodal (Figure 8-1 [b]), consistent with the two predominant tissue compartments examined in this data set (unaffected tissue and DWI lesion). The bimodal distribution of the ADC data rendered them resistant to transformation towards a normal Gaussian distribution, and therefore these data were left unaltered. Therefore, multivariate regression analysis considered the 'natural logarithm of cerebral blood volume', reciprocal of TMAX data, and absolute ADC as predictors of absolute PSC. Owing to the failure of the ADC data to satisfy assumptions of the model, further analyses were performed using only transformed CBV and TMAX data. Finally, both absolute and normalised PSC, and

normalised cerebral blood volume, were entered into the ROC curve analyses for prediction of the presence of a lesion on DWI.

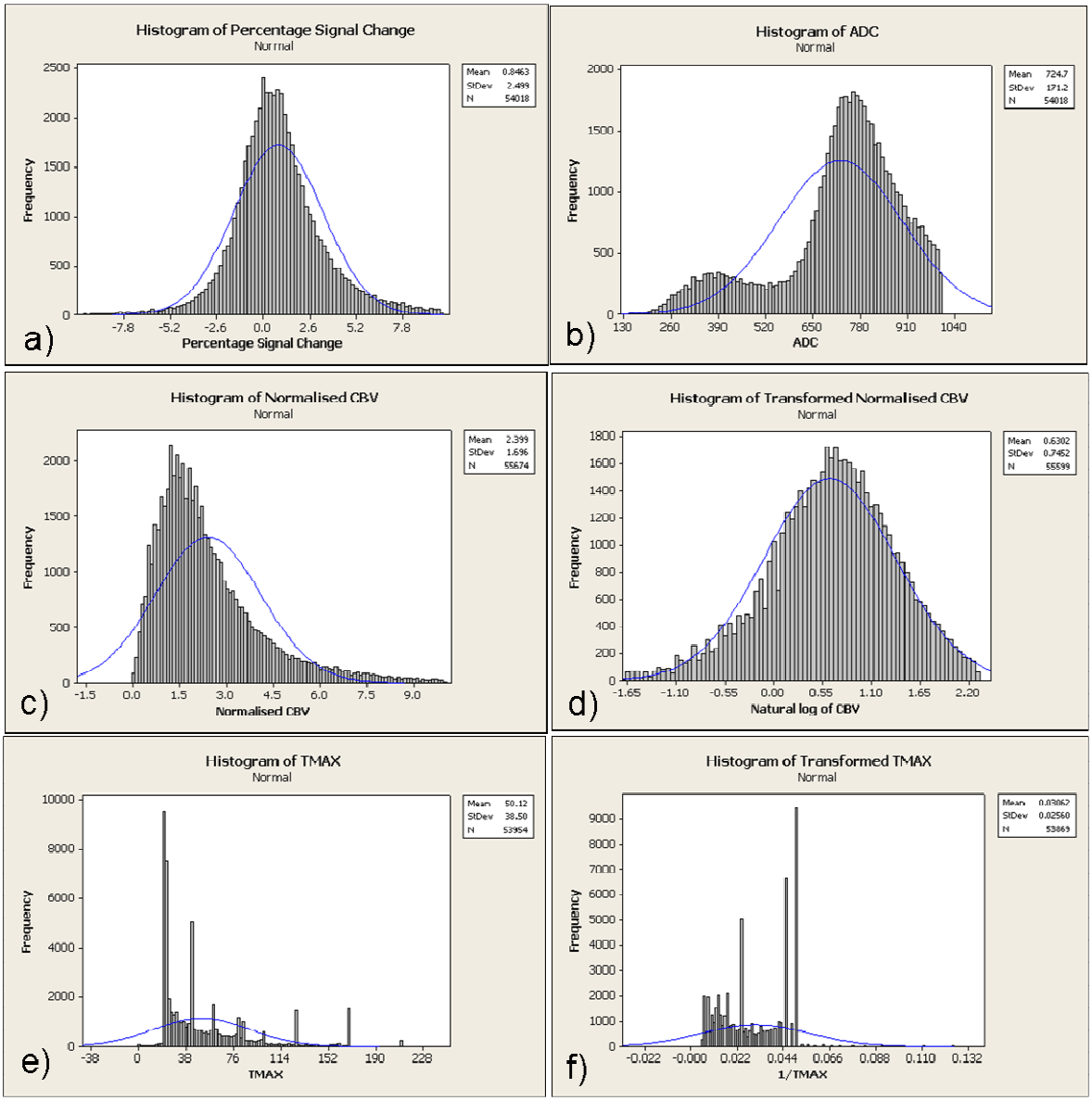

Figure 8-1 Histogram representation of the distribution of data.
The x-axis described the parameter being assessed. The y-axis describes the frequency. The data finally included in the analyses were 'percentage signal change' (a), ADC (b), transformed CBV (d), TMAX (e), and transformed TMAX (f).

8.3.2 MR predictors of Oxygen Challenge induced 'percentage signal change'

8.3.2.1 All voxels

Univariate analyses showed that all three predictors were significantly correlated with normalised PSC (transformed CBV, Rho=0.3, $p<0.0001$; reciprocal

TMAX, Rho = 0.15, p<0.0001; ADC, Rho=0.19, P<0.0001). When transformed CBV, transformed TMAX, and ADC were entered into a multiple linear regression model to predict normalised PSC, transformed CBV (r=0.2, p<0.0001) and ADC (r=0.1, p<0.0001) were independently predictive (n= 53 955 voxels). However, transformed TMAX was not an independent predictor when considering all voxels (r=-0.003, p=0.44). The R^2 for the model was 7.2%. When only transformed TMAX and CBV were entered into the model, again CBV was significantly predictive (r=0.26, p<0.0001), unlike reciprocal TMAX (p=0.61). However, the predictors for these models did not satisfy the requirement for equality of variance (p<0.0001, Kruskal Wallis).

When individual subjects were considered, only transformed CBV was consistently shown to be an independent predictor of normalised PSC. Transformed TMAX and ADC were variably statistically predictive. Data for individual subjects are given below (Table 8).

Subject	Parameter	'r' value	'p' value
	Normalised CBV	0.2	<0.0001
	ADC	0.1	<0.0001
1	Normalised TMAX	*	0.12
	Normalised CBV	0.25	<0.0001
	ADC	*	0.54
5	Normalised TMAX	0.1	<0.0001
	Normalised CBV	0.26	<0.0001
	ADC	0.12	<0.0001
6	Normalised TMAX	*	0.8
	Normalised CBV	0.15	<0.0001
	ADC	0.14	<0.0001
9	Normalised TMAX	0.09	<0.0001
	Normalised CBV	0.12	<0.0001
	ADC	0.09	<0.0001
12	Normalised TMAX	*	0.88
	Normalised CBV	0.14	<0.0001
	ADC	0.08	<0.0001
16	Normalised TMAX	-0.07	<0.0001
	Normalised CBV	0.31	<0.0001
	ADC	0.1	<0.0001
22	Normalised TMAX	0.03	0.02
	Normalised CBV	0.39	<0.0001
	ADC	*	0.97
24	Normalised TMAX	*	0.43
	Normalised CBV	0.14	<0.0001
	ADC	*	0.3
28	Normalised TMAX	*	0.3
	Normalised CBV	0.14	<0.0001
	ADC	*	0.7
31	Normalised TMAX	*	0.7
	Normalised CBV	0.3	<0.0001
	ADC	*	0.15
33	Normalised TMAX	-0.3	<0.0001
	Normalised CBV	0.35	<0.0001
	ADC	*	0.3
35	Normalised TMAX	-0.19	<0.0001

Table 8 Results from multiple linear regression analyses from individual subjects
Only CBV consistently contributed to the prediction of PSC. CBV = cerebral blood volume, ADC = apparent diffusion coefficient. Values for the strength of regression are expressed as the 'r' value but no value is given if there is not statistically significant result.

8.3.2.2 Voxels from within the DWI lesion

A multiple linear regression analysis using only voxels from within the DWI lesion (n=8280) demonstrated that all three predictors which were entered were statistically significant (transformed CBV, r=0.19, p<0.0001; reciprocal TMAX, r = 0.02, p=0.047; ADC, r=0.12, P<0.0001; R^2=8.0%). Both transformed TMAX and CBV remained significant when only these two parameters were entered into the

model, although the correlation with TMAX was very weak (transformed CBV, r=0.25, p<0.0001; reciprocal TMAX, r= 0.03, p=0.006).

8.3.3 Utility of cerebral blood volume and 'Oxygen Challenge' for the prediction of DWI lesion and contra-lateral grey matter

8.3.3.1 Identification of DWI lesion

The ROC curve AUC of normalised PSC for the prediction of the presence of a DWI lesion was '0.70' when considering both grey and white matter voxels (n=13 420 voxels). As an example, a ratio of DWI tissue PSC : to non-DWI lesion tissue PSC of '0.008 : 1.0' predicted the presence of a DWI lesion with a sensitivity of 63% and a specificity of 70%. When considering only grey matter voxels (DWI lesion in the grey matter vs contra-lesional grey matter, n=4851 voxels) the predictive properties of PSC did not improve (AUC=0.68). Normalised CBV was a better predictor of the DWI lesion (AUC=0.85). The ROC curves for normalised PSC and CBV are shown below (Figure 8-2).

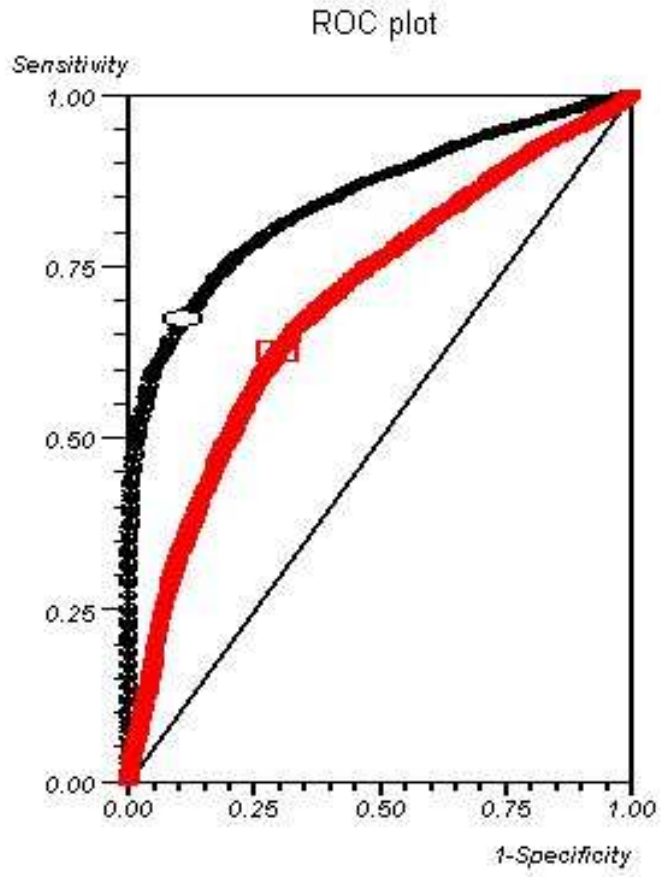

Figure 8-2 ROC curve for CBV and PSC for the prediction of DWI lesion
Data points plotted in black represent values for normalised CBV. Data points plotted in red represent values for normalised PSC. CBV = cerebral blood volume. PSC = percentage signal change

8.3.3.2 Identification of grey matter

In a similar fashion to the prediction of the DWI lesion above, normalised CBV was a better predictor of the presence of grey matter (AUC=0.79) than was normalised PSC (AUC=0.62) (Figure 8-3, n=16 475 voxels).

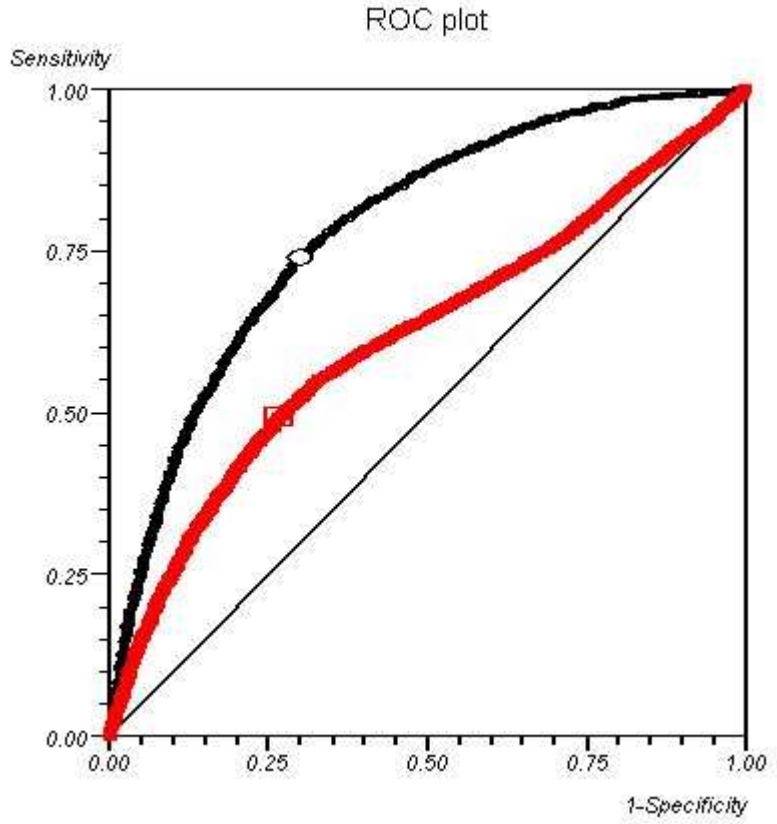

Figure 8-3 ROC curve for CBV and PSC for the prediction of grey matter
Data points plotted in black represent values for normalised CBV. Data points plotted in red represent values for normalised PSC. GM = grey matter, WM = white matter

8.3.3.3 Discrimination of the perfusion-diffusion mismatch from mirror regions

Of the six subjects with PWI-DWI mismatch, ROC curve analyses of all voxels (grey and white matter) revealed a 'cut off' value which discriminated between a lower mismatch voxel PSC value and a higher mirror region voxel PSC value in 2 subjects (subjects 1 and 22). In subject 1 the PSC demonstrated a 'negative' change and in subject 22 the PSC demonstrated a 'positive' but diminished change compared to the mirror region. In the remaining four cases, the ROC

curve discriminated between a higher 'mismatch' voxel PSC value and a lower 'mirror' voxel PSC value, as per the original hypothesis. However, in only one of these subjects was there 'acceptable discrimination' as judged by an AUC of ≥ 0.7 (subject 35; AUC 0.8). Table 9 Table showing ability of PSC to discriminate between mismatch and mirror voxels in individual subjects using the AUC from the ROC analyses. shows that a more homogenous analysis of only white matter voxels did not substantially improve the discriminatory values.

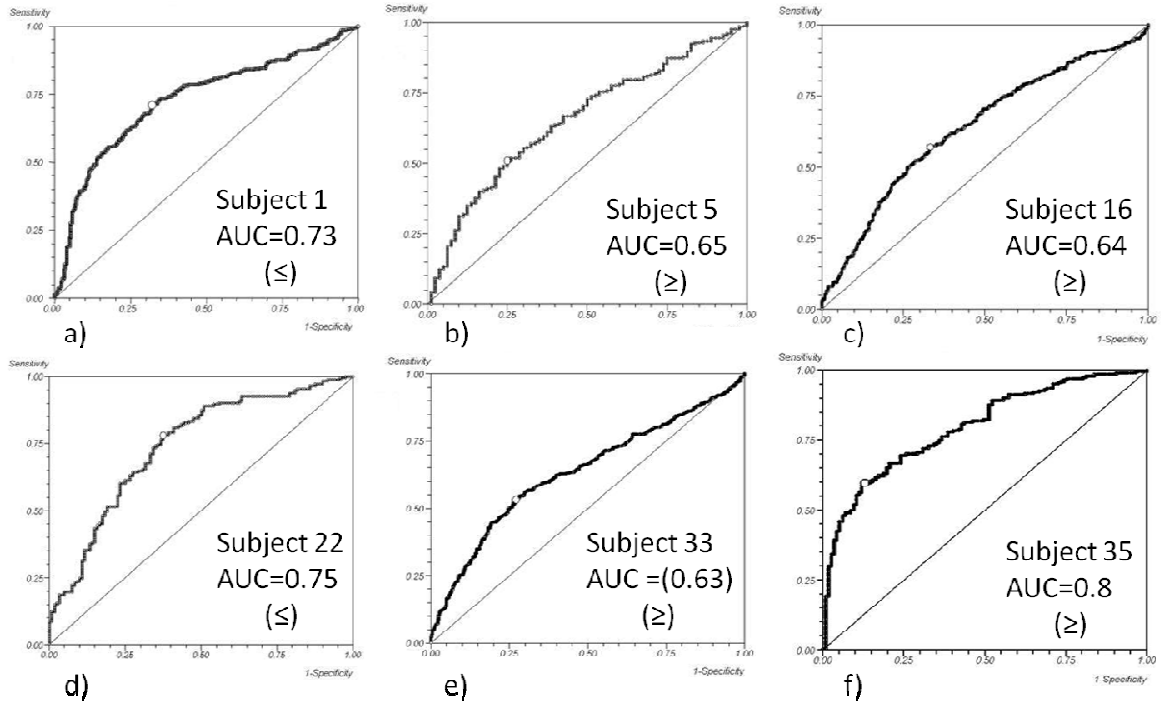

Figure 8-4 Receiver operating characteristic (ROC) curves for individual subjects with perfusion-diffusion mismatch.
X axis = sensitivity, y-axis = 1-specificity. The AUCs show the ability of PSC to discriminate between voxels in the mismatch and associated mirror regions. AUC = area under the curve. '≥' shows cases where the ROC curve distinguishes voxels with higher PSC value in the mismatch region from a lower PSC value in the mirror region, and vice versa for '≤'. Subject 1 = a), Subject 2 = b), Subject 16 = c), Subject 22 = d), Subject 33 = e), Subject 35 = f).

Column1	AUC - All Voxels	AUC White Matter Voxels Only	PSC in Mismatch vs Mirror Region
Subject 1	0.73	0.74	≤
Subject 5	0.65	0.64	≥
Subject 16	0.64	0.65	≥
Subject 22	0.75	0.81	≤
Subject 33	0.63	0.64	≥
Subject 35	0.8	0.8	≥

Table 9 Table showing ability of PSC to discriminate between mismatch and mirror voxels in individual subjects using the AUC from the ROC analyses.
Column 1 = individual subjects, Column 2 shows the AUC derived from both grey and white matter voxels, and Column 3 shows whether the ROC analyses discriminated a higher (≥) or lower (≤) PSC value in the mismatch regions from the mirror region.

8.4 Discussion

This study, which analysed data from individual voxels, follows on from the analyses of 'regions of interest' which have been presented in previous chapters. In order to assess influences on the PSC from Oxygen Challenge, data which would usually be available from stroke MRI protocols (CBV, TMAX, and ADC), were modelled in univariate and multivariate analyses as predictors of PSC from the Oxygen Challenge. In addition, ROC curves were used to assess the predictive capacity of PSC for conventionally defined tissue compartments. These approaches allowed: 1) the potential validation of the Oxygen Challenge technique by showing that PSC is correlated with variables of biological interest; 2) a logical follow on from the 'regions of interest analysis' to confirm results from Chapters 2 and 6 in a manner which is sensitive to spatial heterogeneity; 3) the investigation of factors which may influence the PSC so that these may be accounted for in future studies; 4) to determine the potential for PSC from Oxygen Challenge to discriminate DWI lesions and regions of PWI-DWI mismatch and finally; 5) evaluation of how much existing stroke MRI protocols could predict the response from Oxygen Challenge - if existing protocols can predict the PSC with reasonable accuracy, Oxygen Challenge sequences may provide no additional clinical utility, and vice-versa.

When all voxels from all included patients were considered, there were significant univariate correlations between ADC, CBV and TMAX to PSC data. However, in the multivariate analysis, TMAX became insignificant, suggesting that TMAX was not an independent predictor of PSC. It should be noted that ADC and CBV only accounted for 7.2% of the total variance in PSC. When considering voxels derived only from the DWI lesion, all three parameters predicted the PSC response in multivariate analyses. It should be noted that for all significant correlations, the strength of the correlations was generally weak, with 'r' values of usually no more than '0.3'. Next, it was seen that PSC provided only fair predictive properties for the identification of DWI lesion and grey matter, and in both cases CBV was superior. Finally, it was seen that only one case from six had an ROC curve which showed good discriminatory ability by the hypothesised 'exaggerated' PSC respect to mismatch vs mirror regions.

How may these results be explained and interpreted? Firstly, both univariate and multivariate voxel based analyses have confirmed that CBV has an independent influence of the PSC from Oxygen Challenge. These data are consistent with work presented in this thesis (Chapter 6) which employed univariate analyses of data from 'regions on interest', and also with data from the literature(206, 248). The strengths of the correlations presented in this study were weaker than those presented after analysis of regions of interest. This may be explained, at least partly, due to the combined noise from the standard MR stroke protocol sequences and, in particular, from the PSC maps. Nonetheless, CBV was the only predictor of PSC which was statistically significant in all subjects. Based on these data, those from previous chapters in this thesis, and those from the literature(206, 248), the evidence that CBV influences the Oxygen Challenge result is irrefutable. Therefore, when interpreting the results of PSC Oxygen Challenge, CBV maps should also be acquired and accounted for. Results from these analyses also suggest that other factors also influenced the observed PSC; these were ADC when all voxels were considered, and both ADC and TMAX when only voxels from within the DWI lesion were considered. This is reassuring, and argues the case that other factors, not just CBV, influence the PSC – an argument which underpins the hypothesis of the technique. The precise explanation of how TMAX and ADC influenced PSC is not clear. However,

although suboptimal for this purpose, both may serve as surrogate markers for metabolic activity and tissue viability. For example, ADC values are higher in those with completely reversible DWI lesions, intermediate in those with temporarily reversible DWI lesions, and lowest in DWI lesions which are static and permanent(57). Similarly, it has been shown beyond doubt that the depth of hypoperfusion is related to metabolic activity(19). Although penumbral tissue may theoretically be associated with an infinite TMAX, it has been shown that severe delays in TMAX are predictive of tissue infarction(349) suggesting that, at least in some cases, TMAX may also be a marker of tissue viability, albeit one which is suboptimal. These associations with metabolic activity may explain how TMAX and ADC are predictive of the PSC, independently of CBV.

In the multivariate analysis, only a small proportion of the variance in PSC was accounted for by CBV, TMAX, and ADC. It is unclear what accounted for the remaining 92% of the variance. Noise inherent to the PSC maps is likely to have contributed much of this variance. The stronger correlation between CBV and PSC derived from the ‘regions of interest’ analysis is consistent with this. However, it is not possible to determine if or how much of the variance is independently explained by the OEF of the underlying tissue, as per the hypothesis underlying the technique.

The next part of the analysis showed that, although moderately predictive, PSC maps are inferior to CBV for prediction of the presence of the DWI lesion (and also grey matter). The CBV maps performed well since most of the DWI lesions were hypoperfused, but it is likely they would have performed less well on a data set with patients who had a range of reperfusion statuses. Nonetheless, the PSC maps failed to improve on the predictive properties offered by the CBV data. It could be that the ‘inferiority’ of the PSC maps reflected their greater sensitivity to the variations in metabolic activity within the DWI lesion. It is well established that the DWI lesion is a heterogenous(54) region and although it was considered a distinct imaging tissue compartment it is not a distinct physiological compartment. Given that PSC from Oxygen Challenge is proposed to measure a physiological parameter, with potential advantages over current imaging techniques, one would not expect it to predict a DWI lesion exactly. Indeed, it has been shown that metabolic activity can vary widely within a relatively narrow range of ADC values(182). In addition, signal noise likely also

confounded results (a detailed assessment of the issues related to noise is included elsewhere within this thesis [Chapter 9]). For both of these reasons, there should not be too much emphasis placed on these AUC curves. Nonetheless, encouragement can be taken from the fact that despite these issues, an acceptable area under the ROC curve of '0.7' for prediction of the DWI lesion can still be achieved.

Finally, it was seen that an exaggerated PSC did not robustly predict the PWI-DWI mismatch compartment in all patients. However these findings were expected, since they reflected the results from the 'regions of interest' analysis and are likely to reflect the physiologically heterogenous nature of the PWI-DWI mismatch regions, as has been discussed previously. Nonetheless, it was highly reassuring that in Subject 35, who was imaged in the hyperacute period and who demonstrated a large PSC in the mismatch region on the 'regions of interest' analysis, the capacity of PSC to discriminate the mismatch region from the mirror region voxels was 'excellent'. This result is encouraging and suggests that if noise issues can be minimised and subjects with mismatch can be scanned hyper-acutely, the discriminative capacity of Oxygen Challenge may be clinically acceptable.

This study has a number of limitations which should be acknowledged. Firstly, analysis was restricted to two slices from each included subject. This approach was adopted owing to restriction by the software used, and also the potential size of the spreadsheet used (the maximum number of potential rows is 65 000 in Microsoft Excel 2003.) As was discussed in a previous chapter, relationships between parameters were assumed to be linear for the purposes of the multiple regression analysis, but this may not always be the case(218). Secondly, normalisation of the data was difficult to achieve with these data. The bimodal distribution of ADC rendered these data resistant to transformation, and therefore ADC data should be interpreted with caution. This was the purpose of performing separate analyses without the inclusion of ADC. In addition, it should be noted that the predictors for the multi-variate analyses did not show equality of variance, an assumption of the model, and therefore should be interpreted with caution. Thirdly, the limitations of the PSC maps have previously been

discussed. Next, the multivariate regression analyses assume each voxel to be independent. This assumption cannot be completely satisfied with the current data set. Although there were a large number of voxels analysed, these were derived from only 12 subjects. A larger number of subjects would have been ideal. Moreover, owing to partial volume effects, adjacent voxels may be inherently related to each other. These effects are likely to have been compounded by the smoothing kernel which was applied to the perfusion and Oxygen Challenge data, albeit one which was relatively 'mild'. In addition, it should be noted that the voxel size used was relatively small. The use of a larger voxel size may have reduced the noise associated with these data. Next, the analyses assumed precise co-registration of all images, a procedure for which small errors may have occurred. However, despite these limitations, the large number of voxels assessed is likely to have overcome many of these potential problems. Next, it would have been useful to have investigated thresholds which define the outer border of the penumbra. This could have been achieved by analysing the ROC curve for data from hypoperfused but uninfarcted voxels which subsequently developed infarction and hypoperfused voxels which ultimately escaped infarction at follow up. Although unavailable in this data set, the reperfusion status at follow up would improve the predictive power of such analysis. Such analyses would require more subjects to be scanned at very early hyperacute time points and also at follow up. Finally, it should be noted that an assumption of the multi-variate regression analyses is that data points are independent of each other. Although each voxel was considered as independent for the purpose of these analyses, in reality that intensity value in each voxel is dependent on the adjacent voxels.

In conclusion, this study has a number of implications. Firstly, it confirms the results from Chapter 6 and it is clear that CBV is an independent predictor of PSC, as would be expected from first principles. Therefore CBV should be accounted for when interpreting the PSC, consistent with previous conclusions. Secondly, this study showed that CBV was not the only independent predictor of PSC, and ADC and TMAX were also independent predictors, especially when considering voxels from within the DWI lesions. Given that first principles do not predict an independent influence on T2*-PSC form oxygen challenge, it is likely

that these factors represent surrogate markers of metabolic activity and this is what the technique is ultimately sensitive to – a reassuring suggestion. Finally, in a case with hyperacute mismatch, PSC was shown to be an 'excellent' discriminator between mismatch and mirror regions. Although further good quality imaging from hyperacute cases is required to confirm this, this finding does provide encouragement that this technique may be clinically useful.

9 Oxygen Challenge Results: an Evaluation of Detrimental Influences on Signal

9.1 Introduction

It has previously been discussed that the current series of Oxygen Challenge studies employed a type of MRI sequence commonly used in functional MRI (fMRI) studies. The absolute changes in signal intensity in such studies are usually very small. Results presented in this thesis suggest that the Oxygen Challenge technique is no different. Even in grey matter, increases in T2*-weighted signal intensity were not usually greater than 3-4%. Unfortunately, a number of subjects assessed in the studies reported in Chapter 2 and subsequent chapters were excluded after a failure to observe a 1% increase in T2*-weighted signal in the DWI 'mirror' region after Oxygen Challenge. This led to potentially valuable data being discarded from some of the analyses presented in this thesis. Whilst in some cases the reason for the negligible signal increase in the DWI mirror region was its location predominantly in the white matter, in most cases data were excluded due to excessive noise relative to the signal change. Such exclusion of data is a major issue; study subjects are a scarce resource and the number of subjects available to recruit and scan is always limited. Moreover, the data were acquired by scanning medically unwell stroke patients and by using valuable scanner time.

The strength of signal derived from an MRI scan is termed signal-to-noise ratio (SNR). This term describes the balance between the meaningful signal and the meaningless background signal (noise). Formal calculations of SNR can be made by dividing the mean signal by the standard deviation of noise. A low SNR may occur due to scanning a phenomenon with an inherently weak signal, excessive noise contaminating the images, or a combination of both. For functional MRI studies, if there is a particularly low SNR due to noise then genuine effects may be not be detected(350). Noise may be introduced by a variety of sources including the scanner itself, subject motion(351, 352) and physiological(353) influences resulting from brain pulsation secondary to cardiac(354) and respiratory motion(355).

For the Oxygen Challenge data, an understanding of the nature of noise and the factors which contributed to it may be helpful for two reasons. The first relates to how the data were analysed. For studies presented in this thesis, percentage signal change has generally been calculated by defining the mean of all the pre-Oxygen Challenge time points as being 'baseline'. However, if variability of the baseline data is systematically different between stroke tissue compartments, defining the baseline as the mean of all pre-Oxygen Challenge time points may be problematic. For example, if large drifts in baseline signal intensity were to be seen consistently within the DWI lesion, but baseline signal from normal tissue was found to be stable with very little data variability, comparisons between the DWI lesion and normal tissue with respect to the difference between the baseline and peak signal may not be accurate. When considering whether baseline variability could theoretically be different between stroke tissue compartments and the contra-lesional mirror regions, it is unlikely that factors such as patient motion or scanner related factors will differentially affect tissue compartments compared to their homologous regions in the contra-lesional hemisphere. However, the effect of certain physiological factors may well differ between tissue compartments. In 1995, Biswal and colleagues(268) reported the presence of low frequency fluctuations occurring with a frequency of <0.08Hz (lower than for cardiac and respiratory noise) and which were correlated with other low frequency fluctuations in anatomically distinct regions of the resting brain. This paper supported the concept of functional connectivity and 'resting state' networks. The cause of these low frequency fluctuations is still uncertain but it has been proposed that they represent spontaneous neural activity(356), but cerebral vasomotion(357) may also play a role. Given previous observations that ischaemia alters normal oscillatory activity associated with neuronal metabolism(358) and MRI measured low frequency fluctuations are altered by a variety of neurological disorders, it is possible that these low frequency oscillations are selectively altered in stroke tissue. If this is the case, the baseline T2*-weighted signal intensity in, for example the DWI lesion, may be systematically different from the baseline in the mirror regions, thus potentially confounding results.

The second reason for investigating noise in the Oxygen Challenge data is to gain an understanding of what influences data variability for this technique. This

could potentially highlight patient characteristics which predict noisy data, and even provide an insight into which parameters should be targeted in order to improve SNR in future studies and thereby minimise the exclusion of poor quality data.

In this study, both the amplitude of low frequency fluctuations (ALFF) and the overall variability of the data in the DWI lesion were compared to that from the mirror region in order to ascertain any systematic difference which may prevent the mean of the oxygen time points from being used as the baseline. In addition, the influence of clinico-radiological factors on patient motion, and in turn on overall data variability was also investigated.

9.2 Methods

9.2.1 Quantification of movement

The realignment procedure has already been detailed in Chapter 2. In brief, this was performed using the software package SPM2. Using rigid body transformation, data for six realignment parameters were derived. These were translation in x, y, and z directions (mm) and rotation in pitch, roll and yaw orientations (radians). Movement parameters based on translation were calculated using a procedure previously detailed in the literature(359, 360). In order to derive a measure of the degree of movement with respect to translation from the initial position, a displacement vector (d) was calculated as follows

$$d = \sqrt{x^2 + y^2 + z^2}$$

Where d = displacement vector, x, y, and z are realignment parameters for x, y, and z translations. This was calculated for each of the baseline time points separately and the mean and maximum displacement vectors (d) were expressed for each subject. Next the ‘interscan displacement’ was calculated by expressing the first derivative of the displacement vectors for each interscan interval (d’) according to the following equation;

$$(d_{x+1} - d_x) / (t_{x+1} - t_x)$$

where d= displacement vector and t=time between two successive time points ([x] and [x+1]). Given that each interscan interval was fixed this was assigned a value of '1'. Therefore the interscan displacement (d') was simply calculated as the difference in (d) between scans ($d_{x+1} - d_x$). Again, this was calculated for each of the baseline (pre- Oxygen Challenge) time points separately and the mean and maximum (d') were expressed.

The following movement parameters for each subject were considered in the analyses; mean displacement vector across all baseline time points (mean d), maximum displacement vector across all baseline time points (maximum d), mean inter-scan displacement across all baseline time points (mean d'), maximum inter-scan displacement across all baseline time points (maximum d'), number of 'jerks' [number of times d' was >0.1mm or >0.2mm] and maximum movement in the x-, y-, or z- translations.

9.2.2 Determination of the amplitude of low frequency fluctuations (ALFF)

Again, the pre-Oxygen Challenge baseline data (first 60 time points) were used for this analysis. Data were pre-processed using 'SPM 8.0' software (UCL, UK). Data were realigned to correct for head motion and smoothed using a smoothing kernel of [8,8,8]mm for the full width at half maximum of the Gaussian smoothing kernel in the x,y, and z directions. The software package 'Rest 2007' (http://resting-fmri.sourceforge.net, Beijing Normal University, China) which was run on a 'MATLAB' platform (MATLAB v 7.9.0.529 [R2009b], Mathworks), was used for computation of the ALFF on a voxel by voxel basis. Firstly data were filtered in the range of 0.01-0.08Hz and transformed from the time domain to the frequency domain using a fast Fourier transform (FFT). This yielded a power spectrum, a typical example of which is shown below (Figure 9-1).

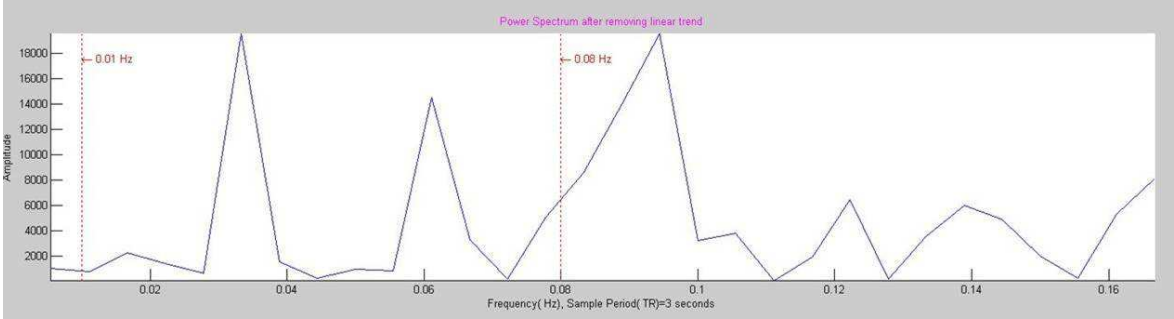

Figure 9-1 Power spectrum from baseline data
Power spectrum, with filtered range indicated by vertical broken lines. The x-axis indicates the frequency scale (Hz) and the is amplitude indicated on the y-axis. This power spectrum was generated from the T2*-weighted signal intensity time series of a representative subject. It suggests two major wave forms between 0.01-0.08Hz; one with a frequency of approximately 0.03Hz and the other with a frequency of approximately 0.06Hz.

On the basis that the power at any given frequency is proportional to the square of the amplitude, the square root of the power was calculated for each frequency value and the average square root across the filtered range was generated by 'REST' software. This was termed the 'ALFF'. Maps of ALFF were subsequently produced by the software on a voxel by voxel basis. The regions of interest which defined the 'DWI lesion', 'PWI-DWI mismatch', 'DWI expansion' and contra-lesional 'mirror' regions and which were employed in Chapter 2 were applied to the ALFF maps and values for the 'mean' ALFF in each tissue compartment were recorded.

9.2.3 Determination of variability of baseline data

The variability of the pre- Oxygen Challenge 'baseline' data (i.e. the first 60 time points) was assessed for the regions of DWI lesion and the 'mirror' region of the DWI lesion. All calculations were performed on 'baseline' data which were normalised to the mean value. As an alternative to assessing data variability using methods based on standard deviation, a method which recognises the 'time series' nature of the data was employed. This method has been adopted by other studies of biological time series(361, 362). The difference between each successive measurement of T2*-weighted signal intensity (i.e. each 'TR') was calculated. This value was then 'squared' and the mean of the 'squared' values derived from each data point was calculated. The square root of this

mean was then expressed as the value for variability as per the following equation;

$$\sqrt{[\sum_{i=1}^{n-1}(X_{i+1} - X_i)^2 /(n-1)]}$$

9.2.4 Statistical analysis

Non-parametric statistical tests were used for all analyses owing to the non-normal distribution of data. Results from statistical evaluations were considered statistically significant at $p<0.05$. In order to address the issue of the effect of stroke on baseline data variability, the data for subjects for whom there was a measurable DWI or PWI lesion (>1ml) were considered for analyses of ALFF and variability of data (n=25), whilst analysis of the movement parameters was considered for the complete data set (n=31).

9.2.4.1 ALFF

The ALFF in stroke tissue compartments was compared to the ALFF from the mirror regions using a Wilcoxon's signed ranks test. This analysis was performed for all subjects and then separately for subjects with large strokes (defined arbitrarily as strokes >50mls), with small strokes (<50ml), and for those with left hemisphere strokes and with right hemisphere strokes. Assessment for a correlation between the ipsilateral : contralateral hemisphere ALFF ratio and DWI lesion volume, NIHSS and the movement parameters was performed using a Spearman's rank correlation analysis. In addition, the correlation between 'time to scan' and ALFF ratio was assessed.

9.2.4.2 Movement parameters

Potential influences on the degree of movement experienced by subjects within the MRI scanner were determined. Univariate correlations between each movement parameter and both DWI lesion volume and NIHSS were evaluated

using a Spearman's Rank Correlation test. Differences in movement parameters were compared between left and right hemisphere strokes and between small and large strokes using a Mann-Whitney U test.

A comparison of the movement parameters from this study with those from a study(360) of volunteers with focal epilepsy was made. The epilepsy study scanned subjects electively using the same MRI 'TR' duration as was used by this study. However, scanning was performed for a longer duration in the epilepsy study and therefore the number of jerks >2mm was normalised by expressing the value 'per 100 scans'. Mann-Whitney U tests were employed to compare movement parameters between this current study and from the epilepsy data.

9.2.4.3 Variablity of Data

Finally, the variability of baseline data was evaluated. Assessment for a correlation between the variability of baseline data from the contra-lesional hemisphere and admission DWI lesion volume, admission NIHSS, movement parameters, and ALFF ratio was performed was again using Spearman's rank correlation analysis. In addition, a Mann-Whitney U test was performed to compare the variability of the baseline data in the contra-lesional hemisphere between those subjects with small and those with large strokes (arbitrarily dichotomised at 50mls) and with left and right hemisphere strokes. Finally, it was determined if there was a difference in the variance of data generated from the DWI lesion and PWI-DWI mismatch region and the contra-lesional hemisphere

9.3 Results

9.3.1 ALFF

An example of an ALFF map is demonstrated by Figure 9-2. Note the differences between grey and white matter in the contra-lesional hemisphere. This distinction is still apparent within the hemisphere ipsi-lateral to the stroke. The signal from within the lateral ventricles also appears to be bright suggesting that the ALFF within this region is large.

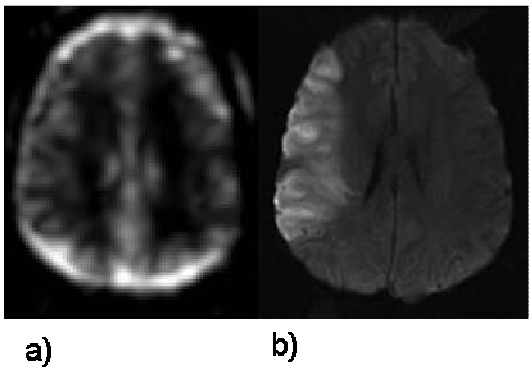

Figure 9-2 Example of an ALFF map
ALFF = amplitude of low frequency fluctuation. a) shows the ALFF map from subject 8 who had a large lesion on Diffusion Weighted Imaging (DWI) as shown in b). On the ALFF map, brighter signal indicates a larger ALFF.

Subjects with a measurable DWI lesion volume (>1ml, n=25) were considered for these analyses. No difference could be detected between the ALFF in the DWI lesion and the contra-lateral mirror region (p=0.49, n=25), suggesting that low frequency fluctuations persist from within the DWI lesion and that their amplitude is maintained. This finding was also found when such comparisons were made using only subjects with large stroke (>50ml, n=10, p=0.32) and with small stroke (<50ml, n=15, p=0.15). Similarly, no ALFF differences could be detected between ipsilateral and contralateral hemisphere when considering only left hemisphere strokes (p=0.23, n=15) and right hemisphere strokes (p=0.62, n=10). There was no correlation between ALFF ratio (ALFF in the DWI lesion normalised to the contra-lesional side) and baseline NIHSS (p=0.56, n=25), baseline DWI lesion volume (p=0.12, n=25), or time since onset (p=0.20, n=25). For subjects with PWI-DWI mismatch, there was no statistically significant difference between the mismatch and contra-lesional hemisphere with respect to ALFF (p=0.81, n=7). There were only four regions of DWI expansion and therefore no statistical analyses were performed. However, no pattern of differences was apparent from the data.

9.3.2 Movement parameters

A summary of the movement parameters is presented in Table 10. Given that the DWI lesion was not the focus of investigation in this case, the contra-lesional

hemisphere for all scans, regardless of DWI lesion volume, was considered in these analyses.

Patient	DWI Volume Day 1 (ml)	Admission NIHSS	Hemisphere	d' max	d' mean	Number of Jerks (0.2mm)	Number Jerks (0.1mm)
1	14	14	Right	0.13	0.03	0	4
2	1	1	Left	0.21	0.08	1	18
4	3	8	Left	0.52	0.13	10	28
5	206	20	Left	0.29	0.05	1	8
6	169	20	Left	0.30	0.10	4	29
8	105	10	Right	0.32	0.11	4	31
9	280	19	Right	0.95	0.12	10	19
10	2	5	Left	0.08	0.03	0	0
11	18	6	Right	0.23	0.05	1	8
12	93	5	Right	0.66	0.10	5	23
13	0	2	Left	0.19	0.04	0	3
14	2	2	Right	0.33	0.04	2	3
16	154	16	Left	0.71	0.13	10	26
17	2	21	Left	0.19	0.06	0	13
18	16	20	Left	0.30	0.10	9	25
19	4	21	Left	0.04	0.01	0	0
20	0	4	Left	0.32	0.10	3	27
21	155	17	Right	0.50	0.14	15	35
22	63	9	Left	0.67	0.06	4	5
23	12	18	Left	1.10	0.16	16	21
24	2	3	Left	0.41	0.10	7	22
25	0	6	Left	0.27	0.07	4	20
26	1	20	Left	1.77	0.23	20	37
28	6	13	Right	0.59	0.14	14	30
29	5	3	Right	0.19	0.04	0	5
30	60	20	Left	0.18	0.05	0	6
31	11	6	Right	0.12	0.04	0	4
32	49	17	Right	0.18	0.06	0	8
33	58	21	Left	0.16	0.02	0	2
34	5	7	Left	0.63	0.11	9	26
35	11	3	Left	0.27	0.07	2	13
Median	*	*	*	0.3	0.07	3	18
Lower Quartile:Upper Quartile	*	*	*	0.19:0.59	0.04:0.11	00:09	05:26

Table 10 Summary of movement parameters
Data from subjects in whom T2*-weighted EPI data was acquired are presented. DWI =diffusion weighted imaging. NIHSS = National Institutes of Health Stroke Scale(257). Mm = millimetres, ml = millilitres.

The median number of head jerks which were greater than 2mm and 1mm was 3 and 18 respectively. Nine subjects had no jerks >2mm and the maximum number of jerks which were >2mm was 20. When jerks of smaller magnitude were considered, only one subject had no jerks greater than 1mm and the maximum number of jerks >1mm was 37. The largest d' max seen was 1.77mm (subject 26) and when considering all subjects, the median d' max was 0.3mm. When considering all subjects, the median "d' mean" was 0.07mm. The comparison of the movement parameters from this study to previously reported subjects with epilepsy(360) is reported below (Table 11).

	Lemieux et al	Current Study	p value
Median maximum d'	1.14	0.3	p<0.001
Median average d'	0.05	0.07	p=0.052
Median number of jerks (>0.2mm) per 100 scans (300s)	2	5	p=0.35

Table 11 Comparison of movement parameters derived from this study to literature based values from elective scanning.
Literature based values derived from a study of electively scanned subjects with focal epilepsy by Lemieux et al(360).

After excluding repeat data which was derived from the same patients in the epilepsy data set(360), there was no statistically significant difference between the number of 'jerks' in the epilepsy data set and this current data set (p=0.35). The mean magnitude of inter-scan displacement (mean d') from this study was not statistically different from that of the epilepsy study (p=0.052), although there was a non-significant trend towards a marginally greater inter-scan displacement in this data set. However, the maximum size of jerk (inter-scan displacement, max d') for all subjects was conversely larger in the epilepsy data set compared to this current stroke data set (p<0.0001). There were four clear outliers in the epilepsy data set with respect to maximum d' (subjects 7, 14, 16 and 21, all had a maximum d'>10mm). When data from these subjects were excluded, the greater mean d' in this current data set compared to the epilepsy data set became statistically significant (p=0.005), but there was no change in the outcome of statistical evaluation from maximum d' and the number of jerks.

There was no correlation between admission NIHSS or DWI lesion volume with any movement parameter evaluated (mean displacement vector [mean d], maximum displacement vector [maximum d], mean inter-scan displacement [mean d'], maximum inter-scan displacement [maximum d'], number of 'jerks' [0.1mm or 0.2mm] or maximum movement in the x-, y-, or z- translations, or pitch, roll, and yaw rotations); p>0.05 in each case. In addition, when left (n=20) and right hemisphere strokes (n=11) were compared, there was no difference demonstrated between groups for any movement parameter (p>0.05 in each case). When DWI lesion volume was dichotomised to large and small strokes, there was no difference between groups with respect to any movement parameter (p>0.05 in each case).

9.3.3 Variability of Data

These analyses focussed on subjects with scans where there was a measurable DWI lesion (n=25). There was no difference in the variability of the data between the DWI lesion and the contra-lesional mirror region (p=0.44, n=25). When the variability of data from the contra-lesional hemisphere was considered, there was no correlation with admission DWI lesion volume, admission NIHSS, or any movement parameter (p>0.05 in each case). When DWI lesion size was dichotomised at 50ml, there was no difference in the variability of the data between large and small strokes (p=0.43). There was no difference in the variability of the contra-lesional data between left (n=15) and right (n=10) hemisphere strokes (p=0.98). When both ALFF data and variability data from the DWI lesion were normalised to the contra-lesional side (i.e. ratio of DWI lesion : mirror), there was a significant positive correlation (r=0.43, p=0.03).

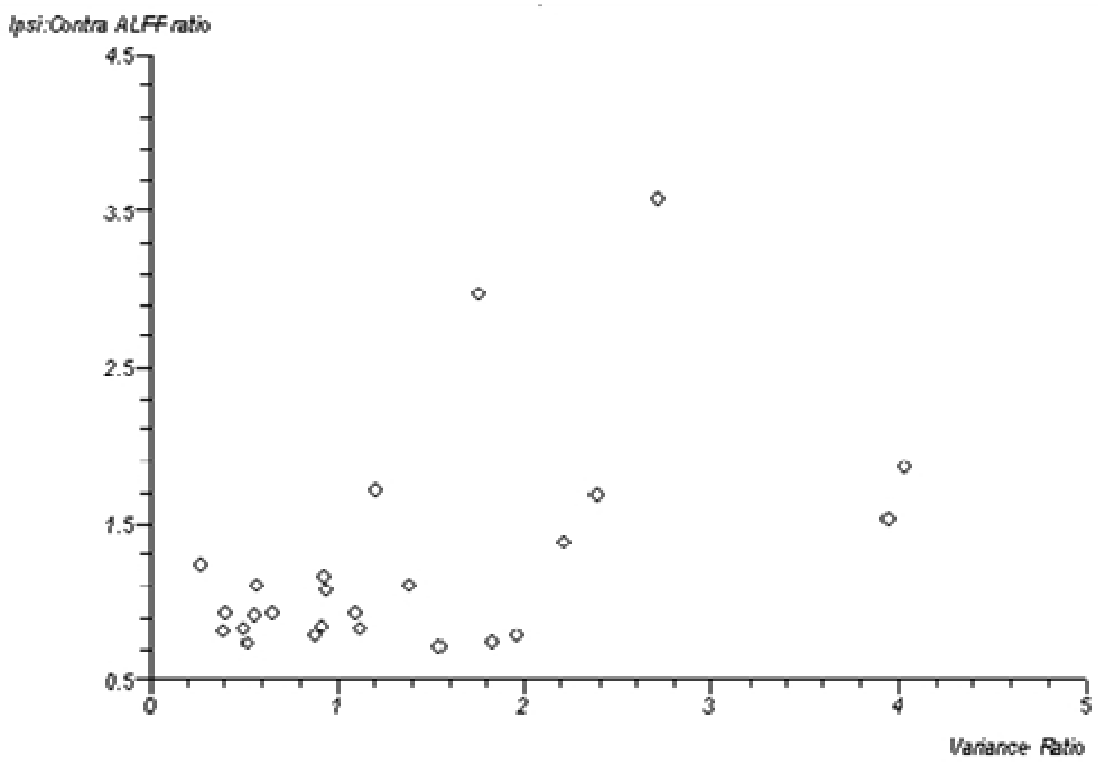

Figure 9-3 Correlation between data variability and amplitude of low frequency fluctuations. The x-axis shows the ratio of the data variability between the left and right hemispheres and the y-axis shows the ratio of the amplitude of the low frequency fluctuations between ipsilateral and contra-lateral hemispheres. There was a positive correlation between ALFF ratio and ratio of data variability as determined by Spearman's rank correlation coefficient (r=0.43, p=0.03).

9.4 Discussion

9.4.1.1 Findings

This study assessed factors with the potential to degrade the quality of the Oxygen Challenge signal. It was seen that the amplitude of low frequency fluctuations (ALFF) within the DWI lesion was correlated to the overall variability of the baseline data from this region. However, there did not appear to be a significant systematic difference in ALFF between stroke tissue compartments and their mirror regions in the contra-lesional hemispheres. This finding was maintained when only large strokes were considered. Moreover, there was no significant difference between the baseline data variability from within the DWI lesion and the mirror regions on the contra-lesional hemisphere. When other potential influences on the Oxygen Challenge signal were considered, there was no clear impact on data variability from the severity of the stroke (defined by either NIHSS or DWI lesion volume), lateralisation of the stroke, or subject motion. When motion parameters were considered in more detail, there was no association of DWI lesion volume or NIHSS to the degree of subject motion, and there did not appear to be a difference between subjects with left and right hemisphere strokes in this data set. Reassuringly, the movement parameters measured in this study of acutely unwell stroke subjects did not show a significant difference in the degree of motion compared to subjects with a diagnosis of epilepsy who were scanned on an elective basis.

9.4.1.2 Interpretation of Findings

Data Variability and ALFF: How should the finding of a lack of statistical difference in ALFF between the DWI lesion (and indeed other stroke tissue compartments) and the mirror region be interpreted? One potential interpretation is that the phenomenon of the resting state network is preserved in acute stroke. However, such a conclusion should not be made definitively from these data. The amplitude of low frequency fluctuations (ALFF) has recently been used to provide a marker of the low frequency fluctuations which contribute to the ‘resting state’ activity(363). Changes in ALFF have been

demonstrated in other neurological disorders such as epilepsy, multiple sclerosis(364), attention deficit hyperactivity disorder (ADHD)(363) and Alzheimer's disease(365). However, although the positive identification of changes in ALFF may be genuine in other studies, the failure to identify differences in ALFF between stroke tissue and mirror regions does not necessarily signify preserved resting state networks. The purpose of this study was to ascertain potential differences in the baseline signal between tissue compartments for the purposes of evaluating the previously implemented technique of examining the T2*-weighted signal intensity-time curves. In this regard, this study has provided a greater confidence for the use of the mean signal of the pre-Oxygen Challenge time points to represent baseline, since there was no difference in ALFF and in overall data variability between stroke tissue and DWI mirror regions. However, resting state networks were not the focus of investigation. For investigation of the effect of ischaemia on resting state networks one would ideally examine a cohort of subjects with a stroke lesion in the same anatomical territory, of the same duration since onset, and perform post processing using analyses such as seed based correlation analysis or independent component analysis(366). Results could then be compared to an age and risk factor matched control data set. In this study, there were a number of limitations of the analysis of the low frequency fluctuations. Firstly, the stroke lesions of subjects varied. This had the effect of restricting analyses of individual subjects separately; group analysis using SPM software was not performed owing to the differences in size and location of the lesions. The next limitation of the clinical variability was that the stroke tissue compartments examined were likely to have been heterogeneous with respect to their pathophysiology, both within regions from individual subjects and between subjects. Within 24h, the DWI lesions were likely to have comprised of a mix of penumbral and core tissue(54) and the mismatch regions were unlikely to have all represented penumbra. Therefore, the responses within a given tissue compartment (e.g. DWI lesion) may not have been consistent - the ALFF may have been pathologically increased in some and decreased in other, thereby limiting the ability of simple statistical tests to detect differences. The second limitation relates to the technique used to examine the low frequency fluctuations. Although the use of ALFF has been successfully employed in a number of studies(363, 367), there are also a number of associated limitations.

The ALFF is the value of the low frequency fluctuation measured in the frequency domain. Therefore, the assessment of low frequency fluctuations for a given region of interest / tissue compartment was summarised into a single value, an approach which is felt by some to eliminate useful physiological data owing to the simplistic mathematical processing(366). In addition, it is now appreciated that ALFF maps are inherently susceptible to noise induced by vascular and respiratory artefacts(368). This is likely to have played a role in the Oxygen Challenge data set. Figure 9-2 shows an example of an ALFF map used in this study. Although it shows the expected appearance of a larger (brighter) ALFF in the grey compared to the white matter(268), the ventricles shows a very large (bright ALFF), which would not be expected if the signal was a pure representation of neuronal activity. This is likely to have represented the artefact from the aforementioned physiological noise. It has been proposed that the use of fractional ALFF(368) may help to eliminate much of this noise; this involves calculating the sum of the amplitudes within the range expected to show low frequency fluctuations (0.01-0.08Hz) and dividing this value by that calculated using a wider frequency range. Although this method has shown promise, it has not been completely validated. A further limitation of this study is that the repetition time of the sequence ('TR') of 3 seconds increases the chances of genuine low frequency fluctuations becoming aliased with cardiac and respiratory noise compared with lower 'TRs'. A final limitation which should be noted is that although the pre-Oxygen Challenge time points were analysed, subjects were not truly 'resting'. For example, a mirror was placed on the head coil in order to allow the patient to see out of the scanner, thus potentially stimulating visual cortex. Subjects may have felt uncomfortable due to stroke related factors, some subjects required verbal reassurance throughout the scanning session and some patients may have been asleep. Although these factors were not routinely recorded, it is likely subjects were heterogeneous in this regard. Therefore they may have been variable cortical activity due to stimuli not been accounted for by this study.

It should be noted that, despite the inherent limitations of the application of ALFF in this study, Liu and colleagues(369) used a very similar method to demonstrate clear changes in the low frequency fluctuations after stroke. These investigators similarly produced maps of peak amplitude in the frequency

domain and showed increased amplitude of low frequency fluctuations in peri-infract tissue. However, that study differed from the current study in that it used a model of experimental stroke in baboons, and examined stroke lesions which were of the same 'age' since onset. As discussed, the Oxygen Challenge data set provided a much more heterogeneous cohort of stroke subjects. Nonetheless, it was still possible to show that the ALFF within the DWI lesion contributes to the overall variability of the data.

Subject Motion: The next observation to consider is that stroke lesion severity (as measured by neurological deficit [NIHSS] or DWI lesion volume) did not seem to be associated with movement parameters. Therefore, in this cohort it could not be shown that subjects with large stroke moved more than subjects with small stroke. Given the large number of factors which may contribute to patient related motion such as impaired cognition, language disorder, individual personality and anxiety state, headache and undetected urinary retention, it is perhaps not surprising that stroke size was not associated with patient motion within the scanner. However, intuitively one may expect this not to be the case. For example, although subjects with large strokes may be agitated, subjects with smaller strokes and in whom cognition is not impaired, may have a greater capacity to appreciate the potentially anxious scenario of MRI scanning. The other point to acknowledge is that this study did not consider subjects who did not have a stroke. It is possible that having had any stroke, regardless of size, is sufficient to cause a different response compared to healthy volunteers. Reassuringly, however, subjects in this cohort did not move to any greater degrees than subjects from an electively scanned cohort published in the literature(360).

Next, it should be noted that part of the reason that movement parameters did not have an effect on data variability is likely to have been due to the realignment procedures. However, it should also be noted that subject motion is likely to have had an effect on a number of parameters which were not considered by this study. For example, motion related factors which are not corrected by realignment include anatomical distortions(352), edge artefacts, and failure of the realignment procedures to realign brain of host artefacts

accurately. Therefore, conclusions about the effect of motion of data refer specifically to the variability of baseline data.

Finally, it should be noted that there are limitations to the description of subject motion. This study examined movement in 6 directions separately and also calculated a vector for the translation. However, there is no standardised technique to express both the degree of translation and rotation as a single value, even though this would be the most representative value.

9.4.1.3 Implications of findings and conclusions

A number of conclusions may be drawn from the data. The first is that low frequency fluctuations, which may represent a combination of vasomotion, neurological activity associated with the resting 'default' state, and aliased physiological noise, are likely to have an impact on the variability of baseline signal, at least within the DWI lesion. Therefore, for future calculations of the 'baseline' one could consider using the immediate pre-Oxygen Challenge time points (e.g. final minute of baseline) rather than a longer preceding period. The second conclusion is that, based on results from this study, the use of the mean of pre-Oxygen Challenge time points is not likely to introduce any systemic bias into the calculation of parameters such as percentage signal change in the DWI lesion and mirror regions. Finally, it can be suggested that subjects with larger strokes with more significant neurological deficit do not necessarily exhibit greater motion within the scanner, and therefore judgements regarding tolerability of MRI should not simply be made on the basis of stroke severity. In fact, in our cohort, the patient motion was similar to that seen in elective studies.

10 Summary and Conclusions

10.1 General considerations

In the work presented here, both existing and novel techniques for the imaging evaluation of hyperacute stroke have been considered. This thesis presented early validation studies derived from the first implementation of the 'Oxygen Challenge' technique in acute ischaemic stroke in humans. This method involved the application of transient hyperoxia during continuous T2*-weighted magnetic resonance imaging which, by exploiting the BOLD effect(208, 209, 370), provides a measure of deoxyhaemoglobin concentration. Since venous deoxyhaemoglobin is dependant on the oxygen extraction fraction, which is in turn dependent of the interplay between $CMRO_2$ and CBF, this technique may be of value in distinguishing tissue compartments following hyperacute ischaemic stroke, on the basis of underlying metabolic activity.

The aims of this thesis were as follows:

1) To implement the Oxygen Challenge technique for the evaluation of acute ischaemic stroke

2) To determine the physiological and pathophysiological influences on Oxygen Challenge results

A summary of findings is presented here.

10.2 Implementation of Oxygen Challenge is feasible

This study showed that implementation of the Oxygen Challenge technique as part of a stroke MR protocol is clinically feasible. Results from this technique can be presented as maps of percentage signal change and viewed along side maps from other MR sequences (Chapter 7). From 35 subjects recruited, Oxygen Challenge data were acquired from 33 subjects. Considering that such scans

were acquired in the context of a medical emergency, a drop out rate of 2/35 may be considered very reasonable. Although some subjects did not have the correct tissue substrate for evaluation, data from 25 subjects were analysed. However, after rigorous quality criteria were applied, data from only 18/25 subjects were analysed, emphasising the need for improvement in the signal-to-noise ratio. A critical analysis of factors potentially detrimental to signal quality did not clearly identify any clinical characteristics which predisposed to a poor signal. However, the amplitude of low frequency fluctuations (ALFF) of the T2*-weighted signal within the DWI lesion was correlated to the variability of data derived from this region. Although changes in ALFF may be due to physiological disturbance due to ischaemia(369), such changes may also be caused by aliasing of physiological T2*-weighted signal to artefacts caused by cardiac and respiriatory motion(368). These results suggested that due attention should be paid to minimising these factors in future studies. Reassuringly there was no difference in baseline variability between the DWI lesion and the 'mirror' regions, suggesting that using the pre-Oxygen Challenge 'baseline' signal for calculations of percentage signal change will not introduce any bias between values for DWI lesions and normal tissue.

10.3 Oxygen Challenge produces a signal increase in healthy tissue

Consistent with the initial hypothesis, application of Oxygen Challenge precipitated increases in T2*-weighed signal intensity in the contra-lesional 'normal' hemisphere (Chapter 2 and Chapter 3). The magnitude of such changes was approximately 2% when considering the 'mirror' regions to the DWI lesion. Such findings are consistent with those found in the literature(242, 249, 251, 252, 269). In addition to the observed signal increase, T2*-weighted signal was seen to return to baseline after cessation of the Oxygen Challenge. This may be explained by the continued extraction of oxygen from the tissue, with replenishment of deoxyhaemoglobin to the measured pool.

10.4 Signal response to Oxygen Challenge is attenuated in the DWI lesion

This study was the first to report changes in T2*-weighted signal intensity after Oxygen Challenge from within a stroke lesion. Results from 17 subjects with DWI lesions >1ml showed that the response to Oxygen Challenge was attenuated in the DWI lesion. This was consistent with reduced extraction of oxygen from the tissue microcirculation by hypometabolic stroke tissue. Although a reduction in cerebral blood volume could also potentially explain these findings, the T2*-weighted signal intensity-time curve remained diminished in two subjects for whom non-nutritional reperfusion was observed, suggesting that the observed changes were indeed due to a metabolic effect. Unlike the pilot animal study(255), regions of signal decrease were also observed within DWI lesions. Although this may have been due to signal drift independent of the Oxygen Challenge, it is possible that owing to the high baseline venous oxygen saturation in these tissue regions, paramagnetic oxygen was offloaded in to the plasma(267). If this explanation is indeed correct, it underlines the potential complexity for the use of hyperoxia as an MRI 'tracer'.

10.5 Signal response to Oxygen Challenge may be exaggerated in the hyperacute region of perfusion-diffusion weighted imaging

Unlike the animal pilot study(255) where an exaggerated signal increase was seen in regions likely to be penumbral, there was no statistically significant effect seen in this study. However, focussing on the subjects with PWI-DWI mismatch who were imaged <9h, there was a trend towards an exaggerated increase in T2*-weighted signal intensity. A possible explanation for the failure to replicate the findings of the animal studies is likely due to the nature of the tissue studied; regions of 'likely penumbra' in this study were small, often imaged late, and derived from very few subjects. Therefore, no definitive conclusions can be made regarding 'penumbral' imaging by this study.

Although the animal pilot study(255) showed an exaggerated signal increase in the borderzone, there was no correction for baseline CBV. Therefore, it remains uncertain if regions of high OEF can be detected by the Oxygen Challenge technique, independent of the influence from cerebral blood volume. The potential ability for the technique to do this hinges on whether enough oxygen can be administered to completely saturate deoxyhaemoglobin in normal tissue. Although increases in venous oxygen saturation of only 10% have been reported after hyperoxia(249), these measurements were insensitive to regional heterogeneity. In this study, the finding of an exaggerated T2*-weighted signal increase in the mismatch region where the CBV was not elevated supports the concept of the Oxygen Challenge technique being partially dependent on underlying OEF.

10.6 Oxygen Challenge may be altered in other regions of metabolic upset

Following the evaluation of the DWI lesion and regions of potential penumbra (PWI-DWI mismatch regions and regions of DWI expansion), it was considered whether other metabolically defined tissue compartments could be evaluated for the purposes of additional validation. Therefore, attention turned towards the phenomenon of crossed cerebellar diaschisis (CCD)(322) which describes contra-lateral hypometabolism of a cerebellar hemisphere secondary to ipsilateral stroke. Given that approximately 50% of stroke subjects have been reported to manifest this phenomenon(328), the potential of Oxygen Challenge to detect this was evaluated. This was only the fourth MRI study to ever evaluate subjects for crossed cerebellar diaschisis, and the only one to use a technique other than PWI. In this study there was a statistically significant reduction in the magnitude of signal increase in the contra-lesional cerebellum for those subjects with large strokes, consistent with hypometabolism. This finding was accompanied by decreased CBV, as expected.

10.7 A number of factors influence the Oxygen Challenge response

Throughout this thesis there was extensive discussion with respect to the influences on T2*-weighted signal intensity. There is a strong body of theoretical(232) and practical evidence(242, 248) that the percentage signal change after hyperoxia is dependent on baseline cerebral blood volume. Results from this study supported this notion. For example, the largest T2*-weighted signal increases were seen in the saggital sinus (a pure blood compartment), followed by cortical grey matter, and least of all white matter (Chapter 3). Moreover, following analysis of regions of interest there was a correlation between CBV and percentage signal change in DWI lesions (Chapter 6). A voxel based analysis for all subjects was consistent with this (Chapter 8), and showed that CBV and ADC were independently predictive of percentage signal change, whereas TMAX was not. However, when only voxels from within the DWI lesion were evaluated, all three parameters were significantly correlated with percentage signal change. This finding is reassuring in that it has been shown that CBV is not wholly predictive of the Oxygen Challenge results. The ADC may be a surrogate marker of underlying metabolic activity(57), albeit one which is suboptimal, supporting the concept that Oxygen Challenge may provide 'metabolic' information. Nonetheless, these results suggest that CBV needs to be considered when interpreting the results of Oxygen Challenge. It should also be noted that the concentration of oxygen influences the magnitude of signal change. In regions of grey matter, higher concentrations of oxygen give rise to larger signal increases, but in regions of low deoxyhaemoglobin concentration, it is possible the reverse may true, due to dissolution of oxygen within the plasma(267). Therefore, results should also be interpreted with knowledge of the administered FiO_2.

10.8 Further work to validate the Oxygen Challenge is warranted

There are two complementary approaches which must be taken for the successful validation of this technique. The first approach must be to improve

the application of the technique in order to achieve the highest quality signal possible. The second approach is to improve understanding of the influence of Oxygen Challenge on the BOLD effect in different tissue compartments. Investigation of both approaches may be performed in tandem.

Firstly, signal-to-noise ratio must be improved. Although subject motion was not shown to be a significant factor in determining the variability of baseline data, due attention to this factor is always necessary. Therefore, comfort of the subjects is critical. For patient studies, where oxygen administration using a 'controlled' system may not be practical, one approach would be to design nasal cannulae specifically to administer high flow oxygen within the MR scanner. This is likely to improve patient comfort since the standard face mask used in this study often fitted tightly between the subject's face and the head coil. Increased space between the head and the coil would also allow additional comfortable padding to be applied in an effort to further limit head motion. Another potential approach to improve signal-to-noise is to apply dielectric pads to the subject's cranium, a technique which has been shown to improve signal and image quality(371, 372).

Next, one should consider the properties of the sequence used. The use of continuous T2*-weighted MRI in this study was similar to typical fMRI studies, and has been invaluable in describing the dynamics of the T2*-weighted signal increase after Oxygen Challenge. However, whilst these sequences may be used further for validation of the technique, such an approach renders the data susceptible to noise. In addition, it requires long scanning times in order to achieve the maximum signal increase, which may not have even always been achieved in data from the hypoperfused regions in this study. Thirdly, the use of the T2*-weighted sequence renders the data very susceptible to artefact from the paranasal sinuses. An alternative approach is to use a sequence similar to that used by An and colleagues(207, 234-236, 238). The multiecho sequence used by this group allows quantitative determination of T2 and T2'. Alternatively one could employ susceptibility weighted images. Such sequences could be acquired at the start and then towards the end of a typical MR stroke protocol, with other images acquired between the two sequences. An interval of at least 10 minutes would be reasonable to allow for equilibration in even the most hypoperfused tissue. Such an approach would allow the acquisition of a single

good quality baseline image and a single good quality Oxygen Challenge image. A difference map could then be used to provide a measure of absolute signal change. This approach may also be more convenient to fit into typical MR stroke protocols.

Next, investigation of a number of different concentrations of oxygen should be investigated with respect to differentiating infarct core, ischaemic penumbra and healthy tissue. This could be achieved using a closed face mask integral to a circuit capable of delivering a fixed concentration of oxygen.

In addition, a detailed examination of the relationship between hyperoxia, venous oxygen saturation and BOLD signal intensity would aid the understanding of the true meaning of signal changes with respect to the differential contributions of cerebral blood volume and venous oxygen saturation. Such evaluation of venous oxygen saturation may be achieved with multiecho MRI sequences(234).

Finally, after sequence optimisation, validation with ^{15}O labelled PET would be ideal.

For all of the analyses described, the most informative patient population should be targeted. Subjects should ideally have persistent arterial occlusion within the first 6h after onset, and should have large regions of PWI-DWI mismatch. For the purposes of validation, a few ‘high yield’ research subjects are likely to be more informative than a larger number of subjects recruited beyond the hyperacute stage.

10.9 Closing remarks

Presented here are the first studies of the application of Oxygen Challenge technique to subjects with acute ischaemic stroke. Although others have encouraged the use of oxygen as an MRI tracer, no studies to date have examined the potential use in stroke subjects. In this study, differences between tissue compartments have been demonstrated, with attenuation in percentage signal change observed within the DWI lesion. The cohort examined in this study did not provide a suitable substrate to examine the response in the penumbra

but there were signals of efficacy. Current limitations of the technique as applied in this study include the relatively low signal-to-noise ratio, and artefacts from paranasal sinuses and iron deposits in the basal ganglia. The technique is also complicated by the potentially bi-modal behaviour of oxygen with respect to T2*-weighted signal, and the ability of oxygen to influence metabolic activity within penumbral tissue. Further investigation is required as to how oxygen influences venous oxygen saturation in stroke tissue compartments, and how such changes in turn influence the Oxygen Challenge results. This study has contributed data to allow a useful insight into the effect of oxygen on T2*-weighted signal intensity in acute ischaemic stroke, and may be the first step towards full validation of this technique for clinical use

11 Appendix A: Acquisition Parameters and Post-processing Algorithms for Current Perfusion Studies Are Heterogeneous

11.1 Introduction

Although much of this thesis is dedicated to the application of novel imaging techniques, it is important to appreciate the current status of penumbral imaging. Chapter 1 discussed the potential of Computed Tomography perfusion (CTp) imaging and Magnetic Resonance (MR) derived Perfusion Weighted Imaging (PWI) to identify 'tissue at risk' after stroke, thereby potentially extending the currently restrictive time windows(38) for treatment and improving safety of treatments within the time window. The latest guidelines from the European Stroke Organisation(373) and American Stroke Association(374) both suggest consideration of perfusion imaging, particularly if patients present beyond the conventional time window and reperfusion therapies are still being considered.

However, despite being based on attractive hypotheses these techniques have still not been proven by large randomised controlled trials(103). Improvements may simply require refinements to the operational criteria for 'tissue at risk' (for example specific thresholds for any given perfusion parameter(123, 159, 304) and consideration of lesion volumes of tissue(125, 375, 376). Moreover, subtle differences in post processing of perfusion imaging can lead to significantly different results (124). Therefore, it is tempting to speculate that a validated and well defined criterion for the penumbra derived from a consistently applied post-processing technique may more accurately define penumbra than present techniques, whilst increasing generalisability between studies. However, an often neglected consideration for perfusion imaging studies is the potential impact of the acquisition parameters on the definition of the penumbra. At present it is not clear if heterogeneity reduces generalisability between studies. Acknowledging that it may be important, however, a consensus statement (317, 318) (the Acute Stroke Research Imaging Roadmap) has recently been published which, amongst other recommendations, proposed optimal

imaging protocol parameters. Adherence to such protocols may promote homogeneity of imaging based stroke studies and therefore clinical applicability of results. In this study the heterogeneity of current perfusion based stroke studies was assessed in order to evaluate current practice and variation within the literature. Moreover, an assessment of the variation of key post processing techniques is made.

11.2 Methods

11.2.1 Search Strategy

This study is based on a search strategy which was developed and implemented as part of a wider series of Systematic Reviews, in collaboration with the Division of Clinical Neurosciences, University of Edinburgh. Three reviewers were involved with the search strategy; KD (thesis author), RT (Clinical Research Fellow, University of Edinburgh) and JW (Consultant Neuroradiologist, University of Edinburgh).Two reviewers (KD and RT) performed the search and disagreements were resolved by a third reviewer (JW). The databases MEDLINE and EMBASE were searched through the Ovid portal from inception to week 4 July 2008 using the search strategy attached in Appendix D. Separate search strategies were performed for MEDLINE and EMBASE databases. The titles / abstracts for all papers retrieved using the specified database search strategy were separately reviewed by both KD and RT. Papers meeting the Inclusion and Exclusion Criteria (stipulated below) were selected. In particular, focus was on the papers which were felt to have contributed to the understanding of the quantitative values derived from perfusion imaging, whilst excluding the papers which simply used perfusion imaging to answer a question unrelated to perfusion imaging itself. To this end, focus was on papers which reported either 1) values for perfusion thresholds, 2) mean perfusion values for tissue compartments or 3) correlation of perfusion deficit volumes with other parameters (see Inclusion Criteria below). In addition, in order to ensure comprehensive coverage of the literature, both KD and RT searched review articles which discussed any aspect of perfusion imaging in human acute stroke subjects (<24h) which were identified by the database search. These articles were searched in reverse chronological order and search was stopped after 10 consecutive review articles

revealed only 1 additional paper (not found by the original search) which evaluated CTp or PWI regardless of purpose. The 'Clinical Trials Registry' in The Internet Stroke Center (www.strokecenter.org) was searched in order to identify additional studies. Abstracts of conference proceedings were not reviewed since it was felt that the restrictive word count would limit the information obtained from them. In order to validate the search strategy, hand searching of two relevant journals (Stroke [KD] and American Journal of Neuroradiology [RT)]) was performed from August 2003 to July 2008 to determine the number of papers 'undetected' by the original search, thereby giving an estimate of its coverage of the literature. A targeted updated search of MEDLINE and EMBASE was performed from July 2008 to week 4 August 2009 by one reviewer (KD). This update also identified papers meeting the Inclusion and Exclusion Criteria below. illustrates the search strategy. The lists of papers generated by two authors (KD and RT) were compared and any discrepancies were discussed with a third reviewer (JW) who arbitrated the decision for final inclusion.

11.2.1.1 Manuscript Inclusion Criteria

1) English Language (owing to the high cost of translation of foreign language articles)
2) Stroke patients <24h assessed and data from whom were distinguishable from other patients
3) Adult patients (≥18 yrs)
4) Papers which reported perfusion characteristics from studies using either first pass CTp or MR derived PWI for the following:
    a. Threshold values for tissue compartments
    b. Mean perfusion values in different tissue compartments
    c. Correlation of deficit volumes on perfusion imaging with lesions on other imaging modalities

11.2.1.2 Manuscript Exclusion Criteria

1) Subjects with hemorrhagic stroke, venous infarction or chronic occlusive cerebrovascular disease

2) Studies of perfusion techniques other than first pass bolus tracking CTp or MR-PWI e.g. arterial spin labelling, CTp from triphasic helical technique or other steady state techniques
3) Studies of technical development / optimisation of imaging parameters for CT or PWI techniques
4) Studies using both duplicate data and analyses from other larger included studies

11.2.2 Data Extraction

Acquisition and post-processing parameters were extracted to standardised data extraction form in Microsoft Excel format (see Appendix D for an excerpt from the form relevant to this study). Two authors (KD and RT) performed this extraction. There was a limited overlap of citations from which the two reviewers extracted data, in order to ensure consistency. A third reviewer (JW) again arbitrated on any inconsistencies.

11.2.3 Comparison to Road Map Criteria

Perfusion acquisition parameters from CTp and PWI studies were compared against those stated by the 'Acute Stroke Imaging Research Road Map'(317, 318). These 'Roadmap' protocols suggest acquisition parameters in different domains. The 'Roadmap' suggests 9 and 10 main categories of acquisition parameters for MR and CT based studies respectively. These are as follows for MR PWI: sequence / image acquisition parameters / image acquisition duration / coverage and slice thickness / slice orientation / contrast material / contrast volume / injection rate / iv access and miscellaneous. For the CT perfusion studies they are; image acquisition rate / gantry rotation / image acquisition parameters / coverage and slice thickness / slice orientation / contrast material / contrast volume / injection rate / iv access and miscellaneous. Different parameters within these categories are specified by the 'Roadmap'. Determination of consistency with the 'Roadmap' was straightforward for parameters which were fixed and easily definable (e.g. single shot gradient echo EPI sequence to be used for PWI). However, consistency with some other parameters was harder to determine. For

example, for PWI, 20ml of gadolinium based contrast was advised for a 100kg patient, but patient weight is not routinely reported in manuscripts. Similarly, although an 'interslice gap' of 0-1mm was recommended and with a matrix of '128x128', the 'Roadmap' allows for adjustment of these parameters to allow for extension of spatial coverage if required. Therefore, a pragmatic comparison of 'Roadmap' parameters to those study parameters within each category which could reasonably be determined from manuscripts was performed (Table 12). Given this, adjustments in approach were as follows; for PWI assessment of 'whole brain coverage with ≥ 12 slices' was substituted for 'brain coverage with ≥ 12 slices'; interslice gap and matrix was not considered since flexibility in these parameters is allowed by the 'Roadmap'; 'phase encoding along the AP direction' was not considered as this is not conventionally reported by clinical manuscripts.; the volume of gadolinium contrast was not considered as the 'Roadmap' suggests a value for a 100kg person and patient weights are not routinely reported in manuscripts. For CTp, adjustments in approach from the 'Roadmap' were as follows; the issue of image duration of each of the 2 phases of the ideal acquisition was simplified to whether 2 phase acquisition was performed. In addition, the 'Roadmap' specified that images should be acquired through the proximal middle/anterior cerebral artery so that acquisition is above the orbits. Since the reporting of data in this fashion would require prior knowledge of this specification (and most papers were published prior to the 'Roadmap') these data were determined by first ensuring coverage of the proximal/middle cerebral artery territories and the basal ganglia, and secondly by determining if there was specific mention of avoidance of the orbits or lenses. Finally, the type of iodinated contrast was not considered as the 'Roadmap' simply gave a 'preference'.

If acquisition parameters were both reported and consistent with the 'Roadmap', they were reported as 'consistent'. If a given acquisition parameter was reported but was performed in a manner inconsistent with the 'Roadmap' they were graded as 'inconsistent'. If the precise acquisition parameter could not be determined we graded them as 'Not reported'. A table illustrating the parameters which were compared is presented (Table 12). Please see the legend for further details.

11.2.4 Consideration of Post Processing Parameters

Finally several post processing parameters were considered. For CT studies these were as follows: 1) arterial input function (AIF) selection methods; 2) AIF selection site; 3) AIF selection lateralisation; 4) venous output function site, and finally; 5) use of deconvolution. For MR studies the parameters considered were: 1) arterial input function (AIF) selection methods; 2) AIF selection site; 3) AIF selection lateralisation; 4) use of deconvolution and, if used; 5) the type of deconvolution.

Acquisition Parameter	Suggested by Roadmap for CT	Suggested by Roadmap for MR
Type of sequence	n/a	Single Shot Gradient Echo EPI
Duration	2 Phase Acquisition	90-120s
Temporal Resolution*	<1000ms*	≤1500ms-2000ms‡
Other technical details	Peak Kilovoltage 80kvp, Current 100mAs	Echo Time 1.5T (35-45ms); 3T (25-30ms), Flip Angle 1.5T (60-90°) 3T (30°)
Magnet Strength	n/a	1.5 or 3.0T
Anatomical Coverage	20mm (minimum) Coverage per bolus	≥12 slices‡
Slice Thickness	5-10mm	5mm
Field of View	~24cm	~24cm
Avoidance of Lenses **	Above orbits**	n/a
Basal Ganglia Coverege**	Yes**	n/a
Slice Orientation Stated	Yes	Yes
Contrast Type	n/a	Gadolinium Use Stated†
Contrast Volume	35-50ml	n/a
Contrast Concentration	350-370mg/m	n/a
Injection Delay	n/a	10s
Injection Rate	4-6ml/s	4-6ml/s
Saline Chaser Described	Yes	Yes
Power Injector Used	Yes	Yes
Cannula Gauage	18-20G	18-20G
Side of Injection	Right	Right
Antecubital Vein Used	Yes	Yes
Post-Processing Parameter	**CT Perfusion**	**MR Perfusion**
Arterial Input Function Selection Method	-	-
Arterial Input Function Selection Method	-	-
Arterial Input Function Selection Lateralisation	-	-
Venous Output Function Site	-	n/a
Use of Deconvolution	-	-

Table 12 Acquisition and post –processing parameters which were considered in this study. The upper part of the table shows the acquisition parameters considered by the 'Roadmap'. The middle and right most column suggest the values considered consistent with recommendations for CT and MR studies respectively. The lower part of the table shows the post-processing parameters considered in this study. b/a = not applicable; EPI = echo-planar imaging; ms = milli-seconds; kvp = peak kilo-voltage; T = Tesla; mA = milli-amp; mm = milli-metre; cm = centi-metre; ml = milli-metres; s = seconds; G = gauge,

11.3 Results

11.3.1 Search Results

The titles and / or abstracts of 7152 papers (6449 and 653 from initial and updated searches respectively) derived from database searching were screened. From these 48 PWI and 20 CTp papers we identified. Hand searching of review articles revealed one additional PWI study and no CTp studies. No additional studies were identified by hand searching Stroke and American Journal of Neuroradiology publications spanning 5 years. This gave a final count of 49 PWI papers and 20 CTp papers which reported perfusion thresholds / average perfusion values / correlations using perfusion deficit volumes. These results are illustrated (Figure 11-1). For the PWI and CTp data, 20/49 and 10/20 papers contributed data for perfusion thresholds for tissue compartments. The PWI studies were conducted between 1998 and 2009 and contributed data from 1810 stroke subjects. The CTp studies were conducted between 1996 and 2009 and contributed data from 840 subjects. The manuscripts of all but 3 studies were received by the publishing journal prior to the publication of the ‘Roadmap’. A list of studies fulfilling the inclusion and exclusion criteria is tabulated (Table 13).

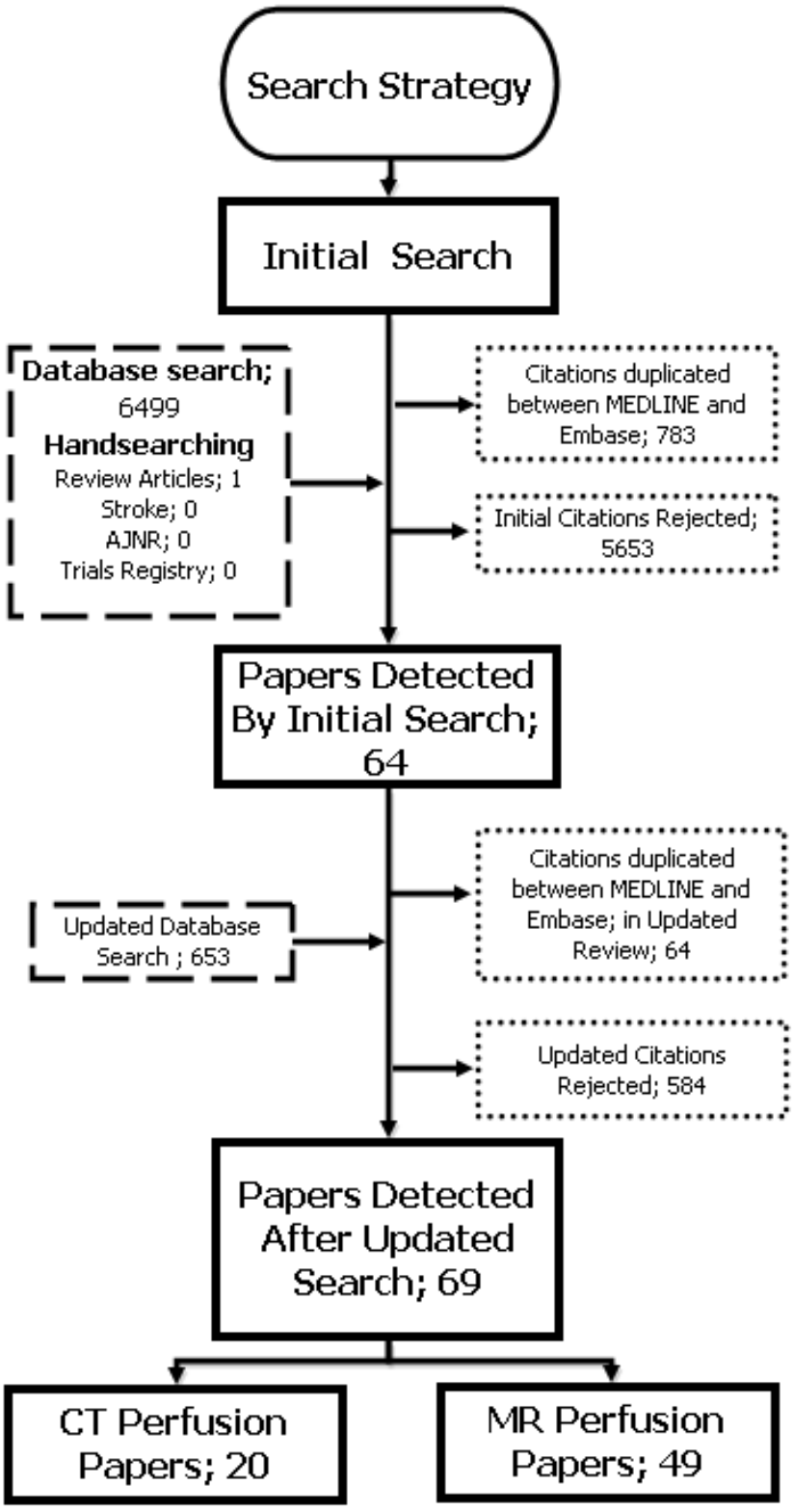

Figure 11-1. Search Strategy
This flow chart details the numbers of citations detected from the initial (top) and updated (bottom) search strategies. Boxes bounded by the broken lines (left) indicate the number of citations screened, whilst boxes with dotted lines indicate the number of citations excluded.

First Author	Journal	Year	Volume	Issue	First Page
CT Studies					
Touho	Surg. Neurol	1996	46	*	135
Klotz	Eur. Jnl Radiology	1999	30	*	170
Rother	Arch Neurol	2000	57	1161	1166
Koenig	Stroke	2001	32	*	431
Nabavi	Stroke	2002	33	*	2819
Wintermark	Annals of Neurology	2002	51	*	417
Disdas	Jnl of Comput Assist Technology	2004	26	6	747
Kloska	Radiology	2004	233	1	79
Schramm	Stroke	2004	35	*	1652
Mair	JNNP	2005	77	*	334
Suzuki	Neurol Med Chir (Tokyo)	2005	45	*	333
Murphy	Stroke	2006	37	*	1771
Schaefer	AJNR	2006	27	*	20
Wintermark	Stroke	2006	37	*	979
Parsons	Neurology	2007	68	10	730
Sparacia	Radiol. Med	2007	112	*	113
Murphy	Radiology	2008	247	3	818
Naito	Radiat. Med	2008	26	*	227
Silvennoinen	AJNR	2008	29	*	118
Hagiwara	Jnl of Comput Assist Technology	2009	32	4	645
MR Studies					
Darbar	Neurology	1998	51	*	418
Beaulieu	Annals of Neurology	1998	46	*	568
Rordorf	Stroke	1998	29	*	939
Karonen	Stroke	1999	30	*	1583
Neumann-Haefelin	Stroke	1999	30	*	1591
Schlaug	Neurology	1999	53	*	1528
Sorensen	Radiology	1999	210	2	519
Karonen	Radiology	2000	217	*	886
Liu	JCBFM	2000	20	*	910
Schellinger	Stroke	2000	31	*	1318
Smith	Jnl of Magnetic Resonance Imaging	2000	12	*	400
Karonen	Computer Methods and Programs in Biomed.	2001	66	*	125
Klutymans	Eur Radiology	2001	10	*	1434
Oppenheim	Stroke	2001	32	*	2486
Parsons	Stroke	2001	32	*	1581
Rohl	Cerebrovasc Diseases	2001	12	*	203
Rohl	Stroke	2001	32	*	1140
Thijs	Neurology	2001	57	*	1205
Aronen	Academic Radiology	2002	9	Suppl 1	S160
Fiehler	Stroke	2002	33	*	2421
Grandin	Radiology	2002	223	*	361
Parsons	Annals of Neurology	2002	51	*	28
Wittsack	Radiology	2002	222	*	397
Butcher	Stroke	2003	34	*	2159
Igarashi	Jnl of Comput Assist Technology	2003	27	*	874
Liu	Neuroradiology	2003	45	*	345
Schaefer	AJNR	2003	24	*	436
Shih	Stroke	2003	34	*	1425
Derex	J Neurol Sciences	2004	225	*	3
Heiss	Stroke	2004	35	*	2671
Nasel	AJNR	2004	25	*	945
Rose	Jnl of Magnetic Resonance Imaging	2004	20	*	941
Rose	Stroke	2004	35	*	2466
Sobesky	Stroke	2004	35	*	2843
Bristow	JCBFM	2005	25	*	1280
Butcher	Stroke	2005	36	*	1153
Kucinski	AJNR	2005	26	*	815
Moon	Korean J Radiology	2005	6	*	75
Seitz	Jnl of Magnetic Resonance Imaging	2005	22	*	199
Simon	JCBFM	2005	25	*	1236
Sobesky	Stroke	2005	36	*	980
Arakawa	Stroke	2006	37	*	1211
Rivers	Stroke	2006	37	*	0
Kane	Stroke	2007	38	*	3158
Akazawa	Neuroradiology	2008	50	*	939
Takasawa	Stroke	2008	39	*	870
Christensen	Stroke	2009	40	*	2055
Olivot	Stroke	2009	40	*	469
Zaro-Weber	Stroke	2009	40	*	2413

Table 13 Table of Studies Fulfilling Inclusion Criteria

11.3.2 Comparison to the 'Acute Stroke Imaging Research Roadmap' Parameters

The results from comparison of image acquisition parameters from derived studies against key features from the 'Roadmap' is presented (Table 14).

For CTp studies several parameters were both reported and consistent with the 'Roadmap'. These included details on anatomical coverage (in >80% of studies), and the volume (70%) and method (75%) of contrast injection. A number of other parameters, however, were frequently reported but not consistent with the 'Roadmap'. For example, only 15% of studies were performed using the recommended '2 phase' acquisition, and the contrast concentration (50%) and injection rate (60%) were frequently performed in a manner other than the method recommended by the 'Road map'. The parameters which were frequently unreported included 'field of view' (85%), acquisition of images from above the orbits / lenses (80%), precise orientation of the image acquisition (90%), and side of injection of contrast (100%). Acquisition parameters were heterogeneous with a large range noted for certain parameters; number of slices (range 1-4), rate of injection (2-20ml/s), electrical parameters (9 different combinations of peak kilovoltage and milliamperes reported), and volume of iodine in contrast (8 combinations in 10 papers which reported this; range 10.5-18.5g)

For MR studies, 92% were reported to have been performed on a scanner with appropriate magnet strength and with appropriate contrast agent. However, the duration of scanning was frequently inconsistent with the 'Roadmap' (63%), and acquisition parameters such as repetition time, echo time, and flip angle, and contrast injection details were also frequently inconsistent or not reported. The acquisition parameters were also noted to be heterogeneous. For example, 17/49 studies used a spin echo sequence, there were 24 combinations of TE/TR, the number of phases of acquisition ranged from 20 to 60 phases, and the number of slices ranged from 7 to 40 slice.

	MR Studies			CT Studies		
Acquisition Parameter	% Consistent	% Not Consistent	% Not Reported	% Consistent	% Not Consistent	% Not Reported
Type of sequence				26	37	37
Duration	15	85	0	6	63	31
Temporal Resolution	70	10	20	53	20	27
TE	6	78	16			
TR	53	20	27			
Flip Angle	8	16	76			
Peak Kv				60	20	20
Current				10	70	20
Magnet Strength	92	6	2			
Anatomical Coverage	49	39	12	80	15	5
Slice Thickness	53	37	10	85	10	5
Field of View	43	37	20	10	5	85
Avoidance of Lenses				10	10	80
Basal Ganglia Coverage				90	0	10
Slice Orientation Stated	6	0	94	10	0	90
Contrast Type	92	8	0	n/a	n/a	n/a
Contrast Volume				70	20	10
Contrast Concentration				10	50	40
Injection Delay	4	25	71			
Injection Rate	49	20	31	35	60	5
Saline Chaser Described	51	0	49	0	0	100
Power Injector Used	55	8	37	74	0	25
Cannula Gauage	10	2	88	30	10	60
Side of Injection	0	0	100	0	0	100
Antecubital Vein Used	31	0	69	70	0	30

Table 14 Comparison of Study Acquisition Parameters to the 'Roadmap'.
The left and right hand side of the table decribes the study acquisition parameters stipulated by the roadmap for MR and CT studies respectively. Values for the percentage (%) of papers consistent with the roadmap guidance are reported. TE = echo time. TR = repetition time. Kv = kilovoltage.

11.3.3 Post-processing Parameters

For the CT papers deconvolution was employed in 8/20 (40%) cases, was not employed in 6/20 cases (30%) and was unclear in 6/20 cases (30%). The specific deconvolution technique was specified in two cases (box-modulation transfer function and closed form non-iterative deconvolution) although the use of a specific commercial software package was described in 14 other cases. The AIF was selected from the internal carotid artery (ICA) in 1/20(5%), from the anterior cerebral artery in 6/20 (30%), from a combination of ICA / MCA in 1/20 (5%), and was not discussed in 12/20 (60%). The AIF was selected from the contra-lateral hemisphere in 4/20 (20%), from either hemisphere in 1/20 (5%) and from a hemisphere not specified in 15/20 (75%). The venous output function was selected from the saggital sinus in 6/20 cases (30%), from dual sites in 2/20 (10%), automatically in 2/20 (10%), and was not discussed in 10/20 (50%).

For MR papers, the use of a deconvolution technique was stated in 31/49 (63%) papers. Twenty three of these 31 papers (74%) used standard singular value decomposition (sSVD), 2/31 (6%) evaluated more than one method which included circular SVD, 2/31 (6%) used standard SVD with bolus delay correction, 1/31 (3%) used Fourier Transform, and in 3/31 (10%) cases deconvolution was employed but the technique was unspecified. The site of the AIF was specified in 23/31 (74%) cases (ICA=3, MCA=19, dual sites=1). The hemisphere used for AIF selection was specified in 19/31 (61%) cases (contralateral in hemisphere in 15 cases, ipsilateral hemisphere in 2 cases, in either hemisphere in 1 case and bilaterally in 1 case).

11.4 Discussion

This systematic review identified 69 papers published up to August 2009 which have contributed to our understanding of perfusion values derived from CT and MRI based studies. Such studies provided data on perfusion thresholds, average perfusion values in certain tissue compartments, and correlation of volumes for

perfusion deficits against other relevant parameters. When compared to the ‘Acute Stroke Imaging Research Roadmap’ many acquisition parameters were frequently unreported, and when reporting of parameters did occur they were frequently inconsistent with the ‘Roadmap’ proposals. Acquisition parameters were frequently heterogeneous. Moreover, the selection of AIF and its employment in deconvolution was varied.

There has been systematic investigation of post-processing parameters(124) such as arterial input function(114), deconvolution(110), perfusion thresholds(123, 159) and operational definitions of the penumbra(52, 125, 375, 376) and these do impact results from perfusion imaging. In this study we observed a variety of AIF selection techniques and a number of different post-processing software packages and deconvolution techniques employed. This is likely to have reduced generalisability of results between studies.

The precise effect of the observed heterogeneity of acquisition parameters on perfusion imaging results is at present unclear since the impact of such heterogeneity has not been systematically investigated. Other than ‘avoidance of lenses’ during CTp studies, which is necessary for safety reasons, all other parameters may theoretically affect perfusion results. Therefore, even if optimal post processing and analysis algorithms are used in future studies, heterogeneity of acquisition parameters between studies has the potential to restrict the generalisability of results and to limit comparison of results between studies. The effect of heterogeneous acquisition parameters combined with heterogeneous post processing (which was also observed here with respect to AIF selection and deconvolution) and variable operational definitions for the penumbra may have a very complex effect on imaging results. This may explain, at least in part, the unanticipated poor performance of CTp and PWI in clinical trials(103). Therefore improved homogeneity of studies with respect to acquisition parameters, in addition to other aspects of perfusion imaging, may be required.

In addition to the frequent heterogeneous reporting of acquisition parameters, some parameters were frequently unreported. The most frequently unreported acquisition parameters included ‘field of view’, description of saline chaser, cannula gauge, side of contrast injection, and MRI flip angle. Such parameters

may be considered less essential to reproducing the study than the more frequently reported parameters such as anatomical coverage and temporal resolution, and therefore the impact of this underreporting may be limited. Nonetheless, the ‘Roadmap’ proposals now give future authors the opportunity to state, at least in a generic manner, that such acquisition parameters have been performed to an agreed standard even if some acquisition parameters are deliberately omitted.

Limitations of this study include a restricted coverage of the literature. Inclusion of potential manuscripts was limited to those which have helped develop understanding of perfusion values (e.g. those reporting perfusion thresholds) rather than studies which have used perfusion imaging as a tool to answer other scientific questions. However, it is likely that the 69 papers included in this study serve as a reasonable representation of the use of perfusion imaging in the wider literature. Other limitations include the use of the ‘Acute Stroke Imaging Research Roadmap’ as a reference. Although this has not been rigorously validated and therefore is arguably not a true ‘gold standard’, it is a consensus statement from leading experts in the field and represents a commonly agreed standard. Therefore it provided a useful reference standard for this study. Finally, it should be noted that the included studies in this review were predominantly performed before the publication of the ‘Roadmap’ and thus a retrospective comparison of published studies to the ‘Roadmap’ meant that precise comparison of the ‘Roadmap’ protocol to the study acquisition parameters was some times difficult for all components. For example, we would not expect a study published prior to the ‘Roadmap’ to explain that the ‘optimal’ interslice gap was sacrificed in order to afford whole brain coverage, since this stipulation by the ‘Roadmap’ was published after the study in question. Therefore a prospectively defined pragmatic comparison was performed for parameters which would be reasonably expected to be reported.

In conclusion, current studies of CT and MRI based perfusion are often heterogeneous and often inconsistent with the recent proposals by the Acute Stroke Imaging Research Roadmap. Moreover, there is variation within the literature with respect to post-processing. This review highlights the areas of such inconsistencies and allows authors of future studies to determine which domains of reporting of acquisition parameters could be strengthened in future

studies. This study emphasises that perfusion imaging is complex and that there is still scope for improvement and development of these techniques. Homogeneous performance and reporting of acquisition parameters in addition to the often discussed post-processing algorithms and operational criteria for the penumbra may help to build consistency and generalisability of future results from perfusion imaging studies. However, given the inherent variability in these techniques, there may still be scope for other imaging techniques to help refine penumbral identification. In the absence of a gold standard MR penumbral imaging technique, development of other novel imaging techniques should be considered.

12 Appendix B: Continued Recruitment to Stroke Studies by Assent Is Critical; A Study of Lesion Volume

12.1 Introduction

Chapter 1 focussed on the application of imaging techniques, predominantly with MRI, which may be routinely implemented for the clinical evaluation of patients. This chapter, however, considers the application of imaging techniques from a research perspective. A typical validation pathway for a novel imaging technique is to test the modality in animal models, then in human volunteers (or control 'healthy' tissue as an alternative) and subsequently in patients with the disease of interest. In this thesis, the validation of a novel MRI technique in stroke patients is presented (Chapter 2 onwards). When testing a new technique in patients, the most relevant data will be generated if the technique is applied to a cohort of subjects who have the biological substrate of interest. Therefore, when testing a technique which may be of use in the evaluation of hyperacute stroke, subjects should be evaluated in the early stages after stroke onset when the likelihood of persistence of 'penumbral' tissue is high. This element can be easily dealt with by stipulating an upper time limit for inclusion. Secondly, recruitment of subjects with adequate lesion volume is important. For example, tissue compartments should be large enough to facilitate accurate measurement of volume without significant errors(342). The minimum volume which is sufficient is likely to depend on the nature and resolution of the modality being tested. Moreover, lesion volume is likely to be important with respect to the pathophysiology of the stroke. For example, subjects with larger DWI lesions are more likely to experience haemorrhagic transformation after intravenous rtPA(377) and those with lesions on DWI of >145ml are likely to develop 'malignant MCA' syndrome(378). The neurological deficit as measured by the NIHSS is correlated with lesion size(379), and an upper limit for the NIHSS is often employed by licences and protocols for rtPA administration. Similarly, subjects with only very minor stroke (and by inference those with small lesions) are often excluded from treatment by thrombolytic therapy. Therefore, findings

from stroke studies recruiting only subjects with small stroke lesions cannot necessarily be generalised to subjects with larger strokes.

For these reasons, in order to recruit subjects with sufficient lesion volume, written assent from relatives was permitted as a method of recruitment of stroke subjects for studies discussed in this thesis (Chapter 2 onwards). This approach is supported by data from the third International Stroke Trial (IST3) which suggested that subjects with more severe stroke were more likely to have been recruited by assent(380). Furthermore, the capacity to consent to trials diminishes with increasing baseline neurological deficit(381). However, an overriding principle of clinical research is that subjects should not be included in studies unless a potential benefit (to the patient or to society) can be demonstrated. In addition, using 'assent' from relatives as a recruitment modality should only be employed if it offers an additional potential benefit compared to restricting recruitment to direct consent. These principles are clearly stated by the Declaration of Helsinki(382) and the European Clinical Trials Directive (ECTD)(383). Additional legislation has been implemented in Scotland (Adults with Incapacity Scotland)(384) which states that research after 'assent' must provide "real and direct benefit to the adult or to other persons having the same incapacity".

Therefore, in order to justify continued recruitment by assent to stroke studies, specific differences between stroke subjects recruited by assent and those recruited by consent should be demonstrated. In addition, cohorts recruited by assent should have qualities which are desirable for study and which are not present in cohorts recruited by direct consent. Thus, it was investigated whether there was a 'biological' difference between those stroke subjects recruited by assent and those by direct consent, to MR imaging based studies at the Institute of Neurological Sciences, Glasgow. In this study, lesion volume was used as the marker of 'biology'.

12.2 Methods

12.2.1 Studies

Clinical stroke studies using MRI at the Institute of Neurological Sciences, for which either digital MRI data or recorded lesion volume data were available, were identified. Data from 3 studies which had previously recruited subjects via both consent and assent were analysed. All studies were approved by relevant ethical committees. Studies 1 and 2 were performed after the introduction of the European Clinical Trials Directive and the Scottish 'Adults with Incapacity' legislation. Study 3 was performed prior to their introduction. The first study (called 'Study 1' for the purposes of description in this chapter) is reported in Chapter 2 of this thesis. This study had no specific minimum neurological deficit required for inclusion but did require clinical evidence of a cortical stroke within 24h of ictus. At the time of data analysis this study was ongoing and therefore only the first 16 subjects with available DWI were included. Images for Study 1 were acquired using a 3.0T scanner. The second study (Study 2) was the Randomized, Controlled Trial of Insulin for Acute Poststroke Hyperglycemia (SELESTIAL) Study(261) which was performed at the Institute of Neurological Sciences, Glasgow. After exclusion of ICH by NCCT, this study required a clinical diagnosis of cortical stroke within 24h. Images for Study 2 were acquired using a 1.5T scanner. Study 3 used data from the subjects recruited at the Institute of Neurological Sciences (Glasgow) for the MRI Substudy of the Intravenous Magnesium Efficacy in Stroke Trial(340). These data contributed to a larger multi-centre study which recruited subjects within 12h after the onset of stroke. This study required a minimum DWI lesion volume of 3ml associated with a clinical diagnosis of stroke and a limb weakness which lasted for at least 1h (and thereby included 'lacunar strokes'(2). Images for Study 3 were acquired using a 1.5T scanner.

It should be noted that treatment decisions were made prior to including subjects in these MR based studies. Therefore, rtPA was administered prior to the images considered in this study.

12.2.2 Consent

All three studies permitted recruitment by written consent or written assent from relatives. There were no definite criteria for recruitment method in any study. In all studies, the decision to recruit a patient using either route was made using clinical judgement. In Study 1, where KD (thesis author) recruited the majority of subjects, this decision was made by KD in close collaboration with the treating physicians. For Studies 2 and 3, the recruiting investigator was either a Stroke Research Fellow or an experienced Consultant Neurologist or Physician. For each subject, the most senior clinical investigator involved in recruitment was recorded

12.2.3 Selection of Subjects

The following selection criteria were applied:

- *Inclusion criteria*
    - Digital MRI data or recorded lesion volume data available
    - Recruitment into one of the 3 aforementioned studies
    - No specific DWI or PWI lesion volume required
- *Exclusion criteria*
    - Method of recruitment into the trial unclear

12.2.4 Clinical Data

The databases for each respective study were interrogated for the following data; 1) age, 2) gender, 3) hemisphere affected (stroke lateralisation), 4) clinical classification according to the Oxfordshire Community Stroke Project (OSCP)(2)), 5) treatment status with respect to recombinant tissue plasminogen

activator (rtPA) and 6) neurological deficit as defined by the National Institutes of Health Stroke Scale(257). If clinical data were not available from the respective clinical databases, clinical case records were retrieved and examined.

In a proportion of subjects, a CT angiogram was performed for clinical purposes. Clinical radiology reports were attained for such cases and the site of arterial occlusion was noted. All clinical reports were made by experienced Consultant Neuroradiologists.

12.2.5 Lesion Volume Data

Study specific MR imaging was acquired after screening with NCCT and subsequent implementation of clinical treatment decisions. Lesion volumes were made using the baseline Diffusion Weighted Imaging (DWI) data for each subject. The DWI acquisition parameters for Study 1 are documented in Chapter 2. All DWI examinations were acquired using B0 and B1000 diffusion gradients. The DWI B1000 data were used for lesion volume measurement. All lesion volumes were measured using the software package 'Cheshire' (Perceptive Informatics, PAREXCEL). The 'autosegmentation' tool was employed in this study. This allowed the delineation of tissue compartments based on local signal intensity and allowed manual refinement according the investigator's discretion. Therefore, in this study, the ultimate lesion volume was based on the investigator's visualisation of the DWI lesion.

KD (thesis author) generated all lesion volume data for Study 1. For Studies 2 and 3 the lesion volume data were attained from the respective clinical databases for each study. These lesion volumes were originally measured by the Clinical Research Fellow who was involved in these respective studies (MTM).

12.2.6 Statistical Analyses

Comparative statistical analyses were performed using Minitab (Version 14.0) software unless otherwise stated. Assessments of the distribution of data were performed using the 'Kolmogorov Smirnov' test and non-parametric statistical tests were employed where normality of the data could not be demonstrated. The Mann-Whitney test was used to compare continuous data from subjects recruited by consent to those by recruited by assent. Data for 'proportions' were compared using the Chi-squared test unless an outcome event had a frequency <5, in which case a Fisher's Exact test was employed. For categorical data of proportions ('clinical syndrome' and 'site of occlusion') the Fisher-Freeman-Halton Exact test was used to compare multiple proportions between groups (StatsDirect v 2.6.2).

Differences in subjects recruited by each of the 3 main investigators were also compared; the Kruskal Wallis statistic was used to compare continuous variables and the Fisher-Freeman-Halton Exact test was again used to compare multiple proportions between groups (StatsDirect v 2.6.2). The Spearman statistic was used to assess the correlation between lesion volume and NIHSS. Lastly NIHSS, lesion volume, age and stroke lateralisation were entered into a binary logistic regression to determine potential predictors for the capacity to consent.

12.3 Results

12.3.1 Recruitment Modality of Subjects

Fifty six subjects were identified in total; 16, 29, and 12 subjects from studies 1, 2, and 3 respectively (one subject was recruited into both Study 1 and Study 2). Thirty eight subjects (68%) were recruited by assent and 18 (32%) by consent. The proportion recruited by consent was 33%, 21% and 58% for studies 1, 2, and 3 respectively.

12.3.2 Influence of Investigator

Three investigators contributed to the majority of the recruitment - KD (thesis author) recruited 14 subjects, KWM (Consultant Neurologist) recruited 13 subjects, and MTM (Clinical Research Fellow) recruited 25 subjects. One other identifiable investigator recruited a single subject to Study 3. There were 3 subjects in Study 3 for whom the recruiting investigator could not be determined. There were no statistically significant differences between the subjects recruited by each investigator with respect to the following variables; baseline NIHSS (n=39, p=0.9), proportion of subjects with left hemisphere stroke (n=56, p=0.5), lesion volume (n=56, p=0.15). There were no statistically significant differences between investigators with respect to the rate of recruitment by assent; 71% (10/14) vs 46% (6/13) vs vs 80% (20/25),[p=0.118].

12.3.3 Differences between Subjects Recruited by Assent versus Consent

states the clinico-radiological variables for subjects in the 'Assent' and 'Consent' groups. There were no differences with respect to the following demographic variables; age, time to imaging, treatment status. There were however, differences in the 'biological' variables of the subjects. There was a significant difference in the clinical stroke classification between subjects (p=0.02) with a much larger proportion of subjects with 'Total Anterior Circulation Stroke' syndromes in the 'Assent' group. The median DWI lesion volume of those were recruited by assent was 18.35 cubic centimetres (cc) (inter-quartile range [IQR] 8.27 – 110.31 cc) and the mean (± Standard Deviation [SD]) was 63.7cc (± 78.5). In the consenting group, the median lesion volume was 2.79 cc (IQR 1.31 – 12.33cc) with a mean (± SD) of 12.1cc (± 23.1). The differences between groups were highly statistically significant (two tailed Mann Whitney test, p=0.0008). A further analysis was performed after excluding the 14 patients treated with rtPA order to ensure that there was no confounding effect of treatment. For this group, the mean, median and IQR volumes were 66cc, 16.9cc and 8.6-118cc for the assenting group and 7.9cc, 3.6cc, and 1.8-9.9cc for

the consenting group, and differences remained significant (p=0.004; n=42). Importantly, there was a dramatic difference between groups for the proportion of subjects who had a lesion volume less than the accepted error implicit for lesion volume measurements. The proportion of subjects in the 'Assent' and 'Consent' groups for whom the DWI lesion was <5cc was 18.4% vs 61% (p=0.002).

There was no significant difference in the site of arterial occlusion between 'Assent' and 'Consent' group when the small subgroup of subjects for whom angiographic data were available were analysed (p=0.594). However, there were 3 cases of occlusion of the Internal Cerebral Artery (ICA) in the 'Assent' group and no cases in the 'Consent' group, thereby suggesting a potential difference between groups.

	Assent Group	Consent Group	Differences Between Groups (p value)
No. of subjects (% of total)	38 (68%)	18 (32%)	***
Mean age (SD)	71 (11.2)	68 (12.7)	0.398
Mean time to imaging (SD)	17.1 (7.1)	14.3 (7.3)	0.143
No of subjects receiving rtPA(% of group)	10 (26%)	2 (11%)	0.2168
Mean time to rtPA, mins (SD)	166 (23)	177 (3.5)	0.564
Clinical syndrome, no. of subjects			0.0231
TACS	20 (53%)	3 (17%)	
PACS	11 (29%)	9 (50%)	
LACS	5 (13%)	6 (33%)	
POCS	2 (5%)	0 (0%)	
Site of occlusion			0.594
ICA	3	0	
M1, MCA	5	1	
M2, MCA	1	1	
PCA	1	1	
Unidentified	13	6	
Left:Right hemisphere stroke	11:07	20:17	0.638
Lesions <5cc (%)	7/38 (18.4%)	11/18 (61%)	0.0024
Median lesion volume (cc) [IQR]	18.35 (8.27-110.3)	2.79 (1.31-12.33)	0.0008

Table 15 Baseline Data in Assenting and Consenting Groups
TACS = Total Anterior Circulation Stroke, PACS = Partial Anterior Circulation Stroke, LACS = Lacunar stroke, POCS = Posterior circulation stroke. ICA = Internal Carotid Artery MCA = Middle Cerebral Artery, PCA = Posterior Cerebral Artery, cc = cubic centimetres. Note one patient in the Assent group had bilateral lesions. .*= statistically significance, p <0.05.

12.3.4 Prediction of Capacity to Consent

There was a positive correlation between DWI lesion volume and baseline NIHSS (r=0.58, P<0.0001). This relationship means that if, hypothetically, only consent was permitted for subject recruitment, the majority of subjects recruited by consent in this cohort would have been ineligible for most previous stroke studies which have used a minimum NIHSS threshold for study inclusion .

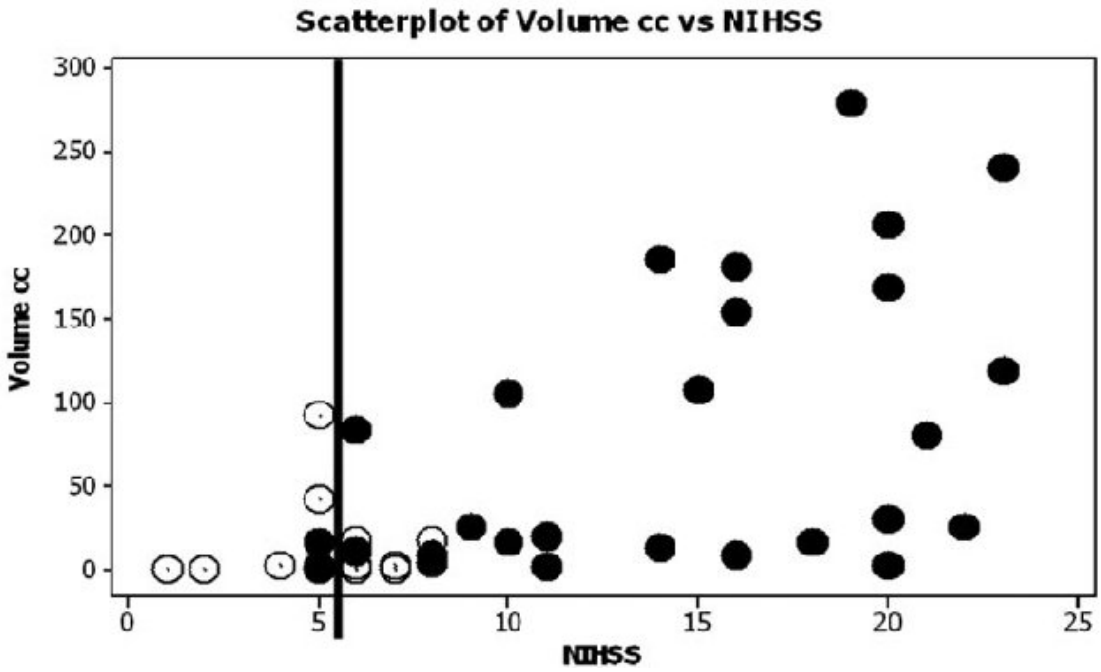

Figure 12-1. Relationship Between Lesion Volume and Baseline NIHSS and the Implication for Clinical Trial Recruitment

The x-axis shows the clinical deficit as measured by the National Institutes of Health Stroke Scale(257) and the y-axis shows the DWI lesion volume on the baseline MR image. The thick vertical line shows a typical 'cut off' NIHSS severity for inclusion into clinical trials(71). The open circles represent subjects recruited by consent and the closed black circles represent subjects recruited by assent. It is clear that the subjects recruited by consent had a much milder (lesser) NIHSS. If, hypothetically, only consent was permitted for this study and a typical NIHSS threshold for study inclusion of NIHSS=6 was implemented, very few of these subjects would have been ultimately recruited into studies. Figure reproduced from When stroke lateralisation, baseline NIHSS, age, and DWI lesion volume were entered into a binary logistic model as predictors for the capacity to consent, baseline NIHSS (p=0.007) and DWI lesion volume were significant (p=0.038). Age was not a significant predictor (p=0.187). Stroke lateralisation was of borderline significance ([p=0.08) but when age was removed from the model the significance level did not improve (p=0.1) whilst NIHSS (p=0.002) and lesion volume (p=0.03) remained significant. When only DWI lesion volume and NIHSS were entered into the model, only NIHSS retained a significant predictive value (p=0.001) whilst DWI lesion volume was borderline non-significant (p=0.054).

12.4 Discussion

This study demonstrates that there are differences between subjects recruited to stroke studies by direct consent compared to those recruited by assent from relatives. There were differences with respect to DWI lesion volume and clinical syndrome.

Why do these differences matter for stroke trials? Firstly, there is good evidence that the severity of stroke as determined by clinical syndrome influences prognosis(2), with subjects with very large established strokes generally having a poor prognosis. Recruiting subjects only by consent would yield a cohort of subjects with mild stroke, many of whom may improve spontaneously, thus potentially limiting the ability of randomised controlled trials to detect differences in end points. Conversely, recruiting subjects with severe strokes and high NIHSS would yield a cohort of subjects with a large ceiling for improvement, thus potentially increasing the ability of trials to detect differences between treatment groups. Secondly, the behaviour of large strokes is different to that of small strokes. For example, there is a high rate of rtPA induced haemorrhagic transformation in subjects with large lesions on DWI(377). Lesions greater than approximately 100ml and which have a marked perfusion deficit are termed to have a 'malignant' profile with respect to the response to thrombolysis(71). Moreover, large lesions greater than 145ml are more likely to develop significant oedema sufficient to cause cerebral herniation(378, 385). Consideration of the volume of imaging 'lesions' (particularly salvageable tissue) is also important when refining the PWI-DWI mismatch hypothesis(125, 376). Parsons and colleagues considered the effects of PWI and DWI lesion volume on the response to rtPA. Excellent outcome was generally seen when DWI lesions were <18ml and benefit from rtPA was seen with lesion up to 25ml, in contrast to lesions >25ml. Therefore, cohorts of subjects with clinically mild strokes associated with small lesion volumes will not provide an adequate substrate for evaluation of the behaviour of larger strokes. Finally, although not statistically significant, proximal occlusions were seen almost exclusively in those recruited by assent. Proximal occlusions are a requirement for some thrombolytic trials such as the follow up studies to DIAS 2 (termed DIAS 3/4). It is unlikely that

many, if any subjects, will be successfully screened for DIAS 3/4 by direct consent.

Next, it was considered if recruitment of subjects purely by consent could have yielded any subjects of interest. Firstly, in the consented group, the third quartile of lesion volume was 12ml, well within the threshold of 18ml suggested by Parsons et al to predict an excellent response to rtPA(376). This suggests if the consented patients were recruited to clinical trials, many would have a good prognosis, regardless of being in a treatment or placebo arm. Differences between groups would be hard to demonstrate. Secondly, even if some subjects within the consented group do provide valuable information, suggests that the absolute number of these subjects would be small. If typical inclusion criteria for imaging based studies such as minimum NIHSS score of 6 (as used in DEFUSE(71)) and minimum lesion volume of 5cc (a threshold suggested by one author's opinion to reduce measurement error(342)) were applied to our population, recruitment by consent alone would have resulted in only 4 patients (7%) being included, all of whom still had relatively small lesions (<20cc). Of the remaining 28 patients where NIHSS data was available, 25 of these could also be included if assent was allowed. Therefore recruiting such valuable subjects to trials by consent only may take an unfeasibly length of time.

In addition to the methodological issues requiring the need for assented subjects, there are also patient-related issues. Recruitment to hyperacute stroke trials occurs in the context of a sudden catastrophic event which often impairs cognitive function. Can valid informed consent really be obtained form patients under such circumstances? It has been demonstrated that even subjects with mild stroke and who recover rapidly may not remember all aspects of the event(386). In addition, Schats and colleagues used sub-arachnoid haemorrhage as an example of a neurological emergency and showed that only 28% of subjects recruited to trials felt retrospectively they had been capable of making a decision for themselves. Therefore, even when consent is taken, it may not be truly valid in all cases.

There are a number of limitations to this study. Firstly, this was a single centre study with a limited number of investigators all practising in the same environment. The decision for recruitment modality was made using clinical

judgement and no specific protocol was used. It is possible, therefore, that the results cannot be generalised to other sites and other countries. The results, however, are consistent with other studies which have suggested a relationship between baseline NIHSS and modality of recruitment, and therefore differences between sites, if present, are likely to be subtle(380). Secondly, recruitment for these studies was made within 12h or 24h of onset after stroke. Acute treatment decisions and implementation, including the administration of rtPA, were made prior to imaging by MR. This may have led to attenuation of lesion volume by previously implemented treatment. Therefore, the recruitment and imaging environment in these studies did not exactly mirror the scenario which would arise if subjects were recruited prior to treatment decisions, such as in thrombolytic trials. Thirdly, the DWI lesion volume was used as the surrogate marker of biological activity of the stroke. The PWI lesion volume was not considered. For a hypothetical hyperacute study where the DWI lesion had not evolved fully this would have led to underestimation of the true extent of the lesion. In this study, no subject had a PWI-DWI mismatch (accordingly to the standard definition of '120%') and therefore simply using the DWI lesion is likely to have provided an accurate measure of lesion extent. Nonetheless, follow up lesions were not considered and therefore, there may have been some DWI lesion expansion after initial imaging. Fourth, two different investigators measured the DWI lesions as different studies were considered by this analysis and no measures of inter-observer reliability were available. In addition, there was no systematic evaluation of intra-observer reliability prior to this study, and these factors constitute a significant limitation.However, to ensure consistency with between raters, the same software package was used and a consensus method of lesion volume measurement was agreed upon prior to the second rater (KD) performing measurements. Moreover, the inter-observer reliability for DWI lesion volume measurement using this package has been shown to be highly reliable (387). Next, there were no power calculations performed for this study. Finally, it should be acknowledged that there is a circularity of argument in this study: subjects recruited by assent were deliberately retrospectively included in order to derive a lesion volume from such subjects, and this was not a prospective study.

In conclusion, this study provides support to the principle that assent of individuals should be permitted in order to allow meaningful results to be generated by stroke studies. Future studies which require subjects with at least moderate neurological deficit should continue to offer the option to recruit by assent. Failure to offer the option of assent of individuals to stroke studies may be ethically unjustified when a moderate neurological deficit is required.

13 Appendix C

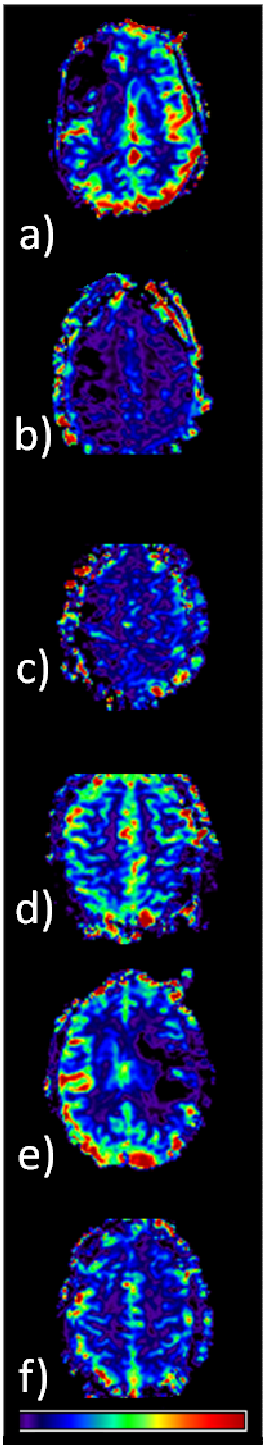

Figure 13-1 Maps of cerebral blood volume (CBV) for subjects with a perfusion-diffusion mismatch.

Lettered labelling and slice position corresponds to those in Figure 7-2. Subjects are a) subject 1, b) subject 5, c) subject 16, d) subject 22, e) subject 33, and f) subject 35. CBV maps were generated using standard SVD deconvolution. The scale bar is given at the bottom of the figure. Higher values for CBV are given towards the right of the scale bar and vice versa. Black regions indicate regions of low CBV where a colour scale could not be assigned. Absolute values are not stated given the limitations of absolute CBV maps previously discussed in the thesis.

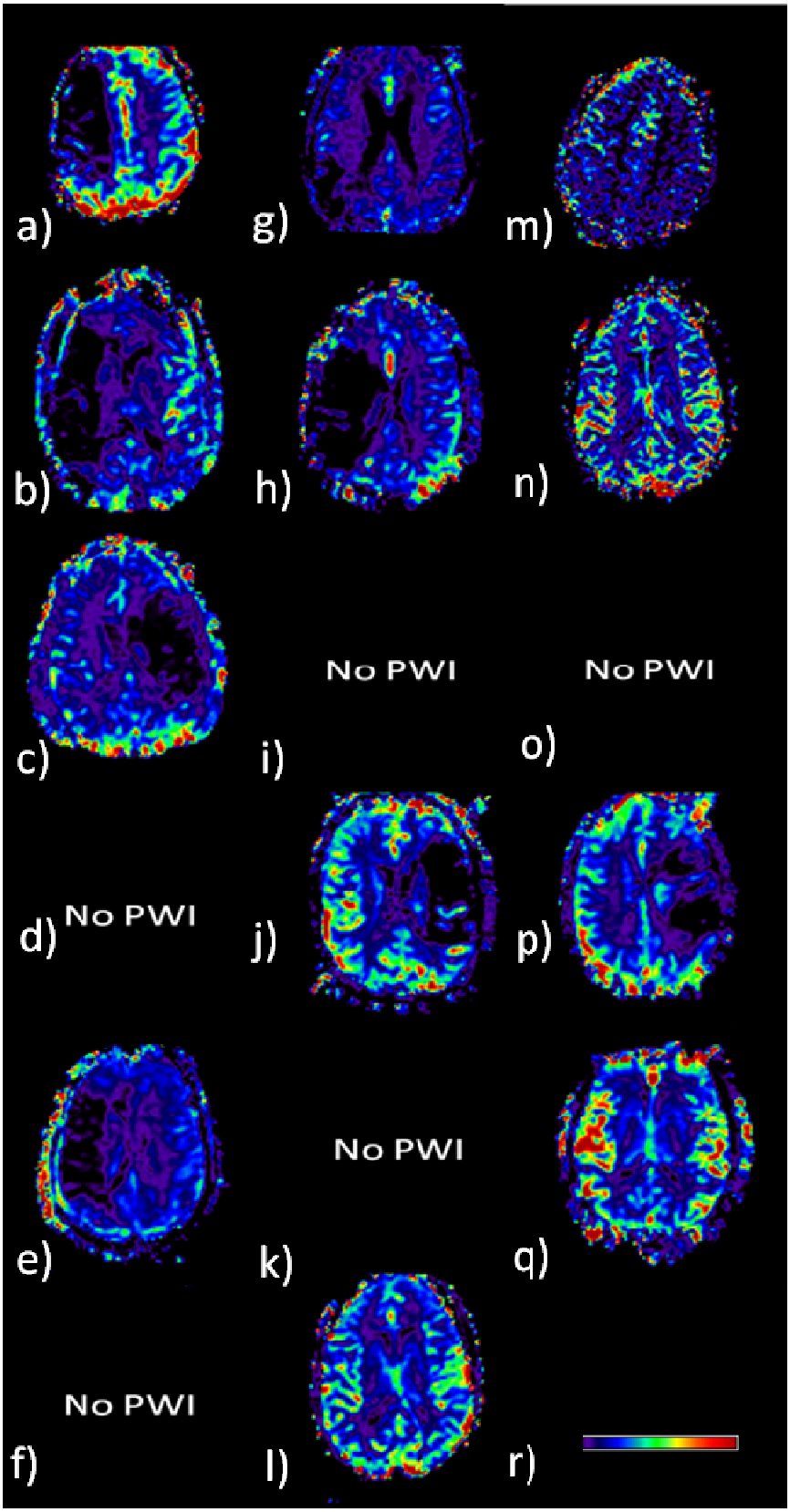
a)
g)
m)
b)
h)
n)
c)
No PWI
No PWI
i)
o)
d)
No PWI
j)
p)
e)
No PWI
k)
q)
No PWI
f)
l)
r)

Figure 13-2 Maps of cerebral blood volume (CBV) for subjects with a diffusion lesion.

Lettered labelling and slice position corresponds to those in **Figure** 7-4. Subjects are a) subject 1, b) subject 5, c) subject 6, d) subject 8, e) subject 9, f) subject 11, g) subject 12, h) subject 16, i) subject 21, j) subject 22, k) subject 23, l) subject 24, m) subject 28, n) subject 30, o) subject 31, p) subject 33, and q) subject 35. CBV maps were generated using standard SVD deconvolution. The scale bar is given at the bottom right hand side of the figure (r). Higher values for CBV are given towards the right of the scale bar and vice versa. Black regions indicate regions of low CBV where a colour scale could not be assigned. Absolute values are not stated given the limitations of absolute CBV maps previously discussed in the thesis.

14 Appendix D

14.1 Medline Search Strategy for Systematic Review of Perfusion Imaging

1. cerebrovascular disorders/ or basal ganglia cerebrovascular disease/ or exp brain ischemia/ or carotid artery diseases/ or carotid artery thrombosis/ or intracranial arterial diseases/ or cerebral arterial diseases/ or exp "intracranial embolism and thrombosis"/ or exp stroke/
2. (isch?emi$ adj6 (stroke$ or apoplex$ or cerebral vasc$ or cerebrovasc$ or cva or attack$)).tw.
3. ((brain or cerebr$ or cerebell$ or vertebrobasil$ or hemispher$ or intracran$ or intracerebral or infratentorial or supratentorial or middle cerebr$ or mca$ or anterior circulation) adj5 (isch?emi$ or infarct$ or thrombo$ or emboli$ or occlus$ or hypoxi$)).tw.
4. tia$1.tw.
5. 1 or 2 or 3 or 4
6. Magnetic Resonance Angiography/
7. (magnetic resonance angiograph$ or mri angiograph$ or perfusion magnetic resonance imaging or perfusion mri).tw.
8. (perfusion adj3 (tomography or ct or cat or pet)).tw.
9. 6 or 7 or 8
10. 5 and 9
11. magnetic resonance imaging/ or diffusion magnetic resonance imaging/ or echo-planar imaging/ or magnetic resonance imaging, cine/ or magnetic resonance imaging, interventional/
12. Positron-Emission Tomography/
13. Tomography, X-Ray Computed/
14. ((magnetic resonance or mr or nmr) adj3 (imaging or tomography)).tw.
15. (mri or positron emission tomography or pet scan$ or diffusion scan$ or diffusion weighted imag$).tw.
16. (computed adj3 tomography).tw.
17. ((ct or cat) adj scan$).tw.
18. radionuclide imaging.fs.
19. 11 or 12 or 13 or 14 or 15 or 16 or 17 or 18
20. Perfusion/
21. cerebral angiography/ or radionuclide imaging/ or radionuclide angiography/
22. exp contrast media/
23. Differential Threshold/
24. (perfusion adj3 (imag$ or parameter$ or differen$ or value$ or threshold$)).tw.
25. (mean transit time or mtt or time to peak or ttp or tmax or t-max).tw.
26. 20 or 21 or 22 or 23 or 24 or 25
27. 5 and 19 and 26
28. 10 or 27

29. limit 28 to humans

30. (haemorrhag$ or

14.2 Embase Search Strategy for Chapter 11's Systematic Review of Perfusion Imaging

1. cerebrovascular disease/

2. cerebrovascular accident/

3. stroke/

4. vertebasilar insufficiency/

5. carotid artery disease/

6. exp carotid artery obstruction/

7. brain infarction/

8. brain stem infarction/

9. cerebellum infarction/

10. brain ischaemia/

11. transient ischemic attack/

12. exp occlusive cerebrovascular disease/

13. (stroke$ or apoplex$ or cerebral vasc$ or cerebrovasc$ or cva or transient isch$ or tia$).tw.

14. (brain or cerebr$ or cerebell$ vertebasilar$ or hemispher$ or intracran$ or intracerebral or infratentorial or supratentorial or middle cerebr$ or mca$ or anterior circulation).tw.

15. (isch?emi$ or infarct$ or thrombo$ emboli$ or occlus$ or hypoxi$).tw.

16. 14 and 15

17. or/1-13,16

18. PET.mp. or Positron Emission Tomography/

19. CT.mp. or Computer Assisted Tomography/

20. Image Analysis.mp. or Image Analysis/

21. computer analysis.mp. or Computer Analysis/

22. MRI.mp. or Nuclear Magnetic Resonance Imaging/

23. magnetic resonance imaging.mp.

24. Diagnostic Imaging/ or Central Nervous System/ or brain imaging.mp. or Neuroimaging/

25. Magnetic Resonance Angiography/ or magnetic resonance angiography.mp.

26. Diffusion Weighted Imaging/ or DWI.mp.

27. PWI-DWI.mp.

28. magnetic resonance imaging/ or diffusion magnetic resonance imaging/ or echo-planar imaging/ or magnetic resonance imaging, cine/ or magnetic resonance imaging, interventional/

29. ((magnetic resonance or mr or nmr) adj3 (imaging or tomography)).mp. [mp=title, abstract, subject headings, heading word, drug trade name, original title, device manufacturer, drug manufacturer name]

30. (mri or positron emission tomography or pet scan$ or diffusion scan$ or diffusion weighted imag$).mp. [mp=title, abstract, subject headings, heading word, drug trade name, original title, device manufacturer, drug manufacturer name]
31. (computed adj3 tomography).mp. [mp=title, abstract, subject headings, heading word, drug trade name, original title, device manufacturer, drug manufacturer name]
32. ((ct or cat) adj scan$).mp. [mp=title, abstract, subject headings, heading word, drug trade name, original title, device manufacturer, drug manufacturer name]
33. exp BRAIN PERFUSION/ or PERFUSION/
34. cerebral angiography.mp. or Brain Angiography/
35. Contrast Medium/ct, ce, rp [Clinical Trial, Intracerebral Drug Administration, Regional perfusion]
36. Differential Threshold/
37. (perfusion adj3 (imag$ or parameter$ or differen$ or value$ or threshold$)).mp. [mp=title, abstract, subject headings, heading word, drug trade name, original title, device manufacturer, drug manufacturer name]
38. (mean transit time or mtt or time to peak or ttp or tmax or t-max).mp. [mp=title, abstract, subject headings, heading word, drug trade name, original title, device manufacturer, drug manufacturer name]
39. (mean transit time or mtt or time to peak or ttp or tmax or t-max).mp. [mp=title, abstract, subject headings, heading word, drug trade name, original title, device manufacturer, drug manufacturer name]
40. perfusion weighted imaging.mp. [mp=title, abstract, subject headings, heading word, drug trade name, original title, device manufacturer, drug manufacturer name]
41. PWI.mp. [mp=title, abstract, subject headings, heading word, drug trade name, original title, device manufacturer, drug manufacturer name]
42. mismatch.mp. [mp=title, abstract, subject headings, heading word, drug trade name, original title, device manufacturer, drug manufacturer name]
43. perfusion.mp. [mp=title, abstract, subject headings, heading word, drug trade name, original title, device manufacturer, drug manufacturer name]
44. perfusion/
45. AIF.mp. [mp=title, abstract, subject headings, heading word, drug trade name, original title, device manufacturer, drug manufacturer name]
46. AIF.mp.
47. Contrast Medium/ or Brain Perfusion/ or Brain Blood Flow/ or Contrast Enhancement/ or Nuclear Magnetic Resonance Imaging Agent/ or arterial input function.mp. or Gadolinium Pentetate/
48. or/18-32
49. or/33-43
50. 16 and 48 and 49
51. (haemorrhag$ or hemorrhag$ or alzheimer$ or dementia or glioma or mening$ or aneurysm$ or coronary).mp. [mp=title, abstract, subject headings, heading word, drug trade name, original title, device manufacturer, drug manufacturer name]
52. 50 not 51
53. limit 52 to human
54. limit 53 to english language

55. limit 54 to "review"

56. 54 not 55

14.3 Modified Excerpt From Excel Data Extraction Sheet; Acquisition Parameters

Please see next page.

MR Data Extraction Parameter	Response	CT Data Extraction Parameter	Response
Scanner Manufacturer	*Free Text Entry*	Scanner Manufacturer	*Free Text Entry*
Magnet Strength (Tesla)	*Free Text Entry*	Jog mode	Yes / No
Sequence	Spin Echo / Gradient Echo	kvp	*Free Text Entry*
Echo Time (TE) (ms)	*Free Text Entry*	mA	*Free Text Entry*
Repetition Time (TR) (ms)	*Free Text Entry*	Gantry Rotation time (s)	*Free Text Entry*
Flip Angle	*Free Text Entry*	Time Resolution (images per second)	*Free Text Entry*
Number of phases	*Free Text Entry*	Orientation Stated	Yes /No
Orientation Stated	Yes /No	Number of slices per series	*Free Text Entry*
Matrix	*Free Text Entry*	Number of series	*Free Text Entry*
Field of View (FOV) (mm)	*Free Text Entry*	Section / Slice thickness (mm)	*Free Text Entry*
Number of Slices	*Free Text Entry*	Avoidance of Lenses?	Yes/No/Unclear
Duration of Scanning (s)	*Free Text Entry*	Duration of Scanning (s)	*Free Text Entry*
Slice thickness (mm)	*Free Text Entry*	Contrast Agent Used	*Free Text Entry*
Interslice gap (mm)	*Free Text Entry*	Concentration of contrast agent	*Free Text Entry*
Contrast Agent Used	*Free Text Entry*	Volume of agent (ml)	*Free Text Entry*
Concentration of contrast agent (mmol/kg)	*Free Text Entry*	Rate of injection (ml/s)	*Free Text Entry*
Volume of agent (ml)	*Free Text Entry*	Delay before injection (s)	*Free Text Entry*
Rate of injection (ml/s)	*Free Text Entry*	Saline Chaser Used	Yes/No/Unclear
Delay before injection (s)	*Free Text Entry*	Power Injector Used?	Yes/No/Unclear
Saline Chaser Used?	Yes/No/Unclear	Side of Injection (r/l)	Left/Right/Unclear
Power Injector Used?	Yes/No/Unclear	Antecubital vein used?	Yes/No/Unclear
Side of Injection (r/l)	Left/Right/Unclear	Gauge of Cannula	*Free Text Entry*
Antecubital vein used?	Yes/No/Unclear	Lowest level Z direction: Coverage of MCA / basal ganglia	Yes/No/Unclear
Gauge of Cannula	*Free Text Entry*	Deconvolution?	Yes /No/ Not described or unclear
Deconvolution?	Yes/No/Unclear	If so, which technique?	*Free Text Entry*
If so, which technique?	*Free Text Entry*	AIF Selection Site	ICA/MCA/ACA/PCA/not specified
AIF Selection Site	ICA/MCA/ACA/PCA/Unclear	AIF Selection Side	Left/Right
AIF Selection Side	Left/Right/unclear	Venous Output Function	Saggital sinus / straight sinus / transverse sinus/ not specified
Coregistration Method	Algorithmic / Visual / Not Done/Unclear	Coregistration Method	Algorithmic / Visual / Not Done/unclear
Definition of ROI	Threshold / Manual / Semi-automatic / Automatic / Unclear	Definition of ROI	Threshold / Manual / Semi-automatic / Automatic / Unclear
Minumum Lesion Size if Applicable	*Free Text Entry*	Minumum Lesion Size if Applicable	*Free Text Entry*
Minimum Mismatch Size if applicable	*Free Text Entry*	Minimum Mismatch Size if applicable	*Free Text Entry*
Software Package Used	*Free Text Entry*	Software Package Used	*Free Text Entry*

15 Appendix E

Subject	Age (yrs)	Gender	Hemisphere	OCSP	Time to Baseline Imaging (hrs)	Admission NIHSS	rtPA Given (mins)
1	55	F	R	TACS	30	14	Yes (150)
2	79	M	L	PACS	24	1	No
5	67	F	L	TACS	22.25	20	Yes (135)
6	68	M	L	TACS	26	20	Yes (150)
8	73	F	R	TACS	21.25	10	Yes (135)
9	76	M	R	TACS	18.5	19	No
11	52	M	R	PACS	18.5	6	No
12	64	M	R	TACS	18	5	Yes (180)
16	67	F	L	PACS	18	16	No
17	85	M	L	TACS	5	21	No
18	52	M	L	TACS	5.5	20	Yes (130)
19	53	F	L	TACS	5.5	21	Yes (150)
21	79	M	R	TACS	6.5	17	Yes (180)
22	64	M	L	PACS	27	9	No
23	75	F	L	TACS	23	18	No
24	79	F	L	PACS	21	3	Yes (180)
26	95	F	L	TACS	6.25	20	Yes (195)
28	78	M	R	PACS	24	13	No
29	54	M	R	PACS	13.5	3	No
30	78	M	L	TACS	4.5	20	Yes (150)
31	67	M	R	TACS	20	6	No
32	85	M	R	TACS	18	17	Yes (125)
33	60	F	L	TACS	6.75	21	Yes (195)
34	70	F	L	PACS	7	7	Yes (165)
35	69	M	L	PACS	7.5	3	No
Median	69	*	*	*	18	16	14 subjects (160 mins)

Figure 15-1. Summary Data for Subjects 25 Subjects with an Acute Ischaemic Stroke Lesion >1ml and Who Were Therefore Considered in the Final Analysis
Subjects are numbered in the order in which they were recruited. OCSP = Clinical Classification by the Oxford Community Stroke Project(2). PACS = partial anterior circulation syndrome, TACS = total anterior circulation syndrome, NIHSS = National Institutes of Health Stroke Scale, rtPA = recombinant tissue plasminogen activator, PWI = perfusion weighted imaging, n/a = not applicable, subject withdrawn from the study, *= missing data.

16 Appendix F

Study	Subjects	Method *Measurement of CBF* *Induction of Hyperoxia*	O_2 Level	CO_2 level	CBF	Comments
Kety and Schmidt (1947)(262)	6 young male volunteers	N_2O technique Variation in Gas Mixtures	↑ FiO_2 0.85-1.00 Arterial O_2 content 16.6 → 18.0%	↔ Blood CO_2 content 50.2 → 50%	↓ 52 → 45 cc/100g/min **13%** decrease in mean	Also noted was an increase in cerebrovascular resistance (vasoconstriction) and an increase in MAP
Lambertsen et al (1953)(288)	8 male volunteers	N_2O technique Variation in Gas Mixtures	↑ Arterial O_2 content 19→21%	↔ 5.3→5.1 kPa	↓ 55 →47 cc/100g/min **15% decrease**	
Ellingsen et al (1987) (289)	4 healthy humans 25-45yrs	Doppler US; average blood velocities Variation of Gas Mixtures	↑ 13.3 → 33.3 kPa	↔↓ $PaCO_2$ 3.3, 4.4, 5.3 kPa ↑ $PaCO_2$ 6.7 kPa	↔ ↓ Reduction by **12.9%**	Blood velocities did not change with hyperoxia unless there was a concomitant increase in CO_2;different CO_2 levels were assessed
Rostrup et al (1995)(251)	6 healthy volunteers (24-28yrs)	Phase contrast MR Varying gas mixtures	FiO_2 1.0		↓ **Reduction in CBF by 27%**	
Omae et al (1998)(290)	8 healthy volunteers	TCD – MCA velocity Varying gas mixtures	↑ 20l O_2 Tc PO2 10.3 +- 2.0 (SD) kPa → 55.1 +- 16.5 (SD) kPa	↔ $tcPCO_2$ 5.1 +- 0.5 → 4.9 +- 0.5 (SD) kPa	↓ 65 +-15 → 52 +- 16 cm/s **20%** **decrease**	This study also looked at hyperbaric oxygen therapy; hyperoxaemia caused by HBO reduced CBF but high atmospheric pressure per se did not reduce the CBF in this study
Berre et al (1999)(291)	20 healthy volunteers, 7 subjects with previous high altitude pulmonary oedema(HAPE), 6 unaffected	TCD – mean velocity MCA Varying gas mixtures	↑ FiO_2 1.0 Mean (SEM) **Healthy volunteer** SaO_2: 96.4 (0.4) → 98.8 (0.2) %	↓ **Healthy volunteers** P_{ETCO2} 5.0(0.1) → 4.7 (0.1) (SEM) kPa ↔	↓ **Healthy volunteers** 69(3) → 60(3) ↓ **Previous HAPO** 63(3) → 53(3)	Decreased heart rate observed with hyperoxia

	high altitude climbers		**Previous HAPO** SaO_2: 96.6 (0.7) → 98.1 (0.4)% **Tolerant Climbers** 97 (0.4) → 99.2 (0.3)	**Previous HAPO** P_{ETCO2} 4.8 (0.2) → 4.8 (0.3) kPa ↓ **Tolerant Climbers** P_{ETCO2} 5.6(0.1) → 5.1(0.1) kPa	↓ **Tolerant Climbers** 58(4) → 49(3) **Overall 12-15% decrease**	
Watson et al (2000)(292)	5 normal male volunteers 32-42 (median 34yrs)	Magnetic resonance phase contrast angiography of carotid and basilar arteries Varying gas mixtures	↑ FiO_2 1.0; 15l/min 96.6%→100%	↓ P_{ETCO2} Decrease 3.7-7.1% (mean 5.2)	↓ **Decreases of 8.99%→26.7% (mean 16.2%) were observed**	A second sub study showed decreases in cerebral blood flow were greater in younger subjects. CBF decreased after 2-4 min of O_2; levels rose to original levels 6 mins after withdrawal
Kolbitsch et al (2002)(293)	39 non-smoking volunteers (TCD n=20, MRI n=19)	TCD – velocity MCA MRI – contrast enhanced perfusion Varying Gas Mixtures	↑ FiO_2 1.0 SaO_2 98+-2 →100 +-1	↔ MRI cohort 40 (+- 0.6) → 40 (+- 0.5) TCD cohort 40 (+- 0.1) → 40 (+- 0.1) CO_2 was maintained at a constant levels	↓ MRI cohort Hyperoxia diminished rCBF in all regions except in parietal and left frontal gray matter (68.08 +- 0.38 to 199.58 +- 1.58 ml/100g/min vs 58.63 +- 0.32 to 175.16 +- 1.51 ml/100g/min ↔ TCD cohort 62 +- 9 → 64 +- 8 cm/s	Changes in velocity as detected by TCD not expected as no changes in parietal and left frontal gray matter on MRI
Johnstone et al (2003)(294)	9 healthy volunteers (6M 3F) age 30-45yrs (mean 33yrs)	TCD – velocity MCA Varying gas mixtures	FiO_2 1.0	↓ ?significance level. Baseline flow	↔ 57.1 +- 11.8cm/s → 55.0 +- 7.6cm/s	This study showed that cerebral haemodynamic responses to a fall in P_{ETCO2} are

				velocities measured prior to manipulation of P_{ETCO2} in separate normoxia (baseline $_{PETCO2}$ 4.85 +- 0.4 kPa) and hyperoxia (baseline P_{ETCO2} 4.62 +-0.4kPa) experiments		modulated by hyperoxia.
Floyd et al (2003)(295)	7 healthy men 21-62yrs. Mean 39 +- 14 (SE) yrs	ASL Varying gas mixtures	FiO_2 1.0 PO_2. 12.2 +- 0.9 kPa →76.9 +- 2.5 kPa	PCO_2 5.8 +- 0.2 → 5.4 +- 0.4 kPa	↓ **32.6% decrease** 53.6+- 6.8→36.1 +- 4.9 kPa	Reduction of CBF in grey and white matter was 32% and 30% respectively. Analysis of data suggests an effect of hyperoxia independent of CO_2

Table 16 Table showing response of CBF to hyperoxia.
Column 1 indicates the manuscript. Column 2 indicates the subject population. Column 3 shows the methods used t. The horizontal solid line separates the methods used to measure cerebral blood flow (upper) and methods used to change inspired oxygen concentration (lower). The fourth, fifth, and sixth columns show the direction of change in arterial oxugen tension, carbon dioxide tension, and cerebrak blood flow respectively, as shown by the arrows, and values which follow. Search Conducted May 2007. CBF – cerebral blood flow; O_2 - oxygen; CO_2 - carbon dioxide; HAPA – high altitude pulmonary oedema kPA – kilopascals; $P_{ET}CO_2$ – end tidal CO_2; $P_{ET}O_2$ – end tidal O_2; N_2O – nitric oxide; A-VO_2 – aterial-venous oxygen difference; MCA – middle cerebral artery; TCD – Transcranial doppler ultrasound; HEPEcc – cubic centimetres; ml – millilitres; s – second; SE – standard error; SE – standard error of the mean; yrs – years; M – male; F – female; pts - patients

17 References

1. Rothwell PM, Coull AJ, Giles MF, Howard SC, Silver LE, Bull LM, et al. Change in stroke incidence, mortality, case-fatality, severity, and risk factors in Oxfordshire, UK from 1981 to 2004 (Oxford Vascular Study).[see comment]. Lancet. [Research Support, Non-U.S. Gov't]. 2004 Jun 12;363(9425):1925-33.
2. Bamford J, Sandercock P, Dennis M, Burn J, Warlow C. Classification and natural history of clinically identifiable subtypes of cerebral infarction. Lancet. 1991 Jun 22;337(8756):1521.
3. Bogousslavsky J, Hachinski VC, Boughner DR. Cardiac and arterial lesions in carotid transient ischemic attacks. ArchNeurol. 1986;43(3):223.
4. Saqqur M, Tsivgoulis G, Molina CA, Demchuk AM, Shuaib A, Alexandrov AV, et al. Residual flow at the site of intracranial occlusion on transcranial Doppler predicts response to intravenous thrombolysis: a multi-center study. Cerebrovascular Diseases. [Multicenter Study
Research Support, Non-U.S. Gov't]. 2009;27(1):5-12.
5. Liebeskind DS. Collaterals in acute stroke: beyond the clot. Neuroimaging clinics of North America. 2005 Aug;15(3):553-73.
6. Saqqur M, Demchuk AM, Hill MD, Dean N, Schebel M, Kennedy J, et al. Bedside emergency transcranial Doppler diagnosis of severe carotid disease using orbital window examination. Journal of Neuroimaging. 2005 Apr;15(2):138.
7. Bisschops RH, Klijn CJ, Kappelle LJ, van Huffelen AC, van der Grond J. Collateral flow and ischemic brain lesions in patients with unilateral carotid artery occlusion. Neurology. 2003 May 13;60(9):1435.
8. Lipton P. Ischemic cell death in brain neurons. Physiological Reviews. [Review]. 1999 Oct;79(4):1431-568.
9. Dirnagl U, Iadecola C, Moskowitz MA. Pathobiology of ischaemic stroke: an integrated view. Trends in Neurosciences. [Research Support, Non-U.S. Gov't Research Support, U.S. Gov't, P.H.S.
Review]. 1999 Sep;22(9):391-7.
10. Dijkhuizen RM, Beekwilder JP, van der Worp HB, Berkelbach van der Sprenkel JW, Tulleken KA, Nicolay K. Correlation between tissue depolarizations and damage in focal ischemic rat brain. Brain research. [Research Support, Non-U.S. Gov't]. 1999 Sep 4;840(1-2):194-205.
11. Symon L, Pasztor E, Branston NM. The distribution and density of reduced cerebral blood flow following acute middle cerebral artery occlusion: an experimental study by the technique of hydrogen clearance in baboons. Stroke. 1974 May-Jun;5(3):355-64.
12. Astrup J, Siesjo BK, Symon L. Thresholds in cerebral ischemia - the ischemic penumbra. Stroke. 1981 Nov-Dec;12(6):723.
13. Baron JC. Mapping the ischaemic penumbra with PET: implications for acute stroke treatment. CerebrovascDis. 1999 Jul-Aug;9(4):193.
14. Hossmann KA. Viability thresholds and the penumbra of focal ischemia.[see comment]. Annals of Neurology. [Review]. 1994 Oct;36(4):557-65.
15. Nedergaard M. Neuronal injury in the infarct border: a neuropathological study in the rat. Acta Neuropathologica. 1987;73(3):267-74.
16. Strong AJ, Tomlinson BE, Venables GS, Gibson G, Hardy JA. The cortical ischaemic penumbra associated with occlusion of the middle cerebral artery in the cat: 2. Studies of histopathology, water content, and in vitro neurotransmitter uptake. Journal of Cerebral Blood Flow & Metabolism. [In Vitro

Research Support, Non-U.S. Gov't]. 1983 Mar;3(1):97-108.
17. Weinstein PR, Hong S, Sharp FR. Molecular identification of the ischemic penumbra. Stroke. 2004 Nov;35(11 Suppl 1):2666-70.
18. Kinouchi H, Sharp FR, Hill MP, Koistinaho J, Sagar SM, Chan PH. Induction of 70-kDa heat shock protein and hsp70 mRNA following transient focal cerebral ischemia in the rat. Journal of Cerebral Blood Flow & Metabolism. [Research Support, U.S. Gov't, Non-P.H.S.
Research Support, U.S. Gov't, P.H.S.]. 1993 Jan;13(1):105-15.
19. Jones TH, Morawetz RB, Crowell RM, Marcoux FW, FitzGibbon SJ, DeGirolami U, et al. Thresholds of focal cerebral ischemia in awake monkeys. Journal of neurosurgery. 1981 Jun;54(6):773.
20. Darby DG, Barber PA, Gerraty RP, Desmond PM, Yang Q, Parsons M, et al. Pathophysiological topography of acute ischemia by combined diffusion-weighted and perfusion MRI. Stroke. 1999 Oct;30(10):2043.
21. Heiss WD, Huber M, Fink GR, Herholz K, Pietrzyk U, Wagner R, et al. Progressive derangement of periinfarct viable tissue in ischemic stroke. JCerebBlood Flow Metab. 1992 Mar;12(2):193.
22. Lassen NA. Autoregulation of Cerebral Blood Flow. Circulation Research. 1964;15(2S1):201-&.
23. Baron JC, Bousser MG, Rey A, Guillard A, Comar D, Castaigne P. Reversal of focal "misery-perfusion syndrome" by extra-intracranial arterial bypass in hemodynamic cerebral ischemia. A case study with 15O positron emission tomography. Stroke. [Case Reports]. 1981 Jul-Aug;12(4):454-9.
24. Sette G, Baron JC, Mazoyer B, Levasseur M, Pappata S, Crouzel C. Local brain haemodynamics and oxygen metabolism in cerebrovascular disease. Positron emission tomography. Brain. 1989 Aug;112(Pt 4):931.
25. Furlan M, Marchal G, Viader F, Derlon JM, Baron JC. Spontaneous neurological recovery after stroke and the fate of the ischemic penumbra. Annals of Neurology. 1996 Aug;40(2):216.
26. Davis SM, Donnan GA, Parsons MW, Levi C, Butcher KS, Peeters A, et al. Effects of alteplase beyond 3 h after stroke in the Echoplanar Imaging Thrombolytic Evaluation Trial (EPITHET): a placebo-controlled randomised trial.[see comment]. Lancet neurology. 2008;7(4):299-309.
27. Muir KW, Buchan A, von Kummer R, Rother J, Baron J-C. Imaging of acute stroke. Lancet neurology. 2006 Sep;5(9):755-68.
28. Hoylaerts M, Rijken DC, Lijnen HR, Collen D. Kinetics of the activation of plasminogen by human tissue plasminogen activator. Role of fibrin. Journal of Biological Chemistry. [Research Support, Non-U.S. Gov't]. 1982 Mar 25;257(6):2912-9.
29. Pennica D, Holmes WE, Kohr WJ, Harkins RN, Vehar GA, Ward CA, et al. Cloning and expression of human tissue-type plasminogen activator cDNA in E. coli. Nature. 1983 Jan 20;301(5897):214-21.
30. Kilic E, Bahr M, Hermann DM. Effects of recombinant tissue plasminogen activator after intraluminal thread occlusion in mice: role of hemodynamic alterations. Stroke. 2001 Nov;32(11):2641-7.
31. Lo EH, Wang X, Cuzner ML, Lo EH, Wang X, Cuzner ML. Extracellular proteolysis in brain injury and inflammation: role for plasminogen activators and matrix metalloproteinases. Journal of Neuroscience Research. [Research Support, Non-U.S. Gov't
Research Support, U.S. Gov't, P.H.S.
Review]. 2002 Jul 1;69(1):1-9.

32. Chen ZL, Strickland S. Neuronal death in the hippocampus is promoted by plasmin-catalyzed degradation of laminin. Cell. [Research Support, Non-U.S. Gov't
Research Support, U.S. Gov't, P.H.S.]. 1997 Dec 26;91(7):917-25.
33. Rogove AD, Siao C, Keyt B, Strickland S, Tsirka SE. Activation of microglia reveals a non-proteolytic cytokine function for tissue plasminogen activator in the central nervous system. Journal of Cell Science. [Research Support, Non-U.S. Gov't
Research Support, U.S. Gov't, P.H.S.]. 1999 Nov;112(Pt 22):4007-16.
34. Tissue plasminogen activator for acute ischemic stroke. The National Institute of Neurological Disorders and Stroke rt-PA Stroke Study Group. NEnglJMed. 1995 Dec 14;333(24):1581.
35. Saver JL, Saver JL. Number needed to treat estimates incorporating effects over the entire range of clinical outcomes: novel derivation method and application to thrombolytic therapy for acute stroke.[erratum appears in Arch Neurol. 2004 Oct;61(10):1599]. ArchNeurol. [Comparative Study
Research Support, U.S. Gov't, P.H.S.]. 2004 Jul;61(7):1066-70.
36. Anonymous. Generalized efficacy of t-PA for acute stroke. Subgroup analysis of the NINDS t-PA Stroke Trial. Stroke. [Clinical Trial
Multicenter Study
Randomized Controlled Trial
Research Support, U.S. Gov't, P.H.S.]. 1997 Nov;28(11):2119-25.
37. Wahlgren N, Ahmed N, Davalos A, Ford GA, Grond M, Hacke W, et al. Thrombolysis with alteplase for acute ischaemic stroke in the Safe Implementation of Thrombolysis in Stroke-Monitoring Study (SITS-MOST): an observational study.[see comment][erratum appears in Lancet. 2007 Mar 10;369(9564):826]. Lancet. [Clinical Trial
Multicenter Study
Research Support, Non-U.S. Gov't]. 2007 Jan 27;369(9558):275-82.
38. Hacke W, Kaste M, Bluhmki E, Brozman M, Davalos A, Guidetti D, et al. Thrombolysis with alteplase 3 to 4.5 hours after acute ischemic stroke. N Engl J Med. 2008 Sep 25;359(13):1317-29.
39. Wahlgren N, Ahmed N, Davalos A, Hacke W, Millan M, Muir K, et al. Thrombolysis with alteplase 3-4.5h after acute ischemic stroke (SITS-ISTR): an observational study
Lancet. 2008;372(1303):7.
40. Lansberg MG, Schrooten M, Bluhmki E. Treatment time-specific number needed to treat estimates for tissue plasminogen activator therapy in acute stroke based on shifts over the entire range of the modified Rankin Scale Stroke. 2009;40:6.
41. Furlan A, Higashida R, Wechsler L, Gent M, Rowley H, Kase C, et al. Intra-arterial prourokinase for acute ischemic stroke. The PROACT II study: a randomized controlled trial. Prolyse in Acute Cerebral Thromboembolism. Jama. 1999 Dec 1;282(21):2003.
42. Investigators IIT. The Interventional Management of Stroke (IMS) II Study. Stroke. [Multicenter Study
Randomized Controlled Trial
Research Support, N.I.H., Extramural]. 2007 Jul;38(7):2127-35.
43. Smith WS, Sung G, Starkman S, Saver JL, Kidwell CS, Gobin YP, et al. Safety and efficacy of mechanical embolectomy in acute ischemic stroke: results of the MERCI trial. Stroke. 2005 Jul;36(7):1432-8.
44. Tomsick TA, Tomsick TA. Mechanical embolus removal: a new day dawning.[comment]. Stroke. [Comment

Editorial]. 2005 Jul;36(7):1439-40.
45. Stejskal E TJ. Spin diffusion measurements: spin echos in the presence of time-dependent field gradient. J Chem Phys. 1965;42:15.
46. Moseley ME, Kucharczyk J, Mintorovitch J, Cohen Y, Kurhanewicz J, Derugin N, et al. Diffusion-weighted MR imaging of acute stroke: correlation with T2-weighted and magnetic susceptibility-enhanced MR imaging in cats. Ajnr: American Journal of Neuroradiology. 1990 May;11(3):423-9.
47. Moseley ME, Cohen Y, Mintorovitch J, Chileuitt L, Shimizu H, Kucharczyk J, et al. Early detection of regional cerebral ischemia in cats: comparison of diffusion- and T2-weighted MRI and spectroscopy. Magnetic Resonance in Medicine. 1990 May;14(2):330-46.
48. Sevick RJ, Kanda F, Mintorovitch J, Arieff AI, Kucharczyk J, Tsuruda JS, et al. Cytotoxic brain edema: assessment with diffusion-weighted MR imaging. Radiology. 1992 Dec;185(3):687-90.
49. Mintorovitch J YG, Shimizu H, Kucharczyk J, Chan PH, Weinstein PR. Diffusion-weighted magnetic resonance imaging of acute focal cerebral ischemia: comparison of signal intensity with changes in brain water and Na+,K(+)-ATPase activity. Journal of Cerebral Blood Flow & Metabolism. 1994 March;14(2):5.
50. Warach S, Gaa J, Siewert B, Wielopolski P, Edelman RR. Acute human stroke studied by whole brain echo planar diffusion-weighted magnetic resonance imaging. Annals of Neurology. 1995 Feb;37(2):231.
51. Yoshiura T, Wu O, Sorensen AG. Advanced MR techniques: diffusion MR imaging, perfusion MR imaging, and spectroscopy. Neuroimaging Clin N Am. 1999 Aug;9(3):439-53.
52. Schlaug G, Benfield A, Baird AE, Siewert B, Lovblad KO, Parker RA, et al. The ischemic penumbra: operationally defined by diffusion and perfusion MRI. Neurology. 1999 Oct 22;53(7):1528.
53. Kidwell CS, Saver JL, Mattiello J, Starkman S, Vinuela F, Duckwiler G, et al. Thrombolytic reversal of acute human cerebral ischemic injury shown by diffusion/perfusion magnetic resonance imaging. Annals of Neurology. 2000 Apr;47(4):462.
54. Guadagno JV, Warburton EA, Jones PS, Day DJ, Aigbirhio FI, Fryer TD, et al. How affected is oxygen metabolism in DWI lesions?: A combined acute stroke PET-MR study. Neurology. 2006 Sep 12;67(5):824.
55. Loh PS, Butcher KS, Parsons MW, MacGregor L, Desmond PM, Tress BM, et al. Apparent diffusion coefficient thresholds do not predict the response to acute stroke thrombolysis. Stroke. 2005 Dec;36(12):2626.
56. Oppenheim C, Grandin C, Samson Y, Smith A, Duprez T, Marsault C, et al. Is there an apparent diffusion coefficient threshold in predicting tissue viability in hyperacute stroke? see comment. Stroke. 2001 Nov;32(11):2486.
57. Kidwell CS, Saver JL, Starkman S, Duckwiler G, Jahan R, Vespa P, et al. Late secondary ischemic injury in patients receiving intraarterial thrombolysis. Annals of Neurology. 2002 01 Dec;52(6):698.
58. Rordorf G, Koroshetz WJ, Copen WA, Cramer SC, Schaefer PW, Budzik RF, Jr., et al. Regional ischemia and ischemic injury in patients with acute middle cerebral artery stroke as defined by early diffusion-weighted and perfusion-weighted MRI. Stroke. 1998 May;29(5):939.
59. Wittsack HJ, Ritzl A, Fink GR, Wenserski F, Siebler M, Seitz RJ, et al. MR imaging in acute stroke: Diffusion-weighted and perfusion imaging parameters for predicting infarct size. Radiology. 2002;222(2):397.
60. Mullins ME, Schaefer PW, Sorensen AG, Halpern EF, Ay H, He J, et al. CT and conventional and diffusion-weighted MR imaging in acute stroke: study in

691 patients at presentation to the emergency department. Radiology. 2002 Aug;224(2):353-60.
61. Lovblad KO, Laubach HJ, Baird AE, Curtin F, Schlaug G, Edelman RR, et al. Clinical experience with diffusion-weighted MR in patients with acute stroke. AJNR Am J Neuroradiol. 1998 Jun-Jul;19(6):1061-6.
62. Gonzalez RG, Schaefer PW, Buonanno FS, Schwamm LH, Budzik RF, Rordorf G, et al. Diffusion-weighted MR imaging: diagnostic accuracy in patients imaged within 6 hours of stroke symptom onset. Radiology. 1999 Jan;210(1):155-62.
63. Fiebach J, Jansen O, Schellinger P, Knauth M, Hartmann M, Heiland S, et al. Comparison of CT with diffusion-weighted MRI in patients with hyperacute stroke.[see comment]. Neuroradiology. 2001 Aug;43(8):628-32.
64. Chalela JA, Kidwell CS, Nentwich LM, Luby M, Butman JA, Demchuk AM, et al. Magnetic resonance imaging and computed tomography in emergency assessment of patients with suspected acute stroke: a prospective comparison.[see comment]. Lancet. 2007 Jan 27;369(9558):293-8.
65. Barber PA, Hill MD, Eliasziw M, Demchuk AM, Pexman JH, Hudon ME, et al. Imaging of the brain in acute ischaemic stroke: comparison of computed tomography and magnetic resonance diffusion-weighted imaging. Journal of Neurology, Neurosurgery & Psychiatry. [Comparative Study
Research Support, Non-U.S. Gov't
Validation Studies]. 2005 Nov;76(11):1528-33.
66. Lovblad KO, Baird AE, Schlaug G, Benfield A, Siewert B, Voetsch B, et al. Ischemic lesion volumes in acute stroke by diffusion-weighted magnetic resonance imaging correlate with clinical outcome. Annals of Neurology. 1997 Aug;42(2):164-70.
67. Seitz RJ, Meisel S, Weller P, Junghans U, Wittsack HJ, Siebler M. Initial ischemic event: perfusion-weighted MR imaging and apparent diffusion coefficient for stroke evolution. Radiology. 2005 Dec;237(3):1020.
68. Davalos A, Blanco M, Pedraza S, Leira R, Castellanos M, Pumar JM, et al. The clinical-DWI mismatch: a new diagnostic approach to the brain tissue at risk of infarction. Neurology. 2004 Jun 22;62(12):2187.
69. Prosser J, Butcher K, Allport L, Parsons M, MacGregor L, Desmond P, et al. Clinical-diffusion mismatch predicts the putative penumbra with high specificity. Stroke. 2005 Aug;36(8):1700.
70. Lansberg MG, Thijs VN, Hamilton S, Schlaug G, Bammer R, Kemp S, et al. Evaluation of the clinical-diffusion and perfusion-diffusion mismatch models in DEFUSE. Stroke. 2007 Jun;38(6):1826.
71. Albers GW, Thijs VN, Wechsler L, Kemp S, Schlaug G, Skalabrin E, et al. Magnetic resonance imaging profiles predict clinical response to early reperfusion: the diffusion and perfusion imaging evaluation for understanding stroke evolution (DEFUSE) study. Ann Neurol. 2006 Nov;60(5):508-17.
72. Tong DC, Adami A, Moseley ME, Marks MP. Prediction of hemorrhagic transformation following acute stroke: role of diffusion- and perfusion-weighted magnetic resonance imaging. Arch Neurol. 2001 Apr;58(4):587-93.
73. Kidwell CS, Alger JR, Di Salle F, Starkman S, Villablanca P, Bentson J, et al. Diffusion MRI in patients with transient ischemic attacks.[see comment]. Stroke. 1999 Jun;30(6):1174-80.
74. Coutts SB, Eliasziw M, Hill MD, Scott JN, Subramaniam S, Buchan AM, et al. An improved scoring system for identifying patients at high early risk of stroke and functional impairment after an acute transient ischemic attack or minor stroke. International Journal of Stroke. 2008 Feb;3(1):3-10.

75. Sylaja PN, Coutts SB, Subramaniam S, Hill MD, Eliasziw M, Demchuk AM, et al. Acute ischemic lesions of varying ages predict risk of ischemic events in stroke/TIA patients.[see comment]. Neurology. 2007 Feb 6;68(6):415-9.
76. Alexander JA, Sheppard S, Davis PC, Salverda P. Adult cerebrovascular disease: role of modified rapid fluid-attenuated inversion-recovery sequences. Ajnr: American Journal of Neuroradiology. [Clinical Trial
Comparative Study
Controlled Clinical Trial]. 1996 Sep;17(8):1507-13.
77. Perkins CJ. Fluid-attenuated inversion recovery and diffusion- and perfusion-weighted MRI abnormalities in 117 consecutive patients with stroke symptoms. Stroke. 2001;32(12):2774-81.
78. Thomalla G, Rossbach P, Rosenkranz M, Siemonsen S, Krutzelmann A, Fiehler J, et al. Negative Fluid-Attenuated Inversion Recovery Imaging Identifies Acute Ischemic Stroke at 3 Hours or Less. Annals of Neurology. 2009;65(6):724-32.
79. Ebinger M, Galinovic I, Rozanski M, Brunecker P, Endres M, Fiebach JB. Fluid-Attenuated Inversion Recovery Evolution Within 12 Hours From Stroke Onset A Reliable Tissue Clock? Stroke.41(2):250-5.
80. Neumann-Haefelin T, Hoelig S, Berkefeld J, Fiehler J, Gass A, Humpich M, et al. Leukoaraiosis is a risk factor for symptomatic intracerebral hemorrhage after thrombolysis for acute stroke. Stroke. [Multicenter Study]. 2006 Oct;37(10):2463-6.
81. Fazekas F, Chawluk JB, Alavi A, Hurtig HI, Zimmerman RA. MR signal abnormalities at 1.5 T in Alzheimer's dementia and normal aging. AJR American Journal of Roentgenology. [Research Support, U.S. Gov't, P.H.S.]. 1987 Aug;149(2):351-6.
82. Noguchi K, Ogawa T, Inugami A, Fujita H, Hatazawa J, Shimosegawa E, et al. MRI of acute cerebral infarction: a comparison of FLAIR and T2-weighted fast spin-echo imaging. Neuroradiology. [Comparative Study]. 1997 Jun;39(6):406-10.
83. Cosnard G, Duprez T, Grandin C, Smith AM, Munier T, Peeters A. Fast FLAIR sequence for detecting major vascular abnormalities during the hyperacute phase of stroke: a comparison with MR angiography. Neuroradiology. [Clinical Trial
Comparative Study]. 1999 May;41(5):342-6.
84. Toyoda K, Ida M, Fukuda K. Fluid-attenuated inversion recovery intraarterial signal: an early sign of hyperacute cerebral ischemia.[see comment]. Ajnr: American Journal of Neuroradiology. 2001 Jun-Jul;22(6):1021-9.
85. Lee KY, Latour LL, Luby M, Hsia AW, Merino JG, Warach S. Distal hyperintese vessels on FLAIR. An MRI Marker for collateral circulation in acute stroke? Neurology. [Original]. 2009;72:6.
86. Gauvrit JY, Leclerc X, Girot M, Cordonnier C, Sotoares G, Henon H, et al. Fluid-attenuated inversion recovery (FLAIR) sequences for the assessment of acute stroke: inter observer and inter technique reproducibility. JNeurol. 2006 May;253(5):631.
87. Warach S, Latour LL, Warach S, Latour LL. Evidence of reperfusion injury, exacerbated by thrombolytic therapy, in human focal brain ischemia using a novel imaging marker of early blood-brain barrier disruption. Stroke. 2004 Nov;35(11 Suppl 1):2659-61.
88. Latour LL, Kang DW, Ezzeddine MA, Chalela JA, Warach S. Early blood-brain barrier disruption in human focal brain ischemia. Annals of Neurology. 2004 Oct;56(4):468.

89. Kidwell CS, Latour L, Saver JL, Alger JR, Starkman S, Duckwiler G, et al. Thrombolytic toxicity: blood brain barrier disruption in human ischemic stroke. Cerebrovascular Diseases. [Research Support, N.I.H., Extramural
Research Support, N.I.H., Intramural
Research Support, Non-U.S. Gov't]. 2008;25(4):338-43.
90. Rauscher A, Sedlacik J, Barth M, Mentzel HJ, Reichenbach JR. Magnetic susceptibility-weighted MR phase imaging of the human brain. AJNR Am J Neuroradiol. 2005 Apr;26(4):736-42.
91. Fiebach JB, Schellinger PD, Gass A, Kucinski T, Siebler M, Villringer A, et al. Stroke magnetic resonance imaging is accurate in hyperacute intracerebral hemorrhage: a multicenter study on the validity of stroke imaging.[see comment]. Stroke. 2004 Feb;35(2):502-6.
92. Linfante I, Llinas RH, Caplan LR, Warach S. MRI features of intracerebral hemorrhage within 2 hours from symptom onset. Stroke. 1999 Nov;30(11):2263-7.
93. Lin DD, Filippi CG, Steever AB, Zimmerman RD. Detection of intracranial hemorrhage: comparison between gradient-echo images and b(0) images obtained from diffusion-weighted echo-planar sequences. AJNR Am J Neuroradiol. 2001 Aug;22(7):1275-81.
94. Nighoghossian N, Hermier M, Adeleine P, Blanc-Lasserre K, Derex L, Honnorat J, et al. Old microbleeds are a potential risk factor for cerebral bleeding after ischemic stroke: a gradient-echo T2*-weighted brain MRI study. Stroke. 2002 Mar;33(3):735.
95. Kakuda W, Thijs VN, Lansberg MG, Bammer R, Wechsler L, Kemp S, et al. Clinical importance of microbleeds in patients receiving IV thrombolysis. Neurology. 2005 Oct 25;65(8):1175-8.
96. Fiehler J, Albers GW, Boulanger JM, Derex L, Gass A, Hjort N, et al. Bleeding risk analysis in stroke imaging before thromboLysis (BRASIL): pooled analysis of T2*-weighted magnetic resonance imaging data from 570 patients.[see comment]. Stroke. [Clinical Trial
Multicenter Study]. 2007 Oct;38(10):2738-44.
97. Chalela JA, Haymore JB, Ezzeddine MA, Davis LA, Warach S. The hypointense MCA sign. Neurology. 2002 May 28;58(10):1470.
98. Kimura K, Iguchi Y, Shibazaki K, Watanabe M, Iwanaga T, Aoki J, et al. M1 susceptibility vessel sign on T2* as a strong predictor for no early recanalization after IV-t-PA in acute ischemic stroke. Stroke. [Letter]. 2009 Sep;40(9):3130-2.
99. Morita N, Harada M, Uno M, Matsubara S, Matsuda T, Nagahiro S, et al. Ischemic findings of T2*-weighted 3-tesla MRI in acute stroke patients. Cerebrovasc Dis. 2008;26(4):367-75.
100. Higashida RT, Furlan AJ, Roberts H, Tomsick T, Connors B, Barr J, et al. Trial design and reporting standards for intra-arterial cerebral thrombolysis for acute ischemic stroke. Stroke. 2003 Aug;34(8):e109.
101. Staroselskaya IA, Chaves C, Silver B, Linfante I, Edelman RR, Caplan L, et al. Relationship between magnetic resonance arterial patency and perfusion-diffusion mismatch in acute ischemic stroke and its potential clinical use. ArchNeurol. 2001 Jul;58(7):1069.
102. Copen W, Gharai LR, Barak ER, Schwamm LH, Wu O, Karmalian S, et al. Existence of the Diffusion-Perfusion Mismatch within 24 Hours after Onset of Acute Stroke: Dependence on Proximal Arterial Occlusion. Radiology. [Original Article]. 2009;250(3):9.
103. Hacke W, Furlan AJ, Al-Rawi Y, Davalos A, Fiebach JB, Gruber F, et al. Intravenous desmoteplase in patients with acute ischaemic stroke selected by MRI perfusion-diffusion weighted imaging or perfusion CT (DIAS-2): a

prospective, randomised, double-blind, placebo-controlled study.[see comment]. Lancet Neurology. 2009 Feb;8(2):141-50.
104. Lansberg MG, Thijs VN, Bammer R, Olivot JM, Marks MP, Wechsler LR, et al. The MRA-DWI Mismatch Identifies Patients With Stroke Who Are Likely to Benefit From Reperfusion. Stroke. 2008 Jul 17.
105. Villringer A, Rosen BR, Belliveau JW, Ackerman JL, Lauffer RB, Buxton RB, et al. Dynamic imaging with lanthanide chelates in normal brain: contrast due to magnetic susceptibility effects. MagnResonMed. 1988 Feb;6(2):164.
106. Simonsen CZ, Ostergaard L, Vestergaard-Poulsen P, Rohl L, Bjornerud A, Gyldensted C. CBF and CBV measurements by USPIO bolus tracking: reproducibility and comparison with Gd-based values. JMagnResonImaging. 1999 Feb;9(2):342.
107. Kiselev VG. On the theoretical basis of perfusion measurements by dynamic susceptibility contrast MRI. MagnResonMed. 2001 Dec;46(6):1113.
108. Perkio J, Aronen HJ, Kangasmaki A, Liu Y, Karonen J, Savolainen S, et al. Evaluation of four postprocessing methods for determination of cerebral blood volume and mean transit time by dynamic susceptibility contrast imaging. MagnResonMed. 2002 May;47(5):973.
109. Ostergaard L, Sorensen AG, Kwong KK, Weisskoff RM, Gyldensted C, Rosen BR. High resolution measurement of cerebral blood flow using intravascular tracer bolus passages. Part II: Experimental comparison and preliminary results. Magnetic Resonance in Medicine. 1996;36(5):726-36.
110. Ostergaard L, Weisskoff RM, Chesler DA, Gyldensted C, Rosen BR. High resolution measurement of cerebral blood flow using intravascular tracer bolus passages. Part I: Mathematical approach and statistical analysis. MagnResonMed. 1996 Nov;36(5):715.
111. van Osch MJ, Vonken EJ, Viergever MA, van der Grond J, Bakker CJ. Measuring the arterial input function with gradient echo sequences. MagnResonMed. 2003 Jun;49(6):1067.
112. Rausch M, Scheffler K, Rudin M, Radu EW. Analysis of input functions from different arterial branches with gamma variate functions and cluster analysis for quantitative blood volume measurements. Magnetic resonance imaging. 2000 Dec;18(10):1235.
113. van Osch MJ, Vonken EJ, Bakker CJ, Viergever MA. Correcting partial volume artifacts of the arterial input function in quantitative cerebral perfusion MRI. MagnResonMed. 2001 Mar;45(3):477.
114. Thijs VN, Somford DM, Bammer R, Robberecht W, Moseley ME, Albers GW. Influence of arterial input function on hypoperfusion volumes measured with perfusion-weighted imaging. Stroke. 2004 Jan;35(1):94.
115. Ebinger M, Brunecker P, Jungehulsing GJ, Malzahn U, Kunze C, Endres M, et al. Reliable Perfusion Maps in Stroke MRI Using Arterial Input Functions Derived from Distal Middle Cerebral Artery Branches. Stroke. 2010;41(41):7.
116. Yamada K, Wu O, Gonzalez RG, Bakker D, Ostergaard L, Copen WA, et al. Magnetic resonance perfusion-weighted imaging of acute cerebral infarction: effect of the calculation methods and underlying vasculopathy. Stroke. 2002 Jan;33(1):87.
117. Calamante F, Gadian DG, Connelly A. Delay and dispersion effects in dynamic susceptibility contrast MRI: simulations using singular value decomposition. MagnResonMed. 2000 Sep;44(3):466.
118. Wu O, Ostergaard L, Weisskoff RM, Benner T, Rosen BR, Sorensen AG. Tracer arrival timing-insensitive technique for estimating flow in MR perfusion-weighted imaging using singular value decomposition with a block-circulant deconvolution matrix. Magnetic Resonance in Medicine. 2003 Jul;50(1):164.

119. Ostergaard L, Chesler DA, Weisskoff RM, Sorensen AG, Rosen BR. Modeling cerebral blood flow and flow heterogeneity from magnetic resonance residue data. JCerebBlood Flow Metab. 1999 Jun;19(6):690.
120. Hacke W, Albers G, Al-Rawi Y, Bogousslavsky J, Davalos A, Eliasziw M, et al. The Desmoteplase in Acute Ischemic Stroke Trial (DIAS): a phase II MRI-based 9-hour window acute stroke thrombolysis trial with intravenous desmoteplase. Stroke. 2005;36(1):66-73.
121. Furlan AJ, Eyding D, Albers GW, Al-Rawi Y, Lees KR, Rowley HA, et al. Dose Escalation of Desmoteplase for Acute Ischemic Stroke (DEDAS): evidence of safety and efficacy 3 to 9 hours after stroke onset. Stroke. 2006 May;37(5):1227.
122. Donnan GA, Baron JC, Ma H, Davis SM, Donnan GA, Baron J-C, et al. Penumbral selection of patients for trials of acute stroke therapy. Lancet neurology. [Review]. 2009 Mar;8(3):261-9.
123. Takasawa M, Jones PS, Guadagno JV, Christensen S, Fryer TD, Harding S, et al. How reliable is perfusion MR in acute stroke? Validation and determination of the penumbra threshold against quantitative PET. Stroke. 2008 Mar;39(3):870.
124. Kane I, Carpenter T, Chappell F, Rivers C, Armitage P, Sandercock P, et al. Comparison of 10 different magnetic resonance perfusion imaging processing methods in acute ischemic stroke: effect on lesion size, proportion of patients with diffusion/perfusion mismatch, clinical scores, and radiologic outcomes. Stroke. 2007 Dec;38(12):3158.
125. Kakuda W, Lansberg MG, Thijs VN, Kemp SM, Bammer R, Wechsler LR, et al. Optimal definition for PWI/DWI mismatch in acute ischemic stroke patients. J Cereb Blood Flow Metab. 2008 May;28(5):887-91.
126. Nagakane Y, Christensen S, Brekenfeld C, Ma H, Churilov L, Parson M, et al. EPITHET Positive Result After Reanalysis Using Baseline Diffusion-Weighted Imaging/Perfusion-Weighted Imaging Co-registration. Stroke. 2011;42:5.
127. Mishra NK, Albers GW, Davis SM, Donnan GA, Furlan AJ, Hacke W, et al. Mismatch-Based Delayed Thrombolysis. A Meta-Analysis. Stroke. 2009 Nov 19.
128. Soares BP, Tong E, Hom J, Cheng S-C, Bredno J, Boussel L, et al. Reperfusion is a More Accurate Predictor of Follow-Up Infarct Volume Than Recanalisation: A Proof of Concept Using CT in ACute Ischemic Stroke Patients. Stroke. 2010;41(41):7.
129. Campbell BC, Christensen S, Butcher KS, Gordon I, Parsons MW, Desmond PM, et al. Regional very low cerebral blood volume predicts hemorrhagic transformation better than diffusion-weighted imaging volume and thresholded apparent diffusion coefficient in acute ischemic stroke. Stroke. Jan;41(1):82-8.
130. Edelman RR, Siewert B, Darby DG, Thangaraj V, Nobre AC, Mesulam MM, et al. Qualitative mapping of cerebral blood flow and functional localization with echo-planar MR imaging and signal targeting with alternating radio frequency. Radiology. [Research Support, Non-U.S. Gov't Research Support, U.S. Gov't, P.H.S.]. 1994 Aug;192(2):513-20.
131. Williams DS, Detre JA, Leigh JS, Koretsky AP. Magnetic resonance imaging of perfusion using spin inversion of arterial water.[erratum appears in Proc Natl Acad Sci U S A 1992 May 1;89(9):4220]. ProcNatlAcadSciUSA. [Research Support, Non-U.S. Gov't Research Support, U.S. Gov't, P.H.S.]. 1992 Jan 1;89(1):212-6.
132. Ye FQ, Berman KF, Ellmore T, Esposito G, van Horn JD, Yang Y, et al. H(2)(15)O PET validation of steady-state arterial spin tagging cerebral blood flow measurements in humans. Magnetic Resonance in Medicine. [Clinical Trial Comparative Study]. 2000 Sep;44(3):450-6.
133. Siewert B, Schlaug G, Edelman RR, Warach S. Comparison of EPISTAR and T2*-weighted gadolinium-enhanced perfusion imaging in patients with acute cerebral ischemia. Neurology. 1997 Mar;48(3):673.

134. Chalela JA, Alsop DC, Gonzalez-Atavales JB, Maldjian JA, Kasner SE, Detre JA. Magnetic resonance perfusion imaging in acute ischemic stroke using continuous arterial spin labeling. Stroke. 2000 Mar;31(3):680.
135. Franke CL, Ramos LM, Van Gijn J. Development of multifocal haemorrhage in a cerebral infarct during computed tomography. Journal of Neurology, Neurosurgery & Psychiatry. [Case Reports
Letter]. 1990 Jun;53(6):531-2.
136. Saenz RC, Saenz RC. The disappearing basal ganglia sign. Radiology. 2005 Jan;234(1):242-3.
137. Grond M, Von Kummer R, Sobesky J, Schmulling S, Rudolf J, Terstegge K, et al. Early x-ray hypoattenuation of brain parenchyma indicates extended critical hypoperfusion in acute stroke. Stroke. 2000 Jan;31(1):133.
138. Muir KW, Baird-Gunning J, Walker L, Baird T, McCormick M, Coutts SB. Can the ischemic penumbra be identified on noncontrast CT of acute stroke? Stroke. 2007 Sep;38(9):2485.
139. Leys D, Pruvo JP, Godefroy O, Leclerc X. Prevalence and significance of hyperdense middle cerebral artery in acute stroke. Stroke. 1992;23(3):317.
140. Kirchhof K, Welzel T, Mecke C, Zoubaa S, Sartor K, Kirchhof K, et al. Differentiation of white, mixed, and red thrombi: value of CT in estimation of the prognosis of thrombolysis phantom study. Radiology. [In Vitro]. 2003 Jul;228(1):126-30.
141. Barber PA, Demchuk AM, Hudon ME, Pexman JH, Hill MD, Buchan AM. Hyperdense sylvian fissure MCA "dot" sign: A CT marker of acute ischemia. Stroke. [Clinical Trial
Research Support, Non-U.S. Gov't]. 2001 Jan;32(1):84-8.
142. Ozdemir O, Leung A, Bussiere M, Hachinski V, Pelz D, Ozdemir O, et al. Hyperdense internal carotid artery sign: a CT sign of acute ischemia.[see comment]. Stroke. [Research Support, Non-U.S. Gov't]. 2008 Jul;39(7):2011-6.
143. Manelfe C, Larrue V, von Kummer R, Bozzao L, Ringleb P, Bastianello S, et al. Association of hyperdense middle cerebral artery sign with clinical outcome in patients treated with tissue plasminogen activator. Stroke. [Clinical Trial Multicenter Study
Randomized Controlled Trial
Research Support, Non-U.S. Gov't]. 1999 Apr;30(4):769-72.
144. Kharitonova T, Thoren M, Ahmed N, Wardlaw JM, von Kummer R, Thomassen L, et al. Disappearing hyperdense middle cerebral artery sign in ischaemic stroke patients treated with intravenous thrombolysis: clinical course and prognostic significance.[see comment]. Journal of Neurology, Neurosurgery & Psychiatry. [Research Support, Non-U.S. Gov't]. 2009 Mar;80(3):273-8.
145. Wardlaw JM, Mielke O, Wardlaw JM, Mielke O. Early signs of brain infarction at CT: observer reliability and outcome after thrombolytic treatment--systematic review. Radiology. [Research Support, Non-U.S. Gov't
Review]. 2005 May;235(2):444-53.
146. Wardlaw JM, Farrall AJ, Perry D, von Kummer R, Mielke O, Moulin T, et al. Factors influencing the detection of early CT signs of cerebral ischemia: an internet-based, international multiobserver study. Stroke. [Comparative Study Multicenter Study
Research Support, Non-U.S. Gov't]. 2007 Apr;38(4):1250-6.
147. Barber PA, Demchuk AM, Zhang J, Buchan AM. Validity and reliability of a quantitative computed tomography score in predicting outcome of hyperacute stroke before thrombolytic therapy. ASPECTS Study Group. Alberta Stroke Programme Early CT Score.[see comment][erratum appears in Lancet 2000 Jun 17;355(9221):2170]. Lancet. 2000 May 13;355(9216):1670-4.

148. von Kummer R, Allen KL, Holle R, Bozzao L, Bastianello S, Manelfe C, et al. Acute stroke: usefulness of early CT findings before thrombolytic therapy. Radiology. 1997 Nov;205(2):327.
149. Patel SC, Levine SR, Tilley BC, Grotta JC, Lu M, Frankel M, et al. Lack of clinical significance of early ischemic changes on computed tomography in acute stroke.[see comment]. Jama. [Research Support, Non-U.S. Gov't]. 2001 Dec 12;286(22):2830-8.
150. Tsivgoulis G, Saqqur M, Sharma VK, Lao AY, Hoover SL, Alexandrov AV, et al. Association of pretreatment ASPECTS scores with tPA-induced arterial recanalization in acute middle cerebral artery occlusion. Journal of Neuroimaging. [Research Support, Non-U.S. Gov't]. 2008 Jan;18(1):56-61.
151. Lev MH, Farkas J, Rodriguez VR, Schwamm LH, Hunter GJ, Putman CM, et al. CT angiography in the rapid triage of patients with hyperacute stroke to intraarterial thrombolysis: accuracy in the detection of large vessel thrombus. Journal of computer assisted tomography. [Evaluation Studies
Research Support, Non-U.S. Gov't
Research Support, U.S. Gov't, P.H.S.]. 2001 Jul-Aug;25(4):520-8.
152. Knauth M, von Kummer R, Jansen O, Hahnel S, Dorfler A, Sartor K. Potential of CT angiography in acute ischemic stroke. Ajnr: American Journal of Neuroradiology. 1997 Jun-Jul;18(6):1001.
153. Hollingworth W, Nathens AB, Kanne JP, Crandall ML, Crummy TA, Hallam DK, et al. The diagnostic accuracy of computed tomography angiography for traumatic or atherosclerotic lesions of the carotid and vertebral arteries: a systematic review. European Journal of Radiology. [Review]. 2003 Oct;48(1):88-102.
154. Chappell F, Wardlaw J, Young GR, Gillard J, Roditi G, Yip B, et al. Carotid Artery Stenosis: Accuracy of Noninvasive Tests--Individual Patient Data Meta-Analysis
Radiology. 2009.
155. Wardlaw JM, Chappell FM, Best JJ, Wartolowska K, Berry E, Research NHS, et al. Non-invasive imaging compared with intra-arterial angiography in the diagnosis of symptomatic carotid stenosis: a meta-analysis.[see comment]. Lancet. [Meta-Analysis
Research Support, Non-U.S. Gov't
Review]. 2006 May 6;367(9521):1503-12.
156. Schramm P, Schellinger PD, Fiebach JB, Heiland S, Jansen O, Knauth M, et al. Comparison of CT and CT angiography source images with diffusion-weighted imaging in patients with acute stroke within 6 hours after onset. Stroke. 2002 Oct;33(10):2426.
157. Schramm P, Schellinger PD, Klotz E, Kallenberg K, Fiebach JB, Kulkens S, et al. Comparison of perfusion computed tomography and computed tomography angiography source images with perfusion-weighted imaging and diffusion-weighted imaging in patients with acute stroke of less than 6 hours' duration. Stroke. 2004 Jul;35(7):1652.
158. Yi CA, Na DG, Ryoo JW, Moon CH, Byun HS, Roh HG, et al. Multiphasic perfusion CT in acute middle cerebral artery ischemic stroke: prediction of final infarct volume and correlation with clinical outcome. Korean Journal of Radiology. 2002 Jul-Sep;3(3):163.
159. Wintermark M, Flanders AE, Velthuis B, Meuli R, van Leeuwen M, Goldsher D, et al. Perfusion-CT assessment of infarct core and penumbra: receiver operating characteristic curve analysis in 130 patients suspected of acute hemispheric stroke. Stroke. 2006 Apr;37(4):979.

160. Roberts HC, Roberts TPL, Smith WS, Lee TJ, Fischbein NJ, Dillon WP. Multisection dynamic CT perfusion for acute cerebral ischemia: The "toggling-table" technique. AmJNeuroradiol. 2001;22(6):1077.
161. Klotz E, Konig M. Perfusion measurements of the brain: Using dynamic CT for the quantitative assessment of cerebral ischemia in acute stroke. European Journal of Radiology. 1999 Jun;30(3):170.
162. Wintermark M, Lau BC, Chien J, Arora S. The anterior cerebral artery is an appropriate arterial input function for perfusion-CT processing in patients with acute stroke. Neuroradiology. 2008 Mar;50(3):227.
163. Kudo K, Terae S, Katoh C, Oka M, Shiga T, Tamaki N, et al. Quantitative cerebral blood flow measurement with dynamic perfusion CT using the vascular-pixel elimination method: comparison with H2(15)O positron emission tomography. Ajnr: American Journal of Neuroradiology. 2003 Mar;24(3):419.
164. Kamath A, Smith WS, Powers WJ, Cianfoni A, Chien J, Videen TO, et al. Perfusion CT compared to $H_2{}^{15}O/{}^{15}O$ PET in patients with chronic cervical artery occlusion. Neuroradiology. 2008;50:7.
165. Wintermark M, Reichhart M, Cuisenaire O, Maeder P, Thiran JP, Schnyder P, et al. Comparison of admission perfusion computed tomography and qualitative diffusion- and perfusion-weighted magnetic resonance imaging in acute stroke patients. Stroke. 2002 Aug;33(8):2025.
166. Eastwood JD, Lev MH, Wintermark M, Fitzek C, Barboriak DP, Delong DM, et al. Correlation of early dynamic CT perfusion imaging with whole-brain MR diffusion and perfusion imaging in acute hemispheric stroke. Ajnr: American Journal of Neuroradiology. 2003 Oct;24(9):1869.
167. Nabavi DG, Kloska SP, Nam EM, Freund M, Gaus CG, Klotz E, et al. MOSAIC: Multimodal Stroke Assessment using computed tomography: Novel diagnostic approach for the prediction of infarction size and clinical outcome. Stroke. 2002 01 Dec;33(12):2819.
168. Mehdiratta M, Schlaug G, Kumar S, Caplan LR, Selim M, Mehdiratta M, et al. Reducing the delay in thrombolysis: is it necessary to await the results of renal function tests before computed tomography perfusion and angiography in patients with code stroke? Journal of Stroke & Cerebrovascular Diseases. 2008 Sep;17(5):273-5.
169. Dittrich R, Akdeniz S, Kloska SP, Fischer T, Ritter MA, Seidensticker P, et al. Low rate of contrast-induced Nephropathy after CT perfusion and CT angiography in acute stroke patients. JNeurol. [Research Support, Non-U.S. Gov't]. 2007 Nov;254(11):1491-7.
170. Hopyan JJ, Gladstone DJ, Mallia G, Schiff J, Fox AJ, Symons SP, et al. Renal safety of CT angiography and perfusion imaging in the emergency evaluation of acute stroke. Ajnr: American Journal of Neuroradiology. [Controlled Clinical Trial
Research Support, Non-U.S. Gov't]. 2008 Nov;29(10):1826-30.
171. Cohnen M, Wittsack HJ, Assadi S, Muskalla K, Ringelstein A, Poll LW, et al. Radiation exposure of patients in comprehensive computed tomography of the head in acute stroke. Ajnr: American Journal of Neuroradiology. 2006 Sep;27(8):1741.
172. Hakim AM, Evans AC, Berger L, Kuwabara H, Worsley K, Marchal G, et al. The effect of nimodipine on the evolution of human cerebral infarction studied by PET. JCerebBlood Flow Metab. 1989 Aug;9(4):523.
173. Wise RJ, Bernardi S, Frackowiak RS, Legg NJ, Jones T. Serial observations on the pathophysiology of acute stroke. The transition from ischaemia to infarction as reflected in regional oxygen extraction. Brain. 1983 Mar;106 (Pt 1)(Pt 1):197.

174. Marchal G, Serrati C, Rioux P, Petit-Taboue MC, Viader F, de la Sayette V, et al. PET imaging of cerebral perfusion and oxygen consumption in acute ischaemic stroke: relation to outcome. Lancet. 1993 Apr 10;341(8850):925.
175. Marchal G, Beaudouin V, Rioux P, de la Sayette V, Le Doze F, Viader F, et al. Prolonged persistence of substantial volumes of potentially viable brain tissue after stroke: a correlative PET-CT study with voxel-based data analysis. Stroke. 1996 Apr;27(4):599.
176. Sobesky J, Zaro Weber O, Lehnhardt FG, Hesselmann V, Thiel A, Dohmen C, et al. Which time-to-peak threshold best identifies penumbral flow? A comparison of perfusion-weighted magnetic resonance imaging and positron emission tomography in acute ischemic stroke. Stroke. 2004 Dec;35(12):2843.
177. Graham GD, Blamire AM, Rothman DL, Brass LM, Fayad PB, Petroff OA, et al. Early temporal variation of cerebral metabolites after human stroke. A proton magnetic resonance spectroscopy study. Stroke. 1993 Dec;24(12):1891.
178. Saunders DE. MR spectroscopy in stroke. Br Med Bull. 2000;56(2):334-45.
179. Saunders DE, Howe FA, van den Boogaart A, McLean MA, Griffiths JR, Brown MM. Continuing ischemic damage after acute middle cerebral artery infarction in humans demonstrated by short-echo proton spectroscopy. Stroke. 1995 Jun;26(6):1007.
180. Felber SR, Aichner FT, Sauter R, Gerstenbrand F. Combined magnetic resonance imaging and proton magnetic resonance spectroscopy of patients with acute stroke. Stroke. 1992 Aug;23(8):1106-10.
181. Gillard JH, Barker PB, van Zijl PC, Bryan RN, Oppenheimer SM. Proton MR spectroscopy in acute middle cerebral artery stroke. Ajnr: American Journal of Neuroradiology. 1996 May;17(5):873.
182. Nicoli F, Lefur Y, Denis B, Ranjeva JP, Confort-Gouny S, Cozzone PJ. Metabolic counterpart of decreased apparent diffusion coefficient during hyperacute ischemic stroke: a brain proton magnetic resonance spectroscopic imaging study. Stroke. 2003 Jul;34(7):e82-7.
183. Singhal AB, Ratai E, Benner T, Vangel M, Lee V, Koroshetz WJ, et al. Magnetic resonance spectroscopy study of oxygen therapy in ischemic stroke. Stroke. 2007 Oct;38(10):2851.
184. Demchuk AM, Christou I, Wein TH, Felberg RA, Malkoff M, Grotta JC, et al. Accuracy and criteria for localizing arterial occlusion with transcranial Doppler. Journal of Neuroimaging. [Research Support, Non-U.S. Gov't Research Support, U.S. Gov't, P.H.S.]. 2000 Jan;10(1):1-12.
185. Delgado-Mederos R, Rovira A, Alvarez-Sabin J, Ribo M, Munuera J, Rubiera M, et al. Speed of tPA-induced clot lysis predicts DWI lesion evolution in acute stroke. Stroke. 2007 Mar;38(3):955.
186. Alexandrov AV, Burgin WS, Demchuk AM, El-Mitwalli A, Grotta JC. Speed of intracranial clot lysis with intravenous tissue plasminogen activator therapy: sonographic classification and short-term improvement. Circulation. 2001 Jun 19;103(24):2897.
187. Molina CA, Montaner J, Abilleira S, Arenillas JF, Ribo M, Huertas R, et al. Time course of tissue plasminogen activator-induced recanalization in acute cardioembolic stroke: a case-control study. Stroke. 2001 Dec 1;32(12):2821.
188. The Thrombolysis in Myocardial Infarction (TIMI) trial. Phase I findings. TIMI Study Group. New England Journal of Medicine. 1985 Apr 4;312(14):932-6.
189. Demchuk AM, Burgin WS, Christou I, Felberg RA, Barber PA, Hill MD, et al. Thrombolysis in brain ischemia (TIBI) transcranial Doppler flow grades predict clinical severity, early recovery, and mortality in patients treated with intravenous tissue plasminogen activator.[see comment]. Stroke. [Clinical Trial Multicenter Study

Research Support, Non-U.S. Gov't
Research Support, U.S. Gov't, P.H.S.]. 2001 Jan;32(1):89-93.
190. Brass LM, Walovitch RC, Joseph JL, Leveille J, Marchand L, Hellman RS, et al. The role of single photon emission computed tomography brain imaging with 99mTc-bicisate in the localization and definition of mechanism of ischemic stroke. Journal of Cerebral Blood Flow & Metabolism. 1994 Jan;14(Suppl 1):S91.
191. Grotta JC, Alexandrov AV. tPA-associated reperfusion after acute stroke demonstrated by SPECT. Stroke. 1998 Feb;29(2):429.
192. Ueda T, Sakaki S, Yuh WT, Nochide I, Ohta S. Outcome in acute stroke with successful intra-arterial thrombolysis and predictive value of initial single-photon emission-computed tomography. Journal of Cerebral Blood Flow & Metabolism. 1999 Jan;19(1):99-108.
193. Mahagne MH, David O, Darcourt J, Migneco O, Dunac A, Chatel M, et al. Voxel-based mapping of cortical ischemic damage using Tc 99m L,L-ethyl cysteinate dimer SPECT in acute stroke. Journal of Neuroimaging. 2004 Jan;14(1):23-32.
194. Spratt NJ, Ackerman U, Tochon-Danguy HJ, Donnan GA, Howells DW, Spratt NJ, et al. Characterization of fluoromisonidazole binding in stroke. Stroke. [Evaluation Studies
Research Support, Non-U.S. Gov't]. 2006 Jul;37(7):1862-7.
195. Saita K, Chen M, Spratt NJ, Porritt MJ, Liberatore GT, Read SJ, et al. Imaging the ischemic penumbra with 18F-fluoromisonidazole in a rat model of ischemic stroke. Stroke. [Research Support, Non-U.S. Gov't]. 2004 Apr;35(4):975-80.
196. Read SJ, Hirano T, Abbott DF, Sachinidis JI, Tochon-Danguy HJ, Chan JG, et al. Identifying hypoxic tissue after acute ischemic stroke using PET and 18F-fluoromisonidazole. Neurology. 1998 Dec;51(6):1617.
197. Markus R, Reutens DC, Kazui S, Read S, Wright P, Chambers BR, et al. Topography and temporal evolution of hypoxic viable tissue identified by 18F-fluoromisonidazole positron emission tomography in humans after ischemic stroke. Stroke. [Clinical Trial
Controlled Clinical Trial
Research Support, Non-U.S. Gov't]. 2003 Nov;34(11):2646-52.
198. Markus R, Reutens DC, Kazui S, Read S, Wright P, Pearce DC, et al. Hypoxic tissue in ischaemic stroke: persistence and clinical consequences of spontaneous survival. Brain. [Research Support, Non-U.S. Gov't]. 2004 Jun;127(Pt 6):1427-36.
199. Takasawa M, Beech JS, Fryer TD, Hong YT, Hughes JL, Igase K, et al. Imaging of brain hypoxia in permanent and temporary middle cerebral artery occlusion in the rat using 18F-fluoromisonidazole and positron emission tomography: a pilot study. Journal of Cerebral Blood Flow & Metabolism. [Research Support, Non-U.S. Gov't]. 2007 Apr;27(4):679-89.
200. Spratt NJ, Donnan G, Howells DW. Characterisation of the timing of binding of the hypoxia tracer FMISO after stroke
Brain Res. [Original]. 2009 2009 1288:8.
201. Heiss WD, Sobesky J, Smekal U, Kracht LW, Lehnhardt FG, Thiel A, et al. Probability of cortical infarction predicted by flumazenil binding and diffusion-weighted imaging signal intensity: a comparative positron emission tomography/magnetic resonance imaging study in early ischemic stroke. Stroke. [Comparative Study]. 2004 Aug;35(8):1892-8.
202. Heiss WD, Kracht LW, Thiel A, Grond M, Pawlik G. Penumbral probability thresholds of cortical flumazenil binding and blood flow predicting tissue outcome in patients with cerebral ischaemia. Brain. 2001;124(1):20.

203. Heiss WD, Kracht L, Grond M, Rudolf J, Bauer B, Wienhard K, et al. Early [(11)C]Flumazenil/H(2)O positron emission tomography predicts irreversible ischemic cortical damage in stroke patients receiving acute thrombolytic therapy.
. Stroke. 2000 Feb;31(2):366.
204. Kohrmann M, Juttler E, Fiebach JB, Huttner HB, Siebert S, Schwark C, et al. MRI versus CT-based thrombolysis treatment within and beyond the 3 h time window after stroke onset: a cohort study. Lancet Neurol. 2006 Aug;5(8):661-7.
205. Frahm J, Haase A, Matthaei D. Rapid NMR imaging of dynamic processes using the FLASH technique. Magnetic Resonance in Medicine. [Research Support, Non-U.S. Gov't]. 1986 Apr;3(2):321-7.
206. He X, Yablonskiy DA, He X, Yablonskiy DA. Quantitative BOLD: mapping of human cerebral deoxygenated blood volume and oxygen extraction fraction: default state. Magnetic Resonance in Medicine. [Research Support, N.I.H., Extramural
Research Support, Non-U.S. Gov't]. 2007 Jan;57(1):115-26.
207. An H, Lin W, An H, Lin W. Cerebral venous and arterial blood volumes can be estimated separately in humans using magnetic resonance imaging. Magnetic Resonance in Medicine. 2002 Oct;48(4):583-8.
208. Ogawa S, Lee TM, Nayak AS, Glynn P. Oxygenation-sensitive contrast in magnetic resonance image of rodent brain at high magnetic fields. MagnResonMed. 1990 Apr;14(1):68.
209. Ogawa S, Lee TM, Kay AR, Tank DW. Brain magnetic resonance imaging with contrast dependent on blood oxygenation. ProcNatlAcadSciUSA. 1990 Dec;87(24):9868.
210. Bandettini PA, Wong EC, Hinks RS, Tikofsky RS, Hyde JS. Time Course EPI of Human Brain-Function During Task Activation. Magnetic Resonance in Medicine. 1992;25(2):390-7.
211. Berens P, Logothetis N, Tolias A. Local field potentials, BOLD and spiking activity - relationships and physiological mechanisms. Nature Precedings. 2010;In press.
212. Pauling L, Coryell CD. The Magnetic Properties and Structure of Hemoglobin, Oxyhemoglobin and Carbonmonoxyhemoglobin. ProcNatlAcadSciUSA. 1936 Apr;22(4):210.
213. Hoppel BE, Weisskoff RM, Thulborn KR, Moore JB, Kwong KK, Rosen BR. Measurement of Regional Blood Oxygen And Cerebral Hemodynamics. Magnetic Resonance in Medicine. 1993;30(6):715-23.
214. Prinster A, Pierpaoli C, Turner R, Jezzard P. Simultaneous measurement of DeltaR2 and DeltaR2* in cat brain during hypoxia and hypercapnia. Neuroimage. 1997 Oct;6(3):191-200.
215. Bandettini PA, Wong EC, Jesmanowicz A, Hinks RS, Hyde JS. Spin-echo and gradient-echo EPI of human brain activation using BOLD contrast: a comparative study at 1.5 T. NMR in Biomedicine. [Comparative Study Research Support, Non-U.S. Gov't
Research Support, U.S. Gov't, P.H.S.]. 1994 Mar;7(1-2):12-20.
216. Thulborn KR, Waterton JC, Matthews PM, Radda GK. Oxygenation dependence of the transverse relaxation-time of water protons in whole-blood at high-field. Biochimica Et Biophysica Acta. 1982;714(2):265-70.
217. Wright GA, Hu BS, Macovski A. Estimating oxygen-saturation of blood invivo with mr imaging at 1.5t. Jmri-Journal of Magnetic Resonance Imaging. 1991;1(3):275-83.
218. Li DB, Wang Y, Waight DJ. Blood oxygen saturation assessment in vivo using T-2* estimation. Magnetic Resonance in Medicine. 1998;39(5):685-90.

219. Turner R, Lebihan D, Moonen CTW, Despres D, Frank J. Echo-planar time course mri of cat brain oxygenation changes. Magnetic Resonance in Medicine. [Note]. 1991 Nov;22(1):159-66.
220. Decrespigny AJ, Wendland MF, Derugin N, Kozniewska E, Moseley ME. Real-time observation of transient focal ischemia and hyperemia in cat brain. Magnetic Resonance in Medicine. 1992;27(2):391-7.
221. Roussel SA, Vanbruggen N, King MD, Gadian DG. Identification of collaterally perfused areas following focal cerebral-ischemia in the rat by comparison of gradient-echo and diffusion-weighted mri. Journal of Cerebral Blood Flow and Metabolism. 1995;15(4):578-86.
222. Jensen UR, Liu JR, Eschenfelder C, Meyne J, Zhao Y, Deuschl G, et al. The correlation between quantitative T2' and regional cerebral blood flow after acute brain ischemia in early reperfusion as demonstrated in a middle cerebral artery occlusion/reperfusion model of the rat. Journal of Neuroscience Methods. 2009 Mar 30;178(1):55-8.
223. Dunn JF, Wadghiri YZ, Meyerand ME. Regional heterogeneity in the brain's response to hypoxia measured using BOLD MR imaging. Magnetic Resonance in Medicine. [Research Support, U.S. Gov't, P.H.S.]. 1999 Apr;41(4):850-4.
224. Jones RA, Muller TB, Haraldseth O, Baptista AM, Oksendal AN. Cerebrovascular changes in rats during ischemia and reperfusion: a comparison of BOLD and first pass bolus tracking techniques. Magn Reson Med. 1996 Apr;35(4):489-96.
225. Tamura H, Hatazawa J, Toyoshima H, Shimosegawa E, Okudera T, Tamura H, et al. Detection of deoxygenation-related signal change in acute ischemic stroke patients by T2*-weighted magnetic resonance imaging. Stroke. 2002 Apr;33(4):967-71.
226. Wardlaw JM, von Heijne A. Increased oxygen extraction demonstrated on gradient echo (T2*) imaging in a patient with acute ischaemic stroke. Cerebrovascular Diseases. [Case Reports]. 2006;22(5-6):456-8.
227. Hermier M, Nighoghossian N, Derex L, Wiart M, Nemoz C, Berthezene Y, et al. Hypointense leptomeningeal vessels at T2*-weighted MRI in acute ischemic stroke. Neurology. [Comparative Study]. 2005 Aug 23;65(4):652-3.
228. Kaya D, Dincer A, Yildiz ME, Cizmeli MO, Erzen C. Acute ischemic infarction defined by a region of multiple hypointense vessels on gradient-echo T2* MR imaging at 3T. Ajnr: American Journal of Neuroradiology. 2009 Jun;30(6):1227-32.
229. Geisler BS, Brandhoff F, Fiehler J, Saager C, Speck O, Rother J, et al. Blood-oxygen-level-dependent MRI allows metabolic description of tissue at risk in acute stroke patients. Stroke. 2006 Jul;37(7):1778-84.
230. Siemonsen S, Fitting T, Thomalla G, Horn P, Finsterbusch J, Summers P, et al. T2' imaging predicts infarct growth beyond the acute diffusion-weighted imaging lesion in acute stroke. Radiology. [Research Support, Non-U.S. Gov't]. 2008 Sep;248(3):979-86.
231. Donswijk ML, Jones PS, Guadagno JV, Carpenter TA, Moustafa RR, Fryer TD, et al. T2*-weighted MRI versus oxygen extraction fraction PET in acute stroke. Cerebrovascular Diseases. 2009;28(3):306-13.
232. Yablonskiy DA, Haacke EM. Theory of NMR signal behavior in magnetically inhomogeneous tissues: the static dephasing regime. Magnetic Resonance in Medicine. 1994 Dec;32(6):749-63.
233. Weisskoff RM, Kiihne S. MRI susceptometry: image-based measurement of absolute susceptibility of MR contrast agents and human blood. Magn Reson Med. 1992 Apr;24(2):375-83.

234. An H, Lin W. Quantitative measurements of cerebral blood oxygen saturation using magnetic resonance imaging. Journal of Cerebral Blood Flow & Metabolism. [Research Support, U.S. Gov't, P.H.S.]. 2000 Aug;20(8):1225-36.
235. An H, Lin W, An H, Lin W. Cerebral oxygen extraction fraction and cerebral venous blood volume measurements using MRI: effects of magnetic field variation. Magnetic Resonance in Medicine. [Research Support, U.S. Gov't, P.H.S.]. 2002 May;47(5):958-66.
236. An H, Lin W, Celik A, Lee YZ. Quantitative measurements of cerebral metabolic rate of oxygen utilization using MRI: a volunteer study. NMR in Biomedicine. [Research Support, U.S. Gov't, P.H.S.]. 2001 Nov-Dec;14(7-8):441-7.
237. Lammertsma AA, Jones T. Correction for the presence of intravascular oxygen-15 in the steady-state technique for measuring regional oxygen extraction ratio in the brain: 1. Description of the method. J Cereb Blood Flow Metab. 1983 Dec;3(4):416-24.
238. An H, Liu Q, Chen Y, Lin W, An H, Liu Q, et al. Evaluation of MR-derived cerebral oxygen metabolic index in experimental hyperoxic hypercapnia, hypoxia, and ischemia. Stroke. [Research Support, N.I.H., Extramural
Research Support, Non-U.S. Gov't]. 2009 Jun;40(6):2165-72.
239. Lee JM, Vo KD, An H, Celik A, Lee Y, Hsu CY, et al. Magnetic resonance cerebral metabolic rate of oxygen utilization in hyperacute stroke patients. Annals of Neurology. [Clinical Trial
Research Support, U.S. Gov't, P.H.S.]. 2003 Feb;53(2):227-32.
240. Ford A, An H, Ponisio R, Vo KD, Derdeyn CP, Powers WJ, et al. Oxygen Metabolic Index Predicts Gray Matter Infarction Better Than Apparent Diffusion Coefficient and Mean Transit Time During Hyper-Acute Ischemic Stroke. Stroke. 2010;41:e204.
241. He X, Zhu M, Yablonskiy DA, He X, Zhu M, Yablonskiy DA. Validation of oxygen extraction fraction measurement by qBOLD technique. Magnetic Resonance in Medicine. [Evaluation Studies
Research Support, N.I.H., Extramural
Research Support, Non-U.S. Gov't
Validation Studies]. 2008 Oct;60(4):882-8.
242. Bulte D, Chiarelli P, Wise R, Jezzard P, Bulte D, Chiarelli P, et al. Measurement of cerebral blood volume in humans using hyperoxic MRI contrast. Journal of Magnetic Resonance Imaging. [Research Support, Non-U.S. Gov't]. 2007 Oct;26(4):894-9.
243. van Zijl PC, Eleff SM, Ulatowski JA, Oja JM, Ulug AM, Traystman RJ, et al. Quantitative assessment of blood flow, blood volume and blood oxygenation effects in functional magnetic resonance imaging. Nature Medicine. [Research Support, Non-U.S. Gov't
Research Support, U.S. Gov't, P.H.S.]. 1998 Feb;4(2):159-67.
244. Grohn OH, Kettunen MI, Penttonen M, Oja JM, van Zijl PC, Kauppinen RA. Graded reduction of cerebral blood flow in rat as detected by the nuclear magnetic resonance relaxation time T2: a theoretical and experimental approach. Journal of Cerebral Blood Flow & Metabolism. [Research Support, Non-U.S. Gov't
Research Support, U.S. Gov't, P.H.S.]. 2000 Feb;20(2):316-26.
245. Kavec M, Grohn OH, Kettunen MI, Silvennoinen MJ, Penttonen M, Kauppinen RA. Use of spin echo T(2) BOLD in assessment of cerebral misery perfusion at 1.5 T. Magma. [Research Support, Non-U.S. Gov't]. 2001 Mar;12(1):32-9.

246. Kettunen MI, Grohn OH, Silvennoinen MJ, Penttonen M, Kauppinen RA, Kettunen MI, et al. Quantitative assessment of the balance between oxygen delivery and consumption in the rat brain after transient ischemia with T2 -BOLD magnetic resonance imaging. Journal of Cerebral Blood Flow & Metabolism. [Research Support, Non-U.S. Gov't]. 2002 Mar;22(3):262-70.
247. Kavec M, Usenius JP, Tuunanen PI, Rissanen A, Kauppinen RA, Kavec M, et al. Assessment of cerebral hemodynamics and oxygen extraction using dynamic susceptibility contrast and spin echo blood oxygenation level-dependent magnetic resonance imaging: applications to carotid stenosis patients. Neuroimage. [Research Support, Non-U.S. Gov't]. 2004 May;22(1):258-67.
248. Davis TL, Kwong KK, Weisskoff RM, Rosen BR. Calibrated functional MRI: mapping the dynamics of oxidative metabolism. ProcNatlAcadSciUSA. 1998 Feb 17;95(4):1834-9.
249. Chiarelli PA, Bulte DP, Wise R, Gallichan D, Jezzard P, Chiarelli PA, et al. A calibration method for quantitative BOLD fMRI based on hyperoxia. Neuroimage. 2007 Sep 1;37(3):808-20.
250. Bulte DP, Chiarelli PA, Wise RG, Jezzard P, Bulte DP, Chiarelli PA, et al. Cerebral perfusion response to hyperoxia. Journal of Cerebral Blood Flow & Metabolism. [Research Support, Non-U.S. Gov't]. 2007 Jan;27(1):69-75.
251. Rostrup E, Larsson HB, Toft PB, Garde K, Henriksen O. Signal changes in gradient echo images of human brain induced by hypo- and hyperoxia. NMR in Biomedicine. [Comparative Study]. 1995 Feb;8(1):41-7.
252. Losert C, Peller M, Schneider P, Reiser M, Losert C, Peller M, et al. Oxygen-enhanced MRI of the brain. Magnetic Resonance in Medicine. [Research Support, Non-U.S. Gov't]. 2002 Aug;48(2):271-7.
253. Kennan RP, Scanley BE, Gore JC. Physiologic basis for BOLD MR signal changes due to hypoxia/hyperoxia: separation of blood volume and magnetic susceptibility effects. Magnetic Resonance in Medicine. [Research Support, Non-U.S. Gov't]. 1997 Jun;37(6):953-6.
254. Wibral M, Muckli L, Melnikovic K, Scheller B, Alink A, Singer W, et al. Time-dependent effects of hyperoxia on the BOLD fMRI signal in primate visual cortex and LGN. Neuroimage. 2007 Apr 15;35(3):1044-63.
255. Santosh C, Brennan D, McCabe C, Macrae IM, Holmes WM, Graham DI, et al. Potential use of oxygen as a metabolic biosensor in combination with T2*-weighted MRI to define the ischemic penumbra. Journal of Cerebral Blood Flow & Metabolism. [Research Support, Non-U.S. Gov't]. 2008 Oct;28(10):1742-53.
256. Pruessmann KP, Weiger M, Scheidegger MB, Boesiger P. SENSE: sensitivity encoding for fast MRI. MagnResonMed. 1999 Nov;42(5):952.
257. Brott T, Adams HP, Jr., Olinger CP, Marler JR, Barsan WG, Biller J, et al. Measurements of acute cerebral infarction: a clinical examination scale. Stroke. 1989 Jul;20(7):864.
258. Gast KK, Puderbach MU, Rodriguez I, Eberle B, Markstaller K, Hanke AT, et al. Dynamic ventilation (3)He-magnetic resonance imaging with lung motion correction: gas flow distribution analysis. InvestRadiol. 2002 Mar;37(3):126.
259. Mapleson WW. Circulation-time models of the uptake of inhaled anaesthetics and data for quantifying them. BrJAnaesth. 1973 Apr;45(4):319.
260. Oldendorf WH. Measurement of the mean transit time of cerebral circulation by external detection of an intravenously injected radioisotope. Journal of Nuclear Medicine. 1984 Feb;25(2):253.
261. McCormick M, Hadley D, McLean JR, Macfarlane JA, Condon B, Muir KW. Randomized, Controlled Trial of Insulin for Acute Poststroke Hyperglycemia. Annals of Neurology.67(5):570-8.

262. Kety SS, Schmidt CF. The Effects of Altered Arterial Tensions of Carbon Dioxide and Oxygen on Cerebral Blood Flow and Cerebral Oxygen Consumption of Normal Young Men. JClinInvest. 1948 Jul;27(4):484.
263. Nakajima S, Meyer JS, Amano T, Shaw T, Okabe T, Mortel KF. Cerebral vasomotor responsiveness during 100% oxygen inhalation in cerebral ischemia. ArchNeurol. 1983 May;40(5):271.
264. Shin HK, Dunn AK, Jones PB, Boas DA, Lo EH, Moskowitz MA, et al. Normobaric hyperoxia improves cerebral blood flow and oxygenation, and inhibits peri-infarct depolarizations in experimental focal ischaemia. Brain. 2007 Jun;130(Pt 6):1631.
265. Mirhej ME. Proton spin relaxation by paramagnetic molecular oxygen. Canadian Journal of Chemistry. 1965;43(5):1130-&.
266. Matta BF, Lam AM, Mayberg TS. The influence of arterial oxygenation on cerebral venous oxygen-saturation during hyperventilation. Canadian Journal of Anaesthesia-Journal Canadien D Anesthesie. 1994;41(11):1041-6.
267. Berkowitz BA. Role of dissolved plasma oxygen in hyperoxia-induced contrast. Magnetic resonance imaging. 1997;15(1):123.
268. Biswal B, Yetkin FZ, Haughton VM, Hyde JS. Functional connectivity in the motor cortex of resting human brain using echo-planar MRI. MagnResonMed. 1995 Oct;34(4):537.
269. Berthezene Y, Tournut P, Turjman F, N'Gbesso R, Falise B, Froment JC. Inhaled oxygen: a brain MR contrast agent? Ajnr: American Journal of Neuroradiology. 1995 Nov-Dec;16(10):2010-2.
270. Murata Y, Sakatani K, Katayama Y, Fukaya C. Increase in focal concentration of deoxyhaemoglobin during neuronal activity in cerebral ischaemic patients. Journal of Neurology, Neurosurgery & Psychiatry. 2002 Aug;73(2):182-4.
271. Fiehler J, Geisler B, Siemonsen S, Saager C, Speck O, Thomalla G, et al. [Visual rating of T2'-blood-oxygen-level-dependent magnetic resonance imaging in acute stroke patients--a pilot study]. Rofo: Fortschritte auf dem Gebiete der Rontgenstrahlen und der Nuklearmedizin. [English Abstract]. 2007 Jan;179(1):17-20.
272. Sakoh M, Ostergaard L, Rohl L, Smith DF, Simonsen CZ, Sorensen JC, et al. Relationship between residual cerebral blood flow and oxygen metabolism as predictive of ischemic tissue viability: sequential multitracer positron emission tomography scanning of middle cerebral artery occlusion during the critical first 6 hours after stroke in pigs. Journal of neurosurgery. 2000 Oct;93(4):647-57.
273. Leenders KL, Perani D, Lammertsma AA, Heather JD, Buckingham P, Healy MJR, et al. Cerebral blood-flow, blood-volume and oxygen utilization - normal values and effect of age. Brain. 1990;113:27-47.
274. Duling BR, Berne RM. Longitudinal gradients in periarteriolar oxygen tension - a possible mechanism for participation of oxygen in local regulation of blood flow. Circulation Research. 1970;27(5):669-&.
275. Hyder F, Shulman RG, Rothman DL. A model for the regulation of cerebral oxygen delivery. Journal of Applied Physiology. 1998;85(2):554-64.
276. Kassissia IG, Goresky CA, Rose CP, Schwab AJ, Simard A, Huet PM, et al. Tracer oxygen distribution is barrier-limited in the cerebral microcirculation. Circulation Research. 1995;77(6):1201-11.
277. Federspiel WJ, Popel AS. A theoretical-analysis of the effect of the particulate nature of blood on oxygen release in capillaries. Microvascular Research. 1986;32(2):164-89.

278. Herman P, Trubel HKF, Hyder F. A multiparametric assessment of oxygen efflux from the brain. Journal of Cerebral Blood Flow and Metabolism. 2006;26(1):79-91.
279. McLeod AD, Igielman F, Elwell C, Cope M, Smith M. Measuring cerebral oxygenation during normobaric hyperoxia: A comparison of tissue microprobes, near-infrared spectroscopy, and jugular venous oximetry in head injury. Anesthesia and Analgesia. 2003;97(3):851-6.
280. Bethune DW, Collis JM. An evaluation of oxygen therapy equipment - experimental study of various devices on human subject. Thorax. 1967;22(3):221-&.
281. Morris EAJ, Smith AJ, Kinsella SM. Performance of standard and reservoir-type Hudson masks in pregnant and non-pregnant subjects. International Journal of Obstetric Anesthesia. 2001;10(4):284-8.
282. Severinghaus JW. Simple, accurate equations for human-blood o2 dissociation computations. Journal of Applied Physiology. 1979;46(3):599-602.
283. Duong TQ, Kim SG. In vivo MR measurements of regional arterial and venous blood volume fractions in intact rat brain. Magnetic Resonance in Medicine. 2000;43(3):393-402.
284. Grubb RL, Raichle ME, Eichling JO, Terpogos.Mm. Effects of changes in paco2 on cerebral blood volume, blood flow, and vascular mean transit time. Stroke. 1974;5(5):630-9.
285. Fox PT, Raichle ME. Focal physiological uncoupling of cerebral blood flow and oxidative metabolism during somatosensory stimulation in human subjects. ProcNatlAcadSciUSA. 1986 Feb;83(4):1140.
286. Waring WS, Thomson AJ, Adwani SH, Rosseel AJ, Potter JF, Webb DJ, et al. Cardiovascular effects of acute oxygen administration in healthy adults. JCardiovascPharmacol. 2003 Aug;42(2):245.
287. Thomson AJ, Drummond GB, Waring WS, Webb DJ, Maxwell SR. Effects of short-term isocapnic hyperoxia and hypoxia on cardiovascular function. JApplPhysiol. 2006 Sep;101(3):809.
288. Lambertsen CJ, Dough RH, Cooper DY, Emmel GL, Loeschcke HH, Schmidt CF. Oxygen toxicity; effects in man of oxygen inhalation at 1 and 3.5 atmospheres upon blood gas transport, cerebral circulation and cerebral metabolism. Journal of applied physiology. 1953 Mar;5(9):471.
289. Ellingsen I, Hauge A, Nicolaysen G, Thoresen M, Walloe L. Changes in human cerebral blood flow due to step changes in PAO2 and PACO2. Acta PhysiolScand. 1987 Feb;129(2):157.
290. Omae T, Ibayashi S, Kusuda K, Nakamura H, Yagi H, Fujishima M. Effects of high atmospheric pressure and oxygen on middle cerebral blood flow velocity in humans measured by transcranial Doppler. Stroke. 1998 Jan;29(1):94.
291. Berre J, Vachiery JL, Moraine JJ, Naeije R. Cerebral blood flow velocity responses to hypoxia in subjects who are susceptible to high-altitude pulmonary oedema. EurJApplPhysiolOccupPhysiol. 1999 Sep;80(4):260.
292. Watson NA, Beards SC, Altaf N, Kassner A, Jackson A. The effect of hyperoxia on cerebral blood flow: a study in healthy volunteers using magnetic resonance phase-contrast angiography. EurJAnaesthesiol. 2000 Mar;17(3):152.
293. Kolbitsch C, Lorenz IH, Hormann C, Hinteregger M, Lockinger A, Moser PL, et al. The influence of hyperoxia on regional cerebral blood flow (rCBF), regional cerebral blood volume (rCBV) and cerebral blood flow velocity in the middle cerebral artery (CBFVMCA) in human volunteers. Magnetic resonance imaging. 2002 Sep;20(7):535.

294. Johnston AJ, Steiner LA, Balestreri M, Gupta AK, Menon DK. Hyperoxia and the cerebral hemodynamic responses to moderate hyperventilation. Acta AnaesthesiolScand. 2003 Apr;47(4):391.
295. Floyd TF, Clark JM, Gelfand R, Detre JA, Ratcliffe S, Guvakov D, et al. Independent cerebral vasoconstrictive effects of hyperoxia and accompanying arterial hypocapnia at 1 ATA. JApplPhysiol. 2003 Dec;95(6):2453.
296. Cremer JE, Seville MP. Regional brain blood-flow, blood-volume, and hematocrit values in the adult-rat. Journal of Cerebral Blood Flow and Metabolism. 1983;3(2):254-6.
297. Yamauchi H, Fukuyama H, Nagahama Y, Katsumi Y, Okazawa H. Cerebral hematocrit decreases with hemodynamic compromise in carotid artery occlusion - A PET study. Stroke. 1998;29(1):98-103.
298. Mickel HS, Vaishnav YN, Kempski O, von Lubitz D, Weiss JF, Feuerstein G. Breathing 100% oxygen after global brain ischemia in Mongolian Gerbils results in increased lipid peroxidation and increased mortality. Stroke. 1987 Mar-Apr;18(2):426.
299. Singhal AB, Dijkhuizen RM, Rosen BR, Lo EH. Normobaric hyperoxia reduces MRI diffusion abnormalities and infarct size in experimental stroke. Neurology. 2002 Mar 26;58(6):945.
300. Henninger N, Bouley J, Nelligan JM, Sicard KM, Fisher M. Normobaric hyperoxia delays perfusion/diffusion mismatch evolution, reduces infarct volume, and differentially affects neuronal cell death pathways after suture middle cerebral artery occlusion in rats. JCerebBlood Flow Metab. 2007 Sep;27(9):1632.
301. Singhal AB. A review of oxygen therapy in ischemic stroke. Neurological Research. 2007;29(2):173-83.
302. Stroke Oxygen Study (SO2S). wwwso2scouk (accessed 1st February 2010).
303. Sobesky J, Weber OZ, Lehnhardt FG, Hesselmann V, Neveling M, Jacobs A, et al. Does the mismatch match the penumbra? Magnetic resonance imaging and positron emission tomography in early ischemic stroke. Stroke. 2005 May;36(5):980.
304. Olivot JM, Mlynash M, Thijs VN, Kemp S, Lansberg MG, Wechsler L, et al. Optimal Tmax threshold for predicting penumbral tissue in acute stroke. Stroke. 2009 Feb;40(2):469-75.
305. Butcher KS, Parsons M, MacGregor L, Barber PA, Chalk J, Bladin C, et al. Refining the perfusion-diffusion mismatch hypothesis. Stroke. 2005 Jun;36(6):1153.
306. Lierse W, Horstmann E. Quantitative anatomy of the cerebral vascular bed with especial emphasis on homogeneity and inhomogeneity in small ports of the gray and white matter. Acta Neurologica Scandinavica Supplementum. [Comparative Study]. 1965;14:15-9.
307. Stys PK, Ransom BR, Waxman SG, Davis PK. Role of extracellular calcium in anoxic injury of mammalian central white matter. ProcNatlAcadSciUSA. 1990;87(11):4212-6.
308. Dohmen C, Kumura E, Rosner G, Heiss WD, Graf R. Adenosine in relation to calcium homeostasis: Comparison between gray and white matter ischemia. Journal of Cerebral Blood Flow and Metabolism. 2001;21(5):503-10.
309. Arakawa S, Wright PM, Koga M, Phan TG, Reutens DC, Lim I, et al. Ischemic thresholds for gray and white matter: a diffusion and perfusion magnetic resonance study. Stroke. 2006 May;37(5):1211.
310. Murphy BD, Fox AJ, Lee DH, Sahlas DJ, Black SE, Hogan MJ, et al. White matter thresholds for ischemic penumbra and infarct core in patients with acute stroke: CT perfusion study. Radiology. 2008 Jun;247(3):818.

311. Murphy BD, Fox AJ, Lee DH, Sahlas DJ, Black SE, Hogan MJ, et al. Identification of penumbra and infarct in acute ischemic stroke using computed tomography perfusion-derived blood flow and blood volume measurements. Stroke. 2006 Jul;37(7):1771.
312. Aquino D, Bizzi A, Grisoli M, Garavaglia B, Bruzzone MG, Nardocci N, et al. Age-related Iron Deposition in the Basal Ganglia: Quantitative Analysis in Healthy Subjects. Radiology. 2009;252(1):165-72.
313. Mrak RE, Griffin WST, Graham DI. Aging-associated changes in human brain. Journal of Neuropathology and Experimental Neurology. 1997;56(12):1269-75.
314. Ashburner J, Friston KJ. Unified segmentation. Neuroimage. 2005 Jul 1;26(3):839-51.
315. Gusnard DA, Raichle ME. Searching for a baseline: Functional imaging and the resting human brain. Nature Reviews Neuroscience. 2001;2(10):685-94.
316. Engelhorn T, Doerfler A. High-molar contrast agents for CNS. Imaging Decisions MRI. 2007;11(4):7.
317. Wintermark M, Albers GW, Alexandrov AV, Alger JR, Bammer R, Baron JC, et al. Acute stroke imaging research roadmap. AJNR Am J Neuroradiol. 2008 May;29(5):e23-30.
318. Wintermark M, Albers GW, Alexandrov AV, Alger JR, Bammer R, Baron JC, et al. Acute stroke imaging research roadmap. Stroke. 2008 May;39(5):1621-8.
319. Lin WL, Paczynski RP, Celik A, Kuppusamy K, Hsu CY, Powers WJ. Experimental hypoxemic hypoxia: Changes in R-2* of brain parenchyma accurately reflect the combined effects of changes in arterial and cerebral venous oxygen saturation. Magnetic Resonance in Medicine. 1998;39(3):474-81.
320. Baskerville TA, Deuchar GA, McCabe C, Robertson CA, Holmes WM, Santosh C, et al. Influence of 100% and 40% oxygen on penumbral blood flow, oxygen level, and T(2)(star)-weighted MRI in a rat stroke model. Journal of Cerebral Blood Flow and Metabolism. Aug;31(8):1799-806.
321. Patronas NJ, Dichiro G, Smith BH, Delapaz R, Brooks RA, Milam HL, et al. Depressed cerebellar glucose-metabolism in supratentorial tumors. Brain Research. 1984;291(1):93-101.
322. Baron JC, Bousser MG, Comar D, Castaigne P. "Crossed Cerebellar Diaschisis" in Human Supratentorial Brain Infarction. Annals of Neurology. 1980;8(1):1.
323. Baron JC, Bousser MG, Comar D, Castaigne P. "Crossed cerebellar diaschisis" in human supratentorial brain infarction. Transactions of the American Neurological Association. 1981 1981;105:459-61.
324. Pantano P, Baron JC, Samson Y, Bousser MG, Derouesne C, Comar D. Crossed cerebellar diaschisis - further-studies. Brain. [Article]. 1986 Aug;109:677-94.
325. Serrati C, Marchal G, Rioux P, Viader F, Petittaboue MC, Lochon P, et al. Contralateral Cerebellar Hypometabolism - A Predictor For Stroke Outcome. Journal of Neurology Neurosurgery and Psychiatry. 1994 Feb;57(2):174-9.
326. Meneghetti G, Vorstrup S, Mickey B, Lindewald H, Lassen NA. Crossed cerebellar diaschisis in ischemic stroke - a study of regional cerebral blood-flow by xe-133 inhalation and single photon-emission computerized-tomography. Journal of Cerebral Blood Flow and Metabolism. 1984;4(2):235-40.
327. Pantano P, Lenzi GL, Guidetti B, Dipiero V, Gerundini P, Savi AR, et al. Crossed cerebellar diaschisis in patients with cerebral-ischemia assessed by spect and i-123 hipdm. European Neurology. 1987;27(3):142-8.
328. Feeney DM, Baron JC. Diaschsis. Stroke. [Review]. 1986 Sep-Oct;17(5):817-30.

329. Sperling B, Overgaard K, Videbaek C, Pedersen H, G B. Remission of crossed cerebellar diaschsis following successful thrombolytic therapy. J Cereb Blood Flow Metab. 1995;15, Supplement 1:1.
330. Kamouchi M, Fujishima M, Saku Y, Ibayashi S, Iida M. Crossed cerebellar hypoperfusion in hyperacute ischemic stroke. Journal of the Neurological Sciences. 2004;225(1-2):65-9.
331. Sobesky J, Thiel A, Ghaemi M, Hilker RH, Rudolf J, Jacobs AH, et al. Crossed cerebellar diaschisis in acute human stroke: a PET study of serial changes and response to supratentorial reperfusion. Journal of Cerebral Blood Flow and Metabolism. 2005;25(12):1685-91.
332. Lin DDM, Kleinman JT, Wityk RJ, Gottesman RF, Hillis AE, Lee AW, et al. Crossed Cerebellar Diaschisis in Acute Stroke Detected by Dynamic Susceptibility Contrast MR Perfusion Imaging. AmJNeuroradiol. 2009;30(4):710-5.
333. Yamada H, Koshimoto Y, Sadato N, Kawashima Y, Tanaka M, Tsuchida C, et al. Crossed cerebellar diaschisis: Assessment with dynamic susceptibility contrast MR imaging. Radiology. 1999;210(2):558-62.
334. Madai V, Altaner A, Stengle K, Zaro Weber O, Heiss WD, von Samson-Himmelstjerna F, et al. Crossed cerebellar diaschisis after stroke: can perfusion-weighted MRI show functional inactivation?
. J Cereb Blood Flow Metab. 2011;Epub ahead of print.
335. Gold L, Lauritzen M. Neuronal deactivation explains decreased cerebellar blood flow in response to focal cerebral ischemia or suppressed neocortical function. ProcNatlAcadSciUSA. 2002;99(11):7699-704.
336. Newman GC, Delucia-Deranja E, Tudorica A, Hospod FE, Patlak CS. Cerebral blood volume measurements by T-2*-weighted MRI and contrast infusion. Magnetic Resonance in Medicine. 2003;50(4):844-55.
337. Sakoh M, Rohl L, Gyldensted C, Gjedde A, Ostergaard L. Cerebral blood flow and blood volume measured by magnetic resonance imaging bolus tracking after acute stroke in pigs - Comparison with [O-15]H2O positron emission tomography. Stroke. 2000;31(8):1958-64.
338. Warach S, Pettigrew LC, Dashe JF, Pullicino P, Lefkowitz DM, Sabounjian L, et al. Effect of citicoline on ischemic lesions as measured by diffusion-weighted magnetic resonance imaging. Citicoline 010 Investigators. Annals of Neurology. 2000 Nov;48(5):713.
339. Warach S, Kaufman D, Chiu D, Devlin T, Luby M, Rashid A, et al. Effect of the Glycine Antagonist Gavestinel on cerebral infarcts in acute stroke patients, a randomized placebo-controlled trial: The GAIN MRI Substudy. CerebrovascDis. 2006;21(1-2):106.
340. Kidwell CS, Lees KR, Muir KW, Chen C, Davis SM, De Silva DA, et al. Results of the MRI Substudy of the Intravenous Magnesium Efficacy in Stroke Trial. Stroke. [Article]. 2009 May;40(5):1704-9.
341. Group MRSC, Phan TG, Donnan GA, Davis SM, Byrnes G. Proof-of-principle phase II MRI studies in stroke: sample size estimates from dichotomous and continuous data. Stroke. 2006 Oct;37(10):2521.
342. Warach S. New imaging strategies for patient selection for thrombolytic and neuroprotective therapies. Neurology. 2001;57(5 Suppl 2):S48.
343. Muir KW. Heterogeneity of stroke pathophysiology and neuroprotective clinical trial design. Stroke. 2002 Jun;33(6):1545.
344. Rodionov R, De Martino F, Laufs H, Carmichael DW, Formisano E, Walker M, et al. Independent component analysis of interictal fMRI in focal epilepsy: Comparison with general linear model-based EEG-correlated fMRI. Neuroimage. 2007 Nov 15;38(3):488-500.

345. Christensen S, Mouridsen K, Wu O, Hjort N, Karstoft H, Thomalla G, et al. Comparison of 10 Perfusion MRI Parameters in 97 Sub-6-Hour Stroke Patients Using Voxel-Based Receiver Operating Characteristics Analysis. Stroke. 2009;40(6):2055-61.
346. Smith SM. Fast robust automated brain extraction. Human Brain Mapping. 2002;17(3):143-55.
347. Latour LL, Warach S. Cerebral spinal fluid contamination of the measurement of the apparent diffusion coefficient of water in acute stroke. Magnetic Resonance in Medicine. 2002;48(3):478-86.
348. Schwamm LH, Koroshetz WJ, Sorensen AG, Wang B, Copen WA, Budzik R, et al. Time course of lesion development in patients with acute stroke - Serial diffusion- and hemodynamic-weighted magnetic resonance imaging. Stroke. 1998;29(11):2268-76.
349. Shih LC, Saver JL, Alger JR, Starkman S, Leary MC, Vinuela F, et al. Perfusion-weighted magnetic resonance imaging thresholds identifying core, irreversibly infarcted tissue. Stroke. 2003 Jun;34(6):1425.
350. Parrish TB, Gitelman DR, LaBar KS, Mesulam MM. Impact of signal-to-noise on functional MRI. Magnetic Resonance in Medicine. [Article]. 2000 Dec;44(6):925-32.
351. Friston KJ, Williams S, Howard R, Frackowiak RSJ, Turner R. Movement-related effects in fMRI time-series. Magnetic Resonance in Medicine. 1996;35(3):346-55.
352. Jezzard P, Clare S. Sources of distortion in functional MRI data. Human Brain Mapping. 1999;8(2-3):80-5.
353. Krueger G, Glover GH. Physiological noise in oxygenation-sensitive magnetic resonance imaging. Magnetic Resonance in Medicine. [Article]. 2001 October;46(4):631-7.
354. Feinberg DA, Mark AS. Human-brain motion and cerebrospinal-fluid circulation demonstrated with mr velocity imaging. Radiology. 1987;163(3):793-9.
355. Maier SE, Hardy CJ, Jolesz FA. Brain and cerebrospinal-fluid motion - real-time quantification with m-mode mr-imaging. Radiology. 1994;193(2):477-83.
356. Pelled G, Goelman G. Different physiological MRI noise between cortical layers. Magnetic Resonance in Medicine. 2004;52(4):913-6.
357. Mayhew JEW, Askew S, Zheng Y, Porrill J, Westby GWM, Redgrave P, et al. Cerebral vasomotion: A 0.1-Hz oscillation in reflected light imaging of neural activity. Neuroimage. 1996;4(3):183-93.
358. Mayevsky A, Ziv I. Oscillations and cortical oxidative metabolism and microcirculation in the ischemic brain. Neurological Research. 1991;13(1):39-47.
359. Salek-Haddadi A, Diehl B, Hamandi K, Merschhemke M, Liston A, Friston K, et al. Hemodynamic correlates of epileptiform discharges: an EEG-fMRI study of 63 patients with focal epilepsy. Brain Research. [Comparative Study Research Support, Non-U.S. Gov't]. 2006 May 9;1088(1):148-66.
360. Lemieux L, Salek-Haddadi A, Lund TE, Laufs H, Carmichael D, Lemieux L, et al. Modelling large motion events in fMRI studies of patients with epilepsy. Magnetic Resonance Imaging. [Research Support, Non-U.S. Gov't]. 2007 Jul;25(6):894-901.
361. Schachinger H, Langewitz W, Schmieder RE, Ruddel H. Comparison of parameters for assessing blood pressure and heart rate variability from non-invasive twenty-four-hour blood pressure monitoring.[Erratum appears in J Hypertens Suppl 1989 Sep;7(9):following 767]. Journal of Hypertension - Supplement. 1989 May;7(3):S81-4.

362. Yong M, Kaste M, Yong M, Kaste M. Association of characteristics of blood pressure profiles and stroke outcomes in the ECASS-II trial. Stroke. [Multicenter Study
Randomized Controlled Trial]. 2008 Feb;39(2):366-72.
363. Zang YF, He Y, Zhu CZ, Cao QJ, Sui MQ, Liang M, et al. Altered baseline brain activity in children with ADHD revealed by resting-state functional MRI. Brain & Development. 2007;29(2):83-91.
364. Lowe MJ, Phillips MD, Lurito JT, Mattson D, Dzemidzic M, Mathews VP. Multiple sclerosis: Low-frequency temporal blood oxygen level-dependent fluctuations indicate reduced functional connectivity - Initial results. Radiology. 2002;224(1):184-92.
365. Li SJ, Li Z, Wu GH, Zhang MJ, Franczak M, Antuono PG. Alzheimer disease: Evaluation of a functional MR imaging index as a marker. Radiology. 2002;225(1):253-9.
366. Cole DM, Smith SM, Beckmann CF. Advances and pitfalls in the analysis and interpretation of resting-state FMRI data. Front Syst Neurosci.4:8.
367. Yang H, Long XY, Yang YH, Yan H, Zhu CZ, Zhou XP, et al. Amplitude of low frequency fluctuation within visual areas revealed by resting-state functional MRI. Neuroimage. 2007;36(1):144-52.
368. Zou QH, Zhu CZ, Yang YH, Zuo XN, Long XY, Cao QJ, et al. An improved approach to detection of amplitude of low-frequency fluctuation (ALFF) for resting-state fMRI: Fractional ALFF. Journal of Neuroscience Methods. 2008;172(1):137-41.
369. Liu YT, D'Arceuil H, He JL, Duggan M, Gonzalez G, Pryor J, et al. MRI of spontaneous fluctuations after acute cerebral ischemia in nonhuman primates. Journal of Magnetic Resonance Imaging. 2007;26:1112-6.
370. Ogawa S, Lee TM. Magnetic resonance imaging of blood vessels at high fields: in vivo and in vitro measurements and image simulation. Magnetic Resonance in Medicine. 1990 Oct;16(1):9-18.
371. Haines K, Neuberger T, Lanagan M, Semouchkina E, Webb AG. High Q calcium titanate cylindrical dielectric resonators for magnetic resonance microimaging. Journal of Magnetic Resonance. 2009;200(2):349-53.
372. Webb A, Kan H, Versluis M, Smith N. Increased signal-to-noise in high field localized spectroscopy of the temporal lobe using newdeformable high-dielectric materials. Proc Intl Soc Mag Reson Med. 2010;18.
373. http://www.eso-stroke.org/pdf/ESO%20Guidelines_update_Jan_2009.pdf (accessed 17th February 2010).
374. Latchaw RE, Alberts MJ, Lev MH, Connors JJ, Harbaugh RE, Higashida RT, et al. Recommendations for imaging of acute ischemic stroke: a scientific statement from the American Heart Association. Stroke. 2009 Nov;40(11):3646-78.
375. Ma H, Zavala JA, Teoh H, Churilov L, Gunawan M, Ly J, et al. Penumbral mismatch is underestimated using standard volumetric methods and this is exacerbated with time. J Neurol Neurosurg Psychiatry. 2009 Sep;80(9):991-6.
376. Parsons MW, Christensen S, McElduff P, Levi C, Butcher KS, De Silva DA, et al. Pretreatment diffusion- and perfusion-MR lesion volumes have a crucial influence on clinical response to stroke thrombolysis
Journal of Cerebral Blood Flow and Metabolism. 2010.
377. Selim M, Fink JN, Kumar S, Caplan LR, Horkan C, Chen Y, et al. Predictors of hemorrhagic transformation after intravenous recombinant tissue plasminogen activator: prognostic value of the initial apparent diffusion coefficient and diffusion-weighted lesion volume. Stroke. 2002 Aug;33(8):2047.

378. Vahedi K, Vicaut E, Mateo J, Kurtz A, Orabi M, Guichard JP, et al. Sequential-design, multicenter, randomized, controlled trial of early decompressive craniectomy in malignant middle cerebral artery infarction (DECIMAL Trial). Stroke. 2007 Sep;38(9):2506-17.
379. Tong DC, Yenari MA, Albers GW, O'Brien M, Marks MP, Moseley ME. Correlation of perfusion- and diffusion-weighted MRI with NIHSS score in acute (< 6.5 hour) ischemic stroke. Neurology. 1998;50(4):864-70.
380. Kane I, Lindley R, Lewis S, Sandercock P, Group ISTC. Impact of stroke syndrome and stroke severity on the process of consent in the Third International Stroke Trial. CerebrovascDis. 2006;21(5-6):348.
381. Demarquay G, Derex L, Nighoghossian N, Adeleine P, Philippeau F, Honnorat J, et al. Ethical issues of informed consent in acute stroke. Analysis of the modalities of consent in 56 patients enrolled in urgent therapeutic trials. CerebrovascDis. 2005;19(2):65.
382. World Medical A. World Medical Association Declaration of Helsinki: ethical principles for medical research involving human subjects. JPostgradMed. 2002 Jul-Sep;48(3):206.
383. Directive 2001/20/EC of the European Parliament and of the Council of 4 April 2001 on the approximation of the laws, regulations and administrative provisions of the member states relating to the implementation of good clinical practice in the conduct of clinical trials on medicinal products for human use. MedEtika Bioet. 2002 Spring-Summer;9(1-2):12.
384. Scotland. Adults with Incapacity (Scotland) Act 2000--excerpt. BullMedEthics. 2000 Apr;(157)(157):8.
385. Oppenheim C, Samson Y, Manai R, Lalam T, Vandamme X, Crozier S, et al. Prediction of malignant middle cerebral artery infarction by diffusion-weighted imaging. Stroke. 2000;31(9):2175-81.
386. Grotta J, Bratina P. Subjective Experiences of 24 patients dramatically recovering from stroke. Stroke. 1995;26(7):1285-8.
387. Luby M, Warach S. Reliability of MR perfusion-weighted and diffusion-weighted imaging mismatch measurement methods. Ajnr: American Journal of Neuroradiology. 2007 Oct;28(9):1674.